UNIVERSITY OF STRATHCLYDE

ADVANCED STRUCTURAL MODELLING AND DESIGN OF WIND TURBINE ELECTRICAL GENERATORS

Pablo Jaen Sola

A thesis presented in fulfilment of the requirements

for the Degree of Doctor of Philosophy

Centre for Doctoral Training in Wind Energy Systems

Department of Electronic and Electrical Engineering

University of Strathclyde

Glasgow, G1 1XW

Scotland, UK

May 2017

This thesis is the result of the author's original research. It has been composed by the author and has not been previously submitted for examination which has led to the award of a degree.

The copyright of this thesis belongs to the author under the terms of the United Kingdom Copyright Acts as qualified by University of Strathclyde Regulation 3.50. Due acknowledgment must always be made of the use of any material contained in, or derived from, this thesis.

Signed:

Date:

Acknowledgments

I would like to express my most sincere gratitude to my principal supervisor Dr Alasdair S. McDonald. I will never forget the opportunity he gave me to carry out this project. Without his moral and technical support, this thesis would not have been possible. I would also like to thank him for the freedom he gave me, for his excellent proof-reading and for all the skills he taught me along this way. I am sure they all will be very useful in my career.

I am grateful to my second supervisor, Dr Erkan Oterkus for his support and valuable advice on materials engineering and composite modelling.

This thesis is the culmination of four years study at the Wind Energy Systems Doctoral Training Centre within the University of Strathclyde and I would like to thank Professor William Leithead who gave me this incredible opportunity. A big thank you is due to Mr Drew Smith who is the person that keeps everything running smoothly in our centre and is always there to give us a hand.

A thank you is also due to my fellow CDT colleagues that have kept me company throughout this process. We created a nice environment where it is actually fun to discuss work.

Finally, but most importantly, I would like to express my eternal gratitude to my parents, Mercedes and Leopoldo and to my elder brother Javier for always being there no matter the distance or the time, and for their unconditional love and patience. I will never be able to explain with words how important you have been for me in this journey and in my entire life.

"Our hours are minutes when we hope to know, but centuries when we know what it is possible to learn"

Antonio Machado

Abstract

This thesis concentrates on direct drive electrical generators for wind energy applications. A variety of wind turbine configurations and generator topologies are reviewed.

Direct drive renewable energy converters introduce a low speed, high torque input into the electrical machine. Due to this, these generators have to be larger and more robust than their high speed counterparts. With very large airgap closing forces, a very stiff structure capable of withstanding the stress is necessary. As a result very heavy machines, with structural ('inactive') material dominating the electromagnetically 'active' material are designed.

In this thesis a stiffness approach is introduced which combines electromagnetic stiffness and structural stiffness for different modes of deflection. This is used to minimise mass of the generator by trading stiffness of rotor and stator structures.

Design tools are presented, validated and utilised to model lightweight supporting structures ('inactive material') for high torque radial flux permanent magnet synchronous generators. Different structural layouts are statically studied, compared and optimised. Making use of low density materials, such as composites, a simplified generator structure is designed and contrasted with its optimised steel counterpart.

As a rotating piece machinery forming part of a bigger and more complex machine, electrical generators are subject to dynamic and external forces coming from the wind turbine rotor. The optimised steel design is looked at from a dynamic viewpoint. Discussions and conclusions highlight the potential design solutions that can be adopted to minimise the mass and therefore the cost of these machines.

v

Table of Contents

List of Figures

XIII

XIV

List of Tables

Nomenclature

Roman letters

A	Area, m^2
A_{arm}	Cross-section area of the arm, m^2
A_{ij}	Extensional and shear stress stiffnesses, N/m
B	Magnetic flux density, Wb/m^2
B_g	Peak flux density in the airgap, T
B_{ij}	Extension-bending coupling stiffnesses, N/m
B_r	Remanent flux density in the airgap, T
b	Beam width in X direction, m
b_p	Magnets width, m
C_i	Balancing constant
D_{ij}	Bending and torsional stiffnesses, N/m
D_s	Distance between holes centres (stator further optimisation), m
d_s	Optimisation holes diameter (stator further optimisation), m
E	Young's modulus, Pa
E_k	Kinetic energy, J
F	Force caused by the normal component of the Maxwell stress, N
F_c	Airgap closing force, N
$\mathscr{F}$	Magnetomotive force, At
$\widehat{\mathscr{F}}$	Peak magnetomotive force, At
$\widehat{\mathscr{F}_1}$	Peak magnetomotive force calculated with analytical model, At
$\widehat{\mathscr{F}_3}$	Peak magnetomotive force calculated with analytical model including third harmonic, At
$\widehat{\mathscr{F}}_{PM}$	Peak magnetomotive force for a permanent magnet machine, At

f	Structure's natural frequency, Hz
G	Shear modulus, Pa
g	Acceleration due to gravity, 9.81 m/s^2
g	magnetically effective airgap width, m
H	Intensity of magnetic field, A/m
H_C	Composite fracture toughness, Pa
h	Beam's height in Y direction, m
h_m	Magnet height, m
h_{ry}	Rotor yoke height, m
h_{sy}	Stator yoke height, m
i	Finite number of bearing radial stiffness
I	Current, A
I	Second moment of area, m^4
k_A	Stiffness of component A, N/m
k_a	Arm stiffness, N/m
k_{ac}	Armed rotor cylinder sub structure stiffness, N/m
$k_{ac,s}$	Armed stator cylinder sub structure stiffness, N/m
$k_{a,eq}$	Arms equivalent stiffness, N/m
k_B	Stiffness of component B, N/m
k_b	Bearing stiffness, N/m
k_{cr}	Carter factor
k_c	Cylinder stiffness, N/m
$k_{c,a}$	Rotor cylinder stiffness for armed structures, N/m
$k_{c,s}$	Stator cylinder stiffness for disc structures, N/m
k_d	Disc stiffness, N/m
k_{eq}	Equivalent stiffness, N/m
$k_{eq,d}$	Equivalent rotor stiffness, N/m
$k_{eq,r}$	Equivalent rotor stiffness, N/m

XVIII

k_{M}	Magnetic stiffness, N/m
k_{r}	Bearing radial stiffness, N/m
k_{s}	Generator structure stiffness, N/m
$k_{\mathrm{s,r}}$	Rotor stiffness, N/m
$k_{\mathrm{s,s}}$	Stator stiffness, N/m
L	Half notch length, m
L	Beam length in the Z direction, m
l	Axial length of machine, m
l_{arm}	Arm length, m
$l_{\mathrm{as,c}}$	Axial length of armed stator cylinder sub structure, m
$l_{\mathrm{c,a}}$	Axial length of armed rotor cylinder sub structure m
$l_{\mathrm{c,s}}$	Axial length of disc stator cylinder sub structure, m
l_{r}	Optimisation hole length, m
M	Moments, Nm
M	Attachment mass, kg
m	Beam mass per unit length, kg/m
$m_{\mathrm{s,r}}$	mass of rotor made with a disc, kg
$m_{\mathrm{s,s}}$	mass of stator made with discs, kg
$m_{\mathrm{s,ar}}$	mass of rotor made with arms, kg
$m_{\mathrm{s,as}}$	mass of stator made with arms, kg
N	Loads, N
N	Total number of bearing radial stiffnesses
n	Number of phases
n	Number of peaks
n_{arms}	Number of support arms
P	Power rating, W
P	Frequency of the wind turbine rotational speed, Hz
$\bar{P}$	Mean value of airgap permeance per unit area, H/m^2
P_{Δ}	Amplitude of variation of the airgap permeance per unit area, H/m^2
p	Number of pole pairs

q	Normal component of Maxwell stress, Pa
R	Radius of machine, m
R	Resistance, Ω
$R_{as,c}$	Armed stator cylinder radius, m
$R_{c,a}$	Armed rotor cylinder radius, m
$R_{c,s}$	Disc stator cylinder sub structure radius, m
R_l	Distance between centres (rotor further optimisation), m
R_m	Radius of the large circumference (rotor further optimisation), m
R_s	Radius of the small circumference (rotor further optimisation), m
r	Radius of the generator's shaft, m
T	Torque, Nm
T	Period of oscillation, sec
T_r	Temperature of the rotor structure, degrees
T_s	Temperature of the stator structure, degrees
t_c	Cylinder casing thickness, m
t_{con}	Cone sub structure thickness, m
t_{cyl}	Rotor conical cylinder sub structure thickness, m
t_d	Disc sub structure thickness, m
$t_{a,s}$	Stator arm's thickness, m
t_{arm}	Rotor arm's thickness, m
$t_{c,a}$	Armed rotor cylinder sub structure thickness, m
$t_{c,as}$	Armed stator cylinder sub structure thickness, m
$t_{s,c}$	Stator cylinder sub structure thickness, m
$t_{s,d}$	Stator disc sub structure thickness, m
V	Potential energy, J
w	Arm width, m
$\dot{y}$	Mass linear velocity, m/s
y_{max}	Spring vertical deformation, m

Greek letters

α_{PM}	Variable used to simplify equation 3.22a
α_{WR}	Variable used to simplify equation 3.21a
γ	Angle between bearing radial stiffnesses, degrees
γ	Deflection mode
δ	Deflection, m
δ	Distance between composite fibres, m
δ_{r}	Rotor deflection, m
δ_{s}	Stator deflection, m
$\delta_{\mathrm{Structural}}$	Structural deflection, m
$\bar{\delta}$	Mean deflection, m
δ_{Δ}	Deflection change respect to the mean, m
ε	Mechanical strain
$\varepsilon_{\mathrm{arm}}$	Arm strain
ε_{r}	Radial strain
κ	Curvatures
θ	Angular displacement, degrees
θ	Cross-section area of a single fibre, m^2
ν	Poisson's ratio
μ_0	Permeability of free space, 4×10^{-7} H/m
μ_{r}	Relative permeability
ρ	Density, $\mathrm{kg/m}^3$
ρ_{c}	Composite material density, $\mathrm{kg/m}^3$
ρ_{PM}	Permanent magnets' density, $\mathrm{kg/m}^3$
σ	Structural stress, Pa
σ	Airgap shear stress, Pa

σ_{arm}	Arm structural stress, Pa
σ_{PM}	Stress during operation in permanent magnet machine, Pa
$\sigma_{\text{N}}^{\infty}$	Residual stress from Mar-Lin formula, Pa
σ_{r}	Radial stress, Pa
σ_{θ}	Angular stress, Pa
τ_{p}	Pole pitch, m
φ	Phase angle, degrees
Φ	Magnetic flux, Wb
ψ	Cone angle, degrees

Abbreviations

AC	Alternating Current
APDL	ANSYS Parametric Design Language
BAT	Buoyant Airborne Wind Turbine
BEM	Blade Element Momentum Theory
CA	Conventional Approach Disc Modelling
CAD	Computer Aided Design
CDT	Centre for Doctoral Training
CMC	Ceramic Matrix Composites
DC	Direct Current
DD	Directly Driven
DFIG	Doubly Fed Induction Generator
DS	Danish Standard
EEDD	Electrically Excited Directly Driven
EMF	Electromotive force
EU	European Union

FE	Finite Element
FEA	Finite Element Analysis
FEMM	Finite Element Method Magnetics
GL	Germanischer Lloyd
IEC	International Electrotechnical Standard
ILSS	Interlaminar Shear Strength
IGBT	Insulated Gate Bipolar Transistors
HAWT	Horizontal Axis Wind Turbine
HVAC	High Voltage Alternating Current
HVDC	High Voltage Direct Current
MMC	Metal Matrix Composites
MMF	Magnetomotive Force
PM	Permanent Magnet
PMC	Polymer Matrix Composites
PMDD	Permanent Magnet Directly Driven
RF	Radial Flux
RTM	Resin Transfer Moulding
rpm	revolutions per minute
UK	United Kingdom
USA	United States of America

Chapter 1

Introduction

1.1 Introduction

Global energy consumption has experienced an important increase since the last century especially in emerging countries, such as China and India. The same trends are shown for the world's population and economic growth [1]. However, the fact that these three factors are highly correlated makes difficult to tackle the problem of climate change. In addition, the recent financial crisis has delayed the development and growth of low carbon and no-carbon technologies [2]. With almost 80% of the electricity demand worldwide coming from the combustion of conventional fossil fuels (coal, oil and gas) [3], the level of greenhouse gases, such as carbon dioxide

(CO_2), methane (CH_4), sulphur dioxide (SO_2) and nitrous oxide (N_2O) [4], released to the atmosphere is causing significant changes in the Earth's mean temperature.
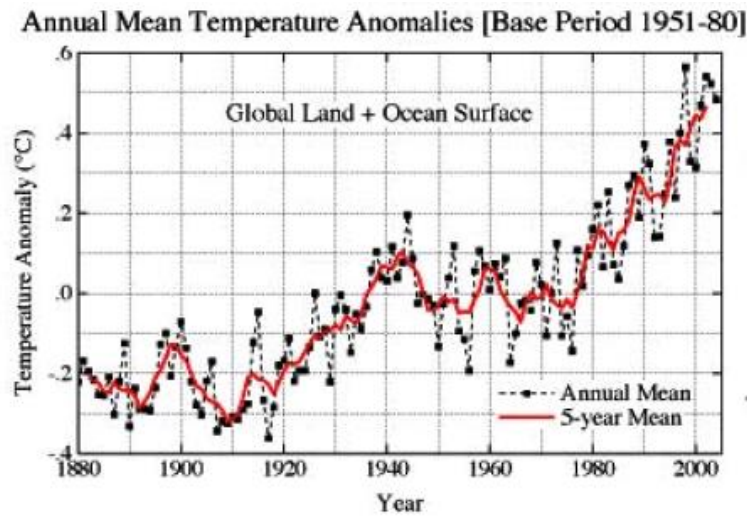
Figure 1.1 Global mean temperature between 1880 and 2000 [5]

Figure 1.1 clearly displays an increase of the global temperature with a sharp slope between 1980 and 2000 due to the growth of greenhouse gas emissions from human activities.

Taking into consideration this clarifying fact, governments have turned their attention on renewable energies. Wind energy is one of the most developed and mature clean technology and has an important role to play in the fight against global warming. Wind resources tend to be greater and steadier offshore and therefore large scale renewable energy projects will be developed further away from shore. For instance, in August 2016, the UK government gave the go-ahead for the world's biggest offshore wind farm off the Yorkshire coast with 300 wind turbines of 7 MW rated power capacity each that will cover an area of more than 480 km^2 in the North Sea [6].

In this context, where the offshore wind sector is becoming a key player, a huge effort is being made worldwide with the main aim of quickly reducing its high levelised cost and making it capable of competing with conventional electricity production technologies.

Offshore wind turbines are placed in harsh environments where the wind speeds tend to be higher, the air has high humidity and salt content, foundations and substations are subject to wave and tidal current loading and access can be limited by wave height. Some of the manufacturers' considerations for wind turbine design are low maintenance requirements, easy access to important components, high capacity factors and assembly with the lightest and cheapest possible crane. Lifting large pieces of equipment offshore, costs between £10k and £100k a day [7]. Thus, lightweight designs are highly desirable.

With large heavy rotating machinery working under tough conditions, minimising the number of moving parts could eventually help diminish the maintenance and mass of the machines. The problems introduced by wind turbine gearboxes could be observed at Scroby Sands, one of the UK's first offshore wind farms. In 2005, 27 intermediate speed and 12 high speed gearbox bearings of the Vestas V-80 wind turbines had to be replaced [8]. In Horns Rev offshore wind farm Vestas again had to remove and replace 80 of V90 gearboxes [9].

Bearing this in mind, the use of brushless direct drive generators, where the electrical machine is directly connected to the wind turbine rotor and the gearbox and the electrical slip rings or brushes are eliminated, can be a potential solution. Without gearbox and brushes maintenance downtimes are significantly reduced. Nonetheless, direct drive generators are quite heavy and robust machines especially designed to withstand large torques and other typical loads present during operation. Therefore, it is also necessary to find a method to minimise its mass. The traditional way is to compare the torque per unit mass between the competing machines. However, these comparisons are usually based only on the machine active mass, which consists of the copper in the windings, permanent magnets and the rotor and stator back iron. According to Hartkopf *et al.* two thirds of the mass of a radial flux electrical machine corresponds to the inactive mass, also known as supporting structure, so this must also be included for an accurate comparison [10]. Significant mass savings leading to machine's substantial cost decrease can be achieved by considering the supporting structure mass during the design stage. In order to carry out this task, it is necessary

to account with versatile tools capable of estimating the minimum generator structural requirements in a quick and precise manner.

1.2 Research question

Can electromagnetic and structural stiffness models be used effectively to minimise the mass of electrical generators for direct drive wind turbines? If so, are there limitations to such an approach?

1.3 Aims of the thesis

The main aims of this thesis are to explore and develop the potential options available for lightweight design of the supporting structure of a direct drive wind turbine generator using stiffness as a framing device. Objectives are as follows:

- To produce design tools which can be used during the design process to accurately estimate the necessary structural stiffness of the machine
- To compare different structural geometries in order to find the lightest configuration capable of dealing with major loads acting on the generator structure
- To optimise the generator steel structure (rotor and stator) with a view to minimise its mass
- To analyse the optimised steel structure from a dynamic viewpoint and generate design tools which can be utilised when looking at the dynamics of the electrical machine
- To explore the distinct structural configurations available so as to identify the one presenting the best characteristics dynamically speaking
- To find an optimum structural generator design using low density materials and compare it with the optimised steel structure

1.4 Thesis layout

The next chapter will introduce the reader to renewables and renewable energy converters concentrating all the attention on the wind energy sector and the different existing types of wind turbines and electrical generators. This section also contains a detailed review of the latest progress in the technology.

Chapter 3 includes the theory behind the design of a radial flux direct drive PM electrical machine supporting structure. A parametric model that couples the electromagnetic and mechanical design has been derived in this chapter, taking disc structures that are utilised to model radial deflection with the main aim of accurately estimating the minimum structural stiffness of the components forming the radial flux generator. The approach has been validated using finite element modelling techniques.

Three distinct techniques for modelling the required machine structural stiffness (FE, analytical and hybrid) are explained in Chapter 4, including a hybrid method produced by the authors which combines the results obtained from dimensional homogeneity studies and the data retrieved from FE analyses.

A comparison between two different types of structural configurations, one made with discs and one made with arms, is presented with a view of finding out the lightest layout. The most suitable structure is studied under different deflection modes and further optimised aiming the minimisation of its mass. Moreover, a conical structural geometry is proposed for study and optimisation taking into consideration its inherent axial stiffness and its excellent radial characteristics.

In Chapter 5, radial flux direct drive PM generator structures are designed and optimised at a small scale and at a large scale using low density materials, such as composites, and compared with optimised steel structures. Using disc sub structures with fibres following conventional and mosaic pattern orientations, significant mass savings could be achieved.

Chapter 6 shows the results achieved from a complete set of modal analyses carried out over the optimised disc steel structure. The available options to avoid the

resonant frequencies of the generator structure are explored and discussed in this chapter. A conical structural configuration is also dynamically tested as its distinct layout showed potential for further dynamic enhancements.

Further discussions on the work completed in this thesis and the conclusions drawn are presented in Chapter 7. Potential improvements and suggestions are made for possible future work.

1.5 References

[1]   BP Statistical Review (2011). BP Energy Outlook 2030. London, UK: World Energy.

[2]   Bloomberg, http://www.bloomberg.com/news/articles/2016-03-03/brazil-s-clean-energy-boom-running-out-of-steam. Last accessed [Online] 19/08/2016.

[3]   O. Edenhofer *et al.*, "IPCC, 2011: Summary for policymakers. In: IPCC special report on renewable energy sources and climate change mitigation", Cambridge University Press, Cambridge, United Kingdom and New York, NY, USA, 2011.

[4]   M. G. Salameh, "Can renewable and unconventional energy sources bridge the global energy gap in the 21st century?", Applied Energy Journal, No. 75, pp. 33–42, 2003.

[5]   J. Hansen *et al.*, "A closer look at United States and global surface temperature change", Geophysical Research Journal, Volume 106, No. 20, pp. 23,947-64, 2001.

[6]   The guardian, https://www.theguardian.com/environment/2016/aug/16/hornsea-project-two-windfarm-second-phase-grimsby. Last accessed [Online] 16/11/2016.

[7]   A. S. McDonald, "Structural analysis of low speed, high torque electrical generators for direct drive renewable energy converters", Ph.D. dissertation, University of Edinburgh, Edinburgh, 2008.

[8]   E. de Vries, 'Trouble spots – Gearbox failures and design solutions', Renewable Energy World, Mar. 2006, 9, (2), pp.37-47.

[9]   J. Wallace, M. Jackson, S. Rogers, "The problem with O&M", Renewable Energy Focus Journal, Volume 9, No. 7, pp. 22-7, January-February 2009.

[10]   T. Hartkopf, M. Hofmann, S. Jöckel, 'Direct-drive generators for megawatt wind turbines'. European Wind Energy Conf., Dublin, Ireland, 1997, pp. 668-671.

Chapter 2

Literature Review

Climate change and global warming are issues that need to be addressed if we want to leave a sustainable planet to future generations. The energy sector is one of the key subjects that must be dramatically redirected. Fossil fuels are rapidly increasing the CO_2 emissions level. According to [1], the World CO_2 emissions released have doubled between the years 1973 and 2010 with 30,000 Mtonnes per year. With an increasing energy demand, caused by the world population growth, a decrease in the use of fossil fuels and a rise in the renewable sources availability have become vital.

In this context, wind energy has an important role to play. Harvesting wind power has been a significant energy source for many years, especially during the 9th

Century when wind mills were utilised to mill grain [2]. At present, modern wind turbines are used to generate electrical power and are usually seen as complete wind farms. Current wind turbines are complex large rotating devices that challenge engineers of all disciplines.

2.1 Wind energy

Wind is produced by the differences in atmospheric pressure, as air moves from high pressure to low pressure regions. Since the Sun's rays reach the Earth's surface with distinct angles, different temperatures between the equator and the poles are set up. Warmer air rises (leading to high pressure), whereas colder air sinks (leading to low pressure). Wind is the flow of air between areas of high and low pressure.

Wind energy is a natural resource present all over the planet that concentrates in certain regions. A steady technological progress in the area, alongside investments and economic support have lead the wind industry to be the quickest growing renewable energy source with a total installed capacity of 432.9 GW at the end of 2015 [3].

Wind turbines can be located both onshore and offshore, although it is true that more than 97 % of the worldwide installed wind capacity is placed on land [3]. This is because the cost of energy is lower onshore due to lower capital costs.

Wind speeds are slower onshore than at the sea surface due to the terrain's roughness that generates friction and creates turbulence. Offshore, the sea roughness can be considered almost zero with good weather conditions (waves influence must be estimated) so that wind speeds are generally higher. In addition, onshore wind farms face certain drawbacks that offshore devices do not. For example, no size and noise restrictions exist for turbines installed offshore making them a suitable alternative for developers globally.

Nevertheless, some significant challenges have to be considered when planning and installing offshore wind parks. The sea is a harsh environment that does not always allow an easy access to the turbines for installation or maintenance. In the installation

case, both the wind speed and wave height must be below certain levels so that cranes and vessels can work safely. It is worth pointing out that if a scheduled maintenance cannot be carried out because of extreme conditions a very high cost produced by the downturn in the turbine availability will be paid by the owner. This is why manufacturing reliable elements at a minimum cost is so important. Lightweight and easy to install structures are of interest although not always possible since generators and other components such as gearboxes can be very complicated and heavy.

2.2 Modern wind turbines

Modern turbines take out the power of the wind by transforming kinetic energy into pressure energy at the rotor plane. Then, by making use of an electrical generator the rotational energy and rotating power of the turbine's main shaft can be converted into electrical energy to be sent to the end consumer through the transmission and distribution systems. As depicted in Figure 2.1, an offshore arrangement comprises an offshore wind turbine (formed by a turbine rotor, a transmission gearbox, an electrical generator and a power converter), a wind farm collector where the power delivered from other wind turbines is gathered and a transmission to shore system that consists of an offshore substation, the HVAC or HVDC cable transmission layout and an onshore substation from where the power is introduced into the national grid.
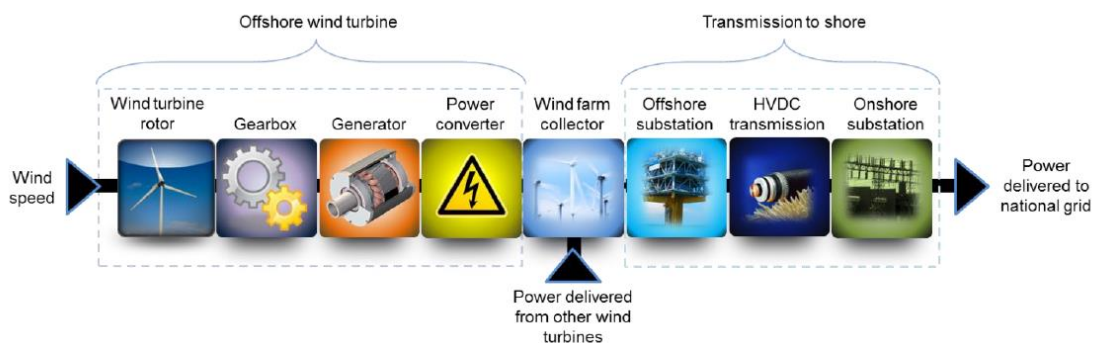
Figure 2.1 Offshore wind turbine arrangement and transmission to shore

Although the final wind turbine layout depends on the manufacturer, four different standard types exist. They can operate at either fixed or variable speed and they can be controlled by either stall or pitch mechanisms:

a) Stall regulated fixed speed wind turbines

The constant speed at which they operate is established by the frequency of the grid. They have induction generators which are directly connected to the grid. The aerodynamic design of the blades makes the turbine stall in high winds reducing the power and the thrust. The only control options to manage the power output are to use a shaft brake and to connect or disconnect the machine from the power system [4]. Some of the most representative models of this type of wind turbines are:

- Nordex N62 1300 kW [5]
- Ecotecnia 62 1300 kW [6]
- REPower 48 600 kW [7]

b) Pitch regulated fixed speed wind turbines

These machines control their torque by pitching the blades. They usually employ pitching mechanisms to start up and above rated wind speed power control to maintain a constant rotor speed. The blades pitch to increase rotor velocity up to operating speed. At this moment, the electrical machine is connected and kept a constant speed. The Nordex N60 (1.3 MW nominal power) is a typical example of a pitch regulated fixed speed wind turbine [5].

c) Pitch regulated variable speed wind turbines

Pitch regulated variable speed turbines use pitch control above rated to regulate the rotor speed and utilises torque control for the generator over the operating range of the wind turbine to permit variable speed operation of the machine. The V90 3 MW Vestas model and N80 2.5

MW Nordex model are examples of pitch regulated variable speed wind turbines [8][5].

2.3 Wind turbine drivetrains

Drivetrains are the area of biggest variation in wind turbine design. Conventional wind turbines are usually formed by a gearbox, a medium or high speed generator and a power converter. A gearbox is a mechanical system which transmits the rotational power of the wind turbine rotor to the electrical machine and increases the rotational speed to match the one of the electrical generator. A generator is a device which converts the mechanical power into electrical power. Generally speaking, two distinct types of electrical generators exist: induction/asynchronous generators and synchronous generators. Induction machines are alternating current (AC) electrical generators that operate by mechanically turning their rotors quicker than the synchronous speed, whereas synchronous machines operate turning their rotors at the synchronous speed. The synchronous speed corresponds to the frequency of the supply current. During operation, the rotor magnetic flux cuts the stator coils producing an active current in the stator coils. Finally, a power converter is an electro-mechanical device that converts electric energy by adjusting its voltage and frequency.

Gearboxes have a limited lifetime that in most cases does not reach the expected wind turbine lifetime. It is normal to replace them at least once in the course of the wind turbine lifetime [9]. It is considered that the higher the number of gearbox stages, the higher the gearbox failure rate [10]. Consequently, manufacturers are studying new methods to replace or just to eliminate the gearbox by introducing the direct drive concept.

A common layout of a fixed speed wind turbine with a squirrel cage induction electrical machine is shown in Figure 2.2. Squirrel cage generators are induction machines that have a rotor made of a ring of conducting bars, short-circuited at both ends by rings forming a squirrel cage. One of the main components within the wind turbine configuration is the soft-starter unit, which is composed by 6 thyristors, and

which function is to control how the magnetic flux is created to decrease current ripple during the generator energising stage. Once the electrical machine has been energised, the soft-starter takes the drivetrain to its operational speed by slowly ramping up the voltage at the generator terminals until it is at the network voltage [11]. This reduces the mechanical stress on the shaft and on the generator, as well as the electrodynamic stresses on the attached power cables and electrical network, extending the lifespan of the system.
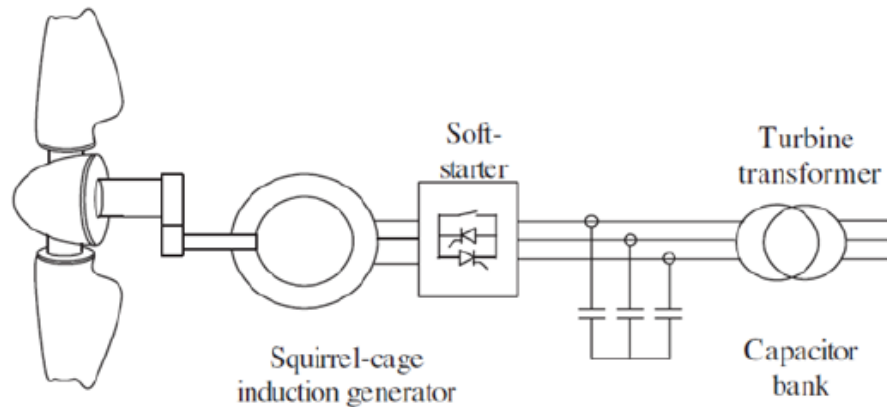
Figure 2.2 Layout of a conventional fixed speed wind turbine [11]

If variable speed turbines are compared with fixed speed ones a considerable reduction in loads is achieved. DFIG (doubly fed induction generator) wind turbines use wound-rotor generators with slip rings. Wound-rotor machines are induction generators where the rotor windings are connected through slip rings to external resistances. By adjusting the resistance, the speed/torque characteristic of the generator can be controlled. A variable frequency converter feeds the rotor winding. It commonly consists of 2 AC/DC + DC/AC IGBT based back-to-back voltage source converters linked by a DC bus [11]. Since with the power electronics converter, the network electrical frequency is decoupled from the rotor mechanical frequency variable speed operation becomes possible.

If the rotational velocity of the wind turbine is low, the rotor of a DFIG turbine can absorb power from the grid through the power converter. On the contrary, if the electrical machine works above synchronous speed, power can be sent to the power

network in the opposite direction through the power converter. Figure 2.3 displays the typical configuration of a DFIG wind turbine.
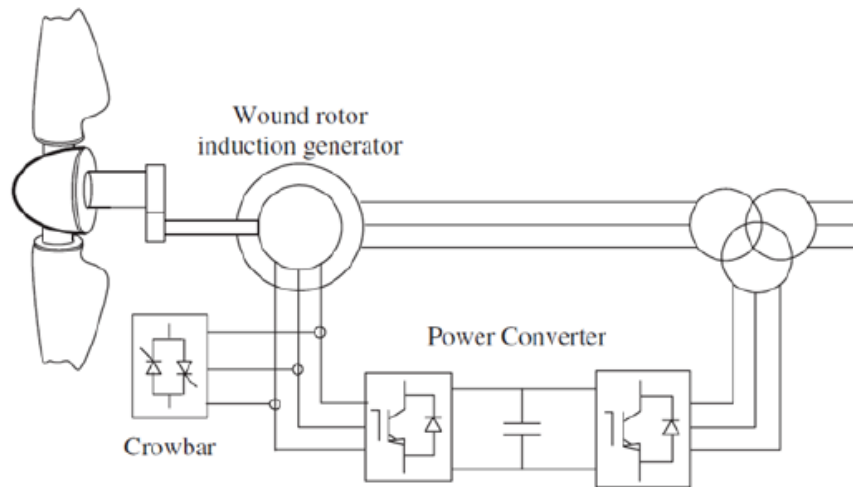
Figure 2.3 Layout of a conventional DFIG wind turbine [11]

As it can be seen, another element used for protection, named crowbar, is present. It is employed to protect the power converter. Over-currents and sudden increases in voltage are typical faults that the crowbar system can cope with.
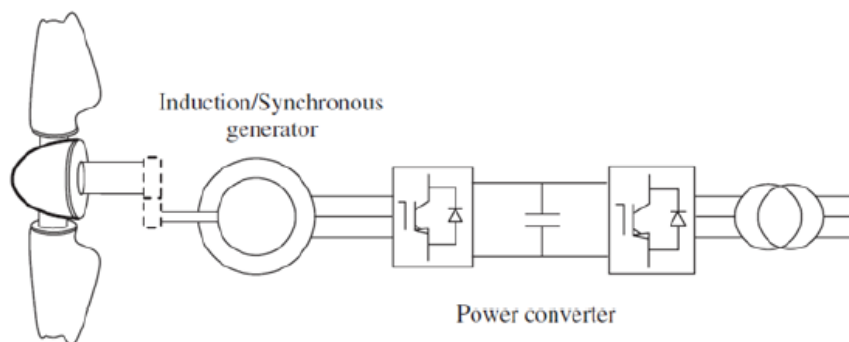
Figure 2.4 Layout of fully rated converter wind turbine [11]

On the other side, there are fully rated converter wind turbines. These can deliver a higher level of control by making use of power converters. The fully rated converter wind turbine can have various different layouts. A broad spectrum of electrical machines can be used and might or might not have gearbox.

Advantages and disadvantages of a brushless synchronous generator with a gearbox and a full converter are detailed in Table 2.1.

Table 2.1 Permanent magnet synchronous generator system advantages and disadvantages

Advantages	Disadvantages
Less complicated grid fault ride-through competences	A larger and more expensive converter is needed
More simple control techniques used	Higher losses in the power converter (fully rated)
Used in both 50 & 60 Hz grids	
Minimized maintenance. Eye-catching for offshore purposes	

With the drop in the power electronics cost a decade ago, this design became eye-catching to manufacturers since they improve grid fault ride-through effectiveness. This type of generators can be used in both 50 and 60 Hz grids meaning that they are also suitable for the North American market, where the frequency of the grid is 60 Hz. The lack of brushes and slip rings minimises its maintenance and as the cost of transporting and lifting equipment in deep waters is very high, this system has become very attractive for offshore purposes.

As the power converter works as the interface between the grid and the generator, the electrical machine is decoupled from the network. As a result, the generator's electrical frequency varies with wind speed variations, whereas the frequency of the grid remains stable, allowing the machine to work at a variable speed [11].

The generator control scheme and power flow is picked in accordance to the sort of power converter layout utilised. The side of the power electronics converter facing the network (inverter) can be configured to keep a constant voltage in the DC bus by applying torque to the generator that is regulated by the side of the converter facing the generator (rectifier). This torque is also controllable by the network side of the converter. Any of the banks can independently absorb or produce reactive power [11].

2.4 Electrical machines

Motors are electrical machines which convert electrical power into mechanical power, whereas generators are electrical machines which convert mechanical power into electrical power. Figure 2.5 illustrates a simple electrical machine with a pole pair (north and south) which creates an electromagnetic field. The wire loop is a rotating armature. When current flows a force acts in an upwards direction on the right hand side of the wire and a downwards direction on the left hand side of the wire. Therefore, a torque is induced and the electrical machine works as a motor. If no current is flowing in the wire but the armature rotates relative to the field, then an induced voltage (EMF) would be induced according to Faraday's Law. At this point, there is no torque resisting the rotation. If some resistive electrical load is connected to the terminals of the wire loop, current will start to flow. A torque will also be developed meaning that work is used to rotate the wire loop. In this case the electrical machine would work as a generator.
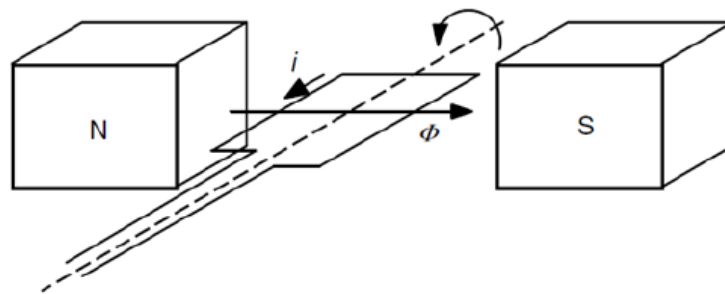
Figure 2.5 Illustration of a simple electrical machine [4]

Electrical generators can be synchronous or asynchronous machines. Synchronous generators are alternating current, 'AC', machines where rotational speed is dependent on the current frequency in the stator and the number of pole pairs. The magnetic fields created by the current on the stator and on the rotor both rotate at the same speed (called synchronous speed). Asynchronous generators are machines in which the magnetic fields of the stator and the rotor do not rotate at the same speed.

16

By changing the magnitude of the rotor field current, the induced EMF can be altered which means that the reactive power produced by a synchronous machine can be controlled. This is an important ability that makes this type of electrical machines suitable to maintain power system stability.
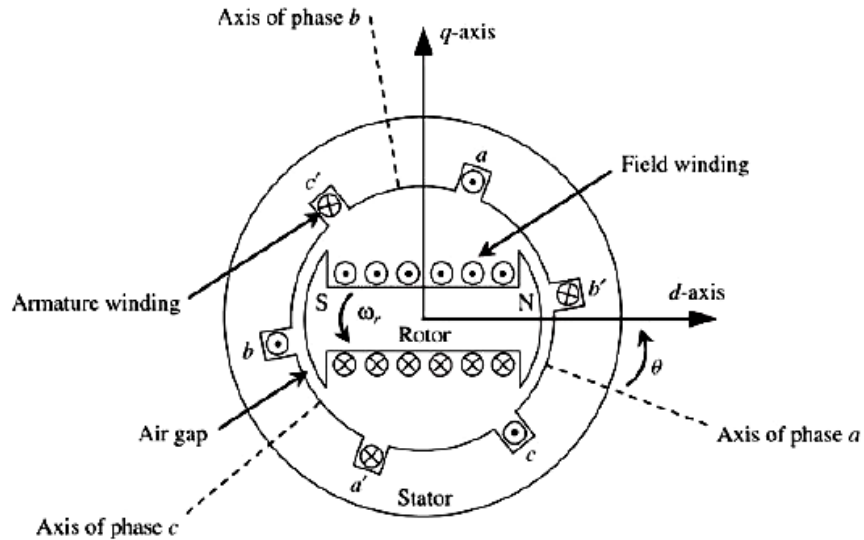
Figure 2.6 Illustration of an AC synchronous generator [11]

Figure 2.6 shows the rotor and the stator of a synchronous machine. The latter is made up of a laminated steel core and a 3 phase winding that at the same time is composed by coils.

2.6 Wind turbine generators

Until 1998, the vast majority of the manufacturers constructed constant speed wind turbines with a 3 stage gearbox, a standard squirrel cage induction generator directly coupled to the grid and a power output below 1.5 MW. Since then, manufacturers started to look at more complex variable speed wind turbines in an attempt to optimise the design of the turbine and its efficiency. Around 2005, wind turbine generators began to be improved by manufacturers so as to meet the grid fault ride-through requirements [12].

In [12], Polinder presents an overview of the available generators for wind turbines and their trends. A good insight of the types of wind turbine generators used in the present day as well as their advantages and disadvantages is given in this comprehensive study. Till recent times, it was thought that constant speed wind turbines were lighter, cheaper and have a more compact design than direct drive turbines that were seen as heavy, large and expensive systems. Nevertheless, companies, for instance Siemens, have found that enhanced direct drive designs have a similar weight to conventional geared converters.

2.6.1 Electrical machines for direct drive wind turbines

As explained, direct drive wind turbines present a number of advantages that make them suitable for offshore purposes. Among them, the removal of the gearbox stands out. With it expensive gearbox matters can be avoided. Moreover, the decrease in the number of moving parts, such as bearings, represents a significant reduction in downtime periods, for example for oil replacement. These features have drawn the attention of some manufacturers and nowadays 20 % of the wind turbines sold worldwide are directly driven.

2.6.2 Excitation techniques

In order to excite an AC synchronous generator different ways exist: Electrical excitation and permanent magnet excitation. Switch reluctance generators are machines in which only the stator is electrically excited.

2.6.2.1 Electrically excited direct drive generators

In electrically excited generators, a DC source magnetizes the rotor poles. This DC source is commonly given through brushes and slip rings. There are two types of rotor poles: salient or cylindrical. Cylindrical poles are the most employed in the wind industry although rotors with salient poles are more common when speaking about direct drive machines. In this type of generators, the rotor poles must be large

enough to generate appropriate room for the excitation windings. The stator of an EEDD is very similar to that of a 3 phase distributed winding introduced into a slotted laminated iron core induction generator. The generator is connected to the grid through a power electronics converter that permits full control of active and reactive power as well as voltage in case of grid fault. In addition, the electrical machine speed can be completely regulated over a broad range of wind speeds.

These machines are relatively easy to manufacture and for large power outputs they provide better power factor and efficiency compared to induction machines. Nevertheless, the constant injection of DC current leads to I_f^2R losses on the field decreasing the overall efficiency. However, since the external electrical excitation can be tuned in accordance to the wind conditions, the voltage can be varied to reduce I_f at lower outputs to minimise losses.

EEDD is currently considered a mature low speed direct drive technology widely used in the wind energy market. The main supplier of EEDD is Enercon, serving 15 % of the whole market and 75 % of direct drive systems installed. As for instance, the prototype E-126, shown in Figure 2.7, that has a 127 m rotor diameter and a 12 m diameter generator. The turbine can generate up to 7.5 MW. The company MTorres also manufactures EEDD turbines with outputs of 2.5 MW [13].

Figure 2.7 7 MW Enercon E-126 [14]

2.6.2.2 Permanent magnet excited direct drive generators

Among the drawbacks of electrically excited systems, efficiency reduction due to I_f^2R losses and maintenance issues because of the use of brushes stand up. Permanent magnet generators can be considered superior to electrically excited machines because of their lower weight, improved efficiency and compactness. These generators do not need external electric excitation since their rotor poles are made of permanent magnet material. The overall efficiency of the machine and the energy capture rate then increases as there are no I_f^2R losses. Besides, the lack of slip rings improves the machine's reliability.

On the side, permanent magnets are costly and difficult to handle during the manufacturing stage. The stationary structure of a PMDD is similar to that of an EEDD although different designs have been proposed [15][16]. For the stator's connection to the grid a fully rated converter is required to convert from variable voltage and frequency to fixed voltage and frequency.

Permanent magnets are made of rare earth materials, e.g. samarium cobalt (SmCo) or neodymium iron boron (NdFeB) which gives high magnetic densities in small geometries and volume. SmCo permanent magnets are typically utilised in high-temperature approaches. In [17], Vilsboll *et al.* states that NdFeB magnets are the most suitable as they generate a larger remnant flux density (1.2 T) and can decrease mass and price of the generator.

At the beginning, the high prices of PM materials discouraged manufacturers from using them for this type of generator. However, the cost of rare earth materials dropped between 1995 and 2005 by a factor of 10. In 2011, the prices went up again due to a number of factors including a rise in demand and the sensitivity to speculation and politics of the supply (95 % of the rare earth material is located in China). Nowadays, prices have stabilized and although the mentioned issues generated a great uncertainty regarding PM use, the future of PMDD generators is promising since rare earths are being found in many other places.

With permanent magnet excitation a simpler and robust electrical machine can be produced. Higher efficiencies and torque densities as well as limited life cost are

some of the advantages that have drawn the attention of big developers such as GE that acquired Scanwind in an attempt to expand into this market [18]. For offshore applications GE has offered a 4 MW design as seen in Figure 2.8.

If a comparison between a PMDD radial flux machines and a conventional generator, (such as a constant speed geared induction machine) is made it can be seen that the PM machine is less efficient at rated power but has greater average efficiency, e.g. 2.3 % higher for a 500 kW machine and 1.6 % higher for a 3 MW machine [19]. Grauers found a PM equivalent to the electrically excited synchronous machine of Enercon with a 94 % smaller diameter and 50 % lower rotor volume. In [20], Bianchi and Lorenzi showed that wound rotor designs are less efficient than permanent magnet designs. On the other side, in [21], the authors found that electrically excited machines have greater mass than PM excited machines whereas in [22], Dubois noted that permanent magnet excitation is more profitable for pole pitches shorter than 100 mm. In [17], Vilsboll *et al.* found that the efficiency of their permanent magnet machines goes up with reducing load as far down as quarter load.

Figure 2.8 4 MW GE (former Scanwind) wind turbine [23]

Other companies entering into this MW scale market are: Siemens with its 3 and 7 MW design, Goldwind (1.5-2.5 MW), STX Windpower (1.5-2.0 MW), Emergya

Wind Technologies 'EWT' (0.5-2.0 MW), Vensys (1.5-2.5 MW), Leitwind (1.5-3.0 MW) and XEMC Darwind (5.0 MW) [24][25][26][27][28][29][30].

With the quick increase of commercial and military applications using PM over the last decade, the industrial capacity for PM machines has grown and this is even highlighted with the rise in the number of manufacturers establishing PM synchronous generators as their first choice for their direct drive wind turbines [31].

2.6 Permanent magnet topologies

Permanent magnet generators are often characterized by the orientation of the magnetic flux as it goes across the air gap, as follows (See Figure 2.9):

- Radial flux
- Axial flux
- Transverse flux

| (a) | (b) | (c) |
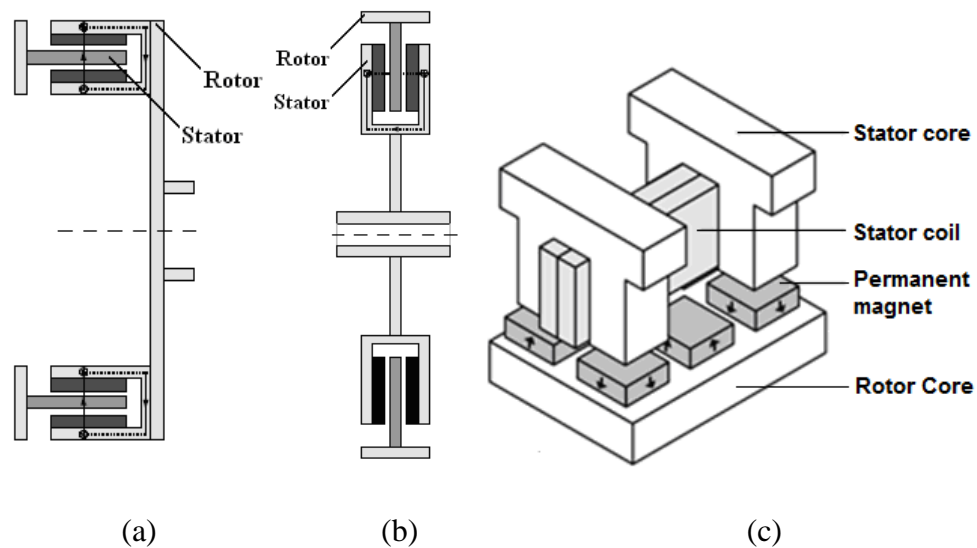
Figure 2.9 PMDD generator topologies; (a) Radial flux; (b) Axial flux; (c) Transverse flux [32][33]

The electrical machine can be slotted or slotless according to the design of the stator. Permanent magnet direct drive generators can also be characterized depending on the

absence or the presence of iron in the core of the stator. As result, they can be either iron cored or air cored machines.

2.6.1 Radial flux PM generators

These machines are so called because of the orientation of flux as it goes across the airgap. They are very similar to wound rotor synchronous generators which are also constructed as radial flux machines. Figure 2.10 displays the configuration of radial flux PM machine.
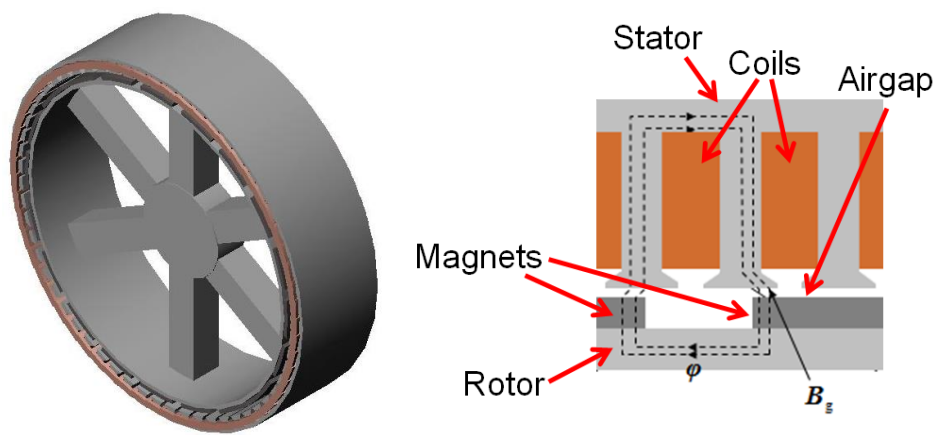
Figure 2.10 PMDD radial flux machine and its components [34]

Some commercial models are out there since the number of manufacturers getting interested in permanent magnet machines has been increasing over the last decade. Most of them have a radial flux configuration [18] [28]. Figure 2.11 shows the layout of the Zephyros/Harakosan Z72 wind turbine with accounts with 1.5 MW power output. The electrical machine is rated at 18.5 rpm and owns a 4 m diameter structure which weighs 47.2 tonnes [35].
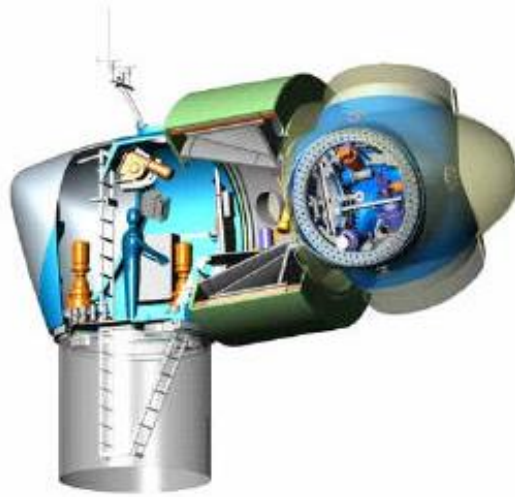
Figure 2.11 Cutaway of the Zephyros/Harakosan Europe Z72 wind turbine [35]

2.6.2 Uncommon radial flux configurations

Aiming for a more compact lightweight design, Sway has developed a model as it is shown in Figure 2.12. With a significant decrease in weight achieved by its novel structural design, considerable tower and foundations optimisations can be made. By having a large diameter ironless stator winding machine with a spoked rotor, the system is 25 to 50 % lighter than conventional designs [36]. Low airgap flux densities and shear stress are likely to be obtained with ironless stators and in spite of higher eddy current and aerodynamic losses are higher than for conventional turbines, developers say that the design's efficiency is about 94 %. Therefore, an overall decrease in cost of electricity per kWh is forecasted over existing machines.

Figure 2.12 ST10 10 MW offshore wind turbine developed by Sway [36]

The C-GEN concept developed by researchers at the University of Edinburgh is also an air cored generator with a modular rotor consisting of C-core modules 50 % lighter than a conventional iron cored PM direct drive generator. Its ease of manufacturing and lightweight design makes it attractive not only for wind energy converters but also for any type of marine power take off [37].

2.6.3 Further variations

An extra variation in permanent magnet direct drive generators is the option of having an inner or an outer rotor. While the outer rotor may lead to a more compact design and the centrifugal forces help magnets seat onto the rotor, the inner rotor facilitates the stator cooling (naturally cooled by external air flow). A reduction in the outer diameter can be achieved by using an outer rotor according to Vensys [28].
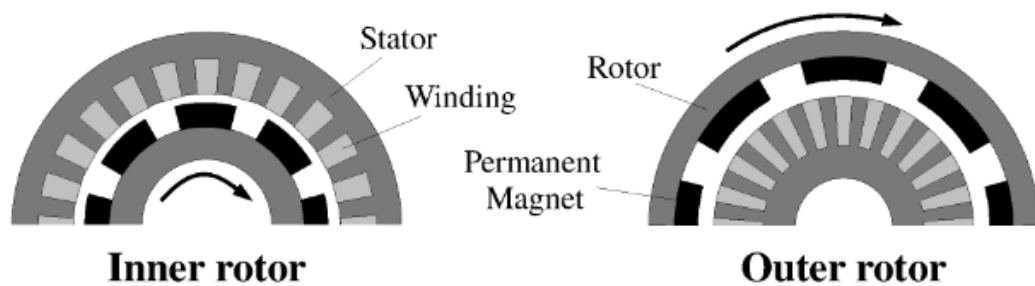
Figure 2.13 Inner and outer rotor generator variants [13]

2.6.4 Surface mounted or buried

In terms of rotor design, a further variation can be introduced. The permanent magnets can be either surface mounted onto or buried into the rotor structure. High energy magnets such as NdFeB are commonly used in surface mounted layouts. They have a remnant flux density that goes above the wanted airgap flux density. Although they are expensive a lightweight design can be produced. When these are mounted on the rotor, they must be mechanically protected and coated since they are prone to corrosion [38].

Buried ferrite magnets can be employed with flux concentration. They are lower energy magnets and are much cheaper (a tenth of the cost per unit mass [39]). Nevertheless, more magnets need to be used (5 times as much magnetic material compared to an equivalent surface mounted machine [38]) and their assembly is more complex and expensive.

According to Vilsboll *et al.* NdFeB magnets are more suitable than ferrite magnets due to a reduction in overall mass, dimensions and price of a 20 kW generator for a wind turbine can be obtained [17].

Several rotor designs for radial flux permanent magnet machines were studied by Lampola such as curved, rectangular and rectangular equipped with shoes PM's surface mounted. The analysis demonstrated that the highest torque to cost of active materials ratio was acquired with curved surface mounted permanent magnets [40].

2.6.3 Axial flux generators

An overview of axial flux machines, focused on axial flux permanent magnet machines is given in [41]. The following features make this type of machines different from conventional ones:

- Airgap is in the axial direction and conductors are radially lined up
- Rotor and stator are discs
- Discs under rotation work as fans

These electrical machines have been suggested for a diverse range of purposes, at different speeds. Some examples include portable generator systems [42], direct drive in-wheel motors [43], generator units in vehicles [44], for propulsion and ship's generators [45] and for aircraft drives [46].

2.6.4 Transverse flux generators

Transverse flux machines are similar to axial ones in that the flux track goes perpendicular to the plane of rotor's rotation. See Figure 2.14. Nevertheless, this type of machines is very different to axial generators. The major difference between

transverse flux permanent magnet generators and RFPM and AFPM is that the TFPM machine permits an increase of the space for the windings without reducing the available space for the main flux. They can also be made with a very small pole pitch compared to other machines. This results in higher force densities that make this type of topology attractive for direct drive purposes.
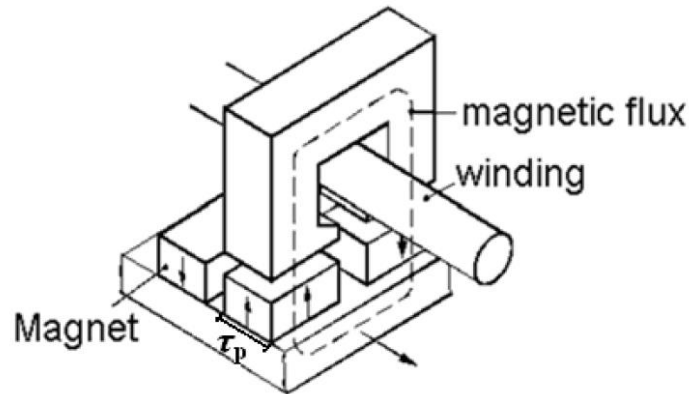
Figure 2.14 A single-sided surface-mounted TFPM machine [47]

2.6.5 PM configurations comparison

An overview of the PM configurations available for wind turbine generators is provided by Dubois in [48]. By making use of documentation about samples, Dubois compares these technologies in accordance to torque density and cost per unit [49]. A comparison of PM layouts for a wide range of turbines with power outputs no larger than 200 kW was carried out by Chen *et al.* [50]. The parameters to make comparison were torque density, mass of the active material, outer radius, total length, overall volume and efficiency. The main conclusions were that axial flux permanent magnet machines have simple winding, low cogging torque and noise, short axial length and higher torque/volume ratio than radial flux machines permanent machines. However, they also have lower torque/mass ratio, larger outer diameter, large amount of permanent magnets and structural instability and difficulties keeping airgap integrity and producing stator cores if compared with the radial machines. Transverse flux machines present higher force densities than the

other 2 configurations, considerably low copper losses and simple winding but it is rather complex to construct which makes it less attractive.

These comparison brings a problem with itself due to it is done by taken into consideration only the active mass (magnets, iron in rotor and stator and copper in windings). Nevertheless, the mass of the inactive material in direct drive machines supposes the majority of the machine's mass. In [21], Hartkopf *et al.* noted that about 2/3 of the total mass corresponds to the supporting structure. If the most suitable permanent magnet topology is to be found then the mass of the inactive material also needs to be considered.

In this thesis, a radial flux surface mounted permanent magnet machine has been assumed. The methodology followed for its analysis can be applied to other types of machines.

2.7 Structural Analysis, Modelling and Design of Direct Drive Generators

Direct drive permanent magnet machines are attractive, however, these electrical machines are currently very large and heavy and therefore expensive. Nevertheless, they are also part of the turbine's structure and withstand significant loads. This section looks in detail how this type of electrical machine have been analysed (considering the loads applied to its structure and the layout of the drivetrain), modelled (simplified models such as disc or armed structures can be used) and finally designed. It is thought that by employing an integrated approach which takes into account the interactions between electrical, thermal and mechanical design aspects of the machine, a reduction in weight could be achieved.

2.7.1 Dimensions of direct drive generators

So as to understand why these generators are large it is essential to consider the torque rating *T*. If the output power of a generator is calculated as follows,

$$P = T\omega \qquad (2.1)$$

where T is the torque produced by the electrical machine and ω is its angular velocity, a large torque must be generated so as to produce high power. The torque produced by a generator can be estimated by considering the generator as a cylinder with a surface shear stress. See Figure 2.15. This can represent the rotor or stator of the radial flux machine.
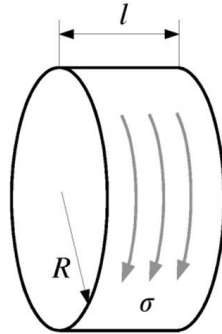
Figure 2.15 Cylinder model of torque produced by a generator [34]

Then, the equation to obtain the torque is,

$$T = 2\pi\sigma R^2 l \qquad (2.2)$$

where σ is the electromagnetic shear stress, R is the radius of the airgap and l is the length in the axial direction. Since there are practical limits to magnetic and electrical loading, a maximum shear stress exists. The typical shear stress for PM machines used by designers is within the range between 25 and 50 kN/m^2 [13].

2.7.2 Forces and moments acting on electrical machines

To keep the airgap clearance between the stator and rotor is vital from the design point of view. The integrity of the entire machine relies on the capacity of the supporting structure to maintain the airgap open and stable. Large direct drive electrical generators are more demanding structurally speaking than conventional generators due to their large surface areas. Larger moments are generated since

forces act at larger distances from the nacelle mounting location. The airgap clearance is about 0.1 % of the airgap diameter for typical designs and a typical maximum permitted deflection is about 10 to 20 % of that clearance. If this threshold is breached, the airgap flux density will vary significantly and hence the loads will also increase. The analysis stage is about recognising the forces acting on the structure and their magnitude. On a radial flux electrical generator different loads such shear, normal, gravitational and thermal, as well as centripetal forces and wind turbine loading, are present.

The shear stress/torque transmission is generated in the area near the airgap where mechanical energy is transformed into electrical energy. In the steady state, the shear force on the rotor is met by an equal but opposite shear force on the stator. That shear force on the stator comes about as current in the slots and the associated magnetic field interact with the rotor magnetic field. See Figure 2.16.
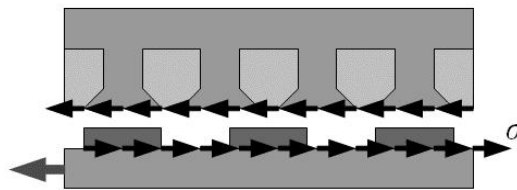
Figure 2.16 Shear loading [34]

The normal stress, also named Maxwell stress, is produced by the effect of attraction that the magnets mounted on the rotor generate between the moving and the stationary parts of the machine. It is the largest load (in order of 200-400 kPa in typical machines) and makes the reduction of machine's weight a difficult task for designers as a stiff and robust structure is needed to withstand it. See Figure 2.17.
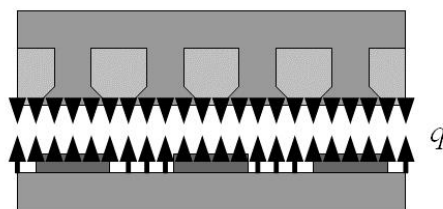
Figure 2.17 Magnetic attraction of the moving and the stationary components of the generator [34]

A key issue to be considered during assembly, transportation and installation is gravity. Generator's weight must be taken into account. In [51] , Stander *et al.* states that segmentation of substructures greater than 4 m (EU) and 5m (USA) can ease manufacturability and transportability. The structural stiffening required to resist gravitational loading can be acquired by arranging the structure geometry rather than utilising stiffer materials. Different examples of stator/rotor yoke structures support are provided: cantilever/Z-profile on one single side, E-profile in the middle or H-profile on both sides. See Figure 2.18.
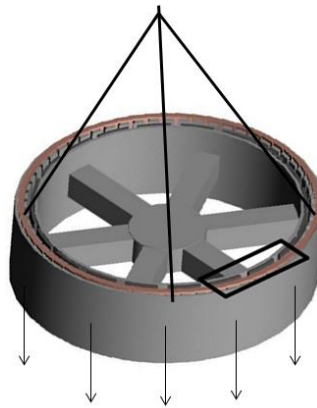
Figure 2.18 Gravitational loading [34]

Since large amounts of heat are generated during electrical machines operation, thermal expansion or contraction of generator's parts has to be taken into consideration. The stator is typically is hotter than the rotor $\Delta T_s > \Delta T_r$. Figure 2.19 illustrates how the deformation caused by thermal expansion or contraction of components can produce significant changes in flux density and therefore in the forces acting on the generator structure.
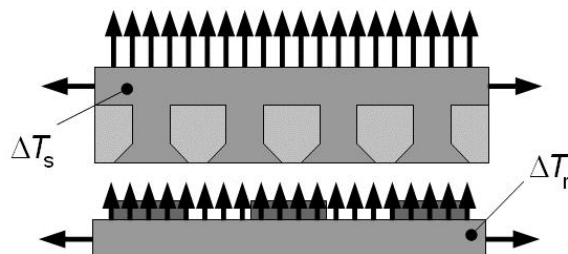
Figure 2.19 Thermal expansion of the generator structure [34]

On the other side, designers need to be aware of centrifugal forces (~3 kPa). These loads are fairly small at low speeds compared to the others.
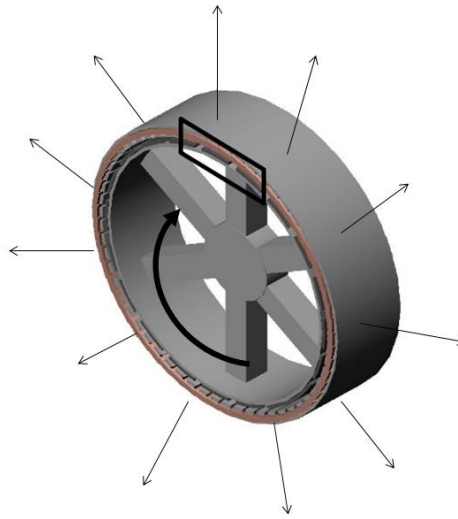
Figure 2.20 Generator's structure under centrifugal forces [34]

2.7.3 Integrating a direct drive generator within the wind turbine

The location and integration of the direct drive generator within the wind turbine and drivetrain are key factors when calculating the loads generated by the rotor blades, rotor blades weight, vertical and horizontal wind shear, yaw error and inertial effects. Next figures show the different existing types of PMDD drivetrain configurations. Figure 2.21 shows how the generator has been mounted upwind of the tower with a single bearing, for example, Zephyros/Harakosan Z72 wind turbine. This type of layout is popular within the market since a single bearing arrangement is allowed leading to a reduction in cost. The generator hangs clear of the turbine, whereas the bearings, which resist enormous loads, can rest on the nacelle's structure. However, it becomes an important structural load path of the wind turbine (its particular conical supporting structure is able to effectively deal with radial and axial loads) and when the electrical machine needs to be either repaired or replaced it is impossible to do it without also removing the rotor
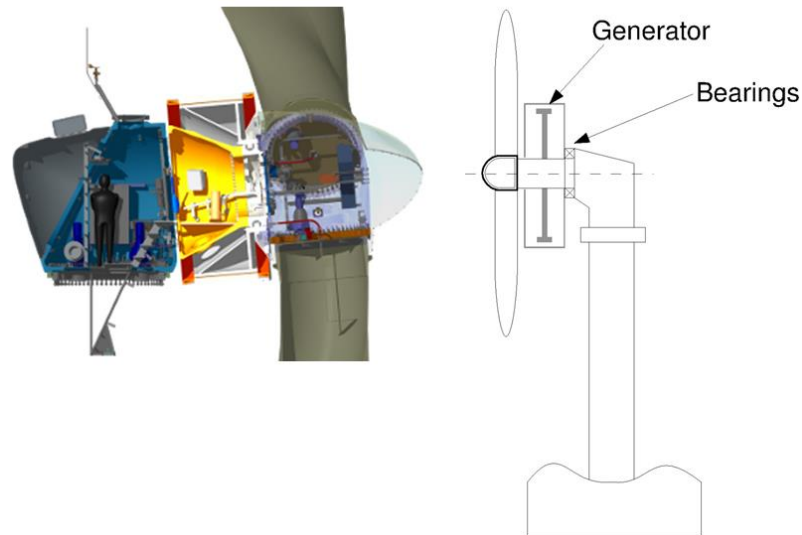
Figure 2.21 Zephyros/Harakosan Z72 wind turbine configuration [13]

An alternative design was proposed by Bywaters *et al.* [31] in the Northern Power Systems WindPACT Drive Train Alternative Design Study Report. The main bearing inner face is attached onto a spindle that carries the stator as well while the outer race is connected to the rotor hub and the rotor of the generator. The spindle is anchored to the turret providing the load path mentioned before. As seen in Figures 2.22 and 2.23, the generator is an integrated component which gives the possibility of shipping an entirely assembled and tested machine to the site where it can be installed onto the turret in one manoeuvre. With the capability of locking the generator rotor to the stator frame, the main bearing can be accessed for maintenance without taking out the generator. In addition, the seals of the bearing can also be repaired or simply replaced without extracting the bearing.
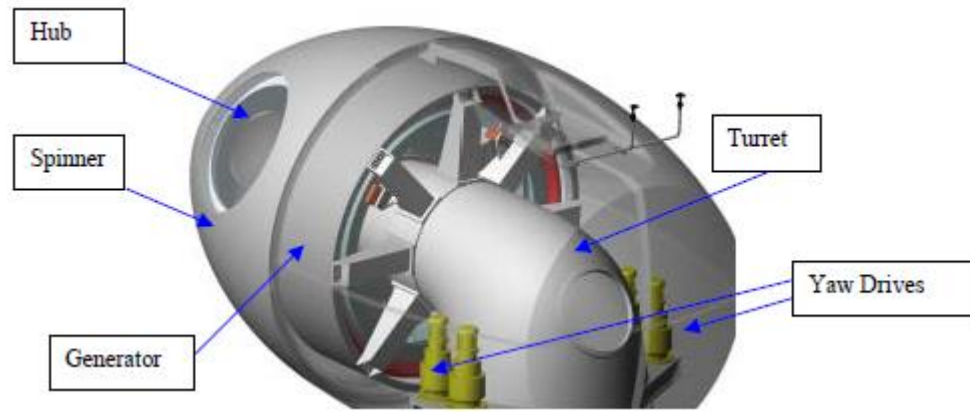
Figure 2.22 PMDD Drivetrain [31]
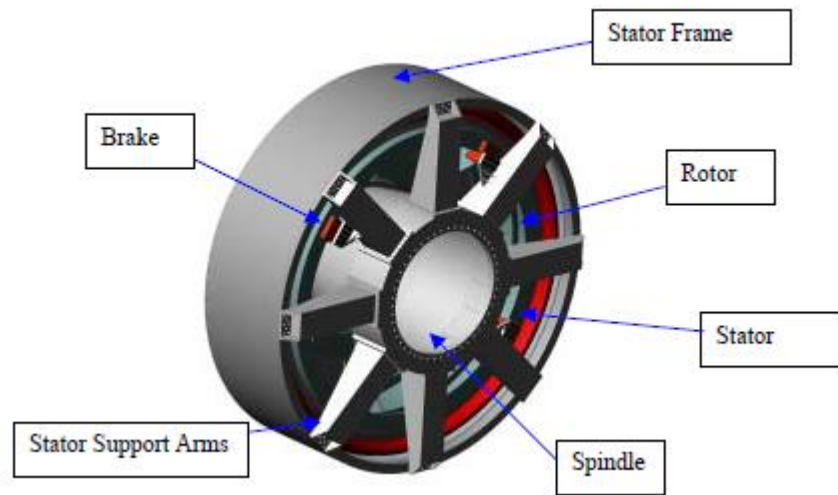
Figure 2.23 PMDD Generator [31]

Figure 2.24 shows the drivetrain configuration of an MTorres 1.5 MW PMDD wind turbine. The generator is located right onto the top of the tower and between bearings.
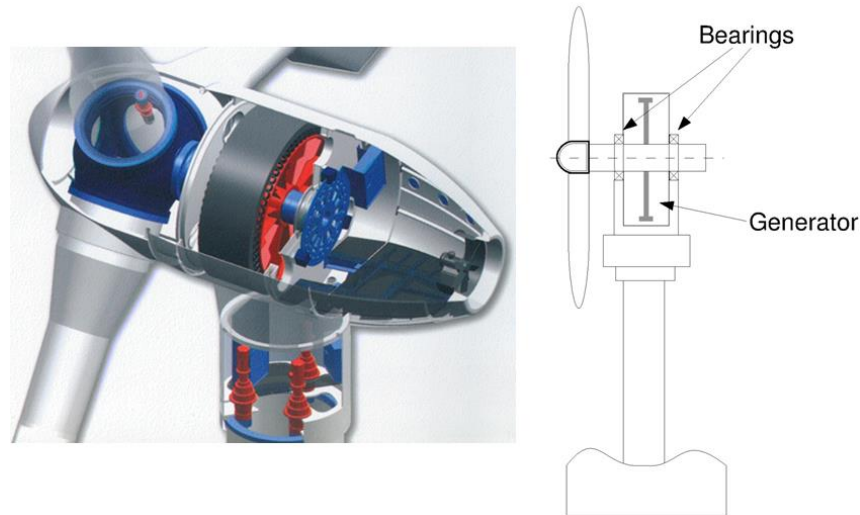
Figure 2.24 MTorres 1.5MW PMDD wind turbine [13]

In Figure 2.25 a GE ScanWind 4.1-113 wind turbine is shown in detail. The generator is located downwind of the tower and the two bearings sit down on nacelle's structure as in the case with the MTorres design. Again for this design, the electrical machine becomes an integral part of the turbine's structure acting as a load path, although major rotor loads have been dealt with by the bearing before reaching the generator. A more robust (in structural terms) and therefore heavier machine is necessary.
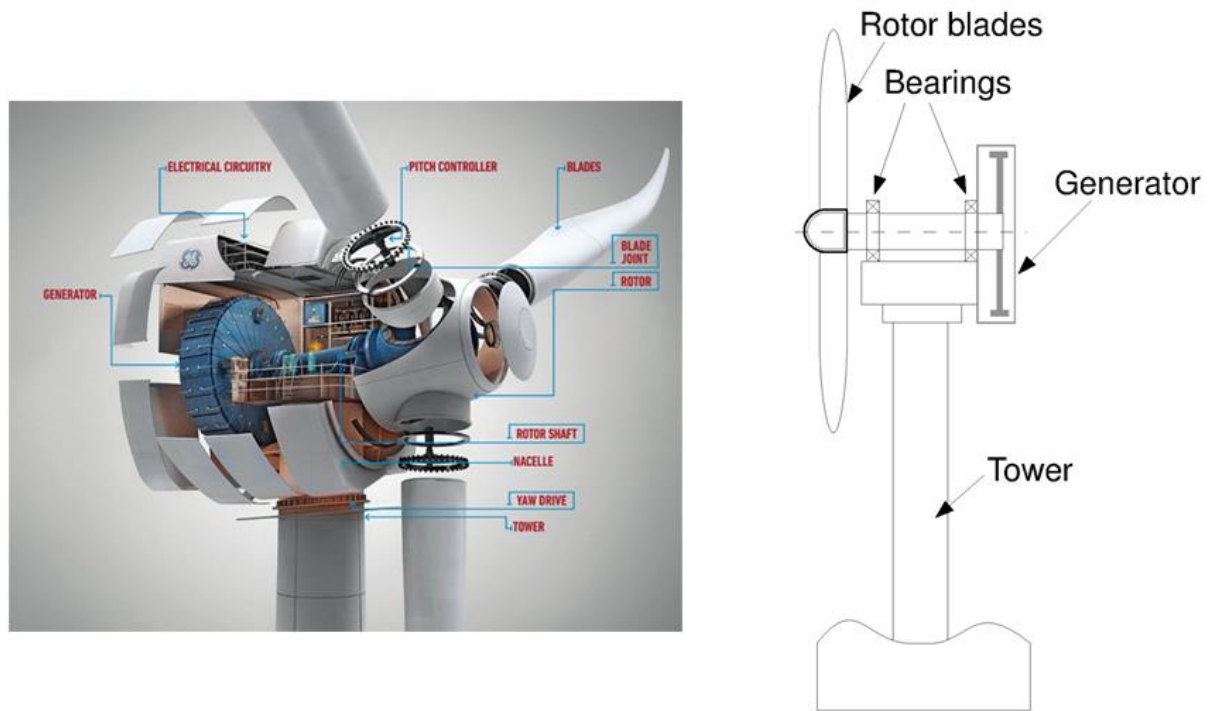
Figure 2.25 GE ScanWind 4.1-113 wind turbine [13]

2.7.4 Design external loads for HAWT: International standards

In [51], Stander *et al.* differentiate between external and internal loads. Hub (including thrust) and gravitational loads are considered external loads whereas internal loads are electromagnetically induced and thermal. External loads have a considerable influence on internal loads. For instance, in case of shaft misalignment due to forces acting on the wind turbine rotor, a substantial increase in the attraction forces within the airgap would be seen. The degree of influence of external loads on electromagnetically induced stresses depends on how well integrated the generator is in the wind turbine structure. In [52], the design loads for horizontal-axis wind turbines are defined according to two different coordinate systems, one respect to the blade and the other respect to the hub.

A more conscious differentiation of the types of stresses is given in the IEC 61400-1, the Germanischer Lloyd rules for certification and the Danish Standard DS 472[53][54][55]. All the loads to be considered when designing a wind turbine component, methods of analysis, material strengths, fatigue properties and the

corresponding safety limits are described in detail in the said international standards, which are used for certification.

2.7.5 Configurations

Different bearing configurations have been described in Section 2.7.3. Looking at the entire drivetrain, Alstom's Pure Torque® drive system corresponds to an innovative design, which separates torque transmission from load support and transfers all the bending and gravitational loads directly to the tower. Two bearings connect the hub to a cast iron structure, while the main shaft is attached to the electrical machine through an elastic coupler, which allows certain degree of misalignment [56].

This system can be also used for conventional geared wind turbines. By making use of this arrangement potential harmful loads for the gearbox or the generator are eliminated elevating so the reliability of the turbine.

Other bearing layouts have been proposed with the main aim of obtaining a more compact lightweight design. In [31], Bywaters *et al.* evaluated a number of bearing configurations on the base of weight, cost, risk, shipping, assembly and serviceability. An integrated configuration suitable for geared and direct drive machines that removes the main shaft has been developed in [57]. For this system, the gearbox or the generator are directly mounted on the outer side of the bearing rotating with the same speed as the hub.

For this investigation, it was assumed that a system such as Alstom's Pure Torque® was utilised as the design of the generator supporting structure was carried out considering only the major internal loads present during the machine operation, in other words, isolating the generator from the rest of the wind turbine.

2.7.6 Integrated design of direct drive machines

In order to design PMDD machines different approaches can be followed. In [13], McDonald proposed an integrated design that considers the interactions between electrical, thermal and mechanical aspects of the generator.
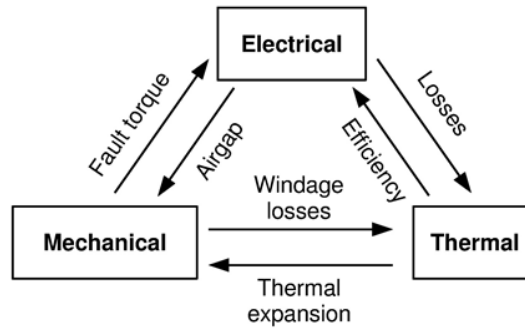
Figure 2.26 Interactions between electrical, thermal and mechanical design aspects of the generator [13]

A multidisciplinary approach is needed to design and manufacture this type of machines due to their size, complexity and cost. A suitable compromise between the priorities of each discipline is required for a proper design. Figure 2.27 shows the flowchart of a conventional process starting from the specifications and giving a privileged position to the aspects of the electrical design followed by mechanical and cooling design aspects to end with the outline.
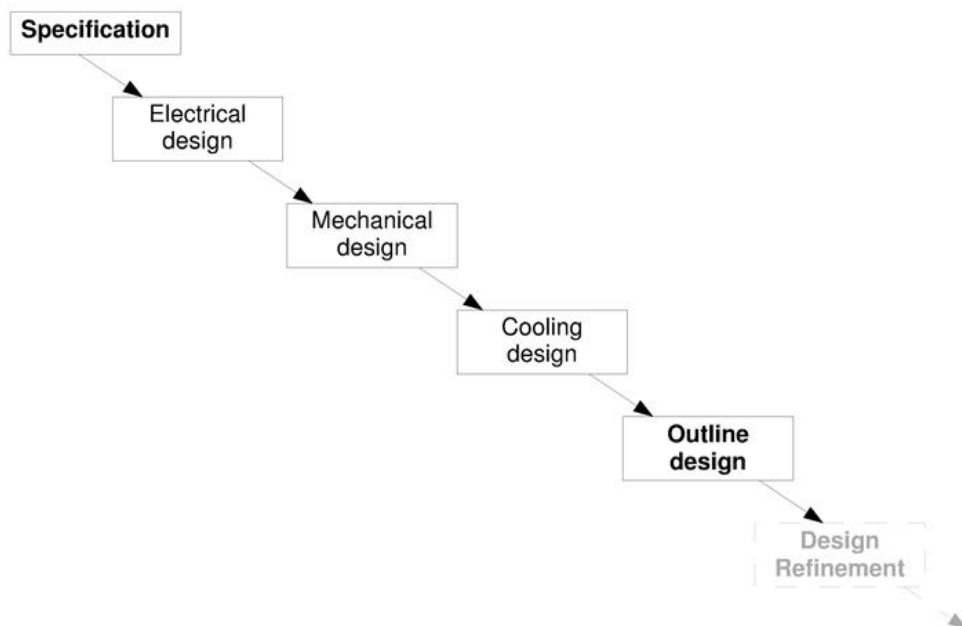
Figure 2.27 Early design stages – traditional approach [13]

However, as said, the idea behind the integrated design is to create a scheme that equally considers the priorities of all the disciplines. Figure 2.28 shows the flowchart of an integrated approach as proposed by McDonald [13].
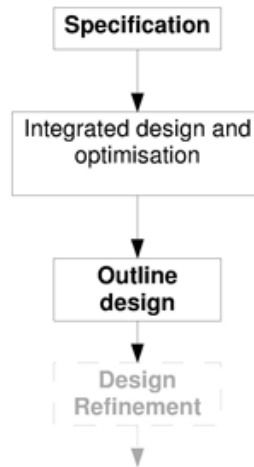
Figure 2.28 Early design stages – integrated approach [13]

Figure 2.29 shows what the priorities of an electrical engineer are so as to have an efficient and resilient generator. The electrical engineer would try to maximize machine's performance (efficiency and power output) employing as little amount of material such as copper and permanent magnet as possible. This characteristic may lead to a reduction in the physical clearance between rotor and stator and a large radius. The type of material and its form is vital (high fill factors of copper and correct design of steel laminations are desired). Electrical insulation is crucial for the electrical engineer too. It is worth pointing out that the electrical design of a 3 MW PMDD generator supposes 52 % of its total cost [13].

Electrical
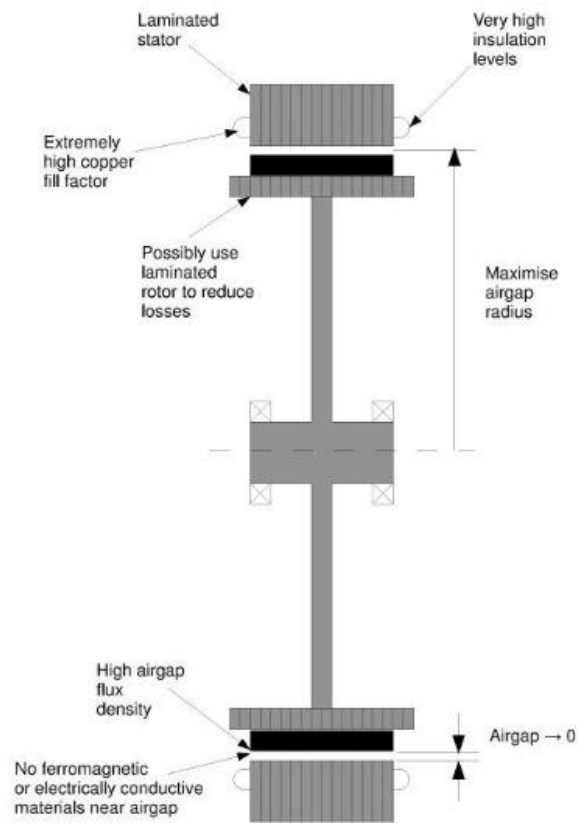
Figure 2.29 Electrical design perspective [13]

On the other side, the mechanical engineer would focus on the physical robustness of the electrical machine, in terms of strain, stress, strength and fatigue.

Suitable safety factors can be achieved utilising low-cost and lightweight assemblies if the mechanical scheme is good. However, the search of robustness might lead to the utilisation of non-optimal materials electromagnetically speaking. The mechanical design can be improved by optimising some electromagnetic parameters which reduce torque ripple and fault torques

Looking at current designs of 5 MW generators is easy to recognize that around 55 % of their total mass comes directly from the mechanical design.

Mechanical
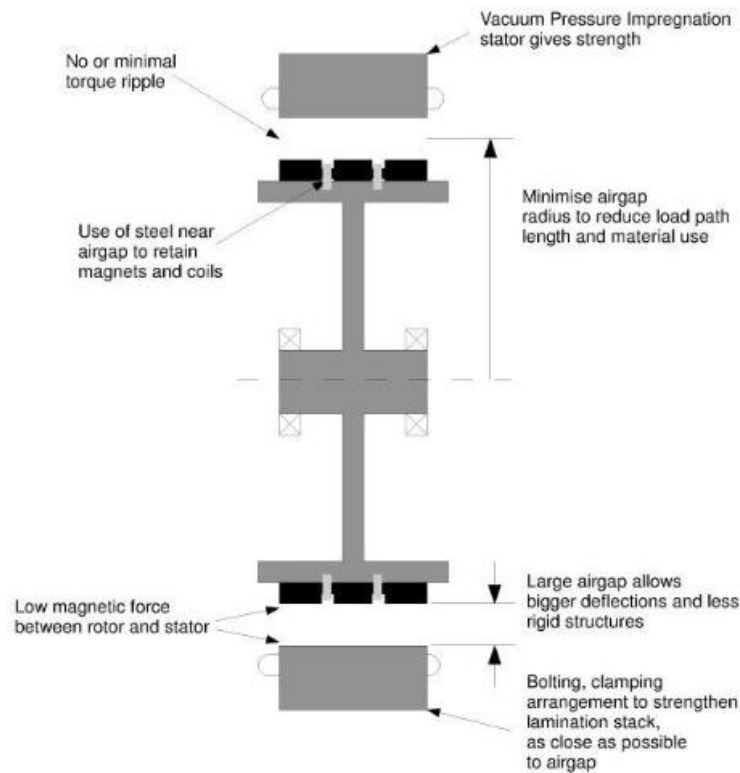
Figure 2.30 Mechanical design perspective [13]

A special set of necessities can be identified for cooling the generator. The specialist in heat transfer would add to and maximize thermal conduction and convection tracks in order to reduce winding temperatures due to some electrical components are temperature dependent. For instance, the resistance of copper is proportional to temperature. Therefore, I^2R losses are proportional to winding temperature as well. Higher efficiencies and power densities can be acquired by decreasing temperature. At the same time, the magnet BH curve is dependent of temperature. High temperatures can cause a significant reduction in magnetic loading as well as to elevate the risk of demagnetization in case of faults.

Thermal
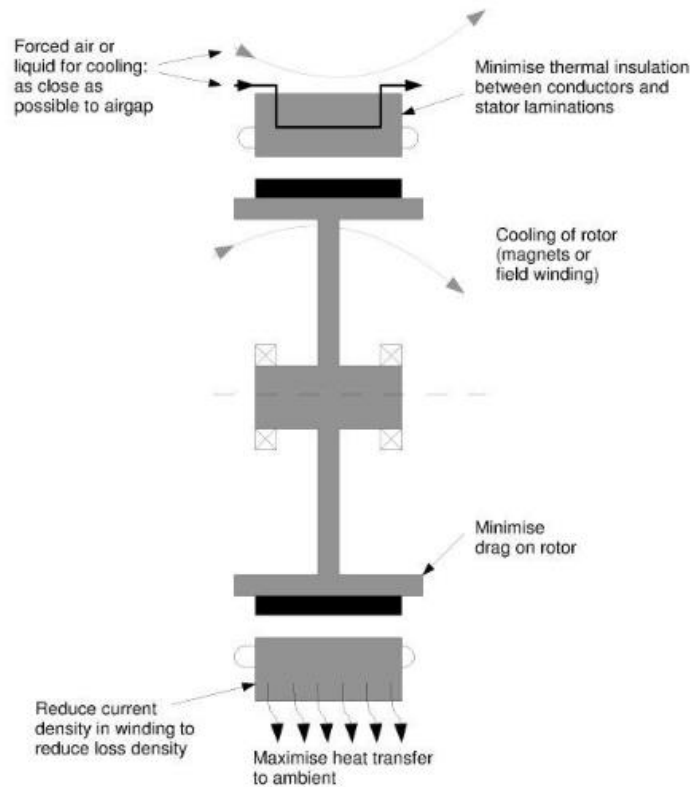
Figure 2.31 Thermal design perspective [13]

From the manufacturing point of view, a considerable cost reduction can be obtained if the design is simplified. Cheaper generators could be constructed if concepts such as modularisation (lower operational costs and labour are achieved as smaller field crews are needed, project timelines are shorter and the use of material is more efficient) and less strict tolerances were introduced. From the logistics viewpoint is also an attractive option since only 4 m diameter structures can be transported by road within the EU.

Manufacturing
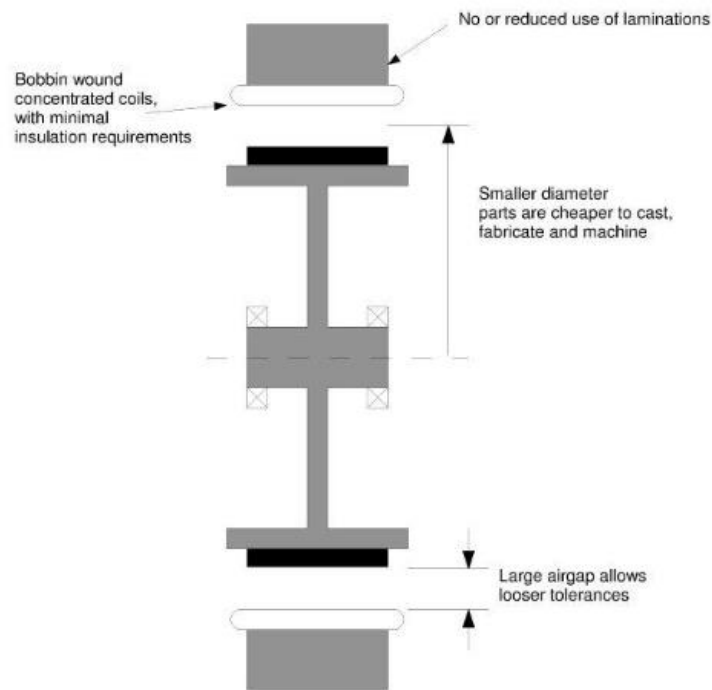
Figure 2.32 Manufacturing design perspective [13]

At this point, it is important to mention that might be an optimum electrical design (in terms of cost, mass and efficiency) but not perhaps a global optimum.

The concept of an integrated design was successfully put in practice with the first 15 kW C-GEN machine prototype. Electromagnetic, structural and thermal issues were considered by making use of a genetic algorithm that tries to maximise the energy yield while minimising material and manufacturing costs [37].

2.7.7 Modelling methods

2.7.7.1 Analytical approaches for structural modelling

Although many different types of structures can be assumed to characterize permanent magnet machines, see Figure 2.33, simple disc and arm structural models, such as shown in Figure 2.34, are more common due to their relative simplicity.
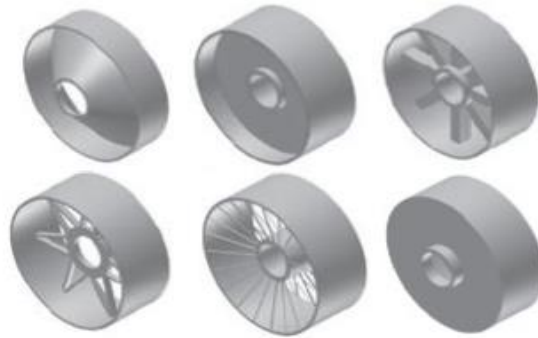
Figure 2.33 Typical rotor structures [51]
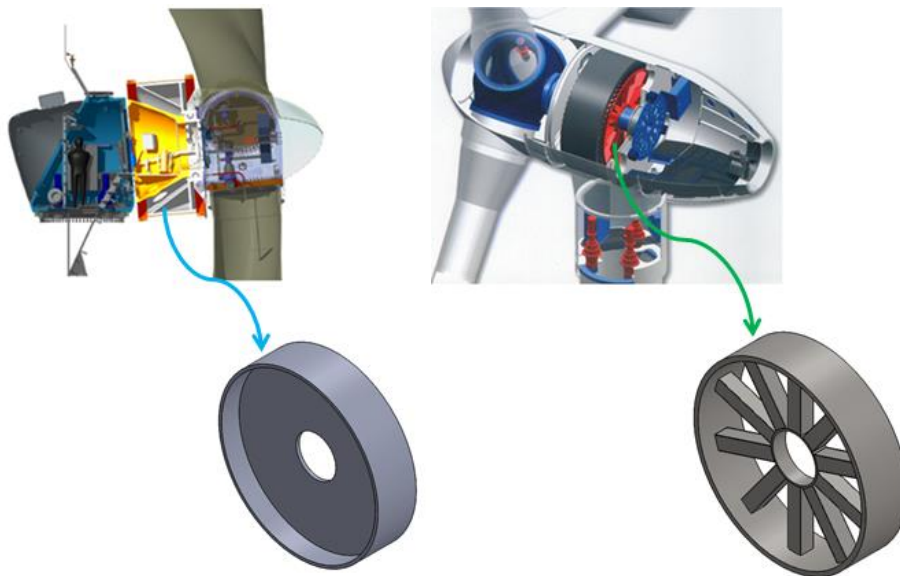
Figure 2.34 a) Zephyros/Harakosan Europe Z72, b) MTorres 1.5 MW

McDonald [58] used these models to link the mechanical and the electromagnetic design in radial flux machines and to estimate radial, axial and tangential deflections in the structure.
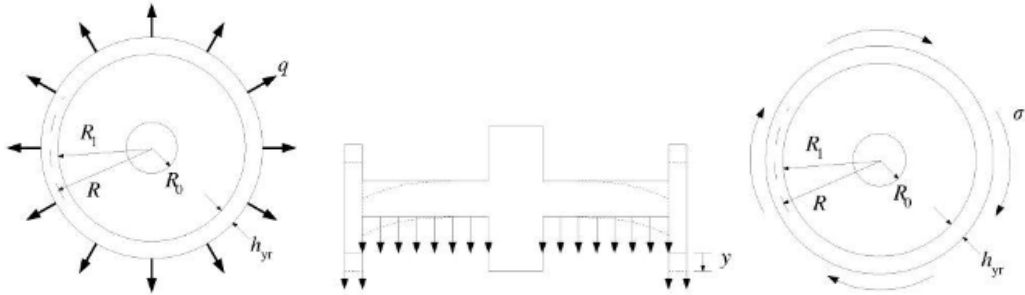
Figure 2.35 Radial flux models: a) radial, b) axial and c) tangential deflection [13]

Axial flux machines can be easily modeled employing disc structures. Structural deflection and dimensions, as well as magnetic forces, can be linked with the model in question.
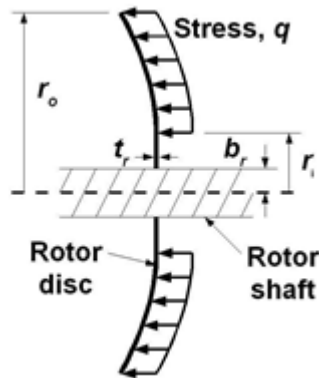
Figure 2.36 Axial flux model [13]

The stress shown here would take the form,

$$q = \frac{1}{2\mu_0} \hat{B}_g^2 sin^2(n\theta) \tag{2.3}$$

where q is the stress, $\hat{B}_g$ is the peak airgap flux density, n is the deflection mode and θ corresponds to the pitch angle. In reality, there are more forces at play in the machine

but it is considered appropriate to neglect these in an early stage design study as the normal component of the Maxwell stress is the largest force by far.

2.7.7.2 Numerical approaches for structural modelling

The behavior of the generator structure can also be modelled using more advanced methods, such as computational finite element techniques. For instance, ANSYS is a widely used commercial piece of software that gives the designer the opportunity to carry out dynamic behavior and fatigue studies. These are considered standard tools whose outcome can be utilized with confidence.

On the other hand, they are in fact computationally expensive so their use is limited. Fine meshes for large volumes own a large number of degrees of freedom which requires more computational power in order to solve the model in a reasonable time.

2.7.7.3 Structural optimization

Making use of an analytical and finite element analysis optimization method, A. Zavvos, A.S. McDonald and M. Mueller tried to minimize the structural mass of a permanent magnet direct drive generator [59]. Three different iron cored generator configurations rated at 5 MW were optimized concluding that a specific transverse flux direct drive topology is the most suitable as its electromagnetic layout helps the structural design. The said topologies were a radial flux and 2 transverse flux PMDD generators, see Figure 2.37, that were simplified using a disc rotor structure and an armed stator structure.

A constant amount of copper per unit of airgap surface area and iron with infinite permeability was assumed so that only the airgap region was modelled [57]. The mass of permanent magnets on the rotor of the machine was calculated as shown:

$$Mass_{PM} = 2\pi Rl \left(\frac{b_m}{\tau_p}\right) h_m \rho_{PM} \tag{2.4}$$

where R is the radius of the rotor, l is the rotor axial length, b_m is the width of the magnet, τ_p is the pole pitch, h_m is the height of the magnet and ρ_{PM} is the permanent magnets' density.
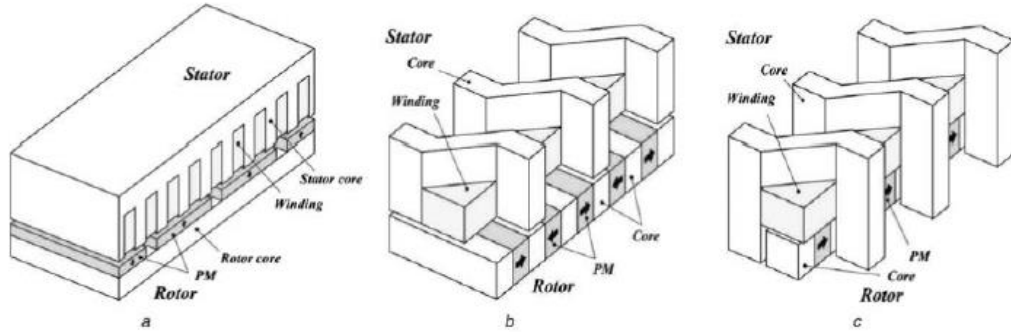
Figure 2.37 Illustrations of the three tested generator topologies: a) radial flux, b) transverse flux No. 1, c) transverse flux No. 2 [59]

(a)

(b)

(c)

(d)
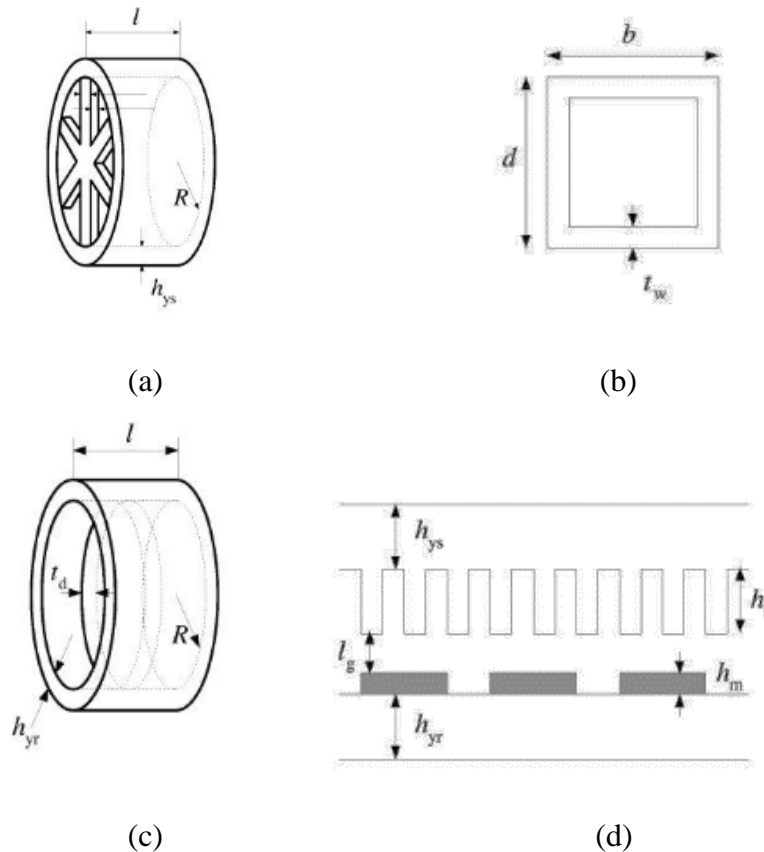
Figure 2.38 Illustration of the variables that were utilised for the optimisation of the generator structures; (a) The variables that describe a structure with arms; (b) The variables that describe arms sub structure; (c) The variables that describe a rotor with discs; (d) The variables that describe the electromagnetic model [59]

Figure 2.38 shows the parameters that were optimised in [59]. The effect on the structural mass of the generator for various structural dimensions was calculated whilst maintaining the structure's aspect ratio ($K_{rad} = l/2R$). The models successfully allowed the designs to be structurally optimised and concluded that out of the three tested, the transverse flux PMDD generator was the lightest option.

2.7.7.4 Modes of deflection

So far the discussion has assumed that local and global deflections are one and the same. This one dimensional model is only correct in a limited case. Actually, the deformation can be different at different parts of rotor and stator. In [60], the authors noted that localized contact can eventually happen because of:

Mode 0: Relative radial expansion of the rotor or radial compression of the stator.

Mode 1: Relative displacement of the rotor and stator.

Mode 2: Distortion of either or both of the circular surfaces into ellipses (known as ovalising).

Mode n: Distortion with ripples, n peaks around the circumference.

In general, the total change in air-gap clearance, δ ($= \delta_r + \delta_s$) can be expressed as a function of circumferential angle around the machine's axis, θ, by equation (2.5),

$$\delta(\theta) = \sum_{0}^{n} \delta_n \sin n(\theta - \varphi_n) \tag{2.5}$$

where $\delta(\theta)$ is the change in airgap clearance at angle θ, δ_n is the amplitude of component n, φ_n is the phase angle of component n, and n is the number of peaks, hence:

$n = 0$ for deformation of mode 0 (Figure 2.39(a));

$n = 1$ for mode 1 (Figure 2.39(b));

$n = 2$ for mode 2 (Figure 2.39(c));

$n \geq 3$ for mode 3 (Figure 2.39(d))and higher.

Often the air-gap deformation is dominated by a uniform mode 0 component with amplitude, $\bar{\delta}$, and a higher order component with amplitude δ_Δ and hence equation (2.6) can be modified:

$$\delta(\theta) = \bar{\delta} + \delta_\Delta \sin n(\theta - \varphi_n) \tag{2.6}$$
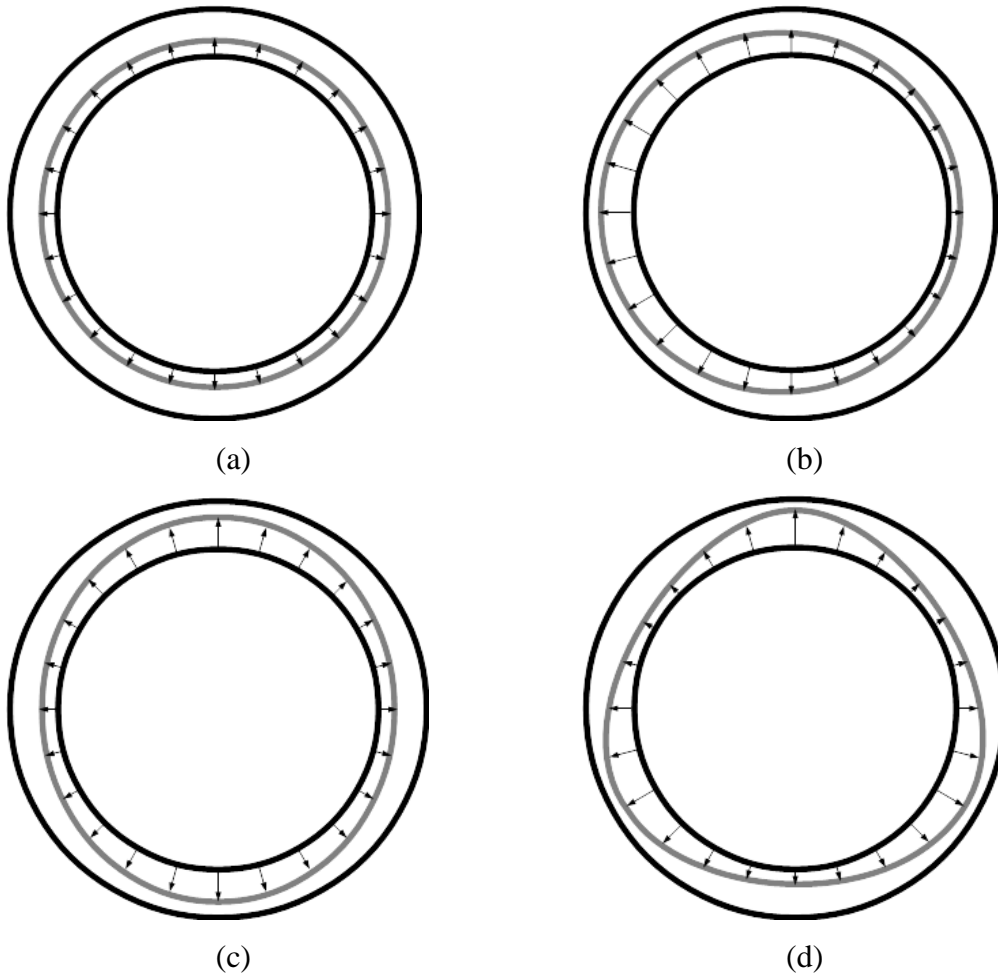
Figure 2.39 A rotor deforming into the airgap towards a stator

(a) Mode 0, uniform deflection, $\boldsymbol{\delta(\theta)} = \bar{\boldsymbol{\delta}}$
(b) Mode 1, eccentricity, $\boldsymbol{\delta(\theta)} = \bar{\boldsymbol{\delta}} + \boldsymbol{\delta_\Delta sin\,(\theta - \varphi)}$
(c) Mode 2, ovalisation, $\boldsymbol{\delta(\theta)} = \bar{\boldsymbol{\delta}} + \boldsymbol{\delta_\Delta sin2(\theta - \varphi)}$
(d) Mode 3, $\boldsymbol{\delta(\theta)} = \bar{\boldsymbol{\delta}} + \boldsymbol{\delta_\Delta sin3(\theta - \varphi)}$

Figure 2.40 is a plot of the airgap clearance for a prototype generator for a Northern Power 1.5MW direct-drive wind turbine [61], showing both the designed and measured air gap clearance, varying with angle. The deflection can be calculated and is shown in Figure 2.41. The machine shows that the actual deflection exceeds the designed limits. In this case the parameters in equation (2.6) can be approximated as $n = 2$, $\bar{\delta} = 9.3$ mm and $\delta_{\Delta} = 6.6$ mm.

In order to understand why different machine designs lead to different mode shapes it is necessary to understand the magnetic air-gap and structural stiffness properties.
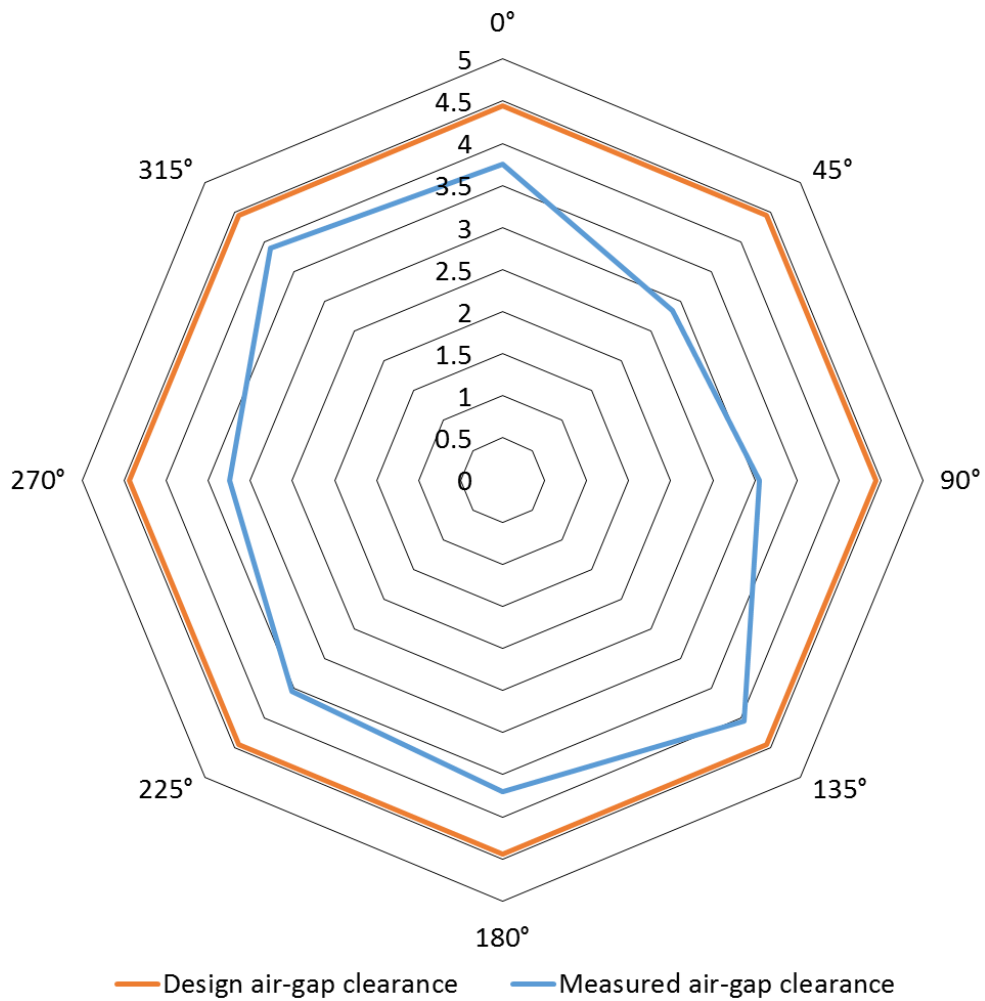
Figure 2.40 Airgap clearance (in mm) for the Northern Power 1.5MW prototype [61]. The values shown here are the mean of the airgap clearance at the upwind and downwind ends of the machine. Clearance is plotted for different angles as seen from the upwind end of the machine

Figure 2.41 Total deflection from designed air-gap clearance (in mm) for the Northern Power 1.5MW prototype [61]

2.8 The Concept of Direct Drive Generator Supporting Structures

The idea of designing a direct drive generator supporting structure utilising composite materials was patented by Siemens Aktiengesellschaft in 2010. Figure 2.42 depicts a cutaway of a direct drive wind turbine with composite material structures for a hollow main shaft (9) and the electrical machine, comprising the rotor (18) and the stator (19) arrangements [62].
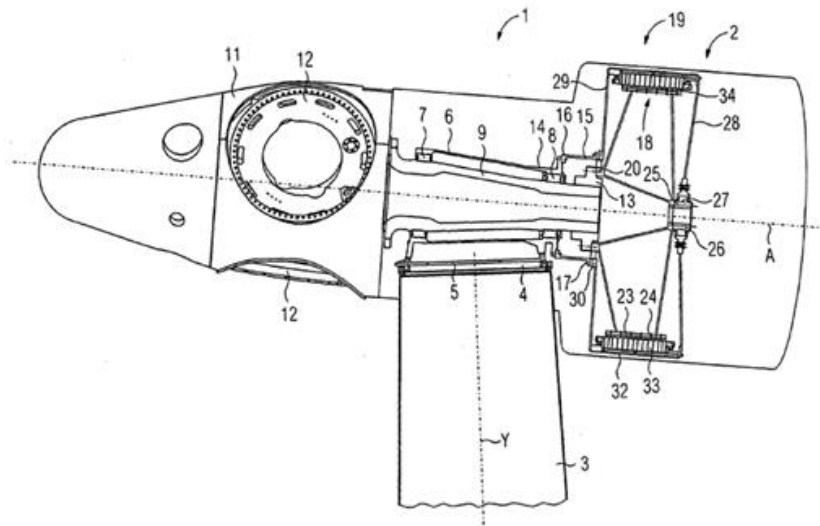
Figure 2.42 Siemens Direct Drive Wind Turbine Cutaway [62]

With the release of this patent, the foundations for the development of an idea that has been widely proposed but not thoroughgoing studied have been set. In this thesis, different structural configurations have been analysed and a potential way of modelling and optimising simplified composite structures for direct drive generators considering mechanical and electromagnetic issues has been proposed.

2.9 References

[1]   I. Ency, "Key World Energy Statistics," 2012.

[2]   E. Hau, Wind Energy: Fundamentals, Technologies, Applications, Economics; 2nd Edition, Berlin: Springer, 2006.

[3]   Global Energy Council Report, "http://www.gwec.net/wp-content/uploads/vip/GWEC-Global-Wind-2015-Report_April-2016_22_04.pdf". [Online]. [Accessed 11 September 2016]

[4]   J. Manwell, J. McGowan and A. Rogers, Wind Energy Explained: theory, design and application, 2nd Edition, John Wiley & Sons Ltd, 2009.

[5]   Nordex AG, www.nordex-online.com, [Online] [Accessed 10 March 2017].

[6]   Ecotècnia, GE Wind, "www.ge.com/wind," [Online] [Accessed 30 September 2016].

[7]   REpower Systems AG, www.repower.de, [Online] [Accessed 10 March 2017].

[8]   Vestas Wind Systems A/S, www.vestas.com, [Online] [Accessed 10 March 2017].

[9]   S. Alshibani and V. Agelidis, "Issues regarding cost estimation of permanent magnet synchronous generators for MW level wind turbines," in IEEE Int. Elect. Mach. Drives Conf; pp. 1629-1634, May 2011.

[10]   K. Smolders, H. Long, Y. Feng and P. Tavner, "Reliability analysis and prediction of wind turbine gearboxes," in EWEC, 2010.

[11]   O. Anaya-Lara, N. Jenkins and J. Ekanayake, Wind Energy Generation: Modelling and Control, 2011.

[12]   H. Polinder, "Overview of the trends in wind turbine generator systems," in IEEE Power Energy Soc. Gen. Meet., pp.1-8, July 2011.

[13]   M. Mueller and A. Zavvos, "Electrical drive technology," in Electrical drives for direct drive renewable energy systems, Woodhead Publishing Limited, 2013, pp. 3-30.

[14]   "www.enercon.de/en-en/Windenergieanlagen.htm," [Online]. [Accessed 30 September 2016].

[15]   D. Bang, "Design of transverse flux permanent magnet machines for large direct-drive wind turbines," Ph.D. thesis, Delft University of Technology,

Delft, The Netherlands, 2010.

[16] E. Spooner and B. Chalmers, "TORUS: A slotless, toroidal-stator, permanent magnet geneator," in International Conference on Electrical Machines, pp.1053-8, Cambridge, 1990.

[17] N. Vilsboll, A. Pinegin, D. Goussarov and J. Bugge, "The experience of designing and testing a 20kW multi pole permanent magnet generator for wind turbines," DEWI Magazine, vol. no. 9, pp. 74-83, August 1996.

[18] Renewable energy world, http://www.renewableenergyworld.com, [Online]. [Accessed 10 March 2017].

[19] A. Grauers, "Design of direct-driven permanent magnet generators for wind turbines," Ph.D. dissertation, Dept. of Electric Power Engineering, Chalmers University of echnology, Goteburg, Sweden, 1996.

[20] N. Bianchi and A. Lorenzoni, "Permanent magnet generators for wind power industry: an overall comparison with traditional generators, pp. 49-54," in IEE Conf. on Opportunities and Advances in International Power Generation , Durham, UK, Mar. 1996.

[21] T. Hartkopf, M. Hofmann and S. Jockel, "Direct-drive generators for MW wind turbines, pp. 668-671," in European Wind Energy Conference, Dublin, Ireland , 1997.

[22] M. Dubois, "Optimized permanent magnet generator topologies for direct-drive wind turbines," Ph.D. dissertation, Dept. of Electrical Engineering, Delft University of technology, Delft, The Netherlands, 2004.

[23] General Electric GE, "www.ge.com/wind," [Online]. [Accessed 30 September 2016].

[24] Siemens, "www.siemens.com/wind," [Online]. [Accessed 30 September 2016].

[25] Goldwind, "www.goldwindglobal.com," [Online]. [Accessed 30 September 2016].

[26] STX WindPower, "www.stxwind.com," [Online]. [Accessed 30 September 2016].

[27] Emergya Wind Technologies, "www.ewinternational.com," [Online]. [Accessed 30 September 2016].

[28] Vensys, "www.vensys.de," [Online]. [Accessed 30 September 2016].

[29] Leitwind, "www.en.leitwind.com," [Online]. [Accessed 30 September 2016].

[30] XEMC Darwind, www.xemc-darwind.com, [Online]. [Accessed 10 March 2017].

[31] G. Bywaters, V. John, J. Lynch, P. Mattila, G. Norton, J. Stowell, M. Salata, O. Labath, A. Chertok and D. Hablanian, "Northern Power Systems WindPACT drive train alternative design study report," Report NREL/SR - 500-35524, 2004.

[32] M. A. Mueller, A. S. McDonald and D. E. Macpherson, "Structural analysis of low-speed axial-flux permanent-magnet machines", IEE Proceedings of Electric Power Applications, Volume 152, No 6, pp. 1417-26, November 2005.

[33] G. Henneberger and M. Bork, "Development of a new transverse flux motor", in Proceedings of IEE Colloquium on New Topologies for PM Machines, Volume 1, pp. 1-6, 1997.

[34] A. McDonald , M. Mueller and H. Polinder, "Structural mass in direct drive permanent magnet electrical generator," IET Renewable Power Generation Special Issue- Selected Papers from EWEC 2007, vol. 2, pp. no. 1, 3-15, March 2008.

[35] C. Versteegh, "Low speed direct drive PM generator for application in the Zephyros Z72 wind turbine," IEE Seminar on Electr. Aspects of Offshore Renewable Energy Systems, NaREC, Blyth, Nothumberland, UK, 2004.

[36] http://www.windpowerengineering.com/design/sway-turbine-reveals-details-10mw-offshore-design/, [Online]. [Accessed 10 March 2017].

[37] O. Keysan *et al.*, "C-Gen, A Lightweigth Direct Drive Generator For Marine Energy Converters," in 5th IET PEMD International Conference, Brighton (UK), 2010.

[38] E. Spooner, A. C. Williamson and G. Catto, "Modular design of permanent-magnet generators for wind turbines", IEE Proc. Electr. Power Appl., 1996,143, (5), pp. 388-395.

[39] O. Danielsson, K. Thorburn, E. Sjöstedt, M. Eriksson and M. Leijon, M, "Permanent magnet fixation concepts for linear generator". Proc. of the Fifth European Wave Energy Conf., Cork, Ireland, Sep 17-20, 2003.

[40] P. Lampola, "Directly driven, low-speed permanent-magnet generators for wind power applications", Ph.D. dissertation, Helsinki University of Technology, Helsinki, 2000.

[41] A. Al-Badi, A. Gastli,H. Bourdoucen and J. Jervase, 'Evolution of axial-field electrical machines'. Science and Technology, Special Review (2000), Sultan

Qaboos University, pp. 227-245

[42]   E. Spooner and B.J.Chalmers, "TORUS": A slotless, toroidal-stator, permanent magnet generator', IEE Proc. B, 1992, 139, (6), pp. 497-506.

[43]   F. Caricchi, F. Crescimbini, F. Mezzetti and E. Santini, 'Multistage axial-flux PM machine for wheel direct drive', IEEE Trans. on Ind. Appl., 1996, 32, (4), pp. 882-888.

[44]   N. Brown, L. Haydock and J.R. Bumby, 'Foresight vehicle: a toroidal, axial flux generator for hybrid IC engine/battery electric vehicle applications'. Proc. SAE Conf. paper 2002-01-0829, Detroit, USA, March 2002.

[45]   F. Caricchi, F. Crescimbini and O. Honorati, 'Modular axial-flux permanent-magnet motor for ship propulsion drives', IEEE Trans. on Energy Conv., 1999, 14, (3), pp. 673-679.

[46]   R. J. Hill-Cottingham *et al.*, 'Plastic structure multi-disc axial flux PM motor'. Conf. Rec. of the 2002 IEEE Ind. Appl. Conf. 37th IAS Annual Meeting. Pittsburgh, PA, USA, 13-18 Oct. 2002, 2, pp. 1274-1280.

[47]   D. Bang, "Design of Transverse Flux Permanent Magnet Machines for Large Direct-Drive Wind Turbines," Ph.D. dissertation, Technical University of Delft, Delft, The Netherlands, 2010.

[48]   M. Dubois, "Review of electromechanical conversion in wind turbines, Final literature review," Technical University of Delft, Electrical Power Processing Group, Delft, The Netherlands, 2000.

[49]   M. Dubois, H. Polinder and J. Ferreira, "Comparison of generator topologies for direct drive wind turbines," in 2000 IEEE Nordic Workshop on Power and Industrial Electronics, pp. 22-26, Aalborg, Denmark, June 2000.

[50]   Y. Chen, P. Pillay and A. Khan, "PM wind generator comparison of differet topologies," in Conf. Rec. of the 2004 IEEE Ind. Appl. Conf. 39th IAS Annual Meeting, Seattle, WA, USA, 2004.

[51]   J. N. Stander, G. Venter, and M. J. Kamper, "Review of direct-drive radial flux wind turbine generator mechanical design," 2011.

[52]   T. Burton, D. Sharpe, N. Jenkins, and E. Bossanyi, Wind Energy Handbook. John Wiley & Sons, Ltd, 2001.

[53]   IEC 61400 International Standard, Third Edition 2005-2008, www.iec.ch [Online] [Accessed 13 March 2017].

[54]   Germanischer Lloyd Industrial Services GmbH, Rules and Guidelines Industrial Services IV, Renewables Certification, 1st July 2010. www.gl-group.com/GLRenewables [Online] [Accessed 13 March 2017].

[55]   Danish Standard DS 472, The Danush Energy Agency's Approval Scheme for Wind Turbines, www.wt-certification.dk [Online] [Accessed 13 March 2017].

[56]   Alstom brochures, www.alstom.com/Global/Power/Resources/Documents/Brochures/wind-powersolutions.pdf, [Online] [Accessed 10 March 2017].

[57]   S. Yagi and N. Ninoyu, "Technical trends in wind turbine bearings", Technical Report Review No. 76, NTN Corporation, Osaka, Japan, 2008.

[58]   A. S. McDonald, "Structural analysis of low speed, high torque electrical generators for direct drive renewable energy converters," Ph.D. dissertation, University of Edinburgh, Edinburgh, 2008.

[59]   M. Mueller, A. Zavvos, and A. S. Mcdonald, "Optimization tools for large permanent magnet generators for direct drive wind turbines," in IET Renewable Power Generation, vol. 7, no.2, pp. 163-171, Mar. 2013.

[60]   P. J. Tavner and E. Spooner, "Light Structures for Large Low-Speed Machines for Direct-Drive Applications." in Proc. International Conference on Electrical Machines, Chania, Greece, 2006.

[61]   G. Bywaters, P. Mattila, D. Costin, J. Stowell, V. John, S. Hoskins, J. Lynch, T. Cole, A. Cate, C. Badger, and B. Freeman, "Northern Power NW 1500 direct-drive generator." Northern Power Systems Inc., Waitsfield, VT, National Renewable Energy Laboratory, Subcontract Rep. NREL/SR-500-40177, Oct. 2007.

[62]   S. O. Lind and H. Stiesdal, "Wind Turbine," Patent WO 2013/083386 A2, June 2013.

Chapter 3

Magnetic Stiffness Modelling of Wind Turbine Electrical Generators

3.1 Introduction

Direct drive electrical generators are low speed high torque machines whose robust and stiff supporting structures are designed to withstand the significant loads present during the assembly (gravitational and attraction forces) and operation stages. The key load to be considered when designing this type of devices is a large force across the air gap which is because of the normal component of the Maxwell Stress. Several approaches were described by McDonald and Mueller in [1] for estimating the mass

of machine structures dealing with uniformly distributed force and deflection, also known as Mode 0. By assuming the rotor and the stator structures were made up of disc and arm sub structures, McDonald linked the electromagnetic and the mechanical design to model radial, tangential and axial deformations in radial flux machines [2]. In [3], Tavner and Spooner introduced a method which describes the challenge in terms of stiffness, focusing the attention on Mode 1 deflection of rotor and stator structures. Following that path, Jaen-Sola and McDonald presented in [4] an electromagnetic model that can be utilised to calculate the required airgap stiffness and therefore the stiffness of the generator structure. Going a step beyond, the authors coupled this model with a parametric structural model, which was produced by making use of finite element methods.

This chapter concentrates on the study of two different electrical machines under distinct deflection modes from a static point of view. An overview of how to model the different modes of generator structural deflection is given. The introduction and use of the magnetic stiffness concept to characterize the behaviour of electrical machines supporting structures is one of the main contributions made in this chapter and the thesis. After this, in the main body of the chapter, the reader will be able to see the development of an analytical model that links the magnetic and the mechanical sides of the design of a conventional wound rotor synchronous generator and a surface mounted permanent magnet generator, which has been developed continuing the work presented in [4].

The analytical parametric model (magnetic) first assumes a deflection value, 'δ', that is distributed along the outer surface of the rotor and the inner surface of the stator in order to calculate the ultimate airgap closing force for deflection modes ranging from 0 to 4. The assumed deflection 'δ' is composed by a mean deflection, '$\bar{\delta}$', and a variable deflection, 'δ_Δ'. Using the said deflection and the resultant force, the airgap stiffness (magnetic), k_M, is found dependent of δ. Finite element analysis of a two pole model and full machine model are used afterwards to validate the analytical models for airgap closing force and stiffness. With the analytical models corroborated, a structural finite element model of the electrical machine is generated. Making use of the airgap closing force computed with the analytical magnetic

approach, a deflection, '$\delta_{Structural}$', is obtained and used to calculate the structural stiffness that will be compared to the already known magnetic stiffness so that the designer can understand if the airgap of the proposed structure will remain stable and what the margin of deformation is. See Figure 3.1.
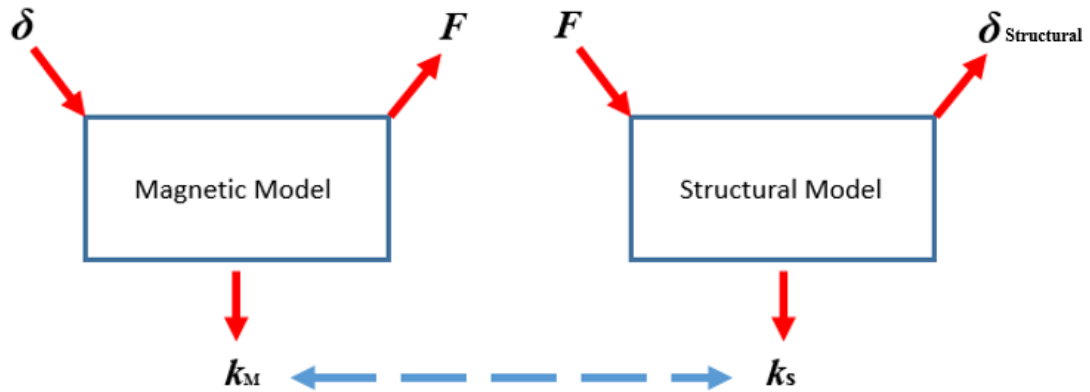
Figure 3.1 Coupling of magnetic and structural models

As said, two different types of generators (surface mounted permanent magnet and wound rotor) were analysed for distinct deflection modes. The achieved outcomes revealed that a stiffer supporting structure is needed to maintain the airgap of a wound rotor machine open and stable. In addition, it was identified that deflection Mode 4 is the most damaging for any of the assumed structures. The conclusions drawn from the obtained results are presented in the last section of this chapter.

3.2 Introduction to the Stiffness Concept

3.2.1 Mechanical Stiffness

In general terms, stiffness is a measure of the resistance offered by an elastic body to a force deforming the body. The stiffness is defined as $k = F/\delta$ where F is the force and δ is the displacement and it can be used to relate any F and δ, whereas a finite element model of a structure only gives δ for one set of F. This concept of stiffness can be expressed in terms of stress (the force per unit area, $\sigma = F/A$), strain (the

change in length divided by the original length, $\varepsilon = \delta/l$) and major dimensions of the body, thus,

$$k = \frac{F}{\delta} = \frac{\sigma A}{\varepsilon l}. \tag{3.1}$$

Normally, one is interested in the strain response to the application of stress. A positive value of stiffness means that as a positive force is applied, the change in length is also positive. Occasionally, the stress itself depends on the strain. This is the case for the magnetic forces in the airgap. Here as the airgap clearance reduces in size (i.e. δ is negative) the magnitude of the forces become larger. Conversely, as the airgap clearance increases in size, the magnitude of the force trying to close the airgap reduces. In this case the stiffness is negative.

In the steady-state and with no external forces applied, stability is achieved and a system is "stiff enough" when the sum of all the values of stiffness is equal to 0 (system is balanced). More stiffness is needed when other forces are introduced. A detailed explanation on this statement is given in Section 3.2.3.

Most systems are made up of multiple bodies each with their own value of stiffness. Two bodies with stiffness k_A and k_B can be combined into an equivalent stiffness depending on whether they are in series (and hence experience the same force but have different displacements),

$$k_{eq} = \frac{k_A k_B}{k_A + k_B}, \tag{3.2}$$

or in parallel (and hence experience the same displacement but different applied forces),

$$k_{eq} = k_A + k_B, \tag{3.3}$$

or mixture of these two cases.

A cross section of a generator structure with a simplified structure for a direct drive wind turbine is shown in Figure 3.2. A radial flux generator is formed by four main

components that in terms of stiffness are as follows: the bearing, k_b, the structure of the rotor, $k_{s,r}$, the magnetic airgap stiffness, k_M, and the structure of the stator, $k_{s,s}$. Combining the bearing and the rotor structure in series gives an equivalent stiffness,

$$k_{eq,r} = \frac{k_{s,r}k_b}{k_{s,r} + k_b}. \qquad (3.4)$$

(a) (b)
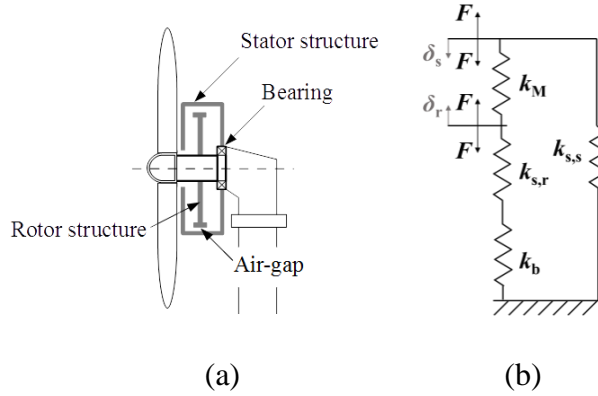
Figure 3.2 (a) Generator structure (b) Shown as stiffness [4]

The magnetic attracting force acting on the rotor and stator surface also acts to deform the rotor and stator structures. These structures have values of stiffness, which are constant for elastic materials below the elastic limit. Equations (3.5a) and (3.5b) express the common force in terms of stiffness and deflection,

$$F_c = k_{eq,r}\delta_r , \qquad (3.5a)$$

$$F_c = k_{s,s}\delta_s . \qquad (3.5b)$$

As they are connected to one another at the generator mounting point, and as they have the same force applied to them both, one can consider them as two bodies with stiffness in series, and so they can be expressed as an equivalent structural stiffness, $k_s = \frac{k_{eq,r}k_{s,s}}{k_{eq,r}+k_{s,s}}$. At one end of this composite structure, the force leads to rotor deflection into the airgap and at the other end the force leads to stator deflection,

$$F = k_s(\delta_s + \delta_r) \qquad (3.6)$$

3.2.2 Magnetic Stiffness

With a force, F, caused by the normal component of the Maxwell stress, acting on the rotor and stator surfaces, the airgap tends to close. The airgap closing force, 'F_c', can be expressed in terms of a magnetic stiffness, 'k_M', assuming a combination of a radial mean deflection, '$\bar{\delta}$', and a variable deflection, 'δ_Δ', which changes with angle 'θ', that alters the airgap clearance;

$$F_c = k_M \left(\bar{\delta} + \delta_\Delta \sin{(n\theta)} \right) \tag{3.7}$$

where n corresponds to the deflection mode and θ to the pitch angle. Figure 3.3 illustrates the airgap closing force calculated with equation (3.7) for $\bar{\delta} = 1$ mm and $\delta_\Delta = 0.5$ mm, at different angles for each deflection mode for $k_M = k_s$.
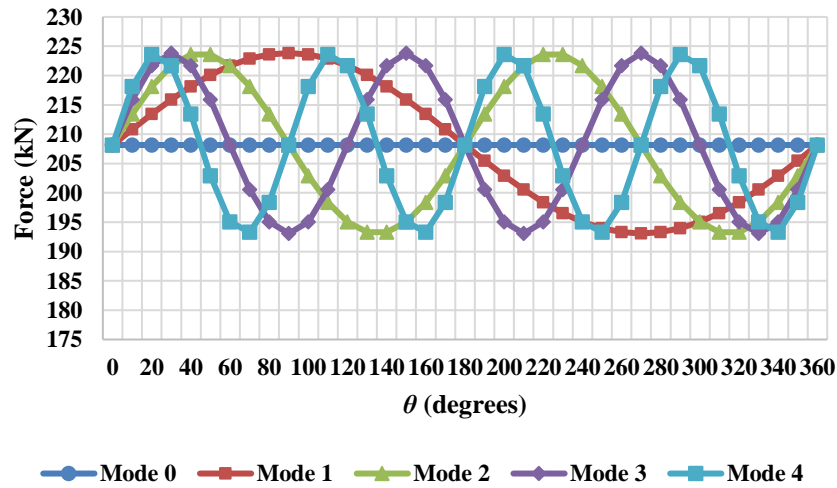
Figure 3.3 Airgap Closing Force vs. Theta

Note that in the figure, the area of the rim is apportioned into 36 parts and that the force for each span of $\beta = 10$ degrees is shown. Table 3.1 illustrates the characteristics of the machine used in the analysis in this chapter. It is based on the direct drive permanent magnet machine in [4].

Table 3.1 Case study generator data

Generator data	
Axial length, 'l_s' (m)	1.2
Rotor radius, 'R' (m)	2.5
Design airgap size, 'g' (m)	0.005
Rotor yoke height, 'h_{ry}' (m)	0.05
Aspect ratio (proportional relationship between width and height)	0.6
Magnet height, 'h_m' (m)	0.01
Magnet width, 'w_m' (m)	0.15
Number of pole pairs, 'p'	88
Pole pitch, 'τ_p' (m)	0.18

The force caused by the normal component of Maxwell stress will be calculated analytically in Section 3.3. So as to develop this model, it was considered the effective magnetic airgap clearance. This means that the changes in stiffness are correlated to the alterations in the size of the airgap. Therefore, expressions describing the airgap behaviour of electrically excited wound rotor machines and permanent magnet generators needed to be produced. Equation (3.8) is suitable to compute the airgap stiffness for electrically excited generators,

$$k_{WR} = \frac{F}{g - \delta} \tag{3.8}$$

where g is the airgap size, whereas equation (3.9) should be used in the case of having a permanent magnet machine (with surface mounted magnets),

$$k_{PM} = \frac{F}{g + \dfrac{h_m}{\mu_r} - \delta} \tag{3.9}$$

where h_m is the height of the magnet and μ_r is the relative permeability of the magnetic material. By introducing these two parameters into the equation, the fact of having surface mounted permanent magnets can be considered. To evaluate the

stiffness of both types of machines for different deflection modes, δ can be substituted by $\bar{\delta} + \delta_\Delta \sin(n\theta)$, which would give us the following

$$k_{\text{WR}} = \frac{F}{g - \bar{\delta} - \delta_\Delta \sin(n\theta)} \tag{3.8a}$$

$$k_{\text{PM}} = \frac{F}{g + \dfrac{h_{\text{m}}}{\mu_{\text{r}}} - \bar{\delta} - \delta_\Delta \sin(n\theta)} \tag{3.9a}$$

3.2.3 Overall Stiffness

As said, in order to keep the integrity of the electrical machine, the airgap must remain open and stable. For this, it is necessary that the magnetic force, 'F_{M}' and the structural force, 'F_{s}', are equal and opposite. No external forces has been considered. If equation (3.7) is manipulated, in equation (3.11), it can be seen that the equivalent structural stiffness of the system must be equal (and opposite in sign) to the airgap magnetic stiffness:

$$F_{\text{M}} + F_{\text{s}} = 0 \rightarrow k_{\text{M}}(\delta_{\text{s}} + \delta_{\text{r}}) + k_{\text{s}}(\delta_{\text{s}} + \delta_{\text{r}}) = 0, \tag{3.10}$$

$$k_{\text{s}} = -k_{\text{M}}. \tag{3.11}$$

Where the structural stiffness, 'k_{s}', will be calculated using finite element techniques. Further methods to estimate the structural stiffness of the electrical generator will be described in the next chapter.

3.3 Magnetic Airgap Stiffness

The concept of magnetic airgap stiffness was introduced in Section 3.2. The need for a versatile quick model that can accurately predict the required magnetic stiffness in several dimensions for different types of machines has led the author to create a 2 dimensional parametric model that can be used for optimization purposes. Equations

will be developed here for the airgap closing force per unit area as a function of deflection and angle for both wound rotor and surface mounted permanent magnet machines. Finally the formulations for the magnetic airgap stiffness will be developed.

As explained in Chapter 2, deflection can be different at distinct zones of rotor and stator [3]. Airgap collapse can take place due to:

Mode 0: Radial expansion of the rotor or radial compression of the stator.

Mode 1: Rotor eccentricity (localized deflection).

Mode 2: Distortion of either or both of the circular surfaces into ellipses.

Mode 3: Distortion with ripples around the circumferences.

The magnetic airgap stiffness expressions for both the wound rotor and the surface mounted permanent magnet machines will be derived attempting to address all of these scenarios.

3.3.1 Airgap closing force per unit area

Magnetic airgap stiffness arises because of the influence of the airgap clearance on the airgap permeance and hence airgap flux density. This in turn affects the airgap closing force. In the case of the airgap closing, the flux density increases and the force per unit area increases. This airgap closing force can be found from the normal component of Maxwell stress σ with equation (3.12), where B is the airgap flux density,

$$\sigma = \frac{B^2}{2\mu_0},$$
(3.12)

and μ_0 is the permeability of free space.

The flux density distribution, B, in the airgap can be found as follows,

$$B(\theta) = \mathscr{F}(\theta)\,\frac{P(\theta)}{A},$$
(3.13)

where $\mathscr{F}(\theta)$ is the MMF set up by the rotor field (winding or magnets) and armature windings current and $P(\theta)/A$ is the magnetic permeance per unit area. This flux density distribution can be found for a generic machine. Having a pole number of $2p$ the main airgap MMF is assumed to be sinusoidally distributed,

$$\mathscr{F}(\theta) = \widehat{\mathscr{F}}\cos(p\theta - \varphi). \tag{3.14}$$

Although the airgap flux density distribution for a surface mounted permanent magnet machine is often more akin to a square or quasi-square wave, equation (3.14) is normally a good approximation with $\widehat{\mathscr{F}}_{PM} = \frac{B_r h_m}{\mu_0 \mu_r} \frac{4}{\pi} \sin\left(\frac{\pi}{2} \frac{w_m}{\tau_p}\right)$, where h_m is the magnet height, w_m is the magnet height, τ_p is the pole pitch and μ_r is relative permeability. It should be noted that because the surface-mounted permanent magnet machine has a larger airgap permeance than conventional salient pole synchronous machines, the MMF per pole will be higher to produce the same flux density (assuming the same number of poles, rating and airgap geometry). Indeed equation (3.13) suggests that for the same airgap flux density, the ratio of MMFs approximates to $\frac{\widehat{\mathscr{F}}_{PM}}{\widehat{\mathscr{F}}} \approx \frac{P}{P_{PM}}$. This is because the final part of equation (3.13) is the magnetic permeance of the airgap. This can be defined in general terms as,

$$\frac{P}{A} = \frac{\mu_0}{l}, \tag{3.15}$$

where A and l are the cross sectional area and length of the region in question. Assuming that the iron in the magnetic circuit is infinitely permeable and ignoring slots then the magnetic permeance reduces to the permeance of the airgap, and $l = g$. Before any deflection occurs, the ratio of magnetic permeance of the airgap of the two machines would be $\frac{P_{PM}}{P} \approx \frac{g}{g + \frac{h_m}{\mu_r}}$.

As the deflection occurs the local airgap changes with the circumferential angle, θ, according to,

$$g(\theta) = g - \delta(\theta) = g - \bar{\delta} - \delta_\Delta \sin(n\theta - \varphi), \tag{3.16a}$$

$$g_{\text{eff,PM}}(\theta) = g + \frac{h_{\text{m}}}{\mu_{\text{r}}} - \delta(\theta) = g + \frac{h_{\text{m}}}{\mu_{\text{r}}} - \bar{\delta} - \delta_{\Delta}\sin(n\theta - \varphi), \tag{3.16b}$$

where g and $g_{\text{eff,PM}}$ are the nominal airgap clearance. The permeance per unit area can be approximated as,

$$\frac{P(\theta)}{A} \approx \bar{P} + P_{\Delta}\sin(n\theta - \varphi), \tag{3.17}$$

where $\bar{P}$ is the mean value of airgap permeance per unit area and P_{Δ} is the amplitude of variation of the airgap permeance per unit area. If δ_{Δ}^2 terms are neglected, then $\bar{P} \approx \frac{\mu_0}{g-\bar{\delta}}$ and $P_{\Delta} \approx \frac{\mu_0}{(g-\bar{\delta})^2}\delta_{\Delta}$. For a surface mounted permanent magnet machine, the magnetic airgap and airgap clearance are no longer one and the same; the mean and amplitude permeance per unit area terms become $\bar{P} \approx \frac{\mu_0}{g+\frac{h_{\text{m}}}{\mu_{\text{r}}}-\bar{\delta}}$ and $P_{\Delta} \approx \frac{\mu_0}{\left(g+\frac{h_{\text{m}}}{\mu_{\text{r}}}-\bar{\delta}\right)^2}\delta_{\Delta}$.

Figure 3.4 shows a comparison between the outcomes achieved for the magnetic permeance per unit area calculated using equations (3.15) and (3.17) for a permanent magnet machine.
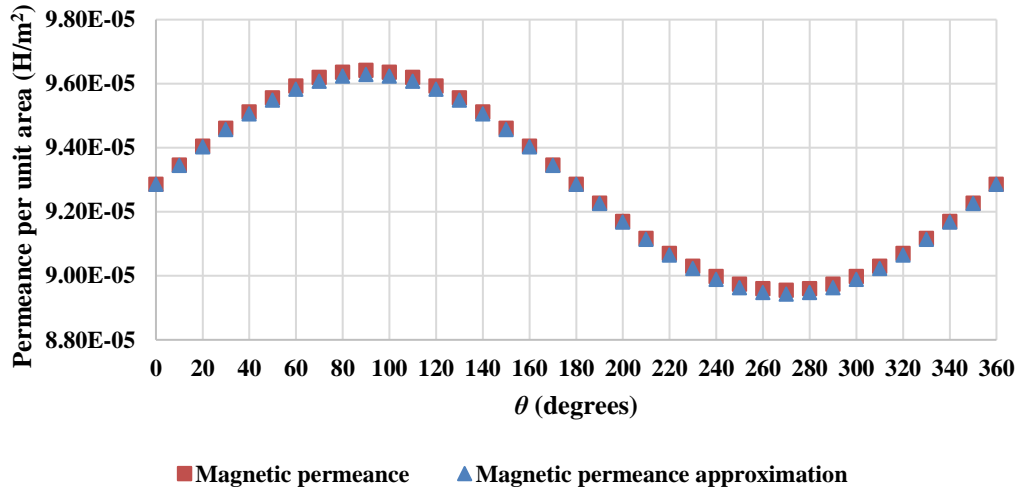
Figure 3.4 Magnetic permeance per unit area comparison. Magnetic permeance per unit area vs. Magnetic permeance per unit area approximation assuming infinite permeability for the back iron and ignoring slots.

So as to evaluate the goodness of fit of the magnetic permeance approximation to the magnetic permeance, the average root-mean-square error (RMSE) was calculated giving a value of 7.77562×10^{-8}. The RMSE corresponds to the sample standard deviation of the differences between the approximated values acquired with the model and the observed values and it is considered a good measure of accuracy statistically speaking. The normalized root-mean-square-error was also computed revealing a value of 1.13 % of residual variance. Thus, the permeance approximation calculated using equation (3.17) was treated as valid.

Substituting equations (3.14) and (3.17) into (3.13) and assuming that φ is changed so that peak deflection is at $\theta = \pi/2$, then it is found that

$$B(\theta) = \widehat{\mathscr{F}} \cos(p\theta)(\bar{P} + P_\Delta \sin(n\theta)) \tag{3.18a}$$

Equation (3.18b) is the corresponding equation but for the permanent magnet machine.

$$B(\theta) = \widehat{\mathscr{F}}_{PM} \cos(p\theta)(\bar{P} + P_\Delta \sin(n\theta)) \tag{3.18b}$$

Here there are two spatial frequencies; a high frequency, p, corresponding to the pole pairs and a lower frequency, n, corresponding to the mode of deflection. By substituting (3.18a) into (3.12) and rearranging and noting that in the case of many pole pairs, the variation in force distribution due to poles (i.e. the compared $\cos(p\theta)$), becomes less significant for structural deflections, then the mean value of $\cos^2(p\theta)$ is ½ and so the stress distribution can be simplified as

$$\sigma(\theta, \bar{\delta}, \delta_\Delta) = \frac{\widehat{\mathscr{F}}^2 \cos^2(p\theta)\mu_0}{2(g-\bar{\delta})^2}\left[1 + \frac{2\delta_\Delta \sin(n\theta)}{g-\bar{\delta}} + \frac{\delta_\Delta^2 \sin^2(n\theta)}{(g-\bar{\delta})^2}\right] \approx \frac{\widehat{\mathscr{F}}^2 \mu_0}{4(g-\bar{\delta})^2}\left[1 + \frac{2\delta_\Delta \sin(n\theta)}{g-\bar{\delta}} + \frac{\delta_\Delta^2 \sin^2(n\theta)}{(g-\bar{\delta})^2}\right]. \tag{3.19a}$$

For Mode 0 ($n = 0$), equation (3.19) becomes (3.20),

$$\sigma_{n=0}(\theta, \bar{\delta}) = \frac{\widehat{\mathscr{F}}^2 \cos^2(p\theta)\mu_0}{2(g-\bar{\delta})^2} \approx \frac{\widehat{\mathscr{F}}^2 \mu_0}{4(g-\bar{\delta})^2} \tag{3.19b}$$

For a surface mounted permanent magnet machine, the equivalent of equation (3.19a) becomes 3.20a, whereas 3.19b becomes 3.20b for Mode 0,

$$
\begin{aligned}
\sigma_{\mathrm{PM}}(\theta, \bar{\delta}, \delta_\Delta) &= \frac{\widehat{\mathscr{F}}_{\mathrm{PM}}^{\,2} \cos^2(p\theta)\mu_0}{2\left(g + \frac{h_{\mathrm{m}}}{\mu_{\mathrm{r}}} - \bar{\delta}\right)^2}\left[1 + \frac{2\delta_\Delta \sin(n\theta)}{g + \frac{h_{\mathrm{m}}}{\mu_{\mathrm{r}}} - \bar{\delta}} + \frac{\delta_\Delta^2 \sin^2(n\theta)}{\left(g + \frac{h_{\mathrm{m}}}{\mu_{\mathrm{r}}} - \bar{\delta}\right)^2}\right] \\[2mm]
&\approx \frac{\widehat{\mathscr{F}}_{\mathrm{PM}}^{\,2}}{4\left(g + \frac{h_{\mathrm{m}}}{\mu_{\mathrm{r}}} - \bar{\delta}\right)^2}\left[1 + \frac{2\delta_\Delta \sin(n\theta)}{g + \frac{h_{\mathrm{m}}}{\mu_{\mathrm{r}}} - \bar{\delta}} + \frac{\delta_\Delta^2 \sin^2(n\theta)}{\left(g + \frac{h_{\mathrm{m}}}{\mu_{\mathrm{r}}} - \bar{\delta}\right)^2}\right]
\end{aligned}
\tag{3.20a}
$$

$$
\begin{aligned}
\sigma_{\mathrm{PM}}(\theta, \bar{\delta}, \delta_\Delta) &= \frac{\widehat{\mathscr{F}}_{\mathrm{PM}}^{\,2} \cos^2(p\theta)\mu_0}{2\left(g + \frac{h_{\mathrm{m}}}{\mu_{\mathrm{r}}} - \bar{\delta}\right)^2} = \frac{\widehat{\mathscr{F}}_{\mathrm{PM}}^{\,2}\,{}^1\!/_2\,\mu_0}{2\left(g + \frac{h_{\mathrm{m}}}{\mu_{\mathrm{r}}} - \bar{\delta}\right)^2} \\[2mm]
&\approx \frac{\widehat{\mathscr{F}}_{\mathrm{PM}}^{\,2}\,\mu_0}{4\left(g + \frac{h_{\mathrm{m}}}{\mu_{\mathrm{r}}} - \bar{\delta}\right)^2}
\end{aligned}
\tag{3.20b}
$$

Figure 3.5 illustrates how the magnetic stress varies with angle for different deflection modes in a permanent magnet electrical machine.
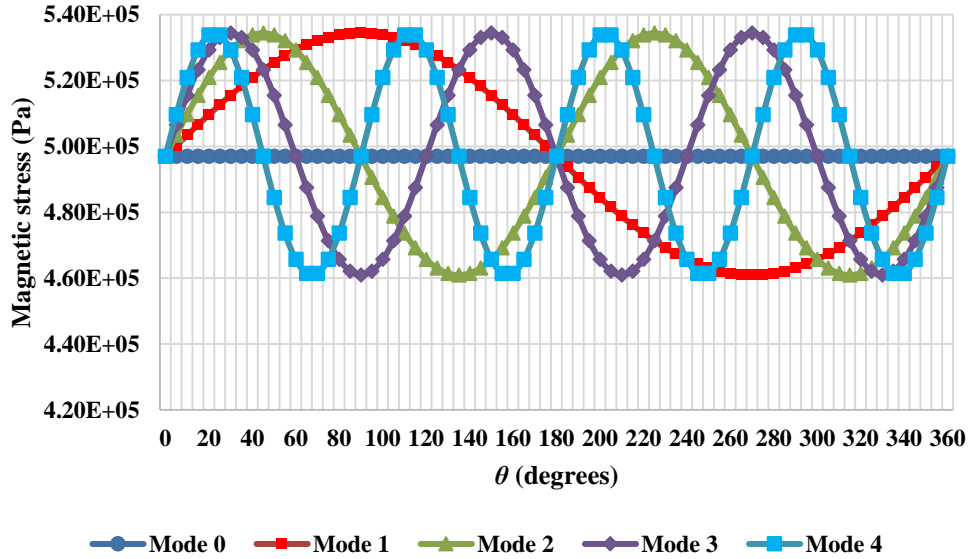
Figure 3.5 Magnetic stress vs. Theta for different deflection modes

70

To find the force on the rotor or stator surface closing the airgap, equation (3.19a) can be integrated over the axial length of the machine, l_s, and over any angle, 'β'. To find the force over for an angle β, we can integrate half an angle either side of the value of θ. For a wound rotor machine, the radial force on an arc of span β centred at angle θ for Modes 1, 2, 3 and 4 is as follows,

$$F_{\text{WR}} = l_s R \int_{\theta - \frac{\beta}{2}}^{\theta + \frac{\beta}{2}} \sigma\big(\theta, \bar{\delta}, \delta_\Delta, \beta\big) d\theta = \frac{\widehat{\mathscr{F}}_{\text{WR}}^{2} l_s R \mu_0}{4\big(g - \delta\big)^4} \alpha_{\text{WR}} \tag{3.21a}$$

with α_{WR} equal to

$$\begin{aligned}
\alpha_{\text{WR}} = \frac{1}{n} \Bigg[& 2\delta_\Delta \left(g - \bar{\delta} - \frac{\delta_\Delta}{4} \sin\left(\frac{n}{2}(\beta - 2\theta)\right) \right) \cos\left(\frac{n}{2}(\beta - 2\theta)\right) \\
& - 2\delta_\Delta \left(g - \bar{\delta} + \frac{\delta_\Delta}{4} \sin\left(\frac{n}{2}(\beta + 2\theta)\right) \right) \cos\left(\frac{n}{2}(\beta + 2\theta)\right) \\
& + \beta n \left(\frac{\delta_\Delta^2}{2} + g - \bar{\delta} \right)^2 \Bigg].
\end{aligned} \tag{3.21b}$$

While for Modes 0 is

$$F_{\text{WR}} = \frac{\widehat{\mathscr{F}}_{\text{WR}}^{2} l_s R \mu_0}{4\big(g - \delta\big)^2} \beta \tag{3.21c}$$

For a surface mounted PM machine, the radial force on an arc of span β centred at angle θ for Modes 1, 2, 3 and 4 is

$$\begin{aligned}
F = l_s R \int_{\theta - \frac{\beta}{2}}^{\theta + \frac{\beta}{2}} & \sigma\big(\theta, \bar{\delta}, \delta_\Delta, \beta\big) d\theta \\
& = \frac{\widehat{\mathscr{F}}_{\text{PM}}^{2} l_s R \mu_0}{4 \left(g + \frac{h_m}{\mu_r} - \bar{\delta} \right)^2} \int_{\theta - \frac{\beta}{2}}^{\theta + \frac{\beta}{2}} \Bigg[1 + \frac{2\delta_\Delta \sin(n\theta)}{g + \frac{h_m}{\mu_r} - \bar{\delta}} \\
& + \frac{\delta_\Delta^2 \sin^2(n\theta)}{\left(g + \frac{h_m}{\mu_r} - \bar{\delta} \right)^2} \Bigg] d\theta = \frac{\widehat{\mathscr{F}}_{\text{PM}}^{2} l_s R \mu_0}{4 \left(g + \frac{h_m}{\mu_r} - \bar{\delta} \right)^4} \alpha_{\text{PM}}
\end{aligned} \tag{3.22a}$$

with α_{PM} being

$$
\alpha_{\text{PM}} = \frac{1}{n}\left[2\delta_\Delta \left(g + \frac{h_m}{\mu_r} - \bar\delta - \frac{\delta_\Delta}{4} \sin\left(\frac{n}{2}(\beta - 2\theta)\right)\right) \cos\left(\frac{n}{2}(\beta - 2\theta)\right) \right.
$$
$$
- 2\delta_\Delta \left(g + \frac{h_m}{\mu_r} - \bar\delta \right.
$$
$$
\left. + \frac{\delta_\Delta}{4} \sin\left(\frac{n}{2}(\beta + 2\theta)\right)\right) \cos\left(\frac{n}{2}(\beta + 2\theta)\right)
$$
$$
\left. + \beta n \left(\frac{\delta_\Delta^2}{2} + g + \frac{h_m}{\mu_r} - \bar\delta \right)^2 \right].
$$

(3.22b)

Whereas for Mode 0 is

$$
F = l_s R \int_{\theta - \frac{\beta}{2}}^{\theta + \frac{\beta}{2}} \frac{\widehat{\mathscr{F}}_{\text{PM}}^{\ 2} \mu_0}{4\left(g + \frac{h_m}{\mu_r} - \bar\delta\right)^2} d\theta = \left[\frac{\widehat{\mathscr{F}}_{\text{PM}}^{\ 2} l_s R \mu_0}{4\left(g + \frac{h_m}{\mu_r} - \bar\delta\right)^2} \theta \right]_{\theta - \frac{\beta}{2}}^{\theta + \frac{\beta}{2}}
$$
$$
= \frac{\widehat{\mathscr{F}}_{\text{PM}}^{\ 2} l_s R \mu_0}{4\left(g + \frac{h_m}{\mu_r} - \bar\delta\right)^2} \beta
$$

(3.22c)

The magnetic stiffness of the same arc for Modes 1, 2, 3 and 4 of a wound rotor machine can be calculated using the following equation

$$
k_{\text{WR}} = \frac{F}{g - (\bar\delta + \delta_\Delta \sin(n\theta))} = \frac{\widehat{\mathscr{F}}_{\text{WR}}^{\ 2} l_s R \mu_0}{4(g - \delta)^4 (g - \bar\delta - \delta_\Delta \sin(n\theta))} \alpha_{\text{WR.}}
$$

(3.23a)

For Mode 0, the stiffness would be computed using equation (3.23b)

$$
k_{\text{WR}} = \frac{F}{\delta} = \frac{\widehat{\mathscr{F}}_{\text{WR}}^{\ 2} l_s R \mu_0 \beta}{4(g - \bar\delta)^3}.
$$

(3.23b)

The magnetic stiffness of the said arc is for Modes 1, 2, 3 and 4 of a PM machine equal to,

$$k_{\text{PM}} = \frac{F}{g - \left(\bar{\delta} + \delta_\Delta \sin(n\theta)\right)} \tag{3.24a}$$

$$= \frac{\widehat{\mathscr{F}}_{\text{PM}}{}^2 l_s R \mu_0}{4\left(g + \dfrac{h_m}{\mu_r} - \bar{\delta}\right)^4 \left(g - \bar{\delta} - \delta_\Delta \sin(n\theta)\right)} \, \alpha_{\text{PM}}$$

whereas for Mode 0 is

$$k_{\text{PM}} = \frac{F}{\delta} = \frac{\widehat{\mathscr{F}}_{\text{PM}}{}^2 l_s R \mu_0 \beta}{4\left(g + \dfrac{h_m}{\mu_r} - \bar{\delta}\right)^3}. \tag{3.24b}$$

3.3.2 Validation using finite element code

Finite element analysis of a two pole model was used to validate the analytical models for airgap closing force and stiffness. Applying correct periodic boundaries this type of model can represent the magnetic flux in the magnetic circuit in a more realistic manner than the simplified lumped parameter approach of the analytical solution. For instance, the analytical solution effectively ignores MMF drops in the iron yokes and teeth and neglects leakage paths but these can be captured in the finite element model.

In this case, a 2D code was utilized (FEMM[5]) and so axial end effects are neglected. To make the model more versatile, the two pole model has been geometrically linearized so that radial lines and arcs are mapped onto vertical and horizontal lines respectively. By changing the airgap clearance by a deflection δ a number of magnetostatic runs were processed and the results were interrogated to find the airgap closing force. Using a force via weighted stress tensor approach the obtained results are shown in Figure 3.6(a)-(c) where the force is plotted against deflection δ, the resulting physical airgap clearance $(g - \delta)$, and the resulting effective magnetic airgap clearance $(g + \dfrac{h_m}{\mu_r} - \delta)$ respectively.
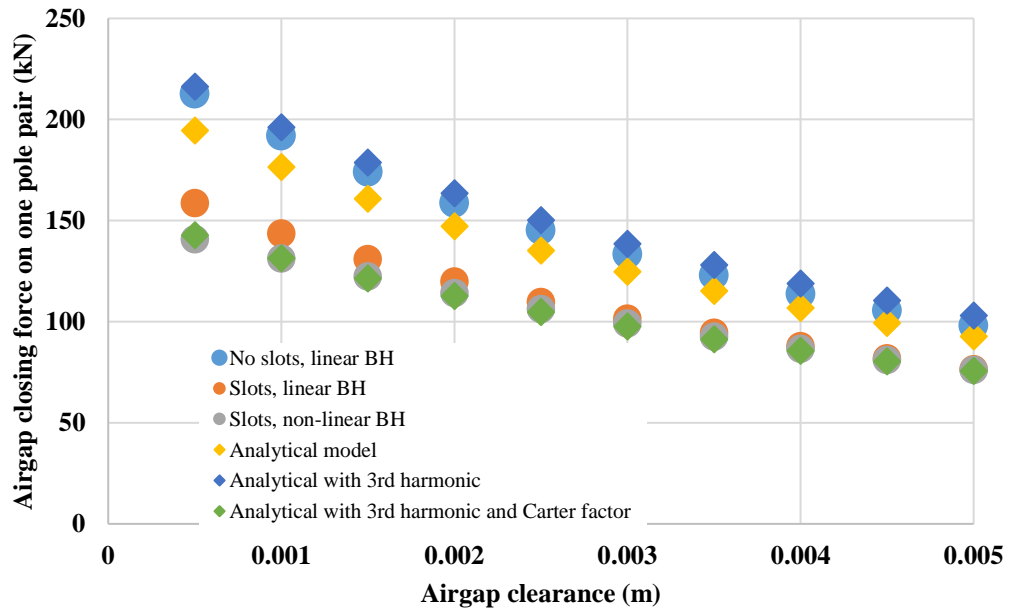
(a)
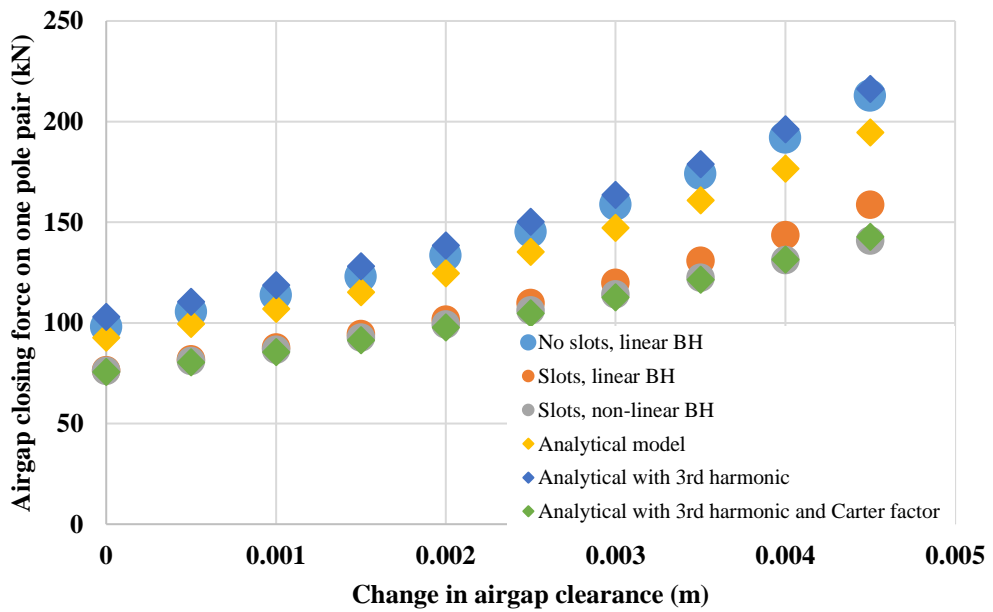
(b)
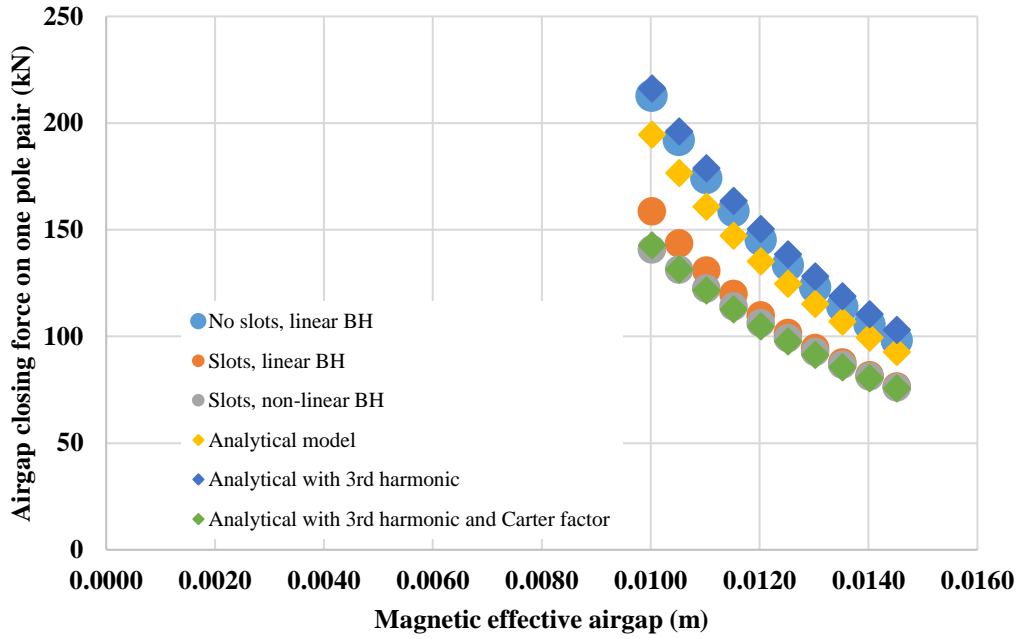
(c)

Figure 3.6 Magnetic airgap stiffness for a pole pair of a PM generator for a direct drive wind turbine, based on [3]. (a) Airgap closing force on one pole pair vs. Airgap clearance (b) Airgap closing force on one pole pair vs. Change in airgap clearance (c) Airgap closing force on one pole pair vs. Magnetic effective airgap

There are 3 FE cases: (i) where the materials are assumed to have linear BH curves and the stator has no slots (similar to the analytical model); (ii) where slotting is introduced but the materials have liner BH curves and (iii) where slotting is present and non-linear BH curves are used.

Also on Figure 3.6(a)-(c) one can see the analytical solutions for the same dimensions and materials using equation (3.22a) for $\delta_\Delta = 0$ and $\bar{\delta} = \delta$ and one pole pair (i.e. $\beta = \frac{2\pi}{p}$).

The analytical model clearly underestimated the force; this can be seen when comparing the results with those of the idealized FE model (i). This suggested that using only the fundamental MMF as an input to the analytical solution is incorrect as it leads to the model neglecting higher order airgap flux density spatial harmonics

and the resulting force contributions. The MMF of a surface mounted permanent magnet of width w_{m} can be written as:

$$\mathscr{F}_{\mathrm{m}}(\theta_{\mathrm{h}}) = \sum_{m=1,2,3,\ldots}^{\infty} \frac{B_{\mathrm{r}} h_{\mathrm{m}}}{\mu_0 \mu_{\mathrm{r}}} \frac{4}{m^2 \pi} \sin\left(\frac{m\pi}{2} \frac{w_{\mathrm{m}}}{\tau_{\mathrm{p}}}\right) \sin(m\theta_{\mathrm{h}})$$ (3.25)

where m is the harmonic order. Including $m = 1$ and $m = 3$ in equations (3.21)-(3.22) leads to amended force equation of

$$F \approx \frac{(\widehat{\mathscr{F}}_1{}^2 + \widehat{\mathscr{F}}_3{}^2) l_{\mathrm{s}} R \mu_0}{4(g + \frac{h_{\mathrm{m}}}{\mu_{\mathrm{r}}} - \bar{\delta})^2} \alpha_{\mathrm{PM}}.$$ (3.26)

This has been plotted in Figure 3.6(a)-(c). This shows better agreement with the idealized FE results (i). When slotting is introduced (FE models (ii) and (iii)) there is a noticeable reduction in force. The analytical model ignores the reduction in permeance due to slotting. This can be taken into account by applying the Carter factor k_{cr}=1.18, to the effective magnetic airgap, in other words,

$$F \approx \frac{(\widehat{\mathscr{F}}_1{}^2 + \widehat{\mathscr{F}}_3{}^2) l_{\mathrm{s}} R \mu_0}{4 k_{\mathrm{cr}}^2 (g + \frac{h_{\mathrm{m}}}{\mu_{\mathrm{r}}} - \bar{\delta})^2} \alpha_{\mathrm{PM}}.$$ (3.27)

The Carter factor was calculated using equation 3.28,

$$k_{\mathrm{cr}} = \frac{\tau_{\mathrm{s}}}{\tau_{\mathrm{s}} - g_1 \gamma}$$ (3.28)

where the slot pitch, $\tau_{\mathrm{s}} = 0.06$ m, the slot width, $w_{\mathrm{s}} = 0.03$ m, $g_1 = g + \frac{h_{\mathrm{m}}}{\mu_{\mathrm{r}}}$ and

$$\gamma = \frac{4}{\pi}\left(\frac{w_{\mathrm{s}}}{2g_1} arctan\left(\frac{w_{\mathrm{s}}}{2g_1}\right) - ln\sqrt{1 + \left(\frac{w_{\mathrm{s}}}{2g_1}\right)^2}\right).$$

The results for equation (3.27) are plotted in Figure 3.6(a)-(c) and show good agreement with the FE models (ii) and (iii). The difference between linear and non-linear materials is relatively modest, if the magnetic circuit is designed to avoid saturation in the default state.

Making use of the same data, a full model of the permanent magnet machine was generated in FEMM for validation. Assuming a linear B-H relationship for the NdFeB magnets and the M19 Steel parts, five different studies were carried out under Mode 1 deflection. As seen no coils have been included in the analysis as it was assumed that the stator electrical connection does not have any influence in the magnetic stiffness result. By looking at Figure 3.7(a), one can see how the north and south poles are clearly differentiated by green arrows pointing up and down that specify the direction of the magnetic flux. An adaptive mesh focused on the airgap area with 514,225 nodes was created for the evaluation.
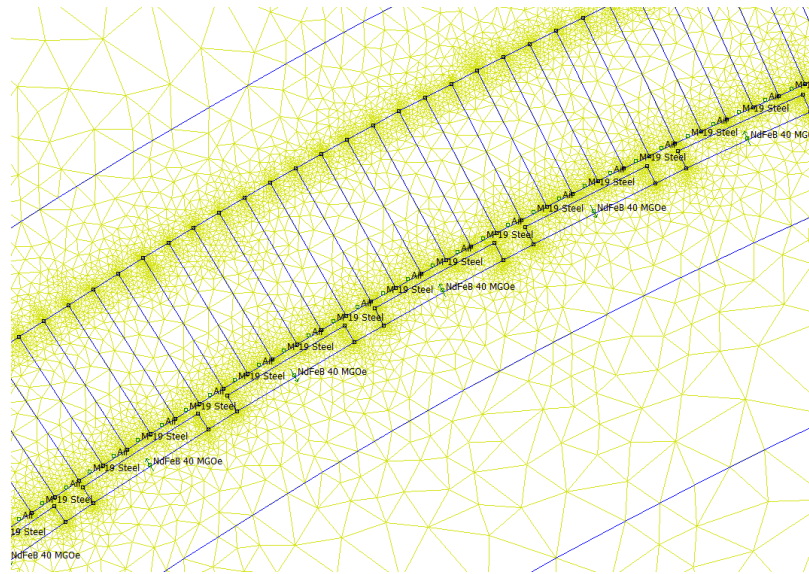
(a)
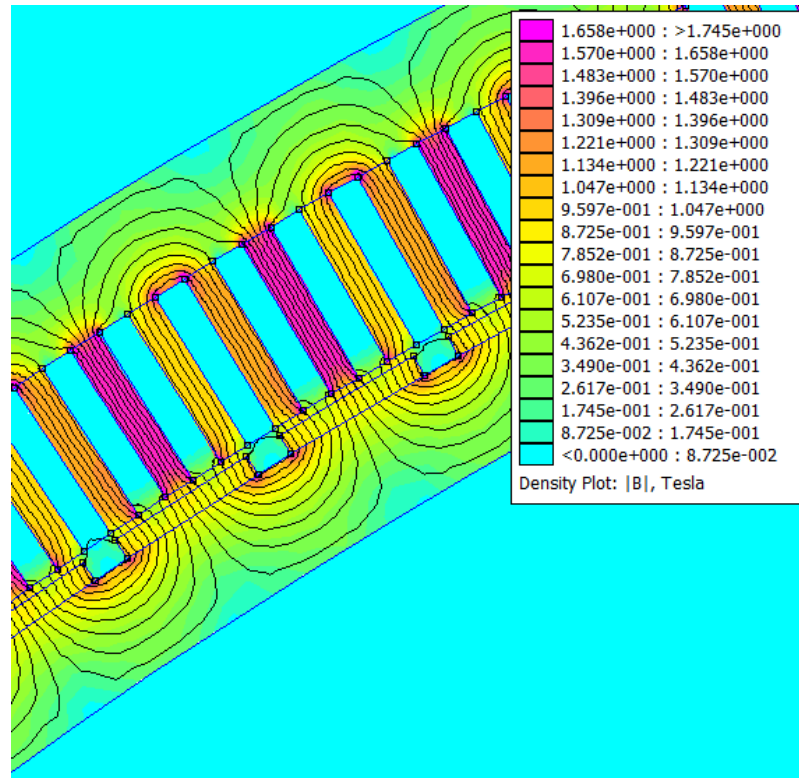
(b)

Figure 3.7 PM generator full model validation; (a) Detailed view of the triangular mesh; (b) Density plot showing the behaviour of the magnetic flux at a particular moment in time

As said, the analysis comprised studies under Mode 1 deflection. To simulate the eccentricity inherent to Mode 1, the rotor structure was shifted horizontally to the left so that the airgap clearance is reduced by a deflection δ. Again, a force via weighted stress tensor approach was utilized. The results achieved are displayed in Figure 3.8, where the airgap closing force is plotted against deflection δ. The analytical solutions can be obtained for the same dimensions and materials using equation (3.27) with $\delta_\Delta = \delta$ and $\bar{\delta} = 0$.
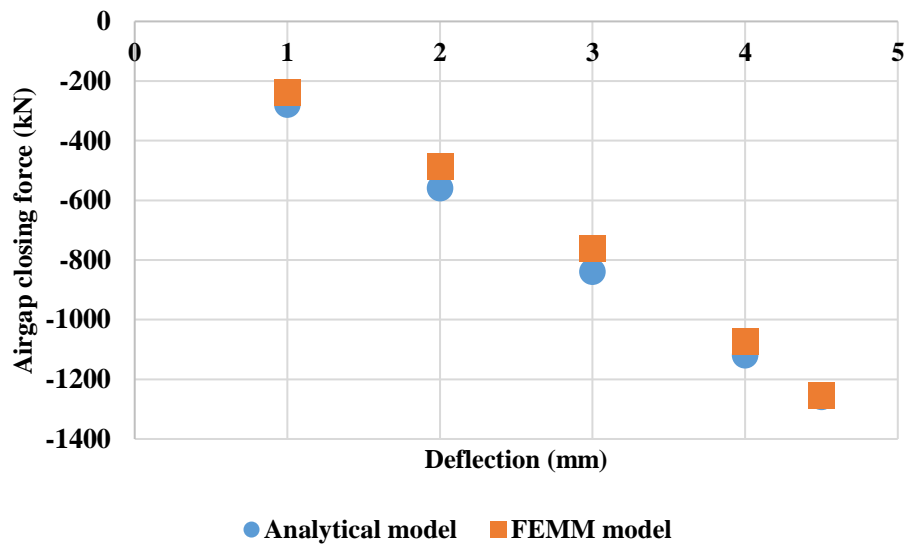
Figure 3.8 Comparison between analytical model and FEMM model (Mode 1 deflection)

As observed, the analytical model slightly overestimates the airgap closing force. Nevertheless, the level of agreement is considered good overall, which means that the analytical model can be used with high level of confidence.

3.4 Case study generator

Magnetic stiffness and structural stiffness are brought together in this section in order to study a 3 MW wind turbine generator. By assuming a deflection, the closing force acting on the airgap can be estimated making use of the magnetic model and utilized to calculate the structural deflection through a structural model. The characteristics of the electrical machine used in this analysis are displayed in Table 3.1 located in Section 3.2.2.

As explained, the required stiffness for the generator structure can be computed in different ways. In this case a structural finite element model of the generator was created in SolidWorks.

For the FE model, the rotor and the stator structures were loaded with radial stresses which were calculated as explained in the previous sub section using the data presented in Table 3.1 and a mean deflection, '$\bar{\delta}$', of 0.001 m and variable deflection,

'δ_Δ', of 0.0005 m. The cylindrical sub structures of both the rotor and the stator were apportioned into 36 parts so that the appropriate forces corresponding to Modes 0, 1, 2, 3 and 4 could be applied. With this, the deflection experienced by the structure was found allowing the structural stiffness of the generator to be evaluated.

The structural radial deflection of each 10 degrees part was measured making use of deflection sensors located on the outer face of each part in the case of the rotor and on the inner face in the case of the stator. See Figure 3.9.
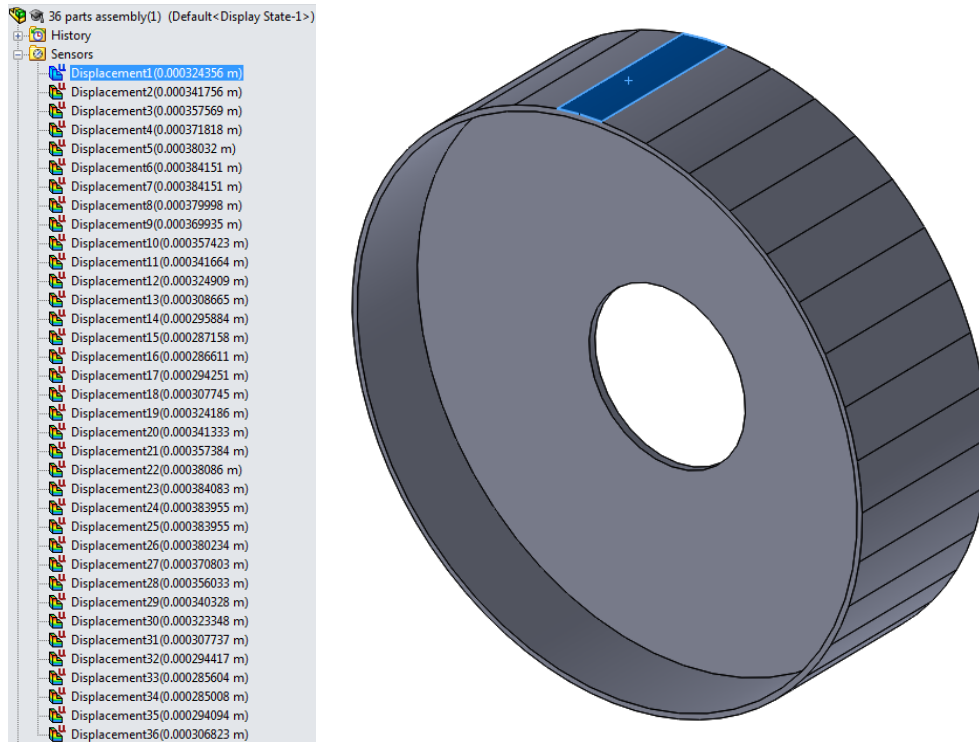
Figure 3.9 Measured structural deflection of rotor

The data retrieved from the structural FE analysis are presented in Figure 3.10.
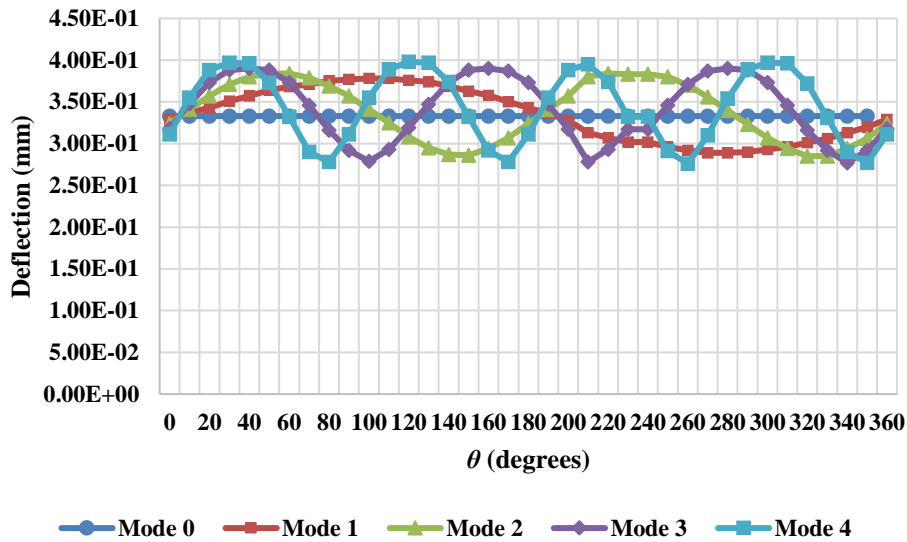
Figure 3.10 Rotor structural deflection (m) vs. Theta (degrees)

It can be appreciated how the structural deformation of the rotor varies according to the mode number (Figure 3.11). If the deflections obtained are plotted against the applied forces, it can be seen that the same gradient (structural stiffness) is maintained throughout the whole range although larger spread is found as the mode number goes up. This increasing might be attributed to the increase in the structural shear stresses with the number of ripples. See Figure 3.11(a)-(e).

(a)

(b)

(c)

(d)

(e)
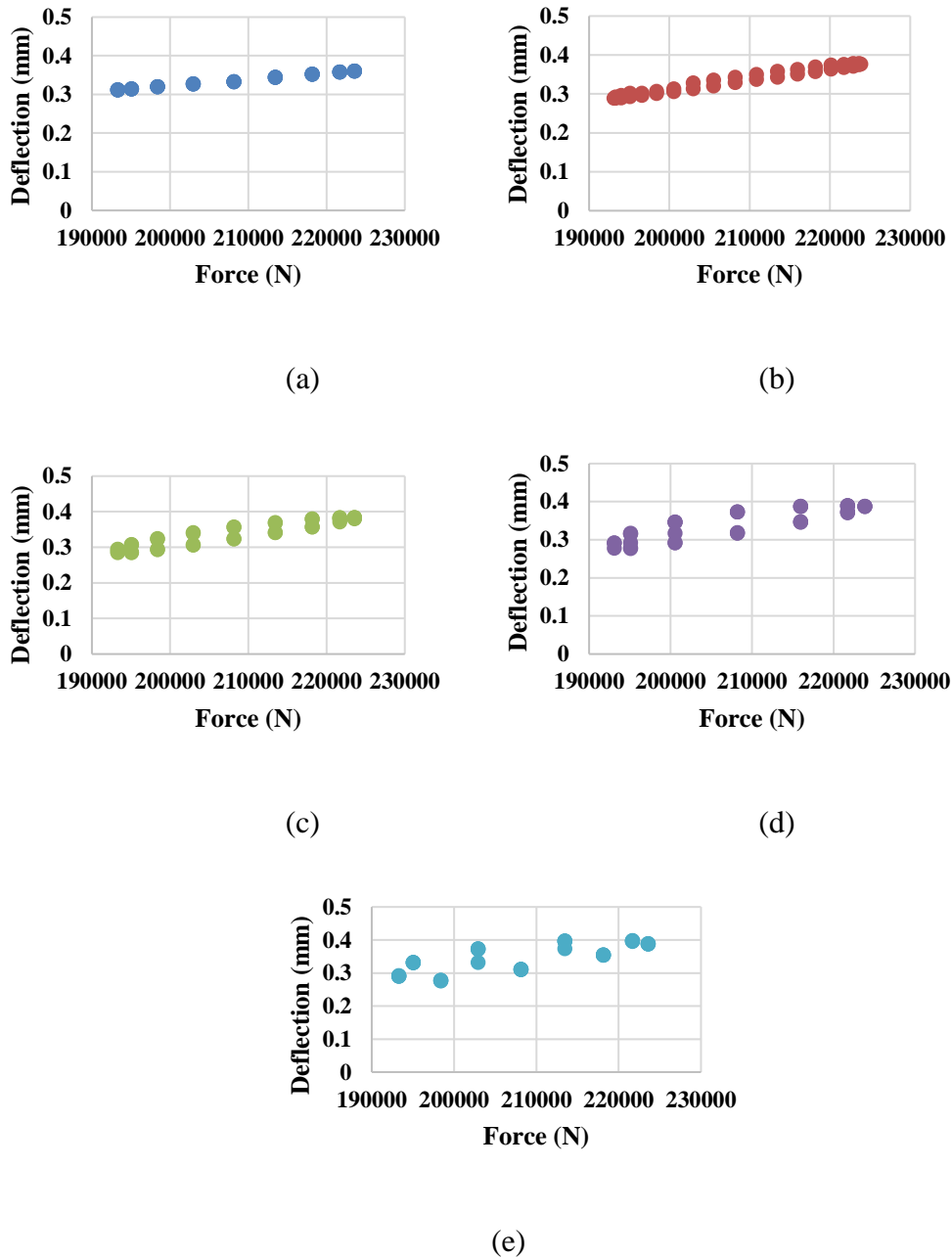
Figure 3.11 Rotor structure deflection vs. Applied Force; (a) Mode 0; (b) Mode 1; (c) Mode 2; (d) Mode 3; (e) Mode 4.

The typical oval shapes shown in the deflection diagrams above were obtained for the corresponding sinusoidal stress applied to the rotor structure according to the deflection mode. As only for Mode 0, a unique uniform load is applied, 36 different finite element studies using 36 distinct loads had to be carried out in order to acquire the straight line displayed in Figure 3.11(a) that lets us know the stiffness. For the

rest of the modes only one study was needed. The loads utilized in the study are as illustrated in the figure above and depend on the deflection mode. So as to know if the structure will be able to resist the load, the absolute value of the magnetic stiffness estimated using the analytical model must be equal or smaller than the structural stiffness calculated with the finite element study. This means that $k_s(\theta) \geq |k_M(\theta)|$. Combining the stiffnesses of the bearing, the rotor and the stator in series as explained is Section 3.2.1, the total stiffness of the generator structure is assessed. The bearing stiffness is assumed constant with a value of 3×10^9 N/m. In order to calculate the equivalent stiffness for each 10 degrees part, the bearing has been modelled as a finite number of radial stiffnesses set in parallel as shown in Figure 3.12, where k_r corresponds to the radial stiffness, γ is the angle between stiffnesses and N is the total number of radial stiffnesses, in our case 36.
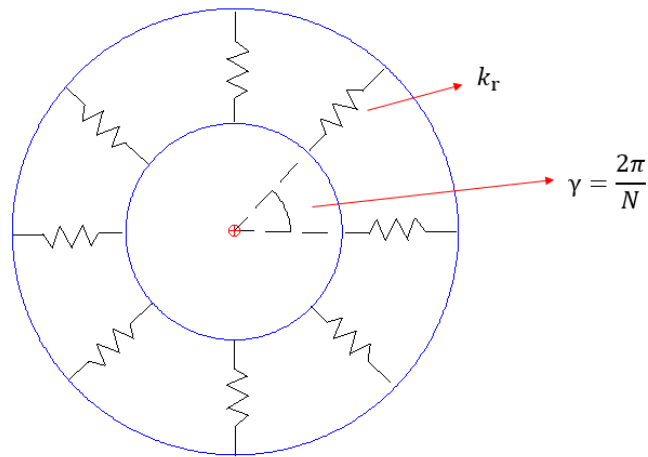
Figure 3.12 Bearing model showed as stiffness

Paying special attention to Mode 1, where a force, *F,* is applied to the top of the structure generating a deflection δ, which gives a stiffness $k_b = F/\delta$, the bearing has been split into a top structure and a bottom structure as depicted in Figure 3.13(a)-(b).

(a)   (b)
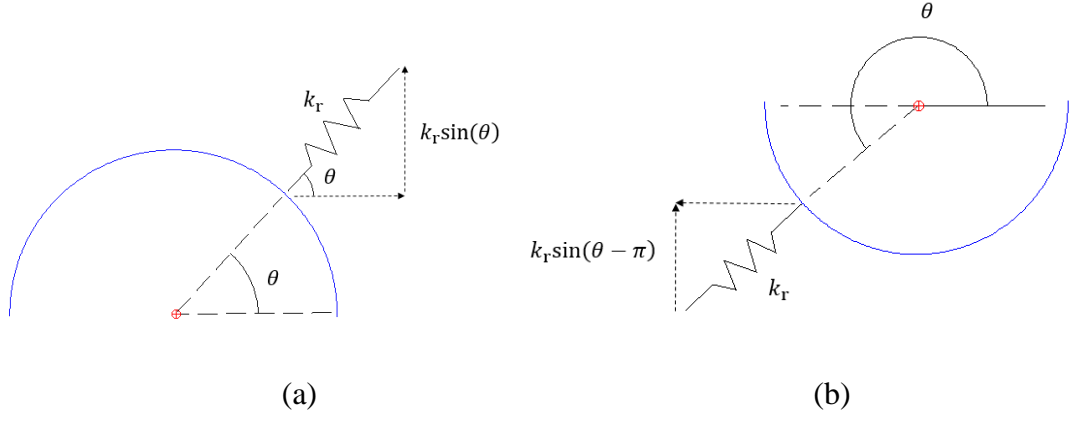
Figure 3.13 Bearing structure split into top and bottom parts; (a) top part; (b) bottom part

The total stiffness of the top structure, k_T, can be calculated using equation 3.29a, where the vertical components of all the radial stiffnesses in the top structure, in this case 18, are added up. Similarly, the stiffness of the bottom structure, k_B, can be estimated making used of equation 3.29b. It is assumed that under Mode 1 deflection, the top bearing structure is under tension, whereas the bottom part works under compression.

$$k_T = \sum_{i=1}^{i=N/2} k_r \sin(i\gamma) \tag{3.29a}$$

$$k_B = \sum_{i=N/2+1}^{i=N} k_r \sin(i\gamma - \pi) \tag{3.29b}$$

Thus, the total stiffness, 'k_b', can be computed as follows,

$$k_b = k_T - k_B = \sum_{i=1}^{i=N/2} k_r \sin(i\gamma) - \sum_{i=N/2+1}^{i=N} k_r \sin(i\gamma - \pi) \tag{3.30}$$

If we know that,

$$\sin(i\gamma - \pi) = -\sin(-i\gamma + \pi) = -\sin(-i\gamma) = -\sin(i\gamma) \tag{3.31}$$

then

$$k_{\mathrm{b}} = k_{\mathrm{T}} - (-k_{\mathrm{B}}) = \sum_{i=1}^{i=\frac{N}{2}} k_r \sin(i\gamma) + \sum_{i=N/2+1}^{i=N} k_r\sin(i\gamma - \pi) \tag{3.32}$$

$$= k_r \sum_{i=1}^{i=N} \sin(i\gamma)$$

Finally, considering the identity

$$\sum_{i=1}^{i=N} \sin(i\gamma) = \frac{\cos\left(\frac{\gamma}{2}\right) - \cos\left(\left(N + \frac{1}{2}\right)\gamma\right)}{2\sin\left(\frac{\gamma}{2}\right)} \tag{3.33}$$

and rearranging equation 3.32, it can be obtained that the stiffness for each 10 degrees section is

$$k_{\mathrm{r}} = \frac{k_{\mathrm{b}}\sin\left(\frac{\pi}{N}\right)}{\cos\left(\frac{\pi}{N}\right) - \cos\left(\left(\frac{N+1}{N}\right)\pi\right)} \tag{3.34}$$

In this case, with N equal to 36, k_{r} shows the value of 1.31×10^8 N/m. Figure 3.14 and 3.15 present the results acquired for the rotor and the stator structures utilizing the FE model.
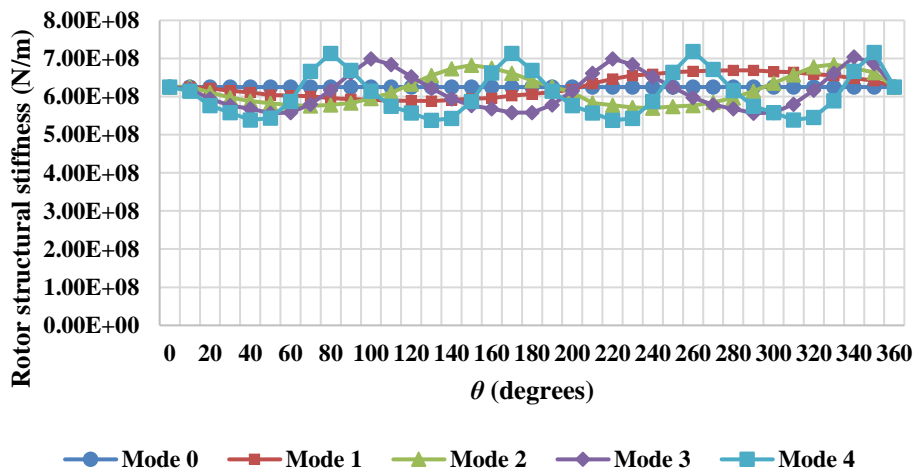
Figure 3.14 Rotor structural stiffness for deflection modes ranging from 0 to 4 vs. Theta
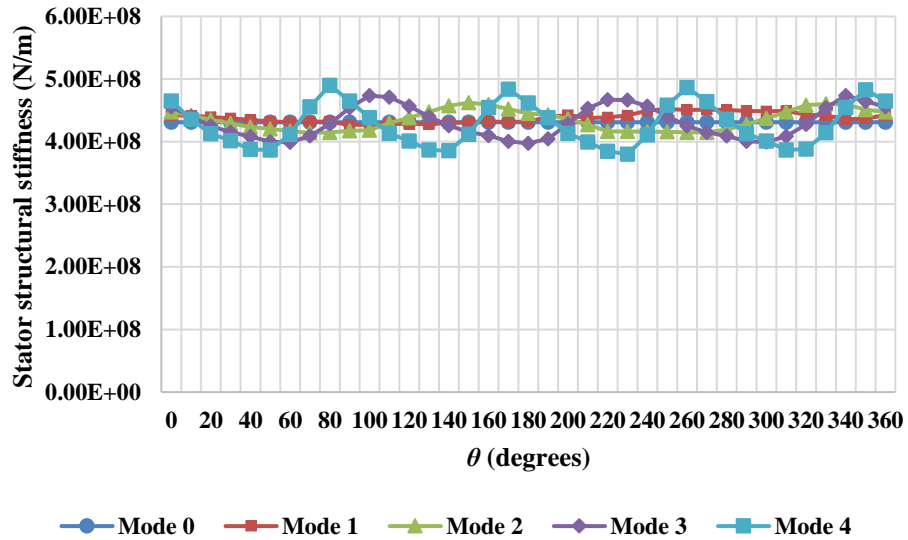
Figure 3.15 Stator structural stiffness vs. Theta

As seen, not all the waves are sinusoidal although they are periodic. Distortions are more pronounced as the mode number increases. This might be again attributed to the alterations in the structural shear stresses with the number of ripples. It can also be appreciated how the rotor structure is stiffer than the stator structure. This is because the structural geometry of the rotor, with the disc acting as a radial support, allows coping with the radial deflection more effectively than that of the stator, where the discs are placed at the edges of rim. Figure 3.16 gives the results of combining the structures in series as mentioned. If these data are compared to those achieved for the necessary magnetic stiffness introduced in Figure 3.17, it can be seen that the structural stiffness is higher than the magnetic stiffness.
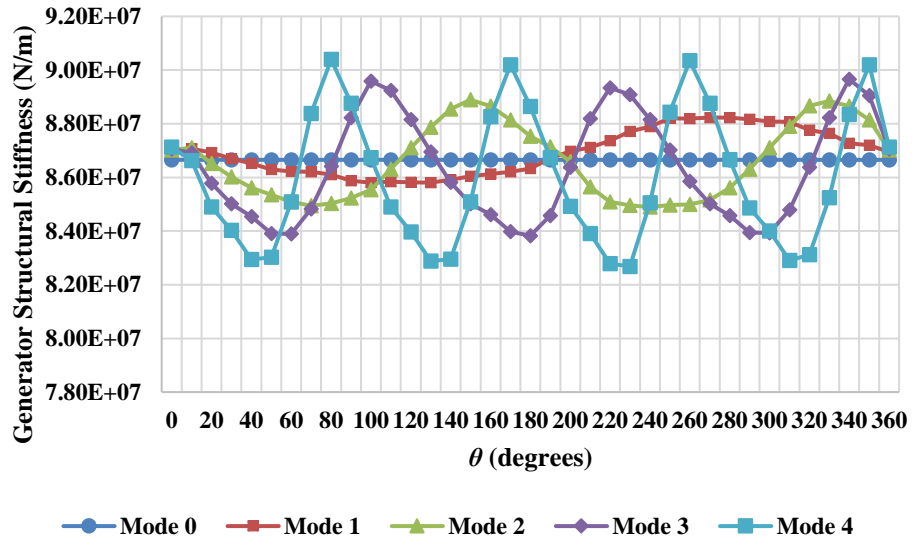
Figure 3.16 Generator structural stiffness vs. Theta

The results achieved for the generator structural stiffness vary about 8.7×10^7 N/m, whereas the magnetic stiffness for each 10 degrees β section is always around -2×10^7 N/m. As observed in Figure 3.17, the sinusoidal waves describing the magnetic stiffness for each mode are asymmetric. This means that the straight line representing Mode 0 does not go through the inflexion points of the rest of the modes and it is because of the extra factor, '$\bar{\delta} + \delta_\Delta \sin(n\theta)$', added to the denominator of the stiffness equation for the rest of the modes.
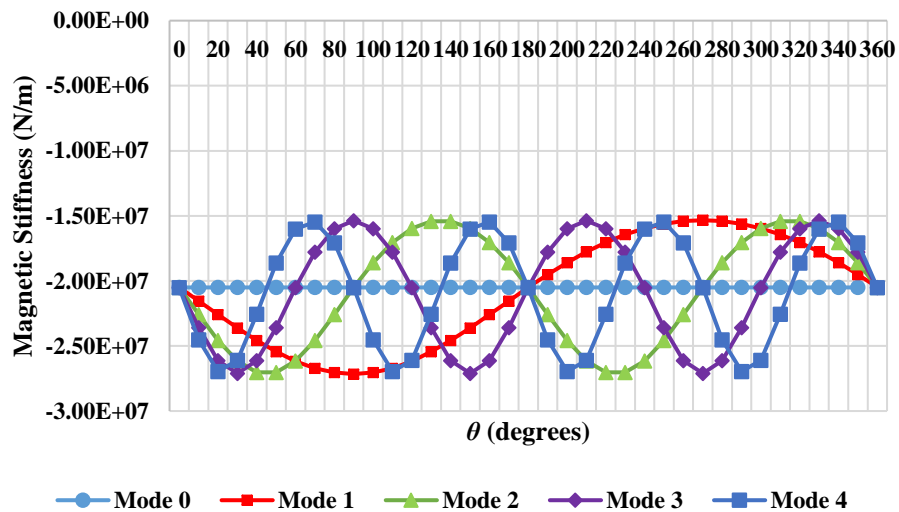
Figure 3.17 Stiffness on beta degree section

In Figure 3.19 the combination of magnetic stiffness and structural stiffness is plotted against the angle for each deflection mode. Four distinct scenarios have been analysed in order to identify the mode giving the lowest value. With $\bar{\delta}$ going from 1 mm up to 4 mm in steps of 1 mm and δ_Δ taking 0.5 mm, 0.75 mm and 1 mm values, all the options have been addressed. See Table 3.2. Since the structure geometry and material are the same, it was assumed, for simplicity, that the generator structural stiffness remains invariant with angle, 'θ', and mode, 'n', for all scenarios, although as it is shown in Figure 3.18, it does depend on the angle and on the deflection mode. As the variation is relatively small and it would only represent a slight alteration in the final result, the assumption was considered valid. Figure 3.18 illustrates the structural stiffness for all the modes and cases 1 to 4. As seen, an average value for the structural stiffness is about 6.2×10^8 N/m for all cases. Nevertheless, it is also important to highlight the fact that the stiffness varies with angle, 'θ', and that the higher the mode, the higher the amplitudes obtained. Mode 4 shows the most unstable behaviour with the lowest stiffness at 4.73×10^8 N/m, as it can be observed in Table 3.2, where the lowest stiffnesses acquired for each mode and case are illustrated. Peaks obtained in Figure 3.18(a)-(e) are because of approximation.
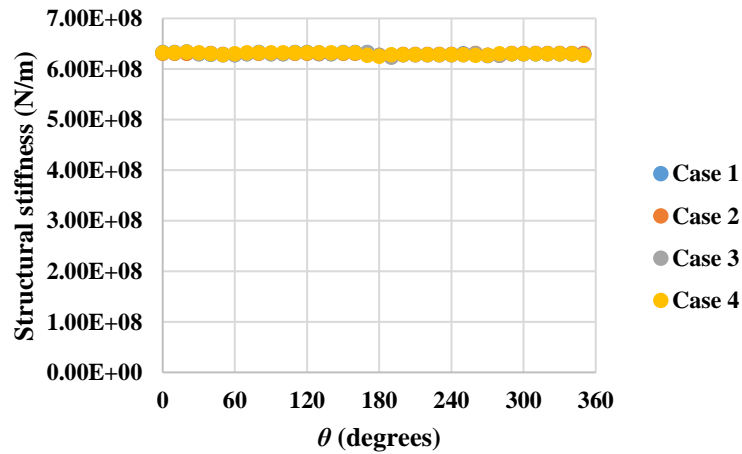
(a)
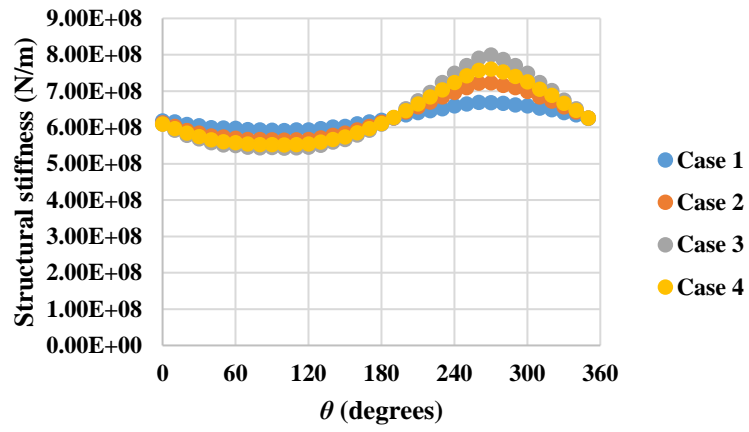
(b)
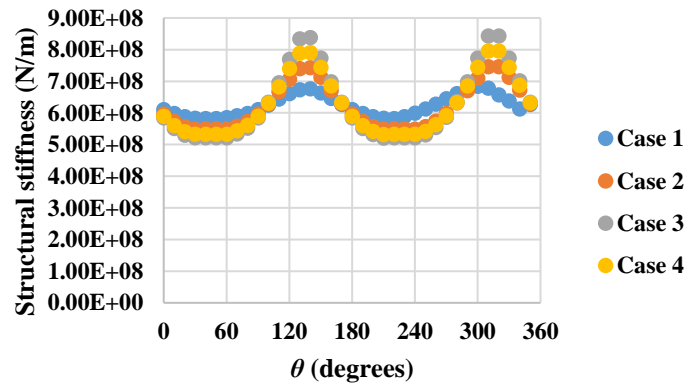
(c)
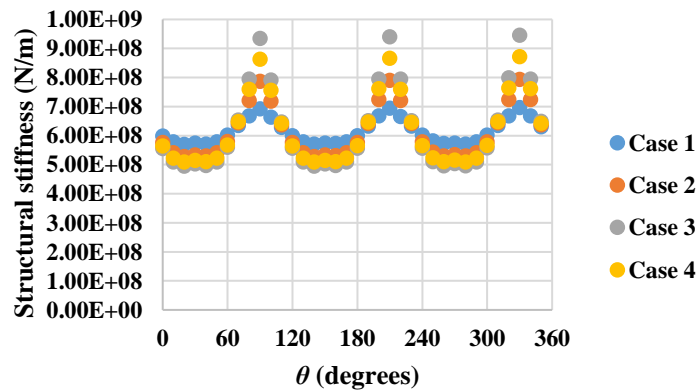
(d)
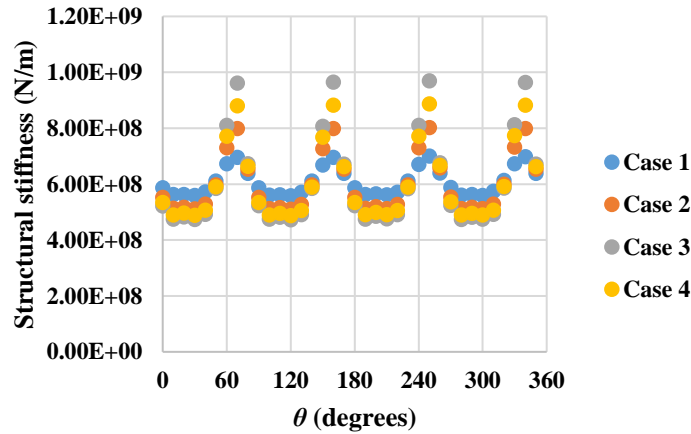
(e)

Figure 3.18 Rotor structural stiffness; (a) Mode 0; (b) Mode 1; (c) Mode 2; (d) Mode 3; (e) Mode 4

Table 3.2 gives the minimum structural stiffness per case (different $\bar{\delta}$ and δ_Δ utilized) and the mode number. If cases 1 and 3 are compared, it can be seen that an increment of 1 mm in variable deflection δ_Δ corresponds to a drop in the minimum stiffness of about 16 %. If cases 2 and 4 are contrasted, it can be observed that an increase of 3 mm in mean deflection represents a decrease in the minimum stiffness of about 5 %. This demonstrates that both deflections exert an influence of different weight over the stiffness of the generator structure.

Table 3.2 Minimum structural stiffness per case and mode

Mode	Case 1		Case 2		Case 3		Case 4	
	$\bar{\delta}=1$mm	$\delta_\Delta=0.5$mm	$\bar{\delta}=1$mm	$\delta_\Delta=1$mm	$\bar{\delta}=1$mm	$\delta_\Delta=1.5$mm	$\bar{\delta}=4$mm	$\delta_\Delta=1$mm
1	5.92×10^8 N/m		5.65×10^8 N/m		5.43×10^8 N/m		5.52×10^8 N/m	
2	5.82×10^8 N/m		5.49×10^8 N/m		5.21×10^8 N/m		5.32×10^8 N/m	
3	5.7×10^8 N/m		5.28×10^8 N/m		4.95×10^8 N/m		5.09×10^8 N/m	
4	5.58×10^8 N/m		5.1×10^8 N/m		4.73×10^8 N/m		4.87×10^8 N/m	

By looking at Figure 3.19, one can appreciate that for the worst case scenario, which corresponds to the collapse of the airgap with the stator structure physically touching

the magnets, the mode presenting the worst performance is Mode 4, having the lowest stiffness value at 5.79×10^7 N/m.
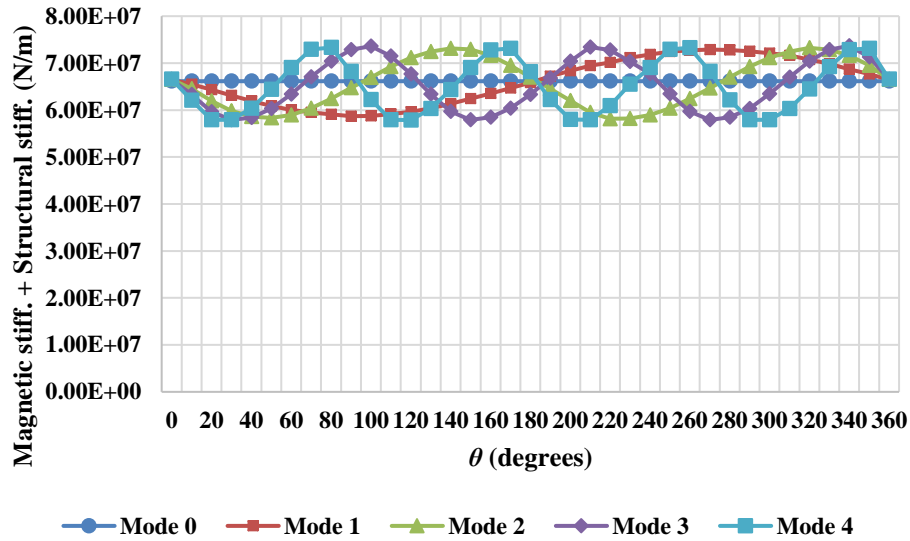
Figure 3.19 Magnetic stiffness + Structural stiffness vs. Theta for the worst case scenario
($\overline{\boldsymbol{\delta}} = 0.004$ m; $\boldsymbol{\delta}_\Delta = 0.001$ m)

It was observed that the structure selected for the study was very stiff and it is rather difficult to appreciate the overall impact of the magnetic stiffness even in the worst case scenario. By carrying out a considerable reduction in the thickness of both disc and rim sub structures of the rotor and the stator a more compliant structure was generated for its study. With higher magnetic stiffnesses, lower overall stiffnesses are achieved and it is expected to see that at some point the total stiffness reach zero values. The thicknesses used for both analyses are given in mm in Table 3.3.

Table 3.3 Thicknesses for stiff and compliant structures

Stiff structure				Compliant structure			
Rotor		Stator		Rotor		Stator	
Cylinder thickness (mm)	Disc thickness (mm)	Cylinder thickness (mm)	Disc thickness (mm)	Cylinder thickness (mm)	Disc thickness (mm)	Cylinder thickness (mm)	Disc thickness (mm)
40	56	25	56	30	40	15	40

A drop in the rotor and the stator masses of 27 % and 31 % respectively was obtained. This corresponds to a total mass reduction of 30 %, which corresponds in this case to an overall stiffness reduction of 21 %. Figure 3.20 displays the results acquired for the rotor and the stator compliant structures. As seen, the equivalent rotor stiffness average is about 4.6×10^8 N/m, whereas the stator stiffness is around 2.6×10^8 N/m.
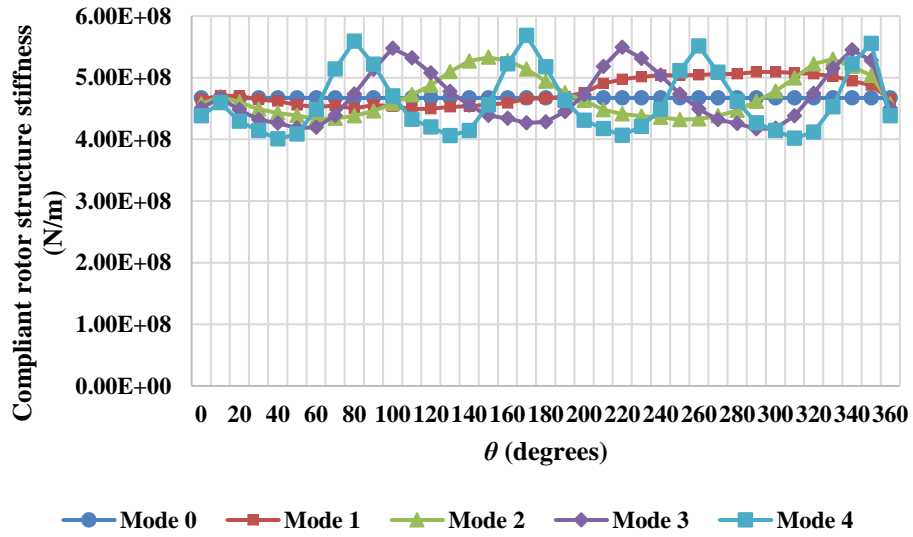
(a)
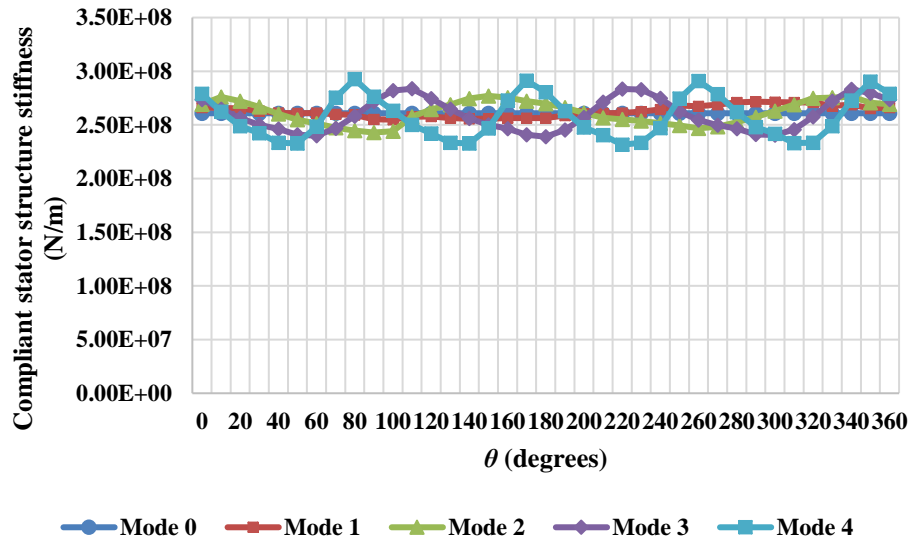
(b)

Figure 3.20 Compliant structure stiffness vs. Theta; (a) Rotor; (b) Stator

The difference between the rotor and stator stiffnesses for both structures stiff and compliant is about 2×10^8 N/m, which brings down the overall stiffness (magnetic + structural). See Figure 3.21.
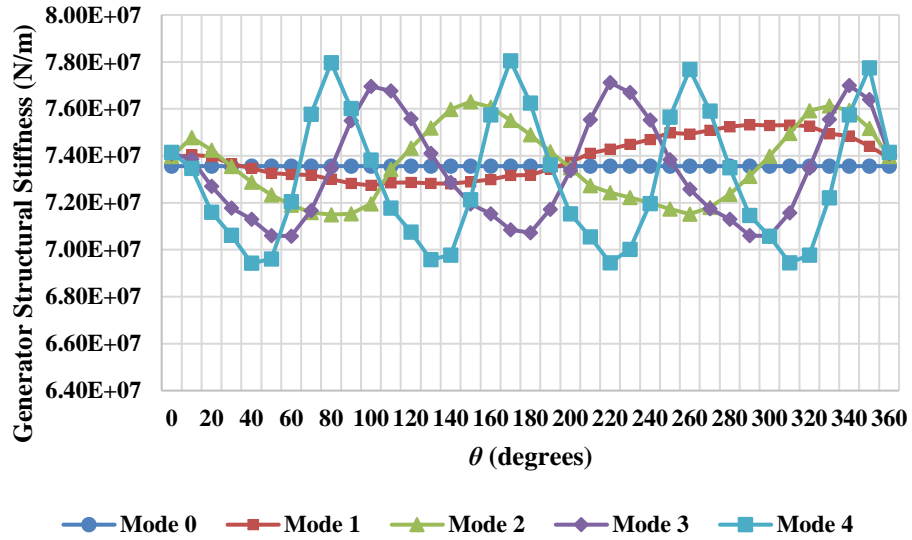
(a)
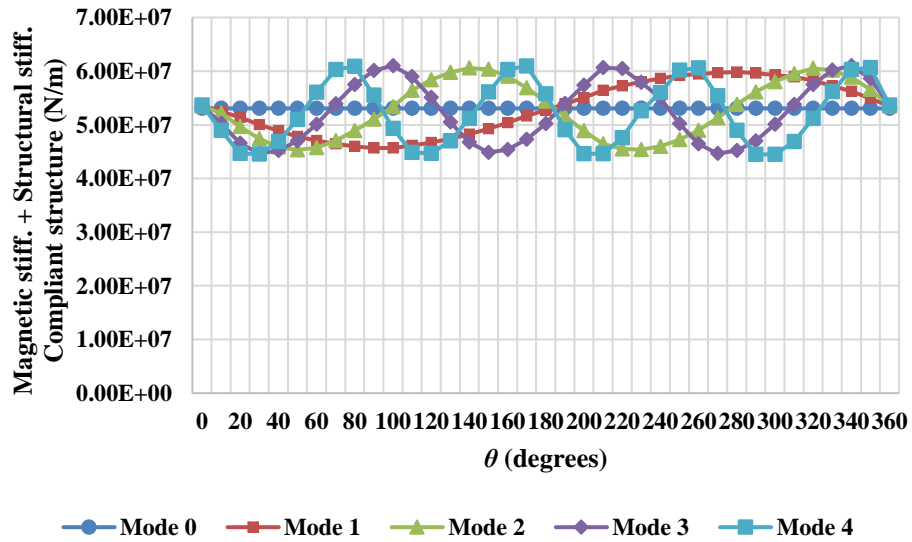
(b)

Figure 3.21 Compliant structure stiffness vs. Theta; (a) Generator structural stiffness; (b) Magnetic + Structural stiffness

In Figure 3.22, a comparison between the stiffnesses for each mode and for each structure is displayed. As observed, a drop in the minimum value of the overall stiffness of more than 1×10^7 N/m is achieved.
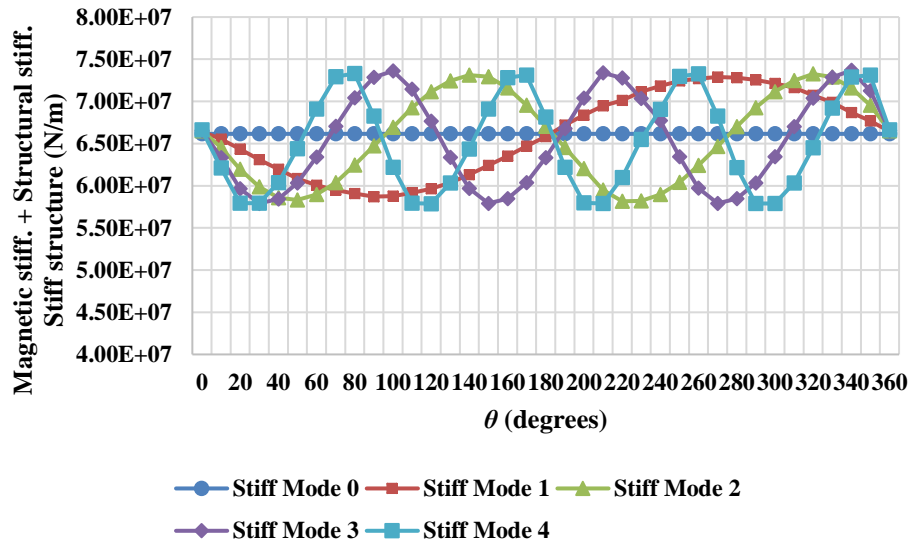
(a)
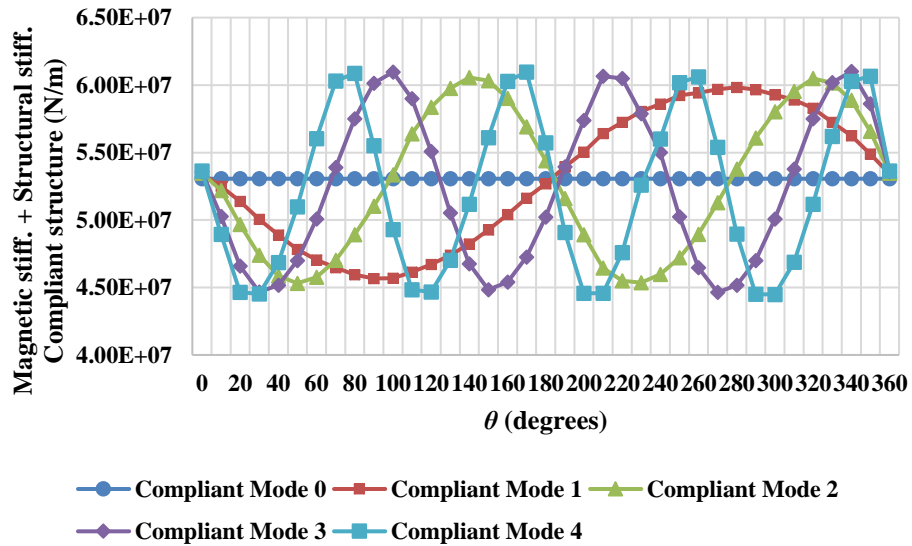
(b)

Figure 3.22 Overall stiffnesses comparison; (a) Stiff structure; (b) Compliant structure

The reduction in thickness of each sub structure forming the machine, revealed a substantial drop of stiffness for this permanent magnet generator. This shows the effect of compliant (lighter) structures and how the approach can be used in the design process.

With both structures fully described and analysed for the PM machine, the stiff structure was studied under the demanding loading conditions of a wound rotor machine. Figure 3.23 illustrates the forces applied on each β degree section. Since the effective airgap size of a wound rotor machine is smaller than that of a PM generator due to the lack of magnets attached to the rotor surface, the forces are one order of magnitude larger in all cases and for all the modes.
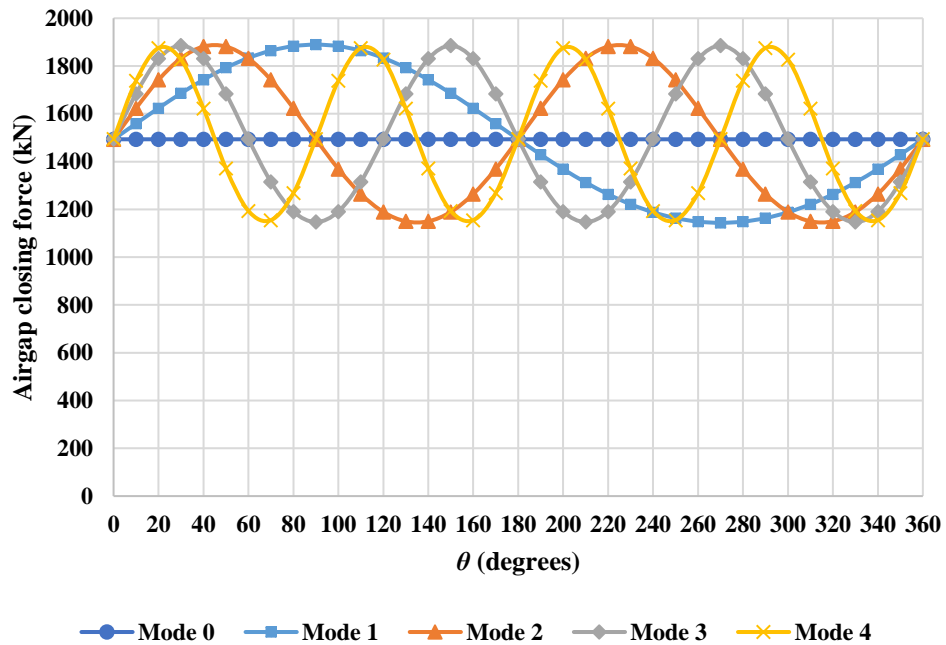
Figure 3.23 Wound rotor machine airgap closing force vs. Theta

Figure 3.24 depicts the magnetic stiffness of the wound rotor generator. Again, if it is compared to its PM counterpart it can be observed that it is one order of magnitude larger, and so it will have a profound impact on the overall stiffness.
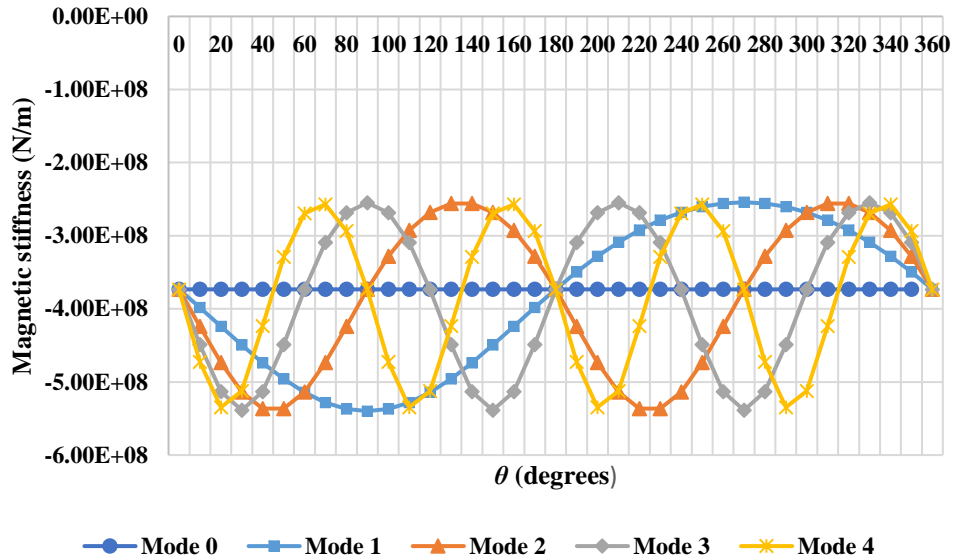
Figure 3.24 Wound rotor machine magnetic stiffness vs. Theta

As predicted, the effect of the large increase in magnetic stiffness produced a very significant drop in the overall stiffness, as seen in Figure 3.25. The negative values for the minimum stiffness means that the structure is not stiff enough to resist the loads and the airgap would close causing the collapse of the overall structure.
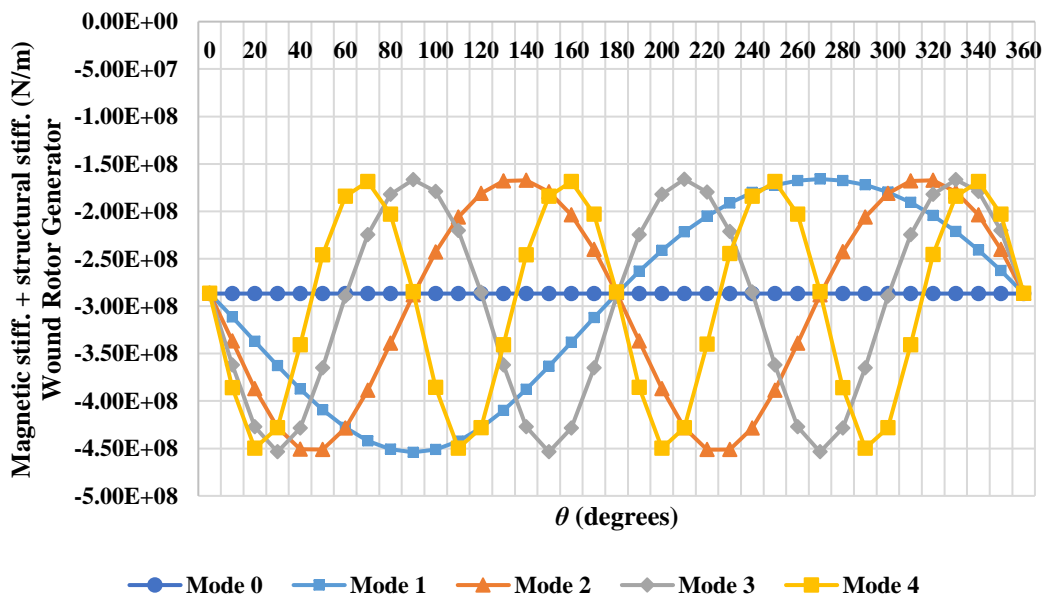
Figure 3.25 Wound rotor overall stiffness vs. Theta

3.5 Discussion

Various approaches exist in order to design a supporting structure for a wind turbine electrical generator capable of withstanding the loads. In this chapter, a stiffness model joining the magnetic and the mechanical designs has been developed. The 2D magnetic model assumes a uniform radial deflection, '$\bar{\delta}$', and a variable deflection, 'δ_Δ', that changes with angle, to estimate the resulting airgap closing force under different modes of deflection. The assumed deflection and the obtained force is then utilized to calculate the airgap stiffness. At this point, a structural model was created and making use of the computed loads a set of finite element analyses was run for a 3 MW machine with a simplified steel structure made with discs. With the deflection, the structural stiffness of the machine could be approximated. A comparison between the airgap stiffness acquired with the magnetic model and the structural stiffness determined if the generator would resist the input loading and what the stiffness margin would be.

3.5.1 Magnetic stiffness model

The magnetic model for the airgap closing force and stiffness of a PM machine was validated using a 2D finite element code. A two pole model with periodic boundaries, neglecting axial effects and geometrically linearized so that radial lines and arcs are mapped onto vertical and horizontal lines, was produced to carry out the task. Three finite element cases were generated: (i) the stator has no slots and the materials have a linear BH behaviour; (ii) the stator has slots and the materials have linear BH curves and (iii) the stator has slots and the materials have no linear BH curves. Comparing the analytical model with the idealised FE model (i), it could be observed how the analytical model underestimated the force. It was proven that the use of the fundamental MMF only, leads to neglecting higher order airgap flux density spatial harmonics and the resulting force contributions. With that, the analytical model was amended to incorporate the 3$^{\text{rd}}$ harmonic achieving better results. Nevertheless, the model did not take into consideration the slotting that according to the FE models (ii) and (iii) significantly reduced the forces. So as to

replicate this behaviour, the Carter factor was introduced into the analytical model. An excellent agreement was achieved, hence the magnetic model was considered valid. A FE magnetic model of a full PM machine was also produced for validation purposes. The retrieved data showed a very good agreement with the analytical results which reinforces the usefulness of the model. The FE magnetic studies did not include coils as it was assumed that the stator electrical connection did not have any influence in the magnetic stiffness final result. It is also necessary to highlight that the effect of the armature reaction which can weaken or strengthen the airgap flux density affecting the airgap closing force was not considered either.

3.5.2 Permanent magnet and wound rotor machines

Two distinct types of generators were analysed: a permanent magnet machine and a wound rotor machine. The main reason to make this differentiation was that a permanent magnet generator has a certain number of magnets attached to the rotor surface that increases the effective size of the airgap $(g + \frac{h_\mathrm{m}}{\mu_\mathrm{r}})$, whereas a wound rotor machine is electrically excited and thus the effective airgap size is equal to the physical airgap clearance 'g'. This means that the existing attractive forces in the airgap of a wound rotor machine are larger than the forces acting on the airgap of a permanent magnet generator. Having this in mind, it can be said that a stiffer and more robust structure is necessary for a wound rotor machine which in turn leads us to have a heavier generator. On the other hand, it is also essential to highlight the fact that the magnetic design of a PM machine can be designed to avoid saturation in the default state, while when a wound rotor machine airgap closes the iron parts of the magnetic circuit go deep into saturation bringing about significant reluctance.

3.5.3 Structural stiffness model

As mentioned, the magnetic study of both machines was completed first assuming a uniform radial deflection and variable deflection which changes with angle, 'θ'. Looking at the results obtained for both cases, it could be understood their effect on the magnetic, structural and overall stiffnesses. The increase of $\bar{\delta}$ supposes a

noticeable decrease in the absolute values of the maximum and minimum magnetic stiffness, whereas the increment in force as the airgap closes causes a substantial reduction of the structural stiffness that puts down the overall stiffness. If δ_Δ is augmented, the absolute value of the maximum magnetic stiffness increases while the minimum stays at the same level. The structural stiffness diminishes and the overall stiffness affected by the increase in the magnetic stiffness and the drop in the structural stiffness goes down although it never reaches a zero value, which means that the structure is eventually very stiff and it would easily support the imposed loading conditions. A more compliant structure was also looked at. A total reduction in mass of 30 % was accomplished. That meant a decrease of 27 % in rotor mass and 31 % in stator mass. After the analysis, it could be observed that the drop in mass corresponded to a decrease in the overall stiffness of 21 %. This gives a clear picture of the trade-off process that should be made during an optimization study. For these analyses it was assumed, for simplicity, that the structural stiffness was totally invariant although it has been demonstrated that it changes with deflection mode, deformation and angle. Nonetheless, as the variation is very small and it would only represent a slight alteration in the final result, the assumption was considered valid.

3.5.4 Modes of deflection

Mode number was another factor that had a significant impact on the distinct stiffnesses. In case of the magnetic stiffness, it could be seen that despite of having different frequencies, all the modes but Mode 0 shared the same maximum value. Mode 0 appeared as a straight line (due to its constant uniform load applied) coinciding with the inflexion points of the curves corresponding to the rest of the modes. Similar behaviour was noticed for the structural and overall stiffnesses, although in the case of the structural stiffness, Mode 4 stood out showing the worst performance with the minimum stiffness at 8.29×10^7 N/m for the stiff structure and 6.94×10^7 N/m for the compliant structure. The overall stiffness presented the same type of shape as the magnetic stiffness, with all the modes but Mode 0 having the same minimum value, which takes us to think that high order modes have to drive the design of any type of electrical machine.

However, it is thought that the model can be utilized not only during the design stage but also after manufacturing and during operation as part of an online airgap condition monitoring system. Manufacturing defects can make the machine more prone to deform following certain patterns, which would turn into high order deflection modes. The model would be able to predict the airgap behaviour and its suitability for operation. As part of a condition monitoring system, the model would be capable of evaluating the time-varying output data and assessing the structural integrity of the machine.

3.6 Conclusion

A stiffness model coupling the electromagnetic and mechanical designs of wound rotor generators and surface mounted permanent magnet machines has been developed. The results of the validation with the FE model showed the usefulness and accuracy of the magnetic analytical tool. In addition, the parametric nature of this analytical model makes it easy to use helping the designer to carry out quick estimations for any deflection mode or deformation, in the early stages of the design or after the manufacturing process. It could also be very handy for optimization purposes or as part of an online condition monitoring system as it could assessed the structural integrity of the machine at any time. On the other hand, it is important to point out that this is a linearized 2D model, which neglects the axial end effects. The dynamic behaviour of the machine is not captured either by the model and no external forces have been considered.

With a view to improve the accuracy of the model, it is thought that all of these features should be included.

Regarding the mechanical model, which is fed by the finite element analyses retrieved data, it can be concluded that it is suitable to calculate the generator structural stiffness. It was assumed that the structural stiffness was invariant although it could be seen that it changes with deformation, '$\bar{\delta}$' and 'δ_{Δ}', deflection mode, 'n', and angle, 'θ'. However, it was observed that the variations were very small and therefore only a slight alteration in the total stiffness result would be obtained. On the

other side, it is thought that the assumption of a constant stiffness for the bearing introduces inaccuracies into the tool. Having said that, the author believes that an accurate stiffness model of the bearing should also be generated and introduced.

A comparison between a very stiff structure and a more compliant structure was made in order to understand the effect of mass reduction in the overall stiffness. It could be seen how for a PM machine both structures were capable of withstanding the loads although it was observed that the compliant structure had more difficulties. In the wound rotor machine case, it could be seen how even the stiff structure was not able to successfully support the loads. Taking this into consideration, the use of the stiffer structure could be associated to a wound rotor machine, while the use of the more compliant structure can be related to a permanent magnet generator due to the inherent characteristics of the wound rotor generator make it more structurally demanding than a permanent magnet electrical machine subject to the same deflection. Hence, it can be concluded that a wound rotor electrical machine is heavier than a permanent magnet generator.

Magnetic and structural stiffnesses were combined together and plotted against the angle in search of the most dangerous mode. By varying the mean and the variable deflection values, twelve different scenarios were assessed obtaining that Mode 4 is the most damaging. Bearing this in mind, designers can tailor the structure with a view to resist this mode in the lightest manner, by just introducing stiffeners in the corresponding direction, by modifying the geometry of the structure or by utilizing distinct structural materials with higher Young's modulus to density ratios.

3.7 References

[1]   A. S. McDonald , M. Mueller and H. Polinder, "Structural mass in direct drive permanent magnet electrical generator," IET Renewable Power Generation Special Issue- Selected Papers from EWEC 2007, vol. 2, no. 1, pp. 3-15, March 2008.

[2]   A. S. McDonald, "Structural analysis of low speed, high torque electrical generators for direct drive renewable energy converters," PhD thesis, University of Edinburgh, Edinburgh, 2008.

[3]   P. J. Tavner and E. Spooner, "Light Structures for Large Low-Speed Machines for Direct-Drive Applications." in *Proc. International Conference on Electrical Machines*, Chania (Greece), 2006.

[4]   P. Jaen-Sola and A. S. McDonald, "Structural Analysis and Characterization of Radial Flux PM Generators for Direct-Drive Wind Turbines", *3rd Renewable Power Generation International Conference (RPG 2014)*, Naples (Italy), Sept. 2014.

[5]   FEMM 'Finite Element Method Magnetics', www.femm.info/, [Online] Last Accessed 28/02/2017.

Chapter 4

Comparison of Methods for Estimating Generator Structural Stiffness

4.1 Introduction

Minimising the structural mass of low speed multi MW electrical machines for renewable energy purposes have become an important object of study as with the reduction in mass a substantial decrease in the machine capital cost can be achieved [1]. In [2], Grauers introduced a procedure which estimated the final cost of a

generator based on its diameter and length, compared to dimensions of reference structures. The excessive weight of the generator structure was highlighted by Hartkopf *et al*. who claimed that 2/3 of a direct drive radial flux electrical machine mass corresponded to the inactive material [3]. Mueller, McDonald and MacPherson claimed in [4] that at multimegawatt ratings the inactive mass of a direct drive axial flux machine it is almost 90 % of the total mass. Several studies have been written on this regard presenting different approaches that can be utilised when designing this type of machines in order to minimize their structural mass [5][6]. Some of them have been already mentioned in Chapters 2 and 3. In these studies, analytical and numerical analysis techniques were used with the main aim of finding the minimum required stiffness so that the machine can withstand the loads. As known, the structural stiffness is the ratio between the force applied on a body and the deflection produced by the force along the same degree of freedom. By having the minimum stiffness, the designers are able to estimate the minimum structural mass in a low cost and fast manner. On the other side, there are studies which suggest the use of magnetic and other innovative types of bearings to reduce the mass [7][8][9]. New lightweight concepts have been also proposed, such as the NewGen one, where the bearings are placed adjacent to the airgap so as to resist the loads and reduce the structural stiffness demand in the rotor, the stator and the shaft [10]. Although these are very promising options, the use of any of these elements have not been included in the analyses presented in this thesis.

The main objective of this chapter is to explain and present the results obtained from analyses carried out using three different approaches to estimate the minimum machine structural stiffness: finite element, analytical and hybrid method. This is a new concept that consists of combination of the data retrieved from finite element studies and the outcomes acquired from dimensional homogeneity analyses. In Section 4.2, a hierarchy of the methods will be given according to their suitability, reliability and speed to accurately estimate the generator stiffness. A description of the techniques and how and where they can be applied is also included in this section. The results obtained from the analyses carried out with these methods over three different structural layouts are presented in Section 4.3. A disc structure arrangement offering the best structural performance under certain loading

conditions will be also tested under distinct modes of deflection. Finally, a further optimisation of the said structure will be made employing finite element tools. A detailed discussion about the data achieved will be introduced in Section 4.4, whereas the drawn conclusions will be presented in Section 4.5.

4.2 Estimating minimum generator structural stiffness

4.2.1 Finding Structural Stiffness through the Combination of Sub Structures Stiffness

The structural stiffness either of the rotor or the stator can be calculated by putting their sub structures together, in series or in parallel as it has been described in Chapter 3. When looking at a rotor or stator structure one can identify coherent structural elements that lend themselves to separate evaluation of stiffness. For instance, the stiffness of a rotor disc structure could be estimated combining in series the stiffness of the disc and the stiffness of the cylinder as follows,

$$k_{s,r} = \frac{k_{s,d}k_{s,c}}{k_{s,d} + k_{s,c}} \tag{4.1}$$

and the total structural stiffness of the generator must be either equal to or higher to k_M (magnetic airgap stiffness) as explained in [11]. A graphical representation of how the rotor structural stiffness can be combined is displayed in Figure 4.1.

Figure 4.1 Rotor structure split into disc and cylinder models [9]

Bearing this in mind and looking at the entire wind turbine, a complete structural stiffness model was defined in the previous chapter employing equations (4.2a) and (4.2b),

$$k_{\mathrm{eq,r}} = \frac{k_{\mathrm{s,r}}k_{\mathrm{b}}}{k_{\mathrm{s,r}} + k_{\mathrm{b}}} \qquad (4.2\mathrm{a})$$

$$k_{\mathrm{s}} = \frac{k_{\mathrm{eq,r}}k_{\mathrm{s,s}}}{k_{\mathrm{eq,r}} + k_{\mathrm{s,s}}} \qquad (4.2\mathrm{b})$$

where $k_{\mathrm{eq,r}}$ and k_{s} correspond to the equivalent rotor structure stiffness and the total structural stiffness, respectively.

So as to satisfy equation (4.2b) with the minimum mass, it is necessary to find a way of evaluating the structural stiffness and mass of rotor and stator structures.

There exist different procedures to calculate the structural stiffness needed by an electrical machine. A hierarchy should be defined considering the advantages and drawbacks of each one. Among the three techniques described in this section, the most sophisticated is the FE method as it is capable of capturing geometric, loading and material features, as well as giving very accurate data. However, this approach is computationally expensive and time consuming and is more suited for final design analysis, rather than early stage optimisation.

The analytical methods presented in this section are able of giving accurate results for Mode 0 and Mode 1 deflection of sub structures, such as arms, in a much quicker manner. In order to estimate the stiffness of advanced structures it is often necessary to combine the stiffness of different sub structures in series. Typically, these analytical tools are precise when the geometry is simple and the loading corresponds to Mode 0. No analytical tools have been proposed for higher modes.

The hybrid procedure combines the data retrieved from dimensional homogeneity studies and a limited number of FE results and fits functions to the outcomes. It is also much quicker than the FE approach and it is able to generate precise results for Mode 0 and Mode 1 deflection of sub structures. This technique is more suited for individual elements as additional independent variables make the function fitting much more challenging although high precision results can also be obtained for complete structures.

4.2.2 A Case Study Generator

For this investigation, a 3 MW machine made up of steel of 4 m diameter and 1.2 m axial length, rotating at 12.7 rpm, as shown in Figure 4.2, has been utilised. In order to estimate the stiffness, dimensions t_c and t_d in the case of the disc structures and $t_{c,a}$ and t_{arm} for the armed structures have been varied. Afterwards, FE studies were carried out so that the radial deflection could be obtained.
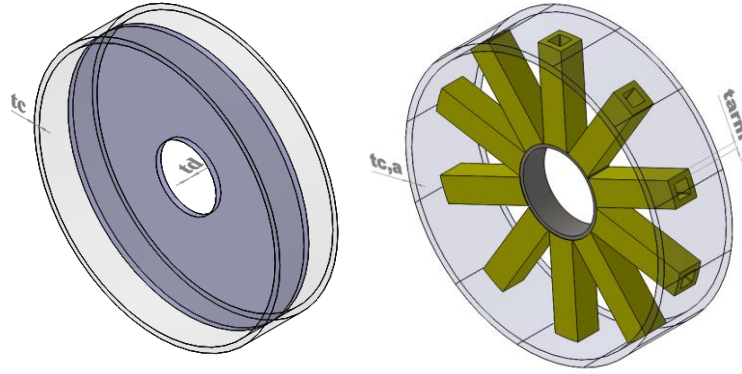
Figure 4.2 Rotor structures with thickness dimensions as altered in this analysis (a) Disc structure (b) Arm structure [12]

Mass of the rotor and stator disc structures was found out with equations (4.3a) and (4.3b), whereas mass of the rotor and stator armed structures was computed using equations (4.4a) and (4.4b).

$$m_{s,r} = \rho[\pi((R + t_c)^2 - R^2)l + \pi(R^2 - r^2)t_d] \tag{4.3a}$$

$$m_{s,s} = \rho[\pi\left((R + t_{s,c})^2 - R^2\right)l + 2(\pi(R^2 - r^2)t_{s,d})] \tag{4.3b}$$

$$m_{s,ar} = \rho[\pi\left((R + t_{c,a})^2 - R^2\right)l + n_{arms}((4t_{arm}w - 4t_{arm}^2)l_{arm})] \tag{4.4a}$$

$$m_{s,as} = \rho[\pi\left((R + t_{c,as})^2 - R^2\right)l + 2(n_{arms}((4t_{arm}w - 4t_{arm}^2)l_{arm}))] \tag{4.4b}$$

Where r is the radius of the shaft and w is the width of the arm structure.

4.2.3 Analytical characterisation of disc and arm structures

Different approaches are available to characterize disc and armed structures. Whereas the use of FE techniques bring on certain difficulties that have been explained in Section 4.2.1, analytical approaches allow the user to find the structural stiffness of the components by introducing their dimensions and their material characteristics into the equation. This technique has been already employed by other authors. For instance, in [5], McDonald derived and validated (using finite element methods) a series of equations for rotor and stator structures made with arms or discs, that can be utilised to accurately calculate their radial deflection under Mode 0 loading and their axial deflection due to gravity for a wide range of dimensions and materials. In this sub section, the author has focussed his attention on the calculation of the stiffness of sub structures, such as discs and arms, under distinct modes of deflection.

Rotor disc model: central hole and loaded boundary

The approach proposed by Benham *et al.* has been used in this paper to examine the stiffness for the disc structure. In [13], the authors assumed a disc structure with a central hole and unloaded boundaries that rotates at a constant velocity and therefore is subjected to stresses induced by centripetal acceleration. Since the approach presented in this paper considered a disc structure with a central hole subject to an expansion load uniformly distributed along its edge and $\omega \to 0$, Benham's model was to some extent modified to match these features and help corroborate the models. The stress-strain relationship is,

$$\varepsilon_r = \frac{\sigma_\mathrm{r}}{E} - \frac{\nu\sigma_\theta}{E} \tag{4.5}$$

with σ_r and σ_θ being the radial stress and the angular stress respectively. If no motion is considered, the radial stress can be calculated either

$$\sigma_\mathrm{r} = X - \frac{Y}{R^2} \tag{4.6a}$$

$$\sigma_\mathrm{r} = X - \frac{Y}{r^2} \tag{4.6b}$$

Any of the following equations can also be utilised to find the angular stress, $\sigma_\theta = X + \frac{Y}{r^2}$ or $\sigma_\theta = X + \frac{Y}{R^2}$.

With no load acting on the central hole

$$X = \frac{Y}{r^2} \tag{4.7}$$

Replacing this into equation (4.6a) and rearranging then

$$Y = \frac{\sigma_r}{\left(\frac{1}{r^2} - \frac{1}{R^2}\right)} \tag{4.8}$$

Radial strain displacement for axial symmetry gives

$$\varepsilon_r = \frac{du}{dr} = \frac{\Delta R}{R} \tag{4.9}$$

Rearranging equation (4.9) and substituting ε_r in equation (4.5) the following results can be achieved,

$$\Delta R = \left(\frac{Y\left(\frac{1}{r^2} - \frac{1}{R^2}\right)}{E} - \frac{v\left(X + \frac{Y}{R^2}\right)}{E}\right) R \tag{4.10}$$

$$k_d = \frac{\sigma_r 2\pi t_d E}{\left(\sigma_r - v\left(\frac{(R^2 + r^2)\left(\frac{\sigma_r}{\frac{1}{r^2} - \frac{1}{R^2}}\right)}{r^2 R^2}\right)\right)} \tag{4.11}$$

A comparison between the results acquired from FE analyses and those achieved with the equation is shown in Section 4.3.2.

4.2.4 Modelling structural stiffness: Finite Element Analysis

Complete rotor and stator structure models were studied utilising finite element methods. For the analyses, the model was constrained at the shaft and evaluated for Mode 1. Considering the variations of the flux density within the electromagnetic circuit, a maximum normal stress of 411 kPa was located on the top of the structure

while the minimum normal stress (335 kPa) was placed at the bottom with the stress varying sinusoidally. To apply the loads correctly, the rim sub structure was divided into 36 parts (of 10 degrees each). This helped us later to deal with different deflection modes without making major changes into the initial model. Note that the maximum structural deflection was limited to a 10 % of the airgap size in any direction. The thicknesses of the cylinders, t_c, the thicknesses of the discs in the case of the disc structures, t_d, and the thicknesses of the arms in the case of arm structures, t_{arm}, were changed and the obtained FE values plotted. For the armed structures, 10 ties of width, $w = 0.35$ m, were employed. In order to carry out the optimisation, a fine tetrahedral mesh with an element size as suggested by the software was used.

a) Rotor analysis

The structure was studied as explained above. Figure 4.3 illustrates a disc rotor structure model constrained at the shaft with a radial load acting on it at the left side and an arm rotor structure at the right side. The material characteristics of this structure made up of steel are: Young's modulus, $E = 2.1 \times 10^{11}$ Pa, Poisson's ratio, $v = 0.3$ and density, $\rho = 7850 \frac{kg}{m^3}$.
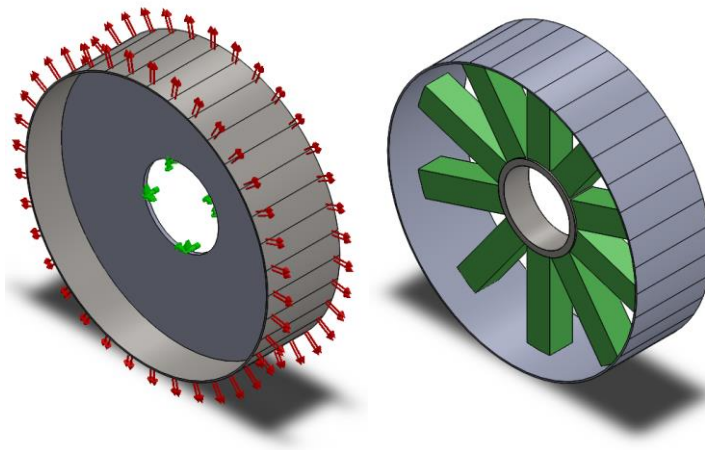
Figure 4.3 Rotor model; Disc structure showing loading conditions and constraints (left side); Arm structure (right side)

b) Stator analysis

For the stator structures the same methodology was put in practice. A sinusoidally distributed compression load acts on the inner face of the stator cylinder, as it is shown in Figure 4.4 (left side). Both discs and arms assemblies are constrained at the shaft. The material properties of these structures are the same as those of the rotor structure.
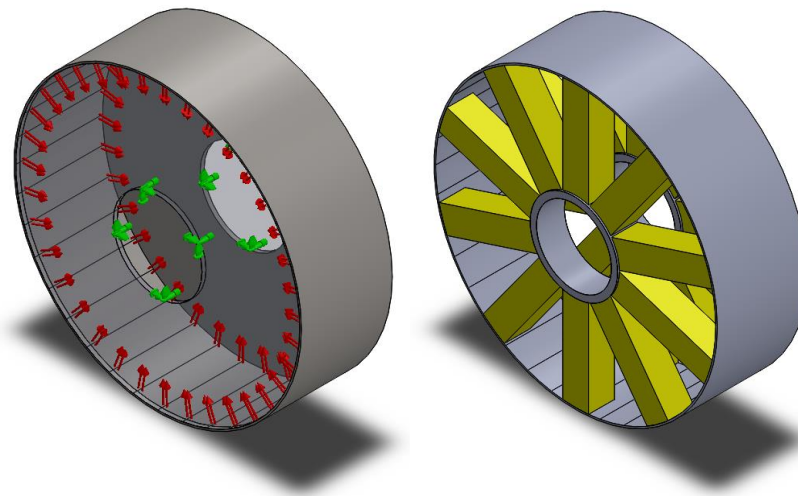
Figure 4.4 Stator model; Disc structure showing loading conditions and constraints (left side); Arm structure (right side)

c) Conical rotor analysis

Although the main purpose of this section is to look at the mentioned type of structures, conical rotor structures have been also proposed in this sub section. Conical rotor structures have been already suggested by other authors, such as Stander in [14], due to the superior axial stiffness that the geometry introduces, as well as, its inherent radial stiffness provided by the cone sub structure. Nonetheless, it is worth highlighting that the optimisation of a rotor cone structure includes other variables that make it more tedious to study. These variables are the position of the cone and the angle of the cone. See Figures 4.5 and 4.6. A rotor cone structure of 4 m diameter and 1.2 m of axial length made of steel was modelled in SolidWorks for its optimisation. Then the structure was constrained at the shaft and the same loading conditions as applied to the disc structure utilised. The element size suggested by the

piece of software for the tetrahedral mesh was accepted. The optimisation process and the results achieved are described and presented in Section 4.3.

| **(1)** | **(2)** | **(3)** | **(4)** | **(5)** |
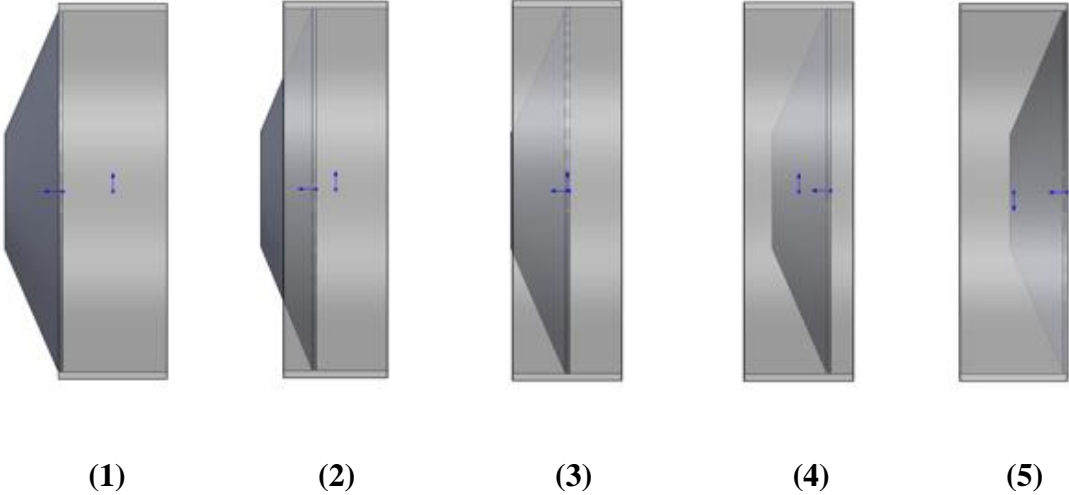
Figure 4.5 View of the different positions for the cone sub structure

Figure 4.6 illustrates the rotor conical structure showing the dimensions as altered in the study. The angle 'ψ' is shown as well for clarification.
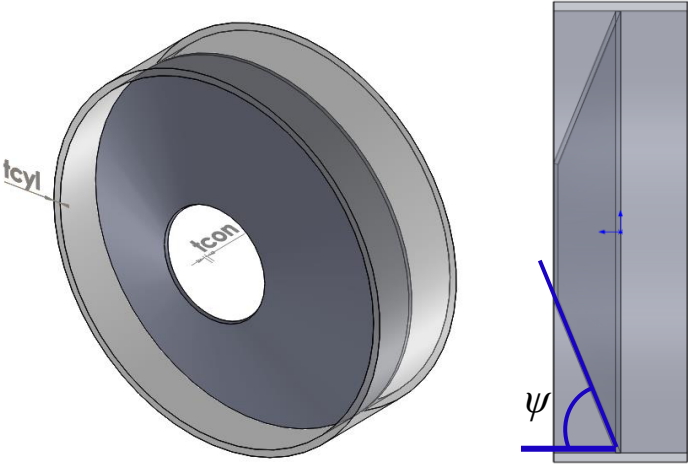
Figure 4.6 Rotor conical structure as altered in the study

4.2.5 Modelling structural stiffness using a hybrid technique: Rotor disc model

Looking at the rotor components separately is possible to find physically meaningful algebraic equations that describe with precision their structural behaviour. In this thesis, analytical techniques based on the principle of dimensional homogeneity have been used [15]. In the case of the disc structure, if it is assumed that its stiffness depends on the Young's modulus, E, thickness, t_d, Poisson's ratio, v, and R-r, where r is the radius of the shaft, we can proceed as follows. Let

$$[k_d] = [E^a t_d^b (R - r)^c] \qquad (4.12)$$

Replacing the dimensional combination for each factor in terms of $[F]$, force, and $[L]$, length, it can be obtained that

$$[FL^{-1}] = [F^a L^{-2a} L^b L^c] \qquad (4.13)$$

Note that the Poisson's ratio is a dimensionless variable.

Equating powers it is obtained that a=1 and -1=-2a+b+c. It can be observed that the analysis is unable to tell the powers of the thickness and the length. Nevertheless, they can be estimated by looking at how they vary with the stiffness, which was approximated using the FE data that were validated with Benham's model. The implementation of a constant was necessary so that the equation could be finally balanced.

$$k_d = \frac{C_1 t_d^2 E (1 + v^2)}{(C_2 t_d + L)\gamma} \qquad (4.14)$$

where $C_1 = 4160$ and $C_2 = 400$. Note that a dimensionless variable, γ, which depends on the mode of deflection, has also been introduced. With it, the stiffness of the rotor components can be calculated taking into consideration the deflection mode. γ is equal to $\frac{\sigma_{radial,max}}{\sigma_{radial,min}}$.

A comparison between the results for Mode 0 obtained with equation (4.14) and data retrieved from the FE simulation studies is shown in Figure 4.7. As it can be seen, a

good agreement was achieved over the whole range. The relationship acquired from the linear regression was $y = x$, with $R^2 = 0.9945$.
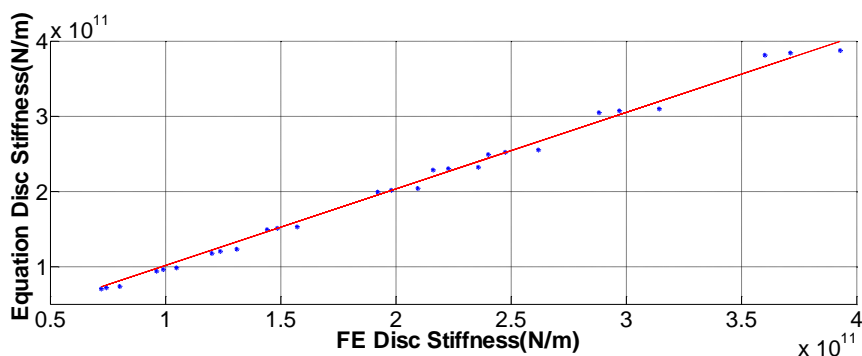
Figure 4.7 Equation vs. FE disc stiffness [11]

4.2.6 Structural optimisation

A detailed description of the different methods that can be used to estimate the minimum required stiffness and structural mass of an electrical machine has been given. Nevertheless, other ways of further reducing the mass of the structure exist. In this section, the shape optimisation add-on tool available in ANSYS Workbench© is presented. Both small and large scale generator structures have been looked at in this chapter. An optimisation study of a small scale generator structure made of steel was run first in order to verify the usefulness of the said tool. Moreover, the creation and analysis of a small scale model at first instance was considered good practice and it could be utilised for other purposes in the future. A 100 kW electrical machine with 0.42 m radius, 0.21 m axial length, 2.08 mm airgap, 140 rpm rotor speed and 6.8 kNm torque was assumed. With a radial expansion load of 400 kPa and a tangential load of 30 kPa applied on the outer face of the rim structure and a gravitational load applied globally according to the Y axis, the shape optimisation study was made. After constraining the structure at the shaft, a fine tetrahedral mesh was produced, and as it can be seen, the red elements, which are mostly placed within the disc sub structure, are the ones that can be removed. See Figure 4.8.

114
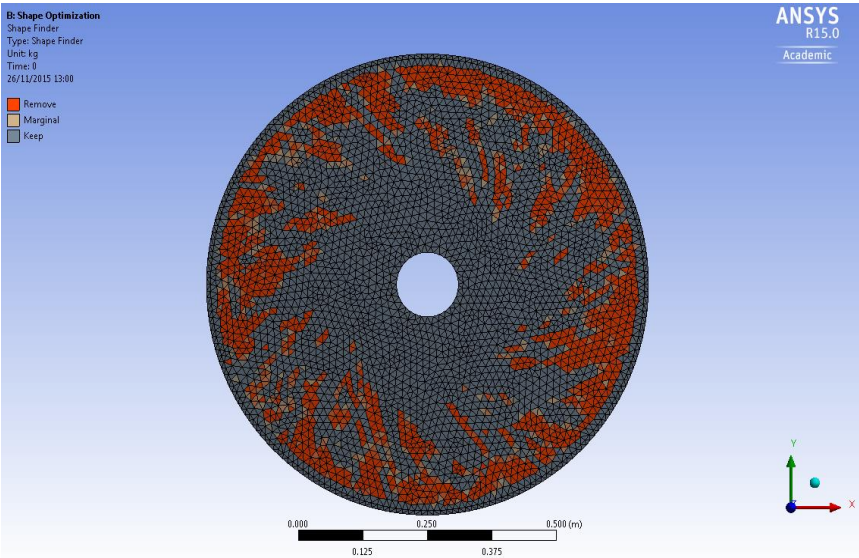
(a)
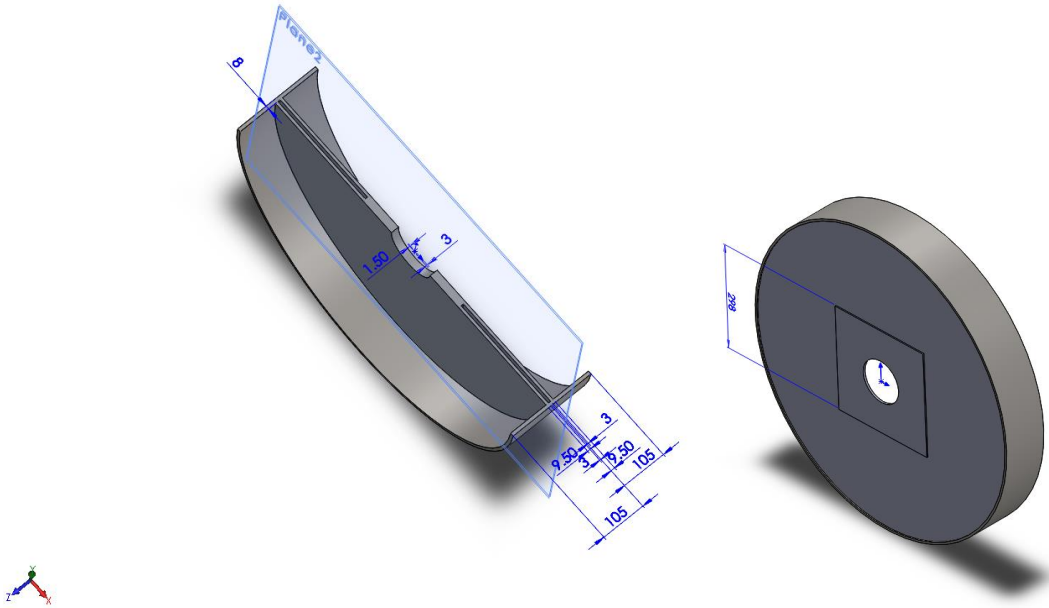
(b)

Figure 4.8 Rotor structure shape optimisation; (a) Rotor structure highlighting the elements to be eliminated; (b) Cutouts of the optimised rotor structure (dimensions shown in mm)

Linking the result to a CAD model in SolidWorks with the same dimensions and material characteristics a handmade removal of material was carried out always taking into consideration the deflection limit, which in this case corresponds to 0.208 mm. An elimination of 6 mm of material could be done for the disc. The same

procedure was followed for the stator acquiring similar data. Having a 6 mm cylinder thickness and 12 mm thickness discs, a removal of 7.5 mm of material from each disc, as it was done with the rotor, could be accomplished. The total mass for a steel generator structure being able to withstand the mentioned loads without deforming more than as stated, is 313.22 kg with 114.76 kg for the rotor and 198.46 kg for the stator. After further optimisation using the ANSYS shape optimisation tool an overall reduction in mass of about 15 % can be achieved. The final structural mass would be 266.7 kg with 91.1 kg for the rotor and 175.6 kg for the stator.
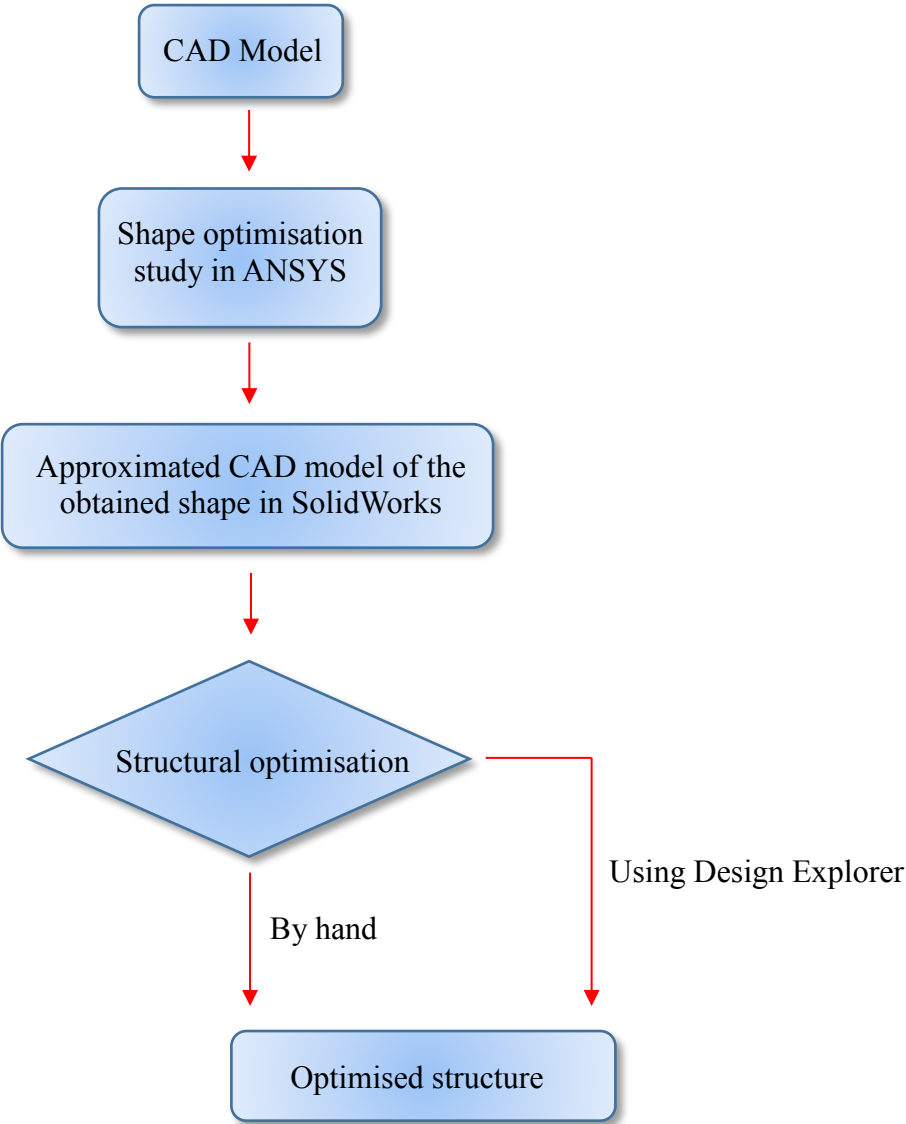
Figure 4.9 Flowchart of the structural topology optimisation process

Figure 4.9 shows a flowchart of the structural topology optimisation process as it was followed. Two different ways of approaching the structural optimisation can be tracked: by hand or using the Design Explorer ANSYS tool coupled to the model in SolidWorks. The first procedure was used to optimise the small scale model, whereas the second was utilised to optimise the large scale one. See Section 4.3.5. Models with relative simple shapes can be easily optimised by hand. However, when the shapes are more complex, the use of an instrument that standardizes the process as Design Explorer does is necessary.

4.3 Results

In this section, outcomes obtained by the three distinct types of methods are given. The FE technique is shown first and the data are utilised as a benchmark to validate the other approaches.

4.3.1 Finite element approach

Figure 4.10 (1), (2), (3) and (4) are contour plots for the disc and arm rotor and stator structures displaying their stiffness for different sub structures thicknesses. In the generator disc structure case, the variables are the thicknesses of the disc and the cylinder sub structures that have been altered as seen in the figure. With the disc thickness in the Y axis and the cylinder thickness in the horizontal axis, the coloured lines plotted represent stiffness. In the case of the generator with arm rotor and stator structures, the variables are the arm sub structure thickness and again the cylinder thickness. As said in Section 4.2.4, the following graphs represent the results obtained from analysing the structures under Mode 1 (localized deformation due to eccentricity) deflection.
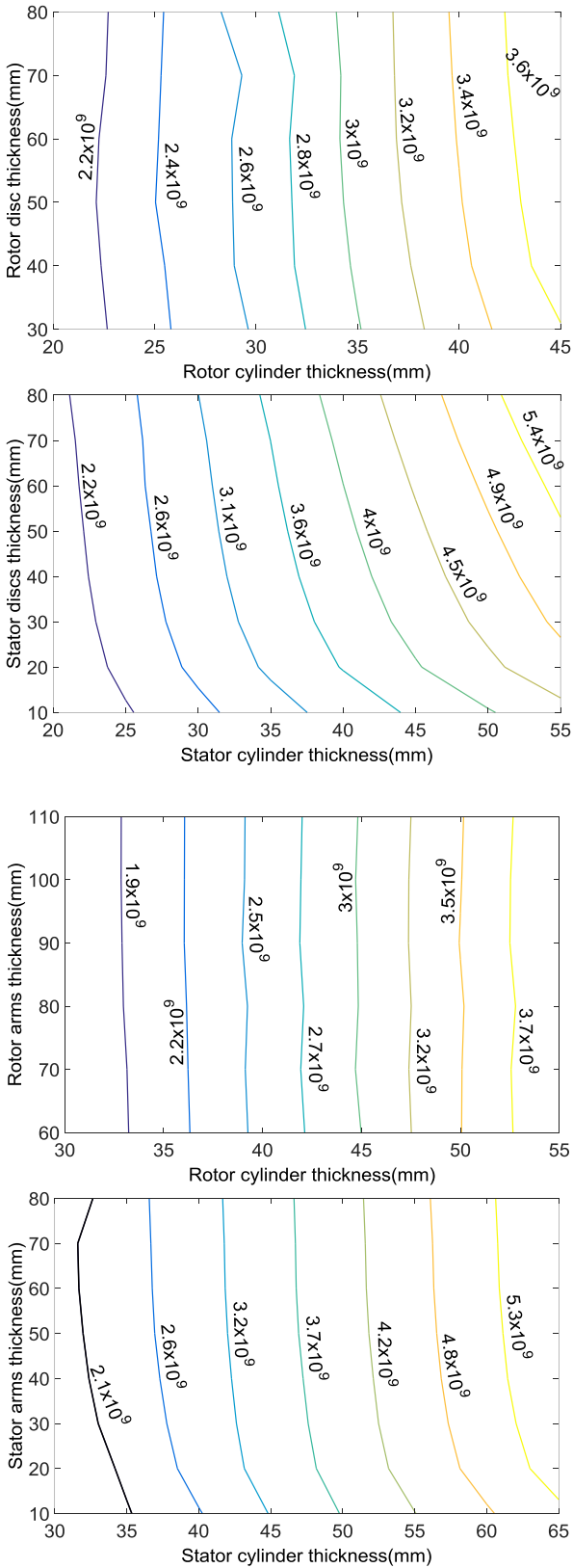
Figure 4.10 2D optimisation for 3 MW rotor and stator disc and arm structures with structural stiffness criterion; (1) Rotor disc structure; (2) Stator disc structure; (3) Arm rotor structure; (4) Arm stator structure

118

By making use of this tool, a quick estimation of either the dimensions or the stiffness needed by the electrical machine structure can be made. These contour plots would result very useful during the early stage of the design.

Different methods for estimating the minimum structural stiffness required have been described and explained in Section 4.2. However, the structures are more prone to deform following certain patterns depending on their geometric configuration. With this in mind the optimised rotor and stator disc structures have been tested under distinct modes of deflection. The characteristics of the electrical machine are the following,

-   Axial length, 'l' = 1.2 m
-   Rotor radius, 'R' = 2 m
-   Airgap, 'g' = 0.005 m
-   Rotor yoke height, 'h_{ry}' = 0.04 m
-   Aspect ratio = 0.6
-   Magnet height, 'l_{m}' = 0.017 m
-   Magnet width, 'b_{p}' = 0.1 m
-   Flux density, 'B_{r}' = 1.02 T

The stiffness of the said components was approximated for deflection modes going from 0 to 4 by using the maximum pressure, which was calculated making use of the data presented above. Its average value corresponded to approximately 518,404 Pa. The rotor structure formed by a disc sub structure with 56 mm of thickness and a cylinder sub structure with a thickness of 40 mm was analysed employing FE techniques as described in the previous section obtaining the results presented in Figure 4.11. As seen, the rotor structure stiffness drops with the mode of deflection. Mode 4 is shown as the most hazardous with a stiffness below 5.6×10^8 N/m and according to the hierarchy of approaches given in this chapter, only finite element methods are able to accurately predict the minimum stiffness needed to comply with the structural requirements for this mode.
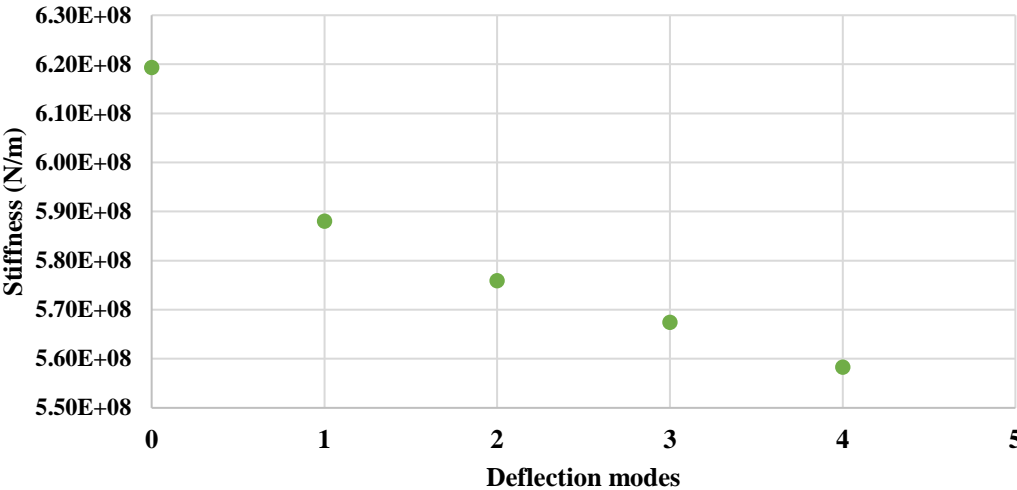
Figure 4.11 Structural Stiffness vs. Deflection Modes (Disc Rotor Structure)

The stator structure is composed by two discs of 40 mm thickness each and a cylinder with a thickness equal to 25 mm. The optimised structure was analysed tracking the procedure defined in Section 4.2.4 and under the same loading conditions as used for the rotor achieving similar results. The structural stiffness goes down again with the deflection mode. As observed, Mode 4 is the most damaging for the structure with a stiffness barely overtaking 4×10^8 N/m. See Figure 4.12.
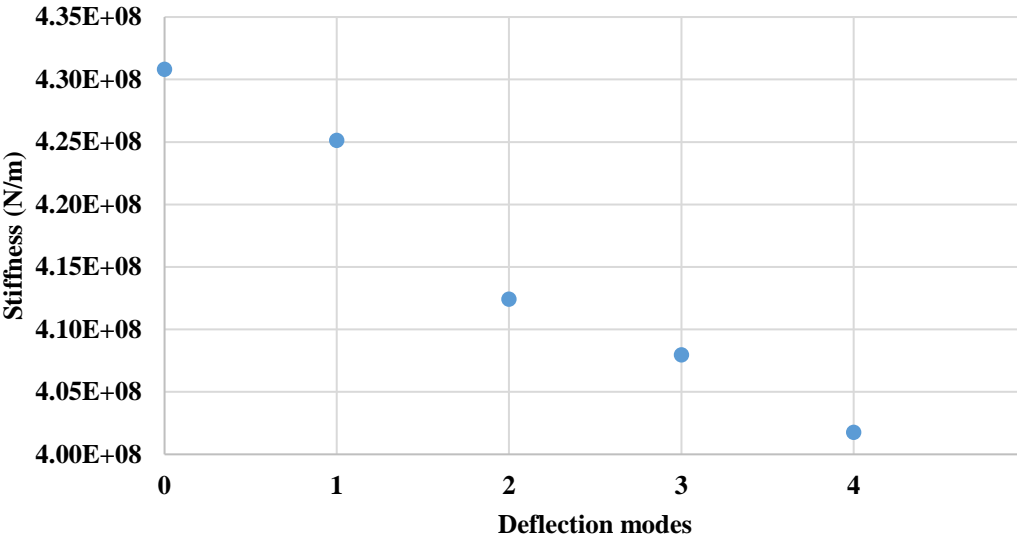
Figure 4.12 Structural Stiffness vs. Deflection Modes (Disc Stator Structure)

4.3.2 Analytical approach

a) Rotor disc sub structure

Figure 4.13 illustrates the comparison between the modified rotor disc sub structure model and the FE results. An excellent agreement is achieved as Benham's model stiffness is equal to the FE stiffness with $R^2 = 1$.
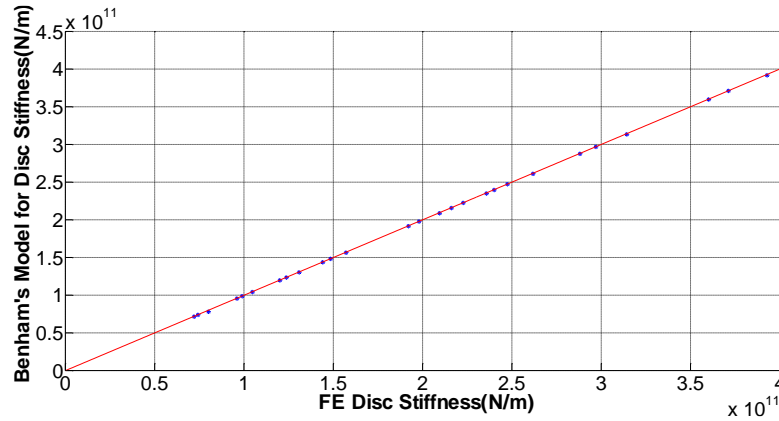
Figure 4.13 Comparison of stiffness calculated from FE and Benham model [11]

However, this approach only works for Mode 0. Hence, an approach that accurately predicts the structural stiffness of this rotor component for different modes of deflection needs to be found.

b) Arms sub structure

The arms are generator sub structures that connect the external cylinder to the main shaft in the case of the rotor. For the stator, these arms, also called ties, are attached to the turret. The aim of the arms is to stiff the generator structure in order to withstand the large loads present during operation as well as during the transportation and installation stages. The modulus of elasticity is,

$$E = \frac{\sigma_{\text{arm}}}{\varepsilon_{\text{arm}}} = \frac{\dfrac{F}{A_{\text{arm}}}}{\dfrac{\delta}{l_{\text{arm}}}} \tag{4.15}$$

where F is the force applied to the structure, A_{arm} is the cross sectional area of the arm, δ is the deflection in the longitudinal direction and l_{arm} is the length of the arm. Reordering the equation

$$E = \frac{Fl_{\text{arm}}}{A_{\text{arm}}\delta} \tag{4.16}$$

With $k = \frac{F}{\delta}$ it is obtained that $E = \frac{k_{\text{arm}}l_{\text{arm}}}{A_{\text{arm}}}$. Rearranging

$$k_{\text{arm}} = \frac{EA_{\text{arm}}}{l_{\text{arm}}}. \tag{4.17}$$

If it is considered that the ties are hollow square structures of width, w, and thickness, t_{arm}, then the cross sectional area

$$A_{\text{arm}} = w^2 - (w - 2t_{\text{arm}})^2 \tag{4.18}$$

Expanding the polynomial expression and rearranging the equation

$$A_{\text{arm}} = 4t_{\text{arm}}w - 4t_{\text{arm}}^2 \tag{4.19}$$

Substituting A_{arm} into equation (4.17) the following expression for the arms structural stiffness can be found,

$$k = \frac{4Et_{\text{arm}}(w - t_{\text{arm}})}{l_{\text{arm}}} \tag{4.20}$$

Due to the relative simplicity of this sub structure, equation (4.20) is supposed to be valid to calculate the required stiffness of the arms for Mode 0 and Mode 1. Figure 4.14 shows a comparison between the data obtained from FE analyses and the values acquired with equation (4.20).
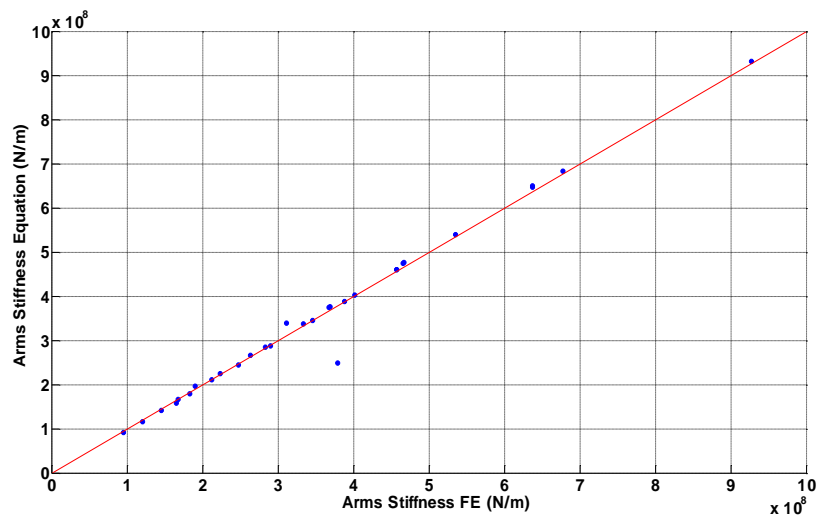
Figure 4.14 Comparison of stiffness estimated with analytical model and FE [6]

As it is shown, a very good agreement has been achieved over the whole range. Fitting a straight line of gradient 1 passing through the origin it is obtained that $R^2 = 0.9829$.

4.3.3 Hybrid approach

Using the hybrid approach, the structural stiffness of several components has been calculated. Equations for the rotor and stator cylinders of the structures made with discs have been obtained. Arm structures have been also looked at acquiring equations for their components. Moreover, equalities for complete rotor and stator structures made with discs and arms have been tried achieving good results in most of the cases.

a) Rotor cylinder model as found from FE results

A similar methodology was tracked for the rotor cylinder. Assuming, $k_c = f(E, t_c, l, R)$, the dimensional analysis was carried out. As it happened with the disc, the study could not predict all the powers of the variables so they had to be found by looking at their variation with the stiffness. Equation (4.21), which accurately describes the behaviour of the cylinder structure, was found after the analysis,

$$k_c = \frac{[C_3 E t_c^2 + C_4(R + l)](1 + v^2)}{(R + l)\gamma} \tag{4.21}$$

where $C_3 = 82.3$, $C_4 = 8.23 \times 10^9$ and l is the cylinder axial length. Again a comparison between the equation results and the data from the FE analyses for mode 0 is presented in Figure 4.15. High accuracy was also achieved according to the relationship obtained from the linear regression, Equation Cylinder Stiffness = FE Cylinder Stiffness with $R^2 = 0.9721$.
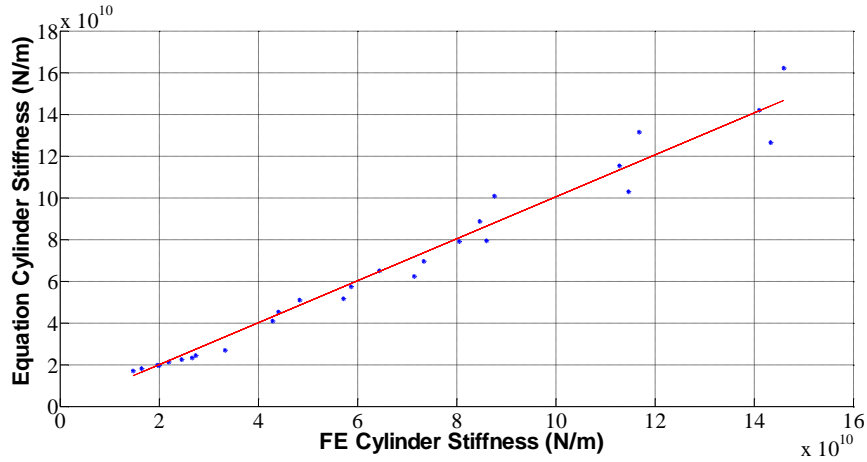
Figure 4.15 Equation vs. FE cylinder stiffness [11]

b) Stator Cylinder Sub Structure Model

As illustrated in Section 4.2.5, a dimensional analysis of the component in question was made. In this particular case it was assumed that the stiffness of the cylinder depends on the Young's Modulus, E, thickness, $t_{c,s}$, length, $l_{c,s}$, radius, $R_{c,s}$ and Poisson's ratio, v. As expected, the study could not predict all the powers of the variables present in the equation, therefore they had to be determined by analysing the variation of each parameter with stiffness. A constant had to be introduced to balance the equation,

$$k_c = C_5 + \left[\frac{C_6 E t_{c,s}^2 l_{c,s}(1 + v^2)}{R_{c,s}^2 \gamma} \right] \tag{4.22}$$

where $C_5 = 3.82 \times 10^{10}$ and $C_6 = 442.14$. Comparing the equation retrieved data and the FE studies results for Mode 0, it can be observed that a reasonable level of accuracy was obtained, as a straight line of gradient 1, passing through the origin, fits the data with an R^2 equal to 0.9225. See Figure 4.16.
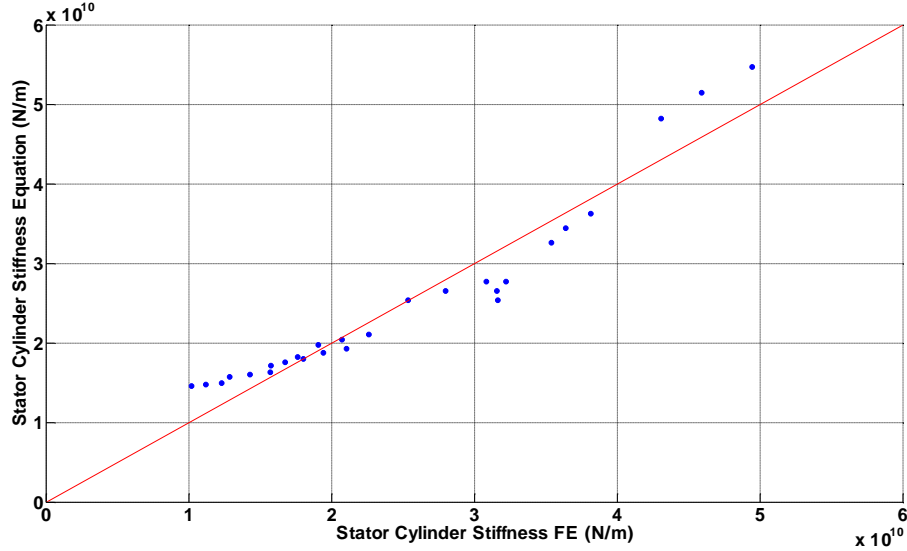
Figure 4.16 Stator cylinder Equation vs. FE [6]

c) Cylinder Sub Structure Model for Armed Rotor

In this case, it was assumed that $k_{c,a} = f(E, t_{c,a}, l_{c,a}, R_{c,a}, v)$. Once the dimensional analysis and sensitivity analysis was completed and the retrieved data were analysed, equation (4.23) was found.

$$k_{c,a} = C_7 + \left[\frac{C_8 E t_{c,a}^2 (1 + l_{c,a}^2)(1 + v^2)}{R_{c,a}^2 l_{c,a} \gamma} \right] \tag{4.23}$$

where $C_7 = 1 \times 10^{10}$ and $C_8 = 86.35$. As seen in Figure 4.17, a fair precision was achieved. Nevertheless, higher volatility can be appreciated for models corresponding to cylinders with very large thicknesses (150 mm). The equality presented the highest accuracy within a range between 5 and 7 metres diameter. The results have a R^2 value of 0.9454 regarding a straight line of gradient 1 passing through the origin.
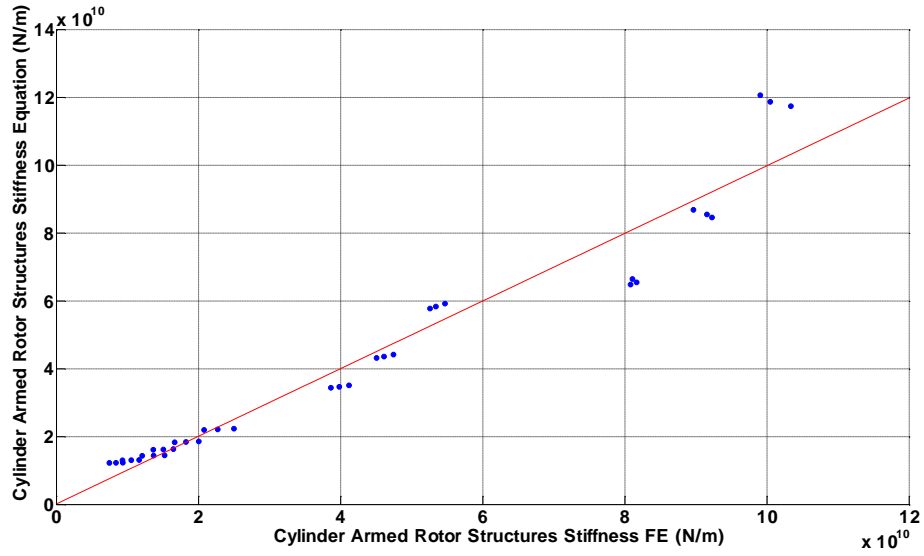
Figure 4.17 Armed rotor cylinder Equation vs. FE [6]

d) Cylinder Sub Structure Model for Armed Stator

Using the same arguments as for Section 4.2.5, the final equation to find the cylinder stiffness is as follows,

$$k_{as,c} = C_9 + \left[\frac{C_{10} E t_{as,c}^2 l_{as,c}(1 + v^2)}{R_{as,c}^2 \gamma} \right] \tag{4.23}$$

with $C_9 = 1.19 \times 10^{10}$ and $C_{10} = 128.44$. A comparison between the results obtained from the equation for the cylinder under Mode 0 deflection and the data acquired from the FE simulation studies was made. As it can be seen in Figure 4.18, a good agreement was achieved again as the data has an $R^2 = 0.9455$.
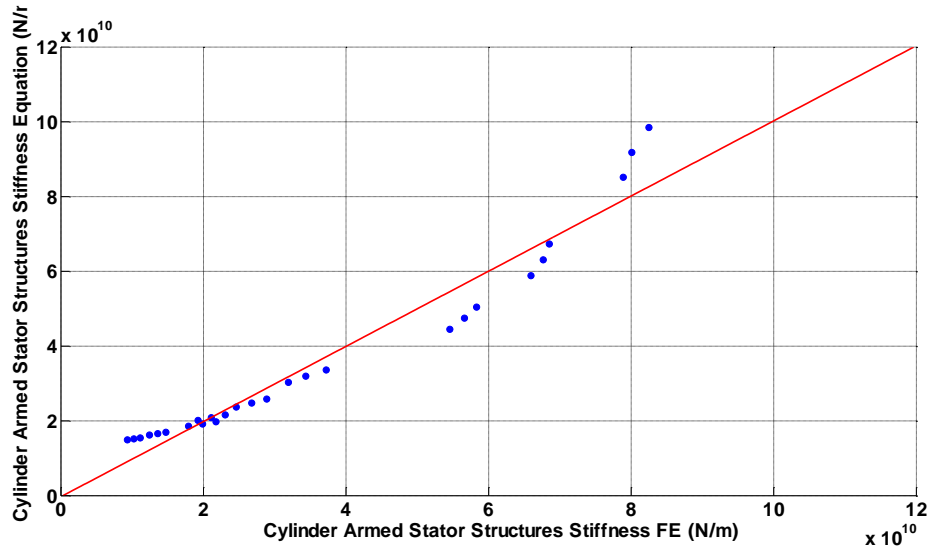
Figure 4.18 Armed stator cylinder Equation vs. FE [6]

e) Rotor and stator structural stiffness model

In order to estimate the structural stiffness of the whole disc rotor, the data for the disc and the cylinder sub structures were introduced into equation (4.1). An overall good agreement was achieved with a R^2 = 0.9828 for a gradient 1 straight line passing through the origin fitting. The component dimensions are shown in Table 4.1. They are the same as the ones that will utilised later on in this chapter to optimise the generator structural mass using the FE approach.

The stator's structural stiffness was predicted by putting together the cylinder, $k_{c,s}$, and the discs sub structures. Because the two discs are in parallel, they are added together to give an equivalent stiffness, $k_{eq,d} = k_{d1} + k_{d2}$.

The same approach that was used to find out the equation of the rotor was utilised in the case of the stator. As the stator discs are constrained in the same way as it was done with the rotor disc, equation (4.14) was considered valid. However, a new formula for the stiffness of the cylinder was needed.

Table 4.1 Disc and arm generator structures data

Disc structure			Arm structure		
General data	**Rotor** t_c **(m)**	**Stator** $t_{s,d}$ **(m)**	**General data**	**Rotor** $t_{c,a}$ **(m)**	**Stator** $t_{c,as}$ **(m)**
$R = 2$ m	0.023	0.054	$R = 2$ m	0.03475	0.038
$r = 0.625$ m	0.026	0.046	$r = 0.625$ m	0.0365	0.039
$l = 1.2$ m	0.029	0.039	$l = 1.2$ m	0.0395	0.04
$v = 0.3$	0.032	0.036	$v = 0.3$	0.042	0.0415
$E = 2.1\times10^{11}$ Pa	0.035	0.034	$E = 2.1\times10^{11}$ Pa	0.045	0.044
Rotor $t_d = 0.04$ m	0.038	0.032	$l_{arm} = 1.375$ m	0.047	0.049
Stator $t_{s,d} = 0.02$ m	0.041	0.03	$w = 0.35$ m	0.05	0.0565
	0.043	0.029	Rotor $t_{arm} = 0.08$ m	0.053	0.0615
			Stator $t_{a,s} = 0.03$ m		

After introducing the results acquired with equations (4.14) and (4.22) into the stator's equation, $k_{s,s} = \frac{2k_d k_c}{2k_d + k_c}$, a low agreement with the FE studies was achieved with a $R^2 = 0.3647$. This is because the equation predicts a higher contribution of the discs to the overall stiffness.

For the armed structures case, having the equivalent stiffness of the arms, $k_{a,eq} = n_{arms} \times k_a$, and the stiffness of the cylinder, $k_{c,a}$, the stiffness of the rotor can be calculated. As it can be seen in Figure 4.19, the data obtained for arm rotor structures shows a good agreement with the FE results having a $R^2 = 0.9091$ for a straight line of gradient 1 intercepting the origin fitting.

The stator's cylinder stiffness was also estimated using the method described in above, but this time considering that there are two sets of 10 arms. A decent agreement was acquired this time as seen in the figure. The data has a $R^2 = 0.8358$ for a linear fitting intercepting the origin. As understood, the equalities tend to overestimate the overall stiffness with the stator structures giving the lowest agreements.
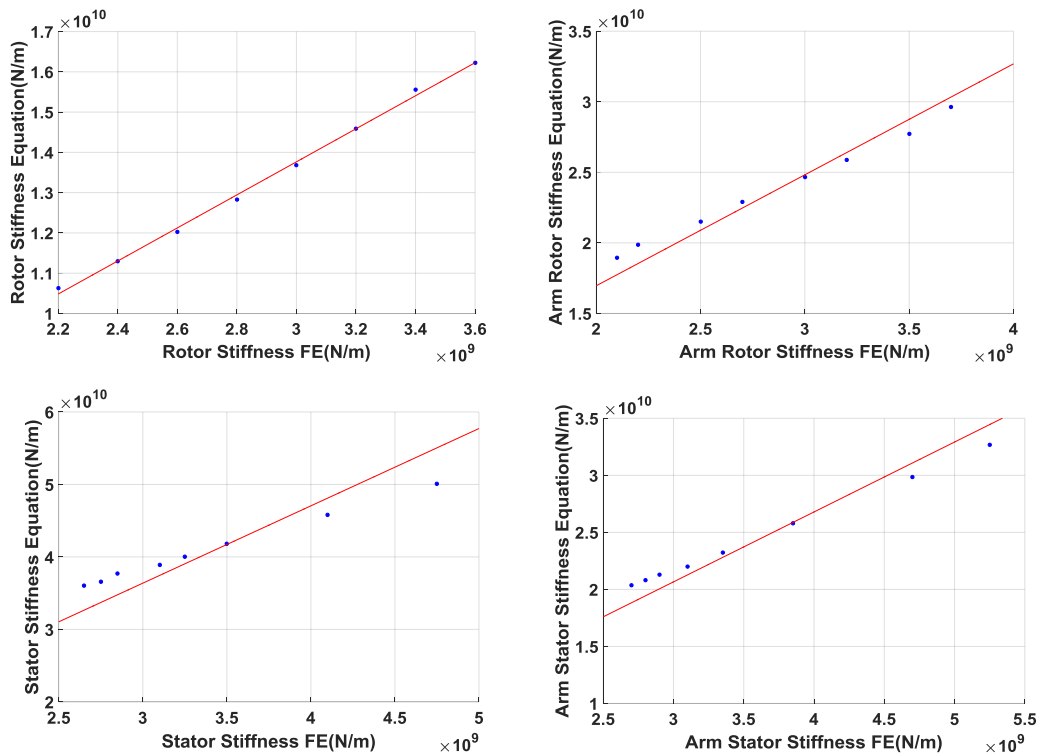
Figure 4.19 Equation Stiffness vs. FE Stiffness for complete structures; (a) Disc rotor structure; (b) Arm rotor structure; (c) Disc stator structure; (d) Arm stator structure

4.3.4 2D optimisation of simplified structures

Going a step beyond in structural optimisation, disc structures mass can be minimized using plots showed in Figure 4.20. For instance, if it is assumed a constant bearing stiffness $k_b = 3 \times 10^9$ N/m and having that the total needed stiffness $k_s = 1 \times 10^9$ N/m (acquired from equation (4.2b)), a comprehensive table gathering all the relevant data can be easily created. As it can be observed, it was identified that the disc of the rotor must have at least 40 mm of thickness whereas the thickness of the stator discs must be over 20 mm due to torque requirements (green lines for rotors and red lines for stators determine the minimum required stiffness in the tangential direction). This necessary stiffness to withstand torque loads was calculated according to the deflections obtained from applying a torque of 2,250 kNm to the structures. This value was retrieved from a simulation study carried out with Bladed over a 3 MW direct drive wind turbine with a PM generator at 12 m/s of wind speed.

Taking all of these features into consideration, the minimum mass of the rotor structure can be calculated for the whole range of structural stiffnesses by looking at the plot displayed in Figure 4.20(a), where the red line states the minimum stiffness in the normal direction. Replacing $k_{s,r}$ and k_b into equation (4.2a), the equivalent rotor stiffness can be computed. Then, substituting $k_{eq,r}$ and k_s into equation (4.2b) and reordering, $k_{s,s}$ can be achieved. With the stator discs thickness and the structural stiffness of the stator known, its mass can be found by entering into the plot displayed in Figure 4.20(b), where the black line determines the minimum required stiffness in the normal direction. The total mass of the generator is estimated by adding up the mass of the rotor structure, $m_{s,r}$, and the mass of the stator structure, $m_{s,s}$.
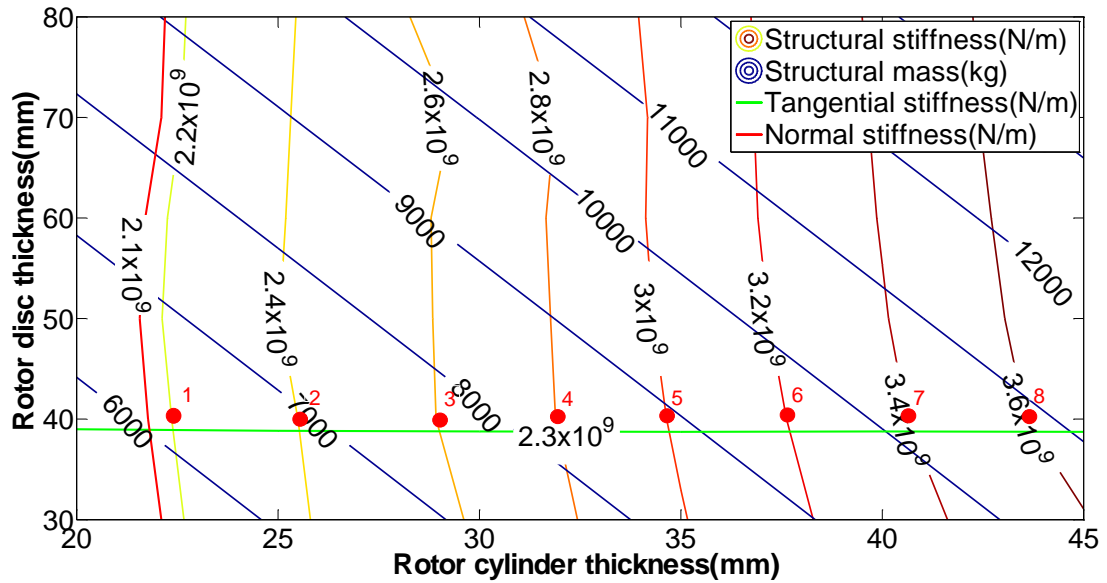
(a)
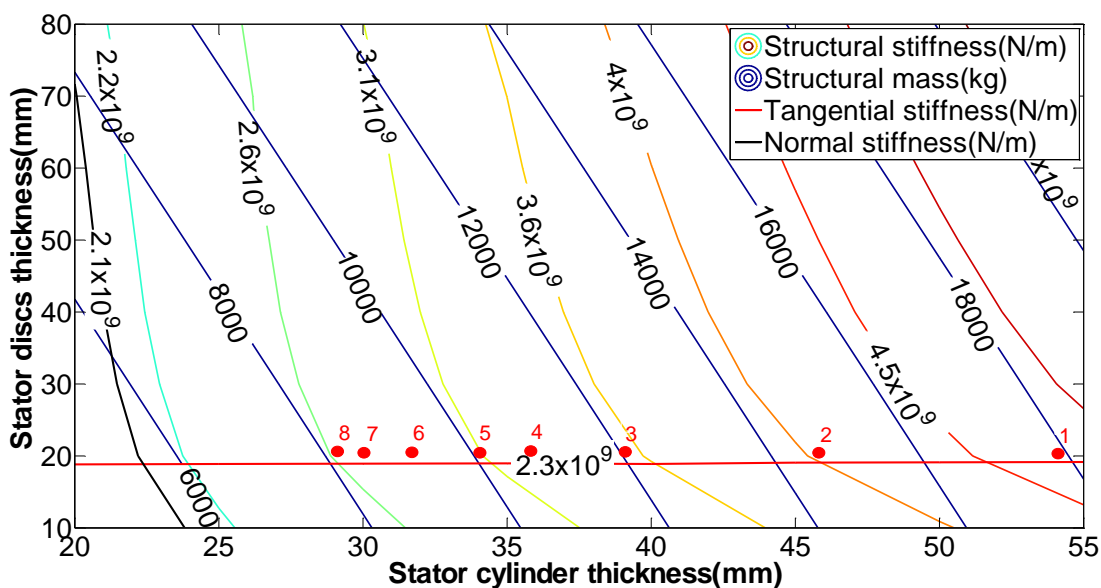
(b)

Figure 4.20 2D optimization for 3MW rotor and stator disc structures with structural stiffness criterion [6]

For this example, it can be seen that the minimum mass of the electrical machine structure, m_s, is 19,260 kg. See Figure 4.21. The models utilised to develop this case study has been highlighted with red dots and their corresponding numbers on the optimization graphs.
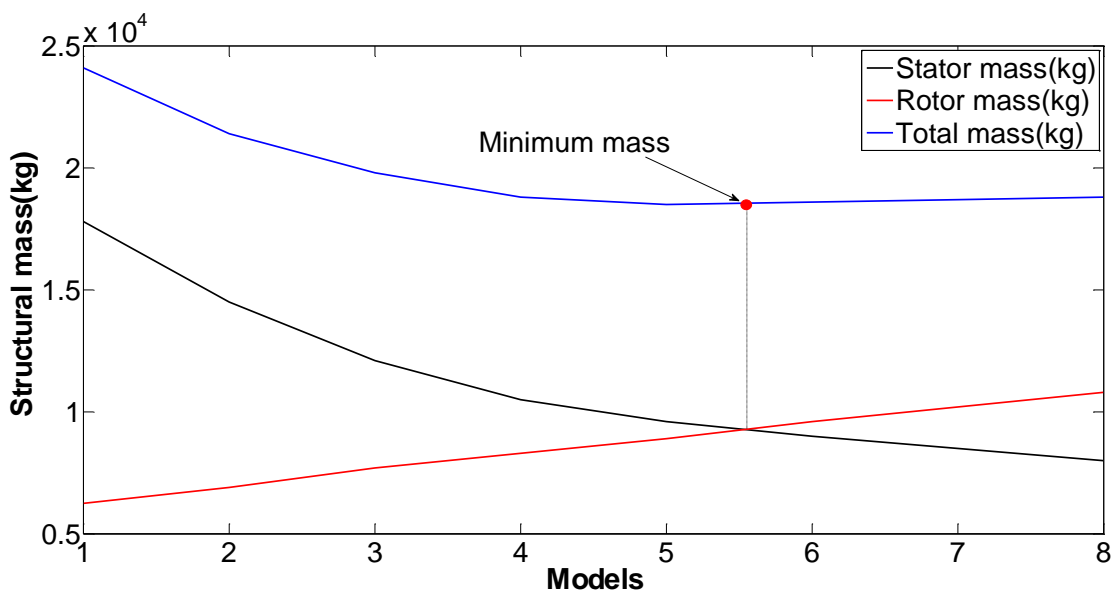
Figure 4.21 Mass optimisation result for disc structures [6]

131

b) Armed Structure

The same methodology was followed for the arm structures case. See Figure 4.22.
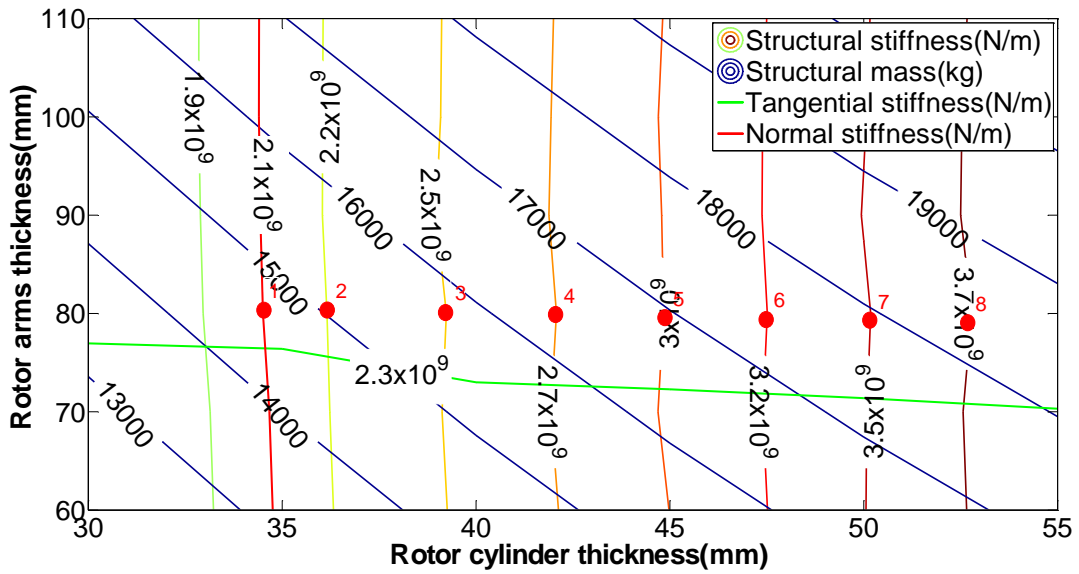
(a)
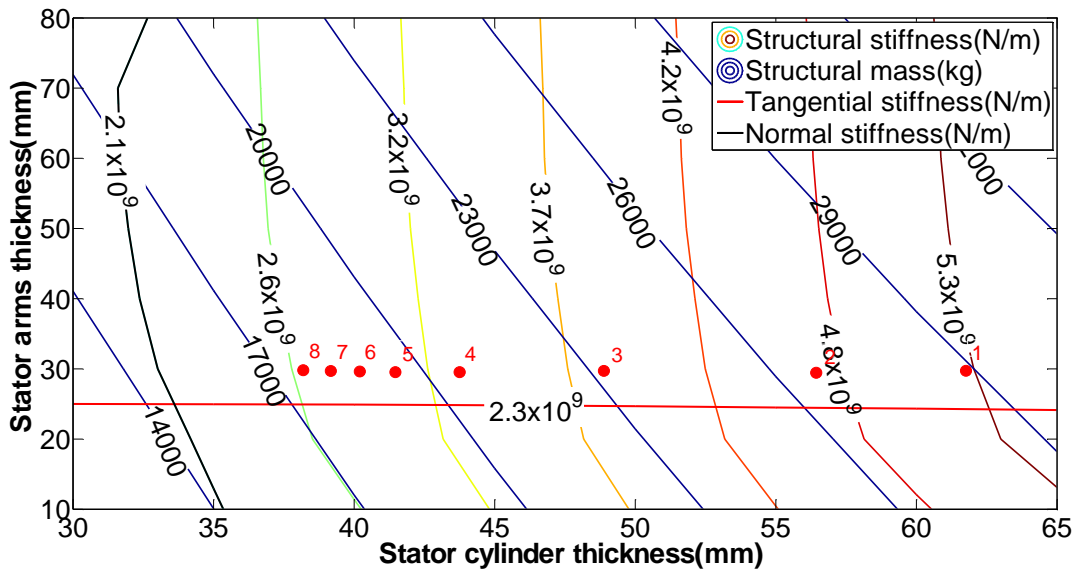
(b)

Figure 4.22 2D optimization for 3MW rotor and stator armed structures with structural stiffness criterion [6]

With $k_b = 3 \times 10^9$ N/m and the total needed stiffness $k_s = 1 \times 10^9$ N/m, the minimum generator mass was 35,500 kg as it can be observed in Figure 4.23.
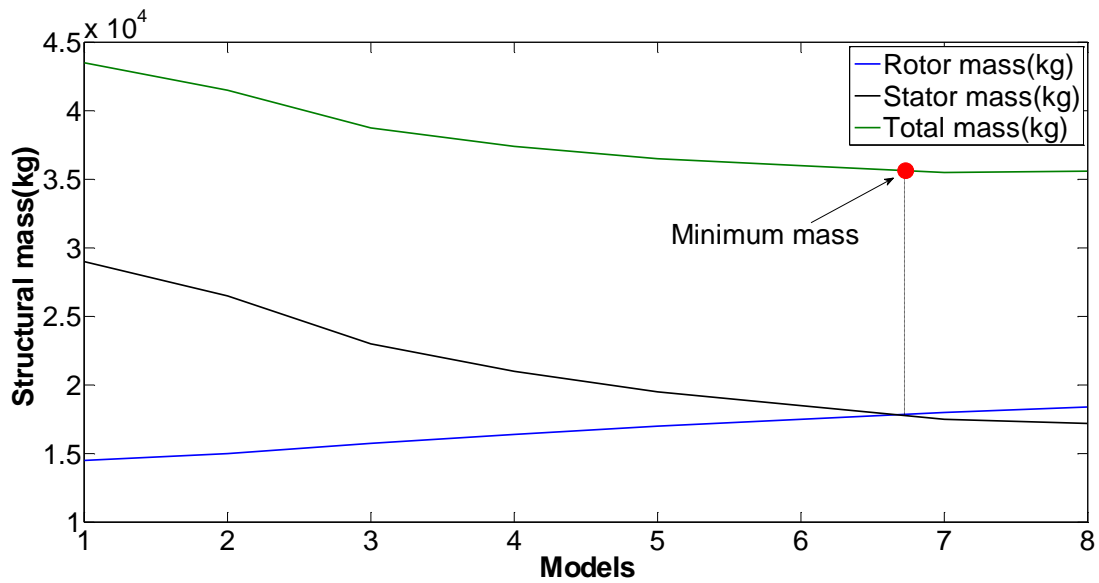
Figure 4.23 Mass optimisation result for armed structures [6]

After a detailed analysis of both types of structures, it could be observed that armed structures were not capable of resisting torque loads as disc structures do unless the thickness of the hollow arms is considerably increased with the consequent rise in mass. It was also noticed that arm structures are slightly weaker than disc structures in the radial direction, as it could be seen from their behaviour under the normal component of the Maxwell stress. If a comparison between these two types of structures supporting the same loads is made, a difference in mass of about 17,000 kg is achieved.

4.3.5 Structural topology optimisation

In this section, the data obtained from the optimisation study of the proposed conical rotor structure are presented, as well as the results achieved from the shape optimization carried out over the large scale model of the generator structure.

a) Conical rotor optimisation

The optimisation study of the rotor structure was carried out as follows,

1. Initial values were given to the thicknesses of the cone and the cylinder (40 mm for the cone and 22 mm for the cylinder).

2. The most suitable position for the cone sub structure was found. By altering the cone angle, 9 different models with five dissimilar cone positions as shown in Figure 4.5 were analysed obtaining the results displayed in Table 4.2.

Table 4.2 Cone structure optimisation results

		Position				
		1	2	3	4	5
Angle (º)	Mass (kg)	$\delta(m) \times 10^{-4}$	$\delta(m) \times 10^{-4}$	$\delta(m) \times 10^{-4}$	$\delta(m) \times 10^{-4}$	$\delta(m) \times 10^{-4}$
30	6873	4.8	4.4	4.8	4.8	4.4
35	7080	4.9	4.6	4.9	4.9	4.4
40	7384	4.7	4.5	4.9	4.9	4.4
45	7775	4.8	4.5	5	5	4.5
50	8281	4.9	4.7	5.1	5	4.6
55	8958	5	4.9	5.3	5.2	4.7
60	9881	5.2	5.1	5.7	5.4	4.9
65	11200	5.7	5.5	5.9	5.7	5.2
70	13205	7.1	6.6	6.7	6.6	5.9

3. As seen, position 5 has the best radial stiffness. In addition it was observed that the overall structural mass decreases with the cone angle. The thickness of each sub structure was increased by 5 mm in order to see which one was introducing more mass into the overall system. After a comparison, it was seen that the cylinder sub structure put about 151 kg more than the cone in any case.

4. With the variables to be targeted (cone angle and cylinder thickness), the optimisation study was defined in SolidWorks. The test settings include the deflection constraint of 0.5 mm in any direction and the goal of minimizing the mass of the whole structure. A complete batch of scenarios was looked at. Having the cone placed at position 5, the angle of the sub structure was varied from 35 to 5 degrees in steps of 5. Each step was study with the cone thickness fixed at 40 mm and the cylinder thickness varying from 22 mm to 14 mm in steps of 1 mm. The best

outcome was acquired for an angle of 10 degrees and a cylinder thickness equal to 20 mm. The overall mass was 6,104 kg and the radial deflection 0.497 mm.

5. So as to complete the rotor conical structure optimisation, it was checked that at that point, the variation of the cone thickness did not introduce any further improvement. For that, the cylinder thickness was diminished to 18 mm while the cone thickness was kept fixed giving a radial deflection of 0.54 mm and a mass of 5,861 kg. Then, the thickness of the cone sub structure was pushed up by 5 mm. The study showed that the deflection had gone down to 0.536 mm whereas the mass had gone up to 6,320 kg. Bearing in mind this result, the author terminated the optimisation process.

b) Large scale disc structure optimisation

Having demonstrated the utility of this ANSYS instrument in Section 4.2.6, it was again utilised to further optimise the large scale model. In this case, different outcomes were obtained for the rotor and the stator structures compared to those of the small scale model. With the structure loaded as specified in Section 4.2.6, the shape optimisation analysis was made revealing that the elements to be removed are not only within the disc sub structure but also in the outer surfaces. In addition, they tracked a certain pattern, as observed in Figure 4.24 that can be utilised to eliminate the material in a standard way making the structure easier to manufacture.
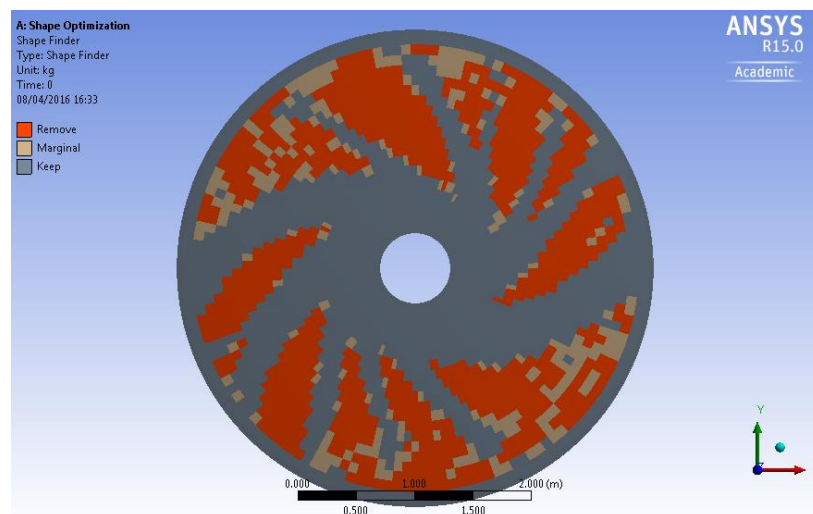
Figure 4.24 Large Scale Rotor Structure Shape Optimisation

Considering the data retrieved from the shape optimisation study, a model in SolidWorks was modified as seen in Figure 4.25(a) trying to standardize the shape of the clusters of elements to be removed. Then, by linking this model to the Design Explorer tool of ANSYS Workbench, the dimensions and the number of those shapes could be altered. Keeping in mind the deflection limit (in this case it is 0.5 mm), the optimum number of gaps was found to be 9. The size of the shapes was maximised so that the maximum amount of material could be taken out. A total number of 57 iterations were necessary to find out the optimum profiles for the rotor structure. Figure 4.25(b) shows the variables as changed in the Design Explorer study with $l_r = 1,265$ mm, $R_s = 135$ mm, $R_m = 2,345$ mm and $R_l = 1,240$ mm.

(a)   (b)
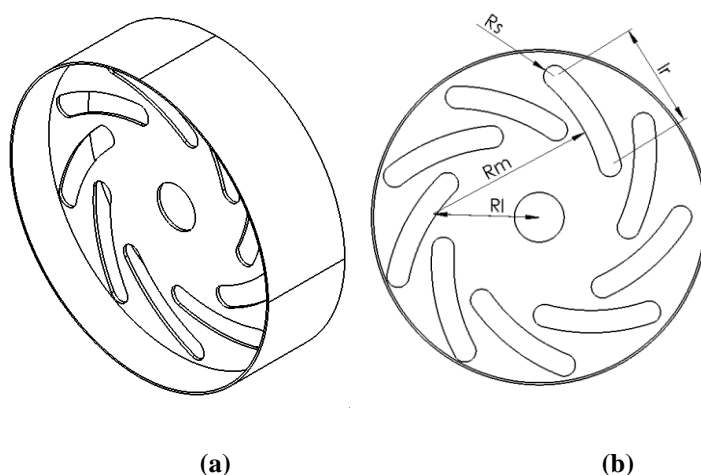
Figure 4.25 Design Explorer Optimisation (Large Rotor Structure)

For the stator structure a similar methodology was followed although a different shape was acquired from the study, as seen in Figure 4.26. The shape was approximated as shown in Figure 4.27(a) with the optimum found at $D_s = 1,400$ mm and $d_s = 1,150$ mm with 5 circular holes. A total number of 23 iterations were needed so as to figure out the optimum values of the two variables.
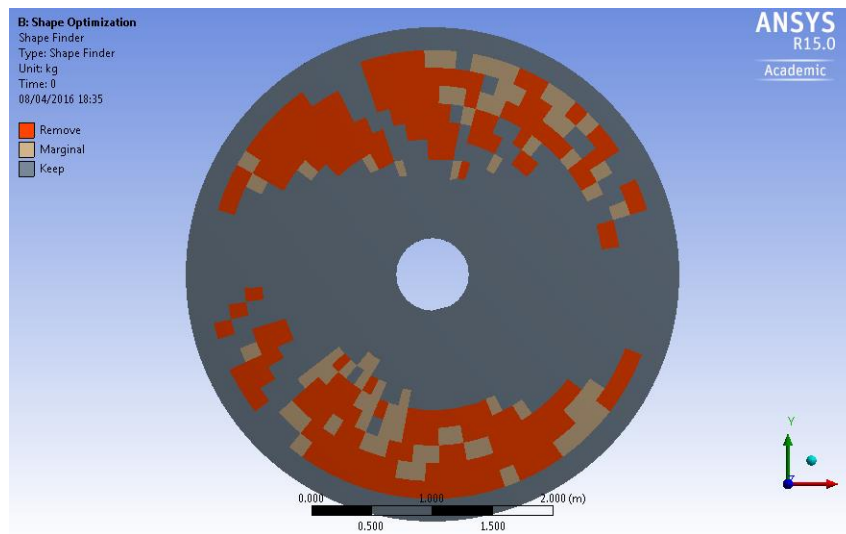
Figure 4.26 Large Scale Stator Structure Shape Optimisation

| (a) | (b) |
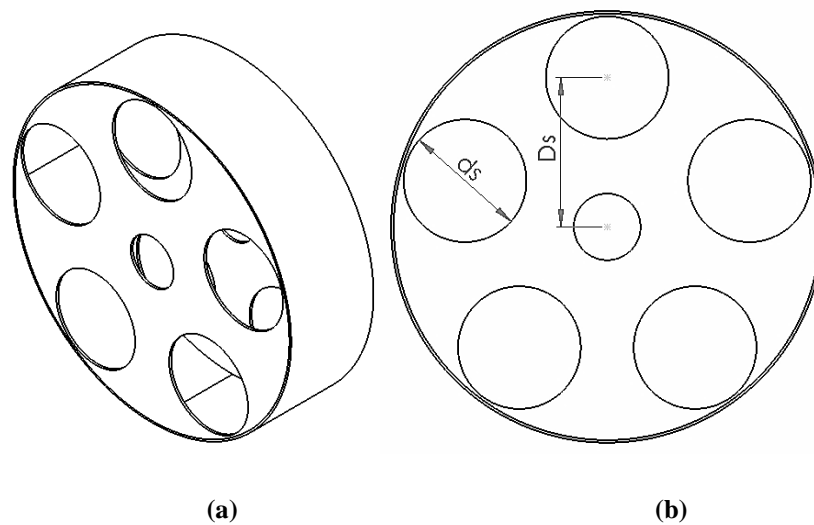
Figure 4.27 Design Explorer Optimisation (Large Stator Structure)

If the mass of the resultant generator structure is compared with a solid disc structure (overall mass of 19,260 kg with 9,809 kg for the rotor and 9,451 kg for the stator) capable of supporting the already said loads, a difference of almost 38 % is achieved. With a total mass of 12,000 kg with the rotor accounting for 5,694 kg and the stator for 6,306 kg a substantial drop in mass was achieved.

4.4 Discussion

There exist different procedures to calculate the structural stiffness needed by an electrical machine. A hierarchy have been defined considering the advantages and drawbacks of each one. Among the three techniques described here, the most reliable is the FE method due to the high precision data that can be obtained for any type of structure under any deflection mode. Nevertheless, this approach it is considered computationally expensive and time consuming. Two distinct structural configurations, arm and disc, were analysed using this method and it could be observed the arm structures were not capable of resisting torque loads as disc structures did unless the thickness of the hollow arms was considerably increased with the consequent rise in mass. It was also noticed that arm structures were slightly weaker than disc structures in the radial direction, as it could be seen from their behaviour under the normal component of the Maxwell stress. After a comparison between these two types of structures supporting the same loads, a difference in mass of about 17,000 kg was achieved, with 19,260 kg for the disc structure and 35,500 for the armed structure.

On the other hand, the analytical method presented here was capable of producing accurate results for Mode 0 deflection of disc and arm sub structures in a much faster way with R^2 not going below 0.9829 in either case. For the disc structure, the approach was developed by modifying an existing model of a rotating disc with a central hole and unloaded boundaries, whereas for the case of the arm, the final expression was obtained by playing with the physical dimensions describing the structure. Last but not least, the hybrid procedure, which was produced by examining the results from the FE studies and utilising the data achieved from dimensional analyses, was also much quicker than the FE approach and it was able to generate precise results for Mode 0 and Mode 1 deflection of disc and arm structures. Excellent agreements between FE data and the results achieved with the expressions were obtained for all the analysed sub structures with R^2 never going below 0.9225. However, when looking at complete structures, the equations did not show that outstanding performance. The lowest agreements between FE data and the results acquired from the equations were achieved for the stator structures, with the disc

arrangement giving the worst outcome (R^2 = 0.3647). It could be understood that the equations tend to overestimate the overall stiffness by giving too much weight to the stiffness of the discs. Considering the applicability and reliability of this method for sub structures, it is thought that better outcomes could be achieved if a more detailed research on the calculation of the stiffness of complete structures is carried out.

Rotor and stator disc structures were tested under different modes of deflection in order to identify which one is the most dangerous and how it would affect the structures. As the data revealed, the stiffness drops with each deflection mode showing its lowest value at Mode 4 in both cases. By taking into account this important feature, the design can be tuned so that the structures can withstand this deflection mode in the most reliable, lightweight and cost effective manner. On the other hand, if the designer is interested in varying the most damaging deflection mode (due to different requirements), it can be done by altering the thicknesses of the sub structures. This is a trade-off process in which the stiffness of the overall structure can be increased for some deflection modes at expense of the others.

Finally, with the optimum disc structure fully described, a further optimisation was carried out using finite element tools. The ANSYS Shape Optimisation© add-on was utilised to identify the areas not contributing to carry the loads. The Design Explorer ANSYS tool was linked to a CAD model in SolidWorks which was produced by looking at the data retrieved from the shape optimisation add-on so that the dimensions of the areas to be removed could be maximised in order to diminish the overall structural mass. Two models were studied. One at a small scale which showed a 15 % reduction in mass whether compared with a solid disc structure capable of supporting the same loading conditions and one at a large scale which gave a drop of 38 % if compared to the disc structure model obtained in Section 4.3.4.

A rotor conical structure at a large scale was also proposed for study due to the excellent radial and axial characteristics that this type of geometry has. After the completion of an optimisation study where the variables to be targeted were the cone angle and the cylinder thickness, it was obtained that the best arrangement compromised a cone sub structure with 40 mm of thickness and 10 degrees of slope

angle and a cylinder thickness of 20 mm. This gave an overall mass of 6104 kg and a radial deflection of 0.497 mm. If a comparison with the optimised disc structure presented in Section 4.3.4 is made a mass reduction of about 37.7 % is achieved.

4.5 Conclusions

Three different techniques have been proposed and verified in this chapter. According to their reliability, suitability and speed to determine the structural stiffness of the components forming the machine it can be said that the first approach to be used would be the hybrid one when studying disc and arm sub structures and complete structures for Mode 0 and Mode 1, whereas the analytical one would be utilised in first instance to analyse Mode 0 deformation of disc and arm sub structures. These two methods give high design freedom as the stiffness can be found by simply introducing the required values describing the structure. They are meant to be used in early design stages, while the FE alternative could be employed either when none of these approaches apply or when data validation is needed. Nonetheless, special attention should be payed when estimating the stiffness of complete rotor and stator structures using the hybrid technique as the equations are prone to overestimate the influence of the discs or the arms into the overall equation. More research is necessary on the area of stiffness calculation of complete rotor and stator structures.

On the other side, the performance of two types of structures arm and disc have been analysed. Due to the high torques present during machine's operation, a high tangential stiffness is needed. Arm structures composed by a cylinder and hollow arms requires high thickness values for the arms which makes the structure heavier than its counterpart made with discs. For this reason it can be concluded that disc structures are more suitable for this type of applications. With the optimum layout identified, its structural performance was tested under different modes of deflection. The studies revealed that the most harmful mode corresponded to mode 4. This data can be considered of vital importance due to the engineers can make a design that avoids this mode by altering the dimensions of the machine or by introducing additional features such as stiffeners.

Further optimisation of the rotor and stator disc structures was accomplished using finite element techniques. A large drop in mass was achieved by removing material following a certain pattern that facilitates the manufacturing of the structure. Looking at the results obtained and the relatively low complex shapes that can be acquired tracking this methodology, the author recommends its use for additional structural optimisations.

The optimisation of another type of structure as the rotor conical one has been completed using the design study optimisation tool. This analysis has opened the door to the exploration of other types of layouts. No further optimisation of this structure was made although as it could be seen, the arrangement showed great potential for structural mass savings. More progress should be made on the research of this structure. Taking into account the results achieved, it can be concluded that rotor conical structures are arrangements that should be considered when designing weight sensitive rotating machinery supporting structures.

4.6 References

[1] A. C. J. A. Versteegh, P. Nl, and H. Nl, "Design of the Zephyros Z72 wind turbine with emphasis on the direct drive PM generator .," 2004, vol. 31, no. 0, pp. 1–7.

[2] A. Grauers, "Design of direct-driven permanent magnet generators for wind turbines," Chalmers University of Technology, Goteborg, Sweden, 1996.

[3] T. Hartkopf and S. Hofmann, M. and Jockel, "Direct-drive generators for MW wind turbines," in *European Wind Energy Conference*, 1997, pp. 668–671.

[4] M. Mueller, A. S. McDonald and D. MacPherson, "Structural analysis of low-speed axial-flux permanent-magnet machines," IEE Proc. Electr. Power. Appl., 2005, 152, (6), pp. 1417-1426.

[5] A. S. Mcdonald, "Structural analysis of low speed, high torque electrical generators for direct drive renewable energy converters," University of Edinburgh, Edinburgh, 2008.

[6] P. Jaen-Sola, A.S. McDonald, "A Comparative Study of Methods for Modelling the Structural Stiffness of Generator Components", *IET Power Electronics, Machines & Drives (PEMD)*, Glasgow (UK), Apr. 2016.

[7] G. Shrestha, H. Polinder, D. Bang, and J. A. Ferreira, "Structural Flexibility : A Solution for Weight Reduction of Large Direct-Drive," in *IEEE Transactions on Energy Conversion*, 2010, vol. 25, no. 3, pp. 732–740.

[8] G. Shrestha, H. Polinder, D. J. Bang, and J. A. Ferreira, "Direct Drive Wind Turbine Generator with Magnetic Bearing," pp. 1–10.

[9] D. Bang, H. Polinder, G. Shrestha, and J. A. Ferreira, "Possible Solutions to Overcome Drawbacks of Direct-Drive Generator for Large Wind Turbines," pp. 1–10.

[10] D. Bang, H. Polinder, G. Shrestha, and J. A. Ferreira, "Promising Direct-Drive Generator System for Large Wind Turbines I . Introduction II . Comparison of Different Generator Concepts."

[11] P. Jaen-Sola and A. S. McDonald, "Structural Analysis and Characterization of Radial Flux PM Generators for Direct-Drive Wind Turbines," *3rd Renew. Power Gener. Conf. (RPG 2014)*, Naples (Italy), 2014.

[12] A. S. McDonald, P. Jaen-Sola, "A New Method for Coupling Structural and Magnetic Models for the Design and Optimization of Radial Flux PM Generators for Direct-Drive Renewable Energy Applications", *IET Renewable Power Generation Journal*, Jan. 2016.

[13] P. Benham, R. Crawford, and C. Armstrong, *Mechanics of Engineering Materials*, Second Edi. Prentice Hall, 1996.

[14] J. N. Stander, G. Venter, and M. J. Kamper, "Review of direct-drive radial flux wind turbine generator mechanical design," 2011.

[15]   R. Pankhurst, *Dimensional Analysis and Scale Factors*. London: The Institute of Physics and The Physical Society, 1964.

Chapter 5

Lightweight materials in generator structures

5.1 Introduction

Lightweight materials such as composites have been considered for applications where structures need to comply with demanding requirements at the lowest possible cost and weight, for example aircrafts, automobiles and ships [1]. In wind turbines, drivetrain weight is highly correlated with machine's capital cost and therefore to its levelised cost too. With less weight on top of the tower, the structural requirements for tower and foundations are less demanding. The reduction in mass means a reduction in the cost of material and manufacturing process, as well as time savings.

In addition, the combination of an adequate design with the decrease in the amplitude of fatigue loads achieved by the drop in mass contributes to enlarge the wind turbine lifespan. In [2], Shrestha *et al.* suggest the use of light structural material, such as aluminium alloy and composites as a method to reduce the weight of direct-drive machines. In 2010, Siemens patented a wind turbine design where both the rotor and the stator structures are made of composite materials [3].

The main aim of this chapter is to produce a lightweight design, using composite materials, that meets all the structural requirements as described in previous chapters in an economic manner. For this, different ways of designing generator structures must be considered. Once the most suitable technique is identified, a rigorous process of optimisation and evaluation have to be completed. So as to check weight savings, a comparison with typical steel structures can be made. At the end of this chapter, a mass comparison between a steel structure, an optimised steel structure, a composite structure modelled by using conventional approaches and a composite structure modelled by using a more advanced methodology will be given. The results will be presented for rotor and stator structures.

Distinct approaches can be utilised to design an advanced composite material structure. In Section 5.2 the most relevant factors to be taken into consideration when designing a composite structure are outlined. Section 5.3 describes in detail the procedure tracked to design the structure and Section 5.5 shows all the results obtained. The last two sections, 5.6 and 5.7, correspond to the discussion of the acquired outcomes and the conclusions reached respectively.

5.2 Composite Materials

5.2.1 What are composite materials and how do we form them?

Composites consist of a bulk material (the 'matrix') and some sort of reinforcement, which is typically in the form of fibres, although particles and flakes are also available. The main task of the fibres is to carry loads, as well as to augment the strength and the stiffness of the matrix. They are much bigger in length than in diameter. This makes them stronger since almost no room for defects is allowed, in

other words, with very small diameters the chances of having an imperfection in the fibre are minimised. Whether an accident occurs and the fibre gets damaged somehow, the effects would be easily noticeable permitting the engineer to take the appropriate measures. In order to have a better binding between the fibres and the matrix, the fibres are treated with chemicals, also known as interface. Figure 5.1 displays the different stages that must be followed when designing advanced composite structures.
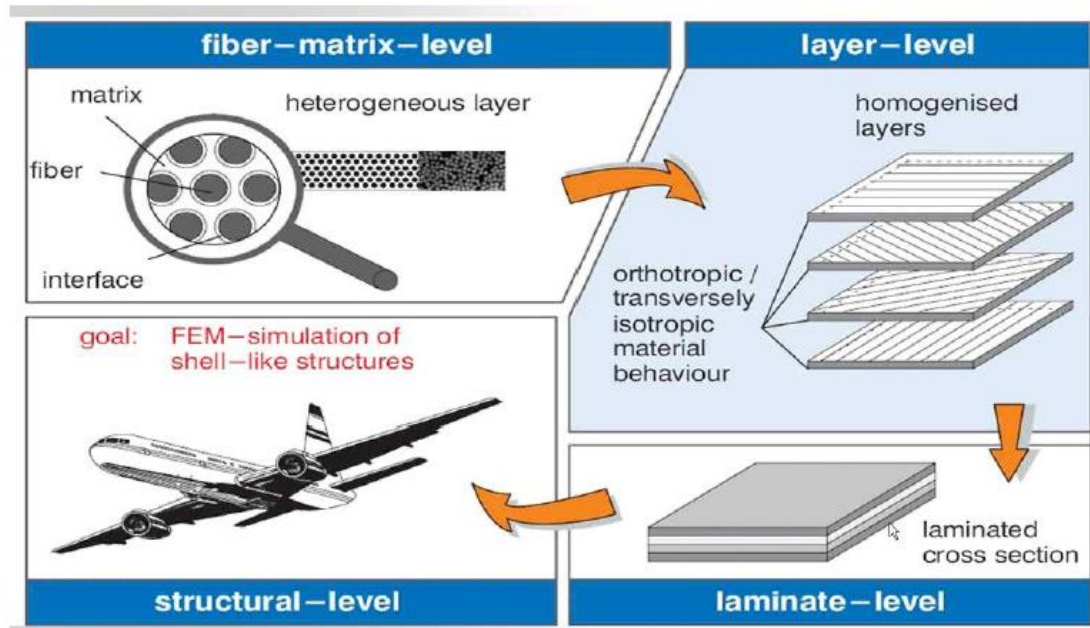
Figure 5.1 Advanced composite structure design stages [4]

The first step in the design of a composite material is to pick a suitable type of fibre. Factors to be considered are the strength and the Young's Modulus. Cost is also a major issue but material properties can be balanced against the cost. Then, according to the project's demands, the type of matrix is chosen. At this point, plies or layers can be formed by combining the fibres and the matrix as shown in Figure 5.1. The higher the fibre volume fraction, the better the mechanical properties of the composite, such as strength and stiffness. At a microscopic level, the distribution and the orientation of the fibres, as well as their properties and the ones of the matrix determine the properties of the composite material. As said, the main objective of the fibres is to carry the loads, hence the higher the volume fraction of the fibres the

better the composite mechanical properties. Nevertheless, it is crucial not to underestimate the importance of the matrix task. In reality, a minimum matrix volume fraction of 30 % is needed, giving a maximum of 70 % for the fibres according to the 'rule of mixtures'. Theoretically, almost 91 % fibre volume fraction can be acquired if the fibres are hexagonally 'close packed' with the fibres touching each other [5].

The main goal of any manufacturing method is to properly wet the fibres with the selected resin and consolidate the laminate in a cost effective and reliable manner. This is achieved by a combination of elevated pressure and temperature. Temperature is needed to initiate and sustain the chemical reactions, while pressure is necessary to consolidate the fibres into the matrix and obtain the maximum volume fractions. Time, also called cure cycle, is a key feature too as it determines the production rate of parts. Cure is a transformation of uncured (liquid stage) or partly cured polymer composites into c-stage (solid stage). Proper cure or cooking must be achieved within the shortest time.

The most common composites currently produced can be split into three different groups:

- Polymer matrix composites (PMC's); these are the most common and are made of a polymer-based resin (plastic) matrix, while the reinforcement is created using glass, carbon or aramid fibres.
- Metal matrix composites (MMC's); MMC's are widely used in the automotive industry and consist of a metal matrix (aluminium) and reinforcement made of either particles or fibres typically of silicon carbide.
- Ceramic matrix composites (CMC's); suitable for very high temperature environments. These are made of a ceramic matrix with a reinforcement usually composed by short fibres or whiskers of silicon carbide and boron nitride [6],[7].

Advanced composite materials can be defined as composites composed by high performance reinforcements of a thin diameter embedded into an epoxy or aluminium matrix. Some examples are graphite/epoxy, Kevlar/epoxy and boron/aluminium composites, which are widely used in the aerospace and naval

aircraft industries (for example F/A-18, AV-8B, SH-60B and CH-53E aircraft) due to their superior strength and stiffness properties [8].

When designing an advanced composite structure many factors need to be considered so that the most suitable material can be chosen.

5.2.2 Carbon fibre and epoxy

As said, reinforcement can be in the form of fibres, flakes and particles and it provides strength and stiffness. There is a plethora of reinforcement types: Glass, Boron, Carbon, Graphite (Carbon + Graphite), Silicon Carbide, Ceramic and Kevlar. In this investigation, carbon fibre has been selected as the type reinforcement to be used in the design of the advanced composite structure forming the generator. Carbon fibre modulus ranges from 40 to 100 million psi and it depends on the manufacturing techniques. The diameter of a fibre is about 7 to 8 μm. Their tensile strength is 13 times higher than that of aluminium. They also have very high stiffness and are electrically conductive. The microstructure of carbon fibres follows an A-B-A packing sequence and the atoms within the layer are held by strong covalent bonds. Fibre density is about 1.8 g/cm^3. This is 65 % of that of aluminium which is much heavier. It is important to notice that carbon fibres are nearly pure carbon and their Young's modulus correlates to the carbonization temperature.

Between the diverse types of matrices, epoxy offers the best properties. This thermoset is an amorphous polymer with the molecules randomly distributed. They have 3 dimensional crosslinks between the molecules. These links are very strong and difficult to break even applying heat. Epoxy is also highly resistant to environmental and solvent attack and has excellent adhesion. It shrinks very little during cure (manufacturing process) and it can be made tougher by embedding thermoplastic interlayers into its structure, also called toughened matrix. Nonetheless, it is an expensive polymer which needs to be cured over long periods at high temperatures. This makes them not suitable for mass production.

By wetting carbon fibres with liquid epoxy and applying the right combination of elevated temperature and pressure, laminates get consolidated. Uniform high

pressure and high temperature contribute to more uniform structure. High quality structures must have the fibres uniformly dispersed over the matrix due to resin rich areas are more prone to microcracking. Nevertheless, if not enough resin is applied (resin starved areas) shear transfer cannot take place.

Composite materials properties can be tailored by combining different percentages of 0, 45, -45 and 90 degrees plies. When weight, strength and stiffness are critical design factors carbon/epoxy outperforms steel and aluminium. If a weight comparison between these three materials is made it can be obtained that steel is 3 times heavier than aluminium and at the same time, aluminium is 2 times heavier than carbon/epoxy. In addition, specific strength of composites (not only carbon/epoxy) is much better that steel and aluminium. To tailor carbon/epoxy structure's elastic constants Figure 5.2 can be used as a reference. It displays how the 4 independent constants that are needed to analyse a 2D orthotropic material behave against orientation of the plies. Note that for defining a 3D orthotropic material 9 independent elastic constants are necessary.
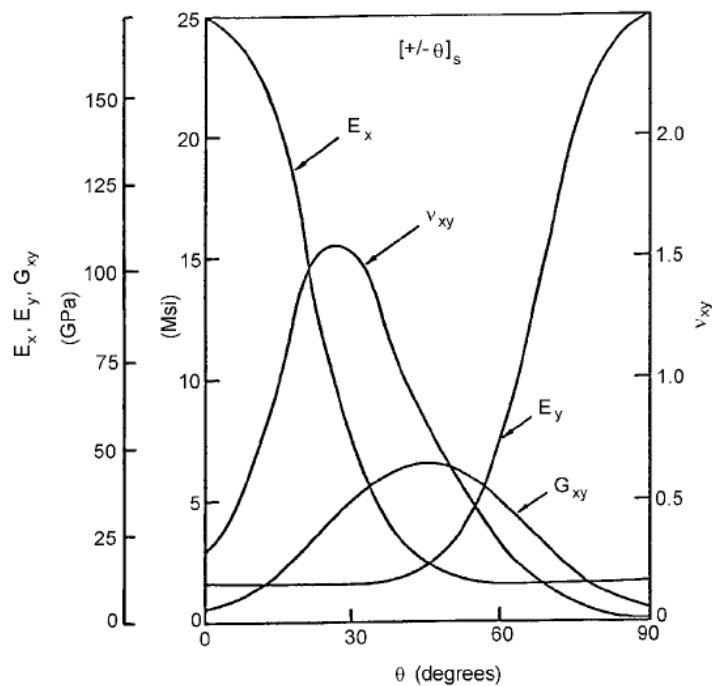
Figure 5.2 Laminate elastic constants for high modulus carbon/epoxy [9]

5.2.3 Manufacturing processes

Amongst the advantages of manufacturing composites are reduced part count, reduced machining and assembly time and minimum number of threaded fasteners (nuts, bolts, etc.,). Different manufacturing processes exist: hand layup, automated layup, resin transfer moulding and vacuum-assisted resin transfer moulding.

Hand layup is a flexible and low capital investment composite manufacturing method involving safety issues and labour intensity as plies are produced by hand, whereas for the automated layup process the fibres are placed using a numerical control machine with 6 degrees of freedom.

On the other hand, resin transfer moulding (RTM) is a very precise and efficient method for which two match-dies are required. In the first instance, dry fibres are placed into the mould. Liquid resin is injected afterwards generating pressure. Finally, the product is heated up. It is considered as a costly and stiff process. Nonetheless, significant savings of money and time can be made since as the high precision offered by this technique helps minimizing trimming and finishing after curing.

Vacuum-assisted resin transfer moulding is easier to carry out and cheaper although it implies a certain loss of quality and mechanical properties. The main difference between this process and common resin transfer moulding is that the resin is applied from the top to the bottom through a hole to be vacuumed later on. This can be produced an uneven distribution of the resin [10].

One example of a composite structure produced by hand layup methods, among others, are wind turbine blades [11]. Automated layup techniques are taking a key role in the production of composite frames of commercial jets [12], whereas resin transfer moulding technologies are applied in the process of truck panels, boat hulls, wind turbine blades again, aerospace and automobile parts, medical composites, bathroom fixtures, car body, helmets and so on [13]. Lastly, the vacuum assisted resin transfer moulding method is typically utilised for aircraft fuselage sections, aircraft landing gear doors, large composite panels, wind turbine blades, high fibre content parts, low void content parts and carbon fibre [14].

Laminates are created by stacking these plies following a certain sequence. The stacking sequence will define the properties of the laminate that will be utilised in the final stage of the advanced structure design.

5.2.4 Advantages and drawbacks of using composites

Composites can meet some of the more advanced material requirements demanded by high performance technologies in a more lightweight manner than metals and alloys. Metals are isotropic and homogenous (they have the same properties in all directions) whereas composites are anisotropic and inhomogeneous (they have the same properties at all points in the body), with properties 400 times better in some directions.

Other advantages for composites are enhanced fatigue and impact resistance, strength, stiffness, corrosion resistance and thermal conductivity [10]. Components made with these materials last longer and need less maintenance and thus, fewer inspections. Larger elements can be designed leading to quicker assemblies. Significant cost savings in manufacturing, machining and assembly processes can be achieved by utilising composites. It is estimated that if well-designed the reduction in the cost of the parts forming an aircraft and the labour wages can be around 25-30 % [10]. Furthermore, as the Young's Modulus to density ratio is very high substantial mass reductions of up to 30 % can be achieved by making use of this type of materials. In the case of airplanes, it is also more efficient to use composites since by reducing their mass the fuel consumption sees itself decreased too [15].

However, composites also present a set of drawbacks that must be taken into account. Fabrication cost is a critical concern. Repair of composite materials is a complex process that requires very skilled labours to detect flaws and cracks. In [16], Su presented a review on the state of the art of Lamb wave-based damage identification approaches for composite structures, showing the latest advances in this technique. Moreover, mechanical characterization of composite structures is more complicated than that of structures made of metal, as composites properties are not equal in all directions.

Composite materials are brittle, therefore higher stresses can be handled with little changes in strain. If a comparison of the structural behaviour between a specimen made of a ductile material, for example steel, and a specimen made of a brittle material, such as composites, both loaded with tension forces is made, ultimate failure of composites occurs without going through a plastic stage as it is shown in Figure 5.3. Energy is absorbed causing internal delamination (separation of layers) that causes the sudden collapse of the structure. This particular characteristic can be considered advantageous in our case as very little deformations are allowed ensuring so that the airgap deflection will be maintained within the limits. However, the fact of not having a plastic stage makes hard to identify any structural damage that can lead to a sudden collapse. In a breakdown event, replacement of the whole machine would be probably required as the composite features make them extremely difficult to repair.
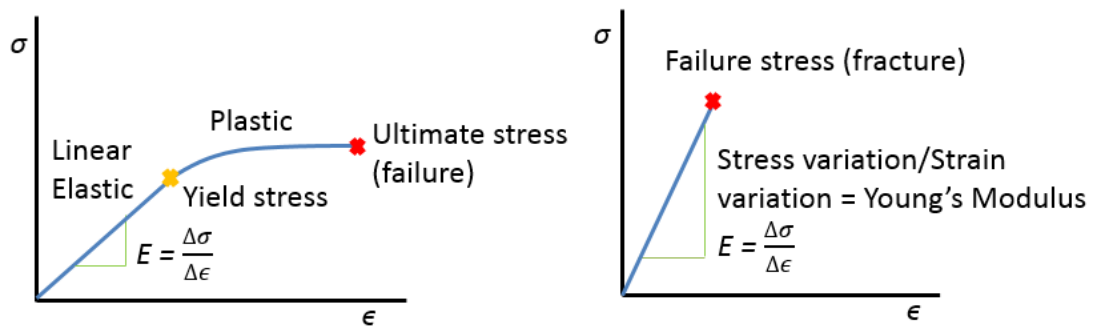
Figure 5.3 Stress-strain curves for Ductile (left) and Brittle (right) materials

5.2.5 Other factors to be considered in design

The thickness of laminates is an issue that needs to be addressed since with thinner laminates (10 to 16 plies for example), the energy from loading deforms the laminate and what is left delaminates the laminate. For thicker laminates, it works the other way around. In other words, the energy is spent on delamination purposes and the remaining is left for the deformation of the laminate itself. The thickness of the laminates is a design choice usually made according to the loads that the structure must withstand. The larger the loads, the thicker the laminates. As very large torque

and radial loads are expected for direct drive machines, the use of thick laminates will be necessary. Bearing all of this in mind, a suitable factor of safety must be taken into account. Figure 5.4 displays an example of delamination acquired during the stator structure design stage.
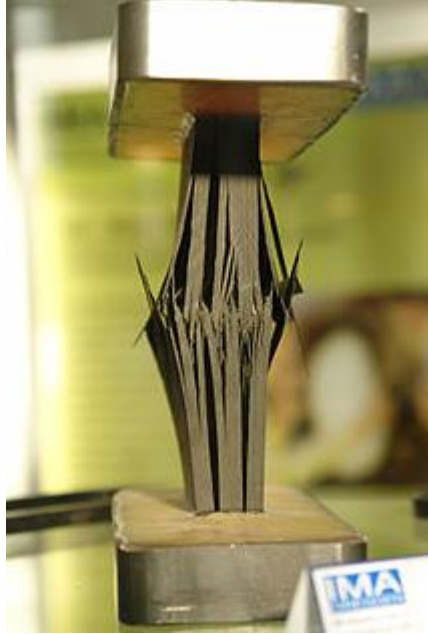
Figure 5.4 Composite structure delamination [17]

Finally, corrosion resistance of composites needs to be considered. Plastics do not corrode even from salt water. Nevertheless, when aluminium, magnesium, cadmium or steel are used with composites a galvanic type of corrosion can happen, as these materials own different electrical properties. To avoid galvanic corrosion, titanium fasteners are required. They are more expensive and they will add more weight.

5.2.6 Establishing the design conditions: loading

The design process starts by looking at the project's requirements. Different types of loads can act on the assembly and the structure must be ready to resist them without being damaged in any way. There are four key loads that every single structure must be able to withstand: tension, compression, shear and flexure.

a) Tension

A composite under tensile loads can respond in many different ways depending on the tensile stiffness and strength of the reinforcement fibres (stiffness and strength properties are higher than the resin based matrix on its own). Figure 5.5 illustrates the four typical loads acting on a composite.

(a)   (b)

(c)   (d)
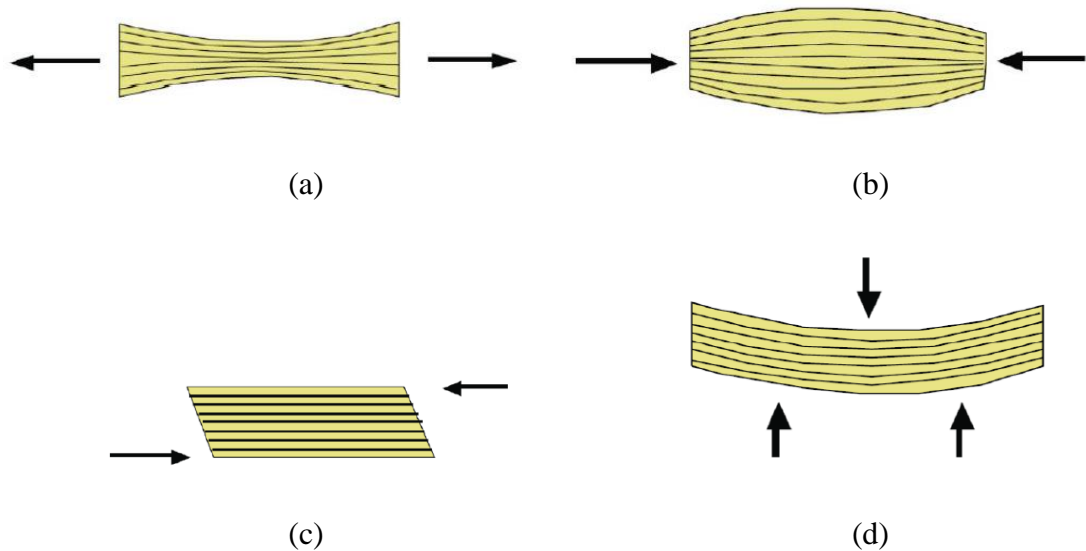
Figure 5.5 Composite loading: (a) Tensile; (b) Compressive; (c) Shear and (d) Flexural [6]

b) Compression

Under compressive loading the adhesive and stiffness properties of the resin system (matrix) are critical in order to maintain the fibres of the reinforcement straight at all times and protect them against buckling.

c) Shear

Under a shear load, the matrix transmits the stresses across the composite. Excellent mechanical properties are desirable, as well as high adhesion to the reinforcement fibres, for the composite to withstand this load, which tries to slide nearby layers of fibres over each other. In a laminate, the interlaminar shear strength (ILSS) is employed to designate this property. This limiting property must be taken in to consideration when approaching a composite structure design. Nonetheless, it is also

convenient to remember that the use of different geometric configurations for the structure and fasteners will affect this property.

In the case of having no matrix, if a fibre breaks the whole structure would become useless. However, with the use of a matrix, shear stress transfer is achieved. This, also called crack arresting system, allows the structure to keep working even if a fibre breaks in that the fibres located within a short distance of the broken fibre are able to recover the stress. This is an indirect contribution of the matrix [18].

d) Flexure

Under flexural loads the structure experiences a combination of tensile load (lower face), compression load (upper face) and shear load (central section of the laminate) as can be seen in Figure 5.5 d).

Fatigue behaviour of composites is a remarkable point to be considered when designing composite structures. With metals, after 10 million cycles only 20 % of their strength remains whereas with composites 95 % of the properties are still usable [10]. Composites work better under tension than under compression. Despite this, their structural behaviour is still better than metals in both cases. In order to design composite structures, stress concentration must be analysed.

Typical understanding of fracture mechanics cannot be employed when designing composite structures because fracture toughness is not a material constant. For composites, a zone of damage can be noticed while for metals the most crucial damage is a sharp crack. Composite fracture mechanics is described by the Mar-Lin mathematical model which is widely used in industry. This model is for predicting the strength of composites with open holes and cut outs. To calculate the mentioned residual strength of the structure, 'σ_N^∞', the Mar-Lin formula is as follows [10],

$$\sigma_N^\infty = \frac{H_C}{2L^m} \qquad (5.1)$$

where H_C is the composite fracture toughness having units of stress, L is the half notch length and the exponent m is related to the stress singularity at the crack tip of the bimaterial interface. The order of singularity depends on the ratio of the shear moduli of the matrix and the fibre, and the Poisson's ratio [10].

5.2.7 Mechanically analysing a composite structure

Since composite materials are composed by two or more elements, their analysis is completely different from that of metals.

Looking at the micromechanics of a lamina, the average properties of the ply can be found by observing the properties of the said ply individual components. The following assumptions when considering the fibres and the matrix are usually made:

- Both fibres and matrix are linearly elastic
- The fibres are infinitely long
- The fibres are spaced periodically either in square-packed or hexagonal packed arrays

Three distinct techniques are available so as to calculate the elastic constants for the composite material founded on micromechanics:

- The use of numerical methods (FE)
- The use of models grounded on the theory of elasticity
- The use of the rule of mixture models based on strength of materials method

If the structure needs to be analysed looking at the macromechanics of a laminate the use of failure theories, such as the Classical lamination theory, and the development of stress-strain relationships are required.

5.2.8 Classical lamination theory

In finding the properties of a laminate, the use of the Classical lamination theory is a must. Superimposing the properties of each ply is not an option. This theory is utilised to estimate internal stress state, dimensional stability of laminated composites and stiffness. It couples extensional, shear, bending and torsional loads

with strain and curvatures. By introducing an environmental load analogy, residual strains and warpage caused by differential shrinkage and swelling of plies in a laminate can be included in lamination theory as well. The ABD matrix shown below describes the united influence of diverse types of loads and moments on laminated plate response. In the equality, N corresponds to loads, M are moments, ε are strains and κ are curvatures. A_{ij} are extensional and shear stiffnesses, B_{ij} are extension-bending coupling stiffnesses and D_{ij} are bending and torsional stiffnesses. For further information on where ABD elements come from see [9].

$$
\begin{bmatrix} N_x \\ N_y \\ N_{xy} \\ M_X \\ M_y \\ M_{xy} \end{bmatrix} = \begin{bmatrix} A_{11} & A_{12} & A_{16} & B_{11} & B_{12} & B_{16} \\ A_{12} & A_{22} & A_{26} & B_{12} & B_{22} & B_{26} \\ A_{16} & A_{26} & A_{66} & B_{16} & B_{26} & B_{66} \\ B_{11} & B_{12} & B_{16} & D_{11} & D_{12} & D_{16} \\ B_{12} & B_{22} & B_{26} & D_{12} & D_{22} & D_{26} \\ B_{16} & B_{26} & B_{66} & D_{16} & D_{26} & D_{66} \end{bmatrix} \begin{bmatrix} \varepsilon_x \\ \varepsilon_y \\ \varepsilon_{xy} \\ \kappa_x \\ \kappa_y \\ \kappa_{xy} \end{bmatrix}
\tag{5.2}
$$

Three distinct factors determine the mechanical behaviour of laminates: symmetry, balanced vs. unbalanced and stacking sequence.

A laminate is considered symmetric whether for every ply to one side of the laminate reference plane with specific material properties, a specific thickness and specific fibre orientation, exists another ply at the same distance on the opposite side of the plane with the same material properties, thickness and fibre orientation. If this is not the case, the laminate is referred to as an unsymmetric laminate. Unsymmetric laminates can have up to six different types of deformation caused by a single applied load. When studying symmetric laminates, all the extension-bending coupling stiffnesses (B elements) are zero. It is important that the elements of the B matrix tend to zero in order to avoid laminate curvature.

A balanced laminate is one which for every ply with specific material properties, a specific thickness and specific fibre orientation, there is another ply somewhere in the laminate with the same specific material properties, specific thickness and

opposite fibre orientation. A_{16} and A_{26} components are always zero for balanced laminates. Therefore, no shear will take place.

Symmetric and balanced laminates are desirable so that neither warpage nor shear can occur. Then, the laminate will nearly behave as an isotropic material.

Matrices B and D are dependent of stacking sequence. So as to reduce deformation, D matrix elements should be as big as possible.

5.3 Composite Structure Modelling

In order to model the supporting composite structure for the electrical machine of a direct drive wind turbine, a disc structure was selected and a finite element approach adopted. As Abdul-Aziz and Uddin propose for flywheels in [19] and [20] respectively, the ANSYS Parametric Design Language (APDL) was employed to carry out this task as it allows easy parametric changes in material, geometry, mesh, loads and boundary conditions.

The material selected was carbon-epoxy due to its excellent strength-to-weight ratio. Table 5.1 shows the material properties used for study,

Table 5.1 Material properties for a filament wound disc [20]

E_X	2.03×10^{11} Pa
E_Y	1.12×10^{10} Pa
E_Z	1.12×10^{10} Pa
v_{XY}	0.33
v_{YZ}	0.45
v_{XZ}	0.33
G_{XY}	8×10^9 Pa
G_{YZ}	3.8×10^9 Pa
G_{XZ}	4.2×10^9 Pa
ρ_c	1,600 kg/m^3
δ	5×10^{-6} m
θ	1.96×10^{-11} m^2

where E corresponds to the Young's modulus, G is the shear modulus, v, is the Poisson's ratio, ρ_c is the density, δ is the distance between fibres and θ is the cross-section area of a single fibre. Data for the Shear modulus in the YZ and XZ planes where estimated using equation 5.3:

$$G = \frac{E}{2(1+v)} \qquad (5.3)$$

Assuming a perfect bonding between fibres and matrix, the distance between fibres, δ, and the cross-section area of a single fibre, θ, were picked so that the highest possible fibre volume fraction can be obtained. The fibre volume fraction utilised in these analyses was 90%.

The type of element utilised in the analysis was Shell281. As seen in Figure 5.6, it owns eight nodes (I, J, K, L, M, N, O and P) with six degrees of freedom at each node: translations in the X, Y and Z axes, and rotations about the X, Y and Z axes. It is suitable for studying thin to moderate-thick shell structures. The element accounts

for consequential effects of distributed pressures [21]. Figure 5.6 displays the geometry, node locations and the element coordinate system.
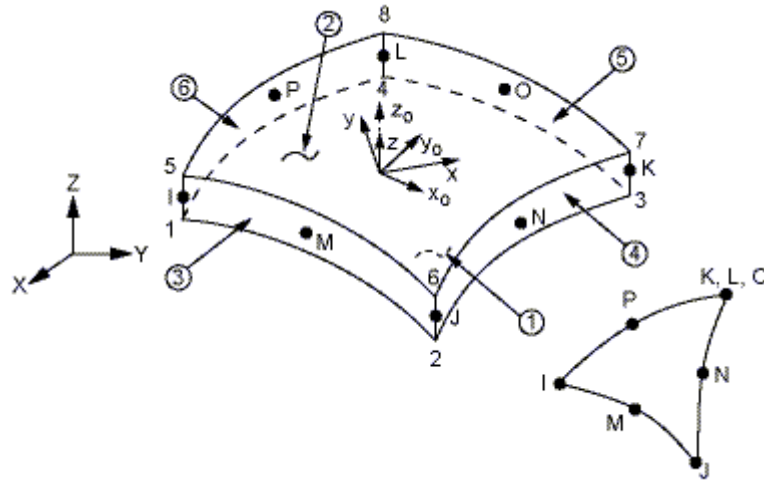
Figure 5.6 Shell281 Geometry [21]

The model of the structure was created using the GUI tool available in ANSYS APDL. It was constrained at the shaft and three different sorts of loads were applied to the generator structure:

- Radial expansion load acting on the rim sub-structure of 400 kPa corresponding to the Maxwell stress. This corresponds to an airgap flux density of 1 T.

- Tangential load again acting on the rim of 30 kPa corresponding to the shear stress. This loading was divided by four and applied in the form of forces of 120kN for the large scale model and 5.5 kN for the one at a small scale, to the keypoints located at the cylinder midspan and equally spaced. This can be seen in Figure 6.6.

- Gravitational loading in the Y axis of 9.81 $m.s^{-2}$. Gravity was also tested in the Z direction in order to consider the weight effect during the generator's transportation stage.

Figure 5.7 depicts in detail all the loads acting on a generator rotor disc structure model.

- Radial expansion load = 400 kPa
- Shear load = 30 kPa
- Gravitational load (Y) = 9.81 m.s^{-2}

Cylinder sub structure
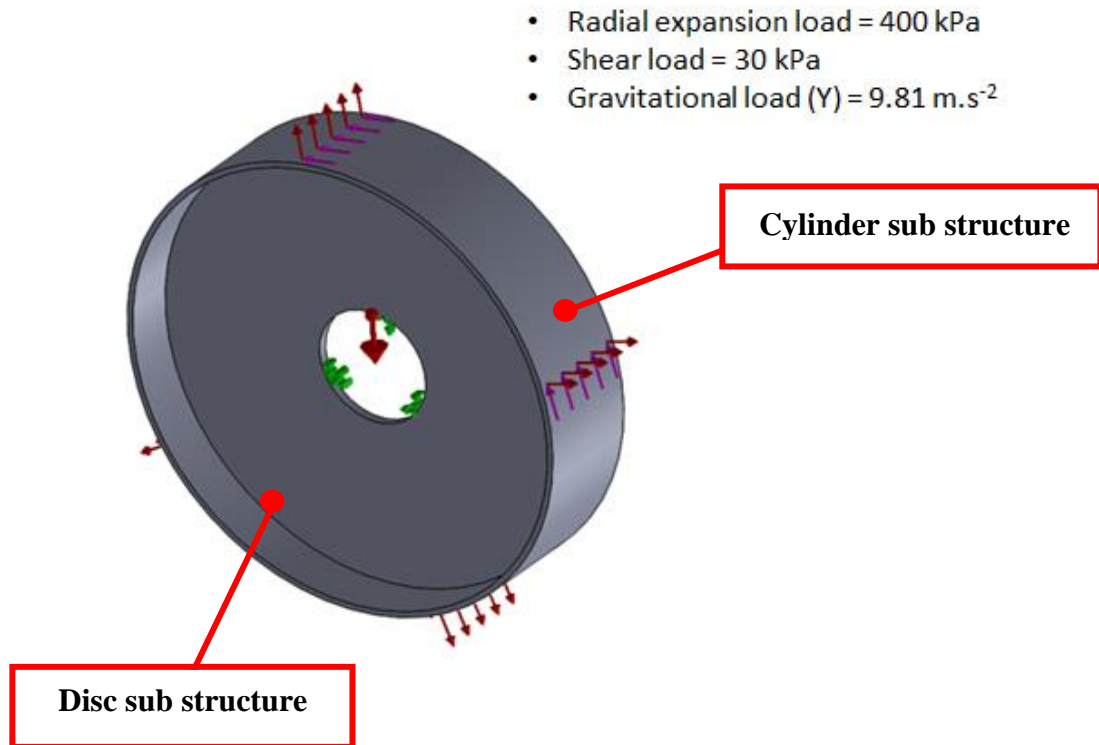
Disc sub structure

Figure 5.7 Loads acting on the generator rotor structure

Two distinct methods were used when creating the model of the disc that would be merged with the outer cylinder sub structure lately: the conventional approach and the mosaic pattern disc approach as stated by Morozov in [22].

In the conventional approach (CA), the disc is modelled as a laminated circular plate consisting of a certain number of plies; see Figure 5.10, whereas the mosaic pattern disc is composed by four plies of different thicknesses and orientations depending on the corresponding area. For this model, the disc area is divided into sub areas as it can be seen in Figure 5.11.

Electrical machines structures for direct driven wind turbines were modelled according to at both small and large scales. The benefits of composites are likely to be different at these scales, and so two case studies were performed. At the small scale, a 100 kW buoyant airborne wind turbine, also known as BAT, created by Altaeros Ltd. [23] was investigated. This device shares much of the wind turbine technology with its grounded cousins and also introduces additional constraints. One such limitation is the requirement of the turbine equipment to be lightweight. With

this is mind, the design of the supporting structure for a generator of 0.42 m radius and 0.21 m axial length rotating at 140 rpm and with a torque of 6.8 kNm was started first following the conventional approach to then continue with the more complex one. In the early stages, it was thought that fibre reinforcement of certain plies could enhance the stiffness characteristics of the machine modelled using the more complicated configuration. This option was tried, as shown in Figure 5.12, and discarded as it was observed that it did not introduce any further noticeable improvement to the design. The mesh for the small scale model was created following the same procedure as stated in the following section. However, it is important to highlight that the size for the quads of the inner/outer areas was 0.05m, whereas for the rest was of 0.005 m. The elements in the areas at the edges had to be refined twice.

Having the small scale structure modelled and tested, it was proceeded to draft a 3 MW large scale case study model. The same approaches were tracked to design this structure of 2 m radius and 1.2 m axial length again with the purpose of minimising its mass.

With the composite structures finished, a mass comparison with models made of steel (AISI 304) and designed to comply with the same structural requirements, this means, as already mentioned, that deflection in all directions must remain below the stipulated limit of 10 % of the airgap size. For the small scale model that is equal to 0.208 mm, whereas for the large scale it is equal to 0.5 mm.

Two electrical machine supporting structures made with discs have been modelled following the methodology described in this section, one at small scale and one at large scale corresponding to 100 kW and 3 MW wind turbines, respectively.

So as to come up with a design that can fulfil the structural requirements stated a factorial design of experiments was developed for both the small scale and large scale models. For the models with conventional configurations a design of experiments process was completed for each section (disc and cylinder). For the more mosaic pattern composite structure a design of experiments process was carried out for every area forming the disc structure and for the cylinder.

After those procedures were terminated it was obtained that a stacking sequence of 90/0/45/0/90 was the one presenting less deflection for both the disc and the cylinder of the CA structures no matter the size. With this in mind, an optimisation process of the thicknesses of the plies was made. It was observed that the influence of the 90 degrees and the 45 degrees plies in the cylinder was negative and elevated the deflection in the sub-structure for both the small and the large scale models. Therefore, they were removed. The deflection for each attempted stacking sequence of the laminates forming the CA structure with 5 mm plies is given in Table 5.2.
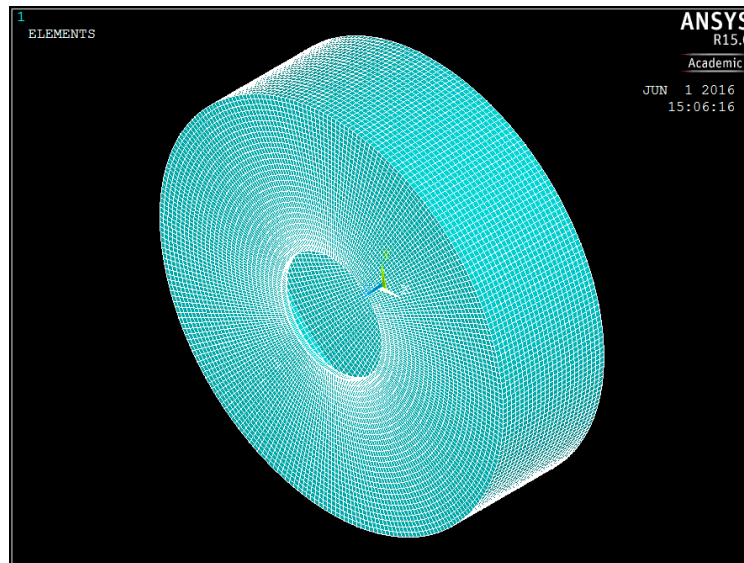
Figure 5.8 Stator structure according to the conventional method

5.4 Investigation

5.4.1 Conventional Approach

For this model, the construction of a mesh of an adequate density was determined by an independence study which gave a result of 0.05 m quad element size. A mapped mesh was used as depicted in Figure 5.8 for the generator with a CA disc sub structure. The orientation of all the fibres within this model was set according to the original Cartesian coordinate framework and it was assigned to each element through the creation of two different sections, one for the disc sub-structure and one for the cylinder sub-structure. In order to find the best stacking sequence for either the disc or the cylinder a factorial experimental design was carried out [24]. Three different

thicknesses (0.005 m, 0.01 m and 0.02 m) and three different fibre orientations of 45, 0 and 90 degrees were assumed. All the possible combinations for the stacking sequence (keeping symmetry), see Table 5.2, and thicknesses were tried as stated by the factorial design. For each stacking sequence, the thicknesses of two orientations were fixed to 0.005 m, whereas the one remaining was changed.

After attempting the 54 possible combinations, it was found that 90/0/45/0/90 was the most suitable for the disc and the cylinder sub-structures. The deflection results obtained for the six stacking sequences with all the plies with 0.005 m thickness are given in Table 5.2.

Table 5.2 CA Composite Structure Stacking Sequence

Stacking Sequence	Outer Ply (1)	Inner Ply (1)	Mid Ply	Inner Ply (2)	Outer Ply (2)	Deflection (mm) for 0.005 m ply thickness
1	90	0	45	0	90	0.139
2	0	90	45	90	0	0.14
3	45	0	90	0	45	0.14
4	45	90	0	90	45	0.141
5	90	45	0	45	90	0.14
6	0	45	90	45	0	0.14

The last step was to optimise the thickness of plies taking into consideration the deflection limit. In the cylinder case, it was observed that the 45 and 90 degrees plies did not introduce any improvement in the stiffness of the overall generator structure, hence they were removed, leaving the 0 degrees ply alone, which corresponds to the hoop direction. Figure 5.9 depicts a flowchart describing the process, while in Figure 5.10, the composite material fibre orientations utilised in this investigation can be recognised.
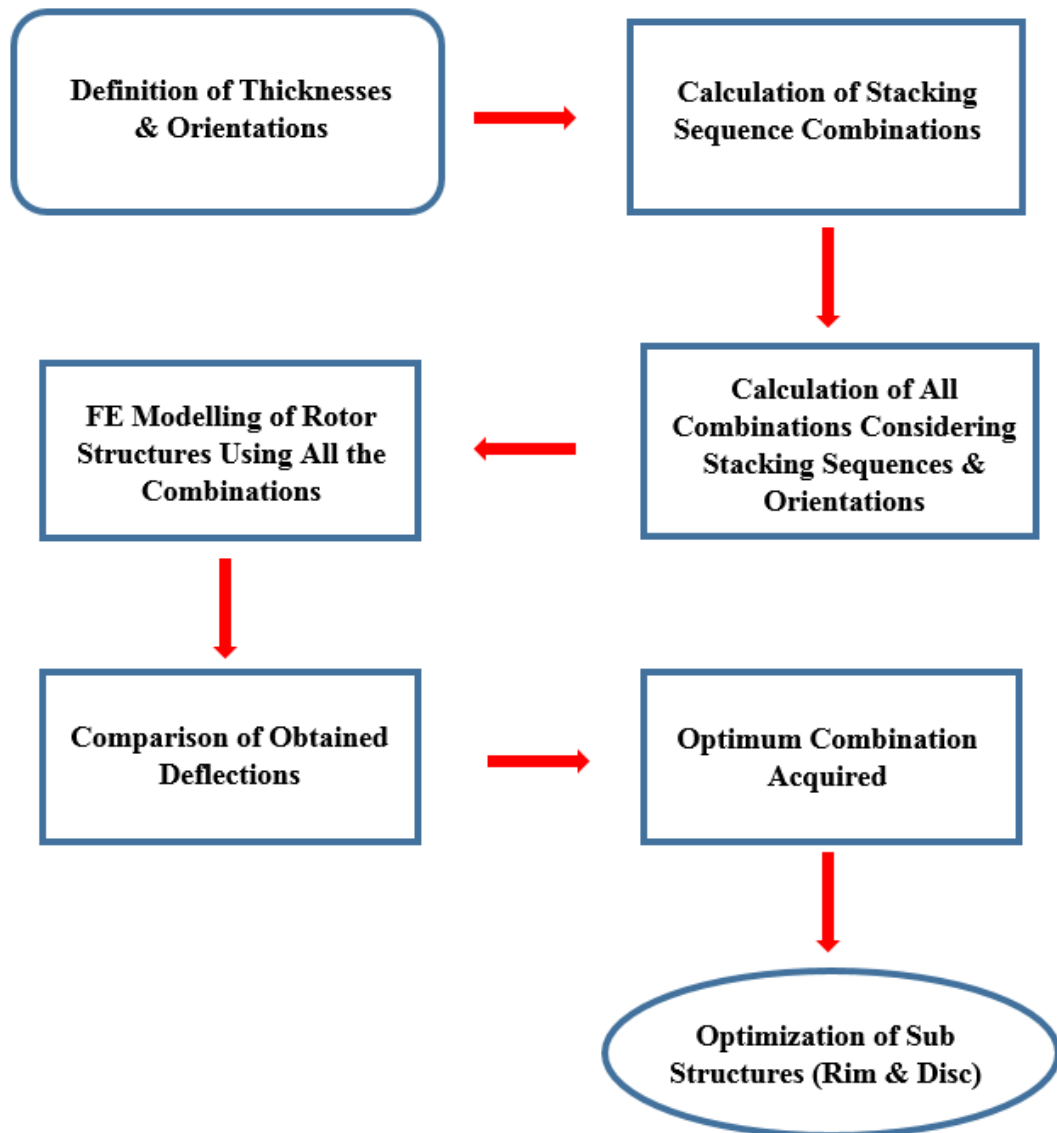
Figure 5.9 CA composite structure design process used in this chapter

(a)   (b)

(c)
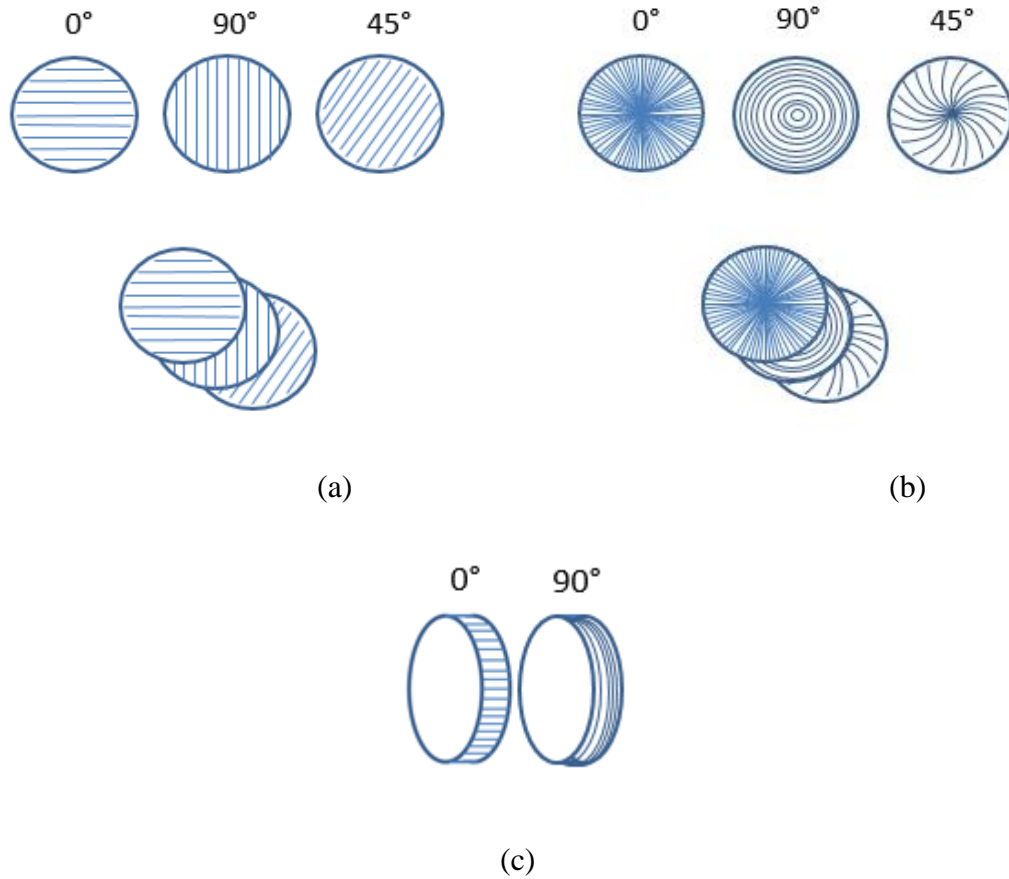
Figure 5.10 Example of Composite Fibre Orientations & Stacking Sequences for the Generators Components; (a) Following a Cartesian Coordinate Frame; (b) Following a Cylindrical Coordinate Frame; (c) For the Cylinder Sub Structure Following a Cylindrical Coordinate System

5.4.2. Mosaic Pattern Approach

For the mosaic pattern disc sub-structure, 5 cylindrical coordinate systems were created so that the orientation of the fibres in the different areas could be assigned. Eleven unlike sections were generated for the disc, while for the cylinder only one was needed. Afterwards, the sections were applied to the areas. In the first instance, a quarter of the rotor was developed and then reflected in the X direction with the YZ plane acting as a mirror. Finally, the resultant structure was again mirrored in the Z axis direction. The same procedure was utilised to model the stator structure. See Figure 5.11.
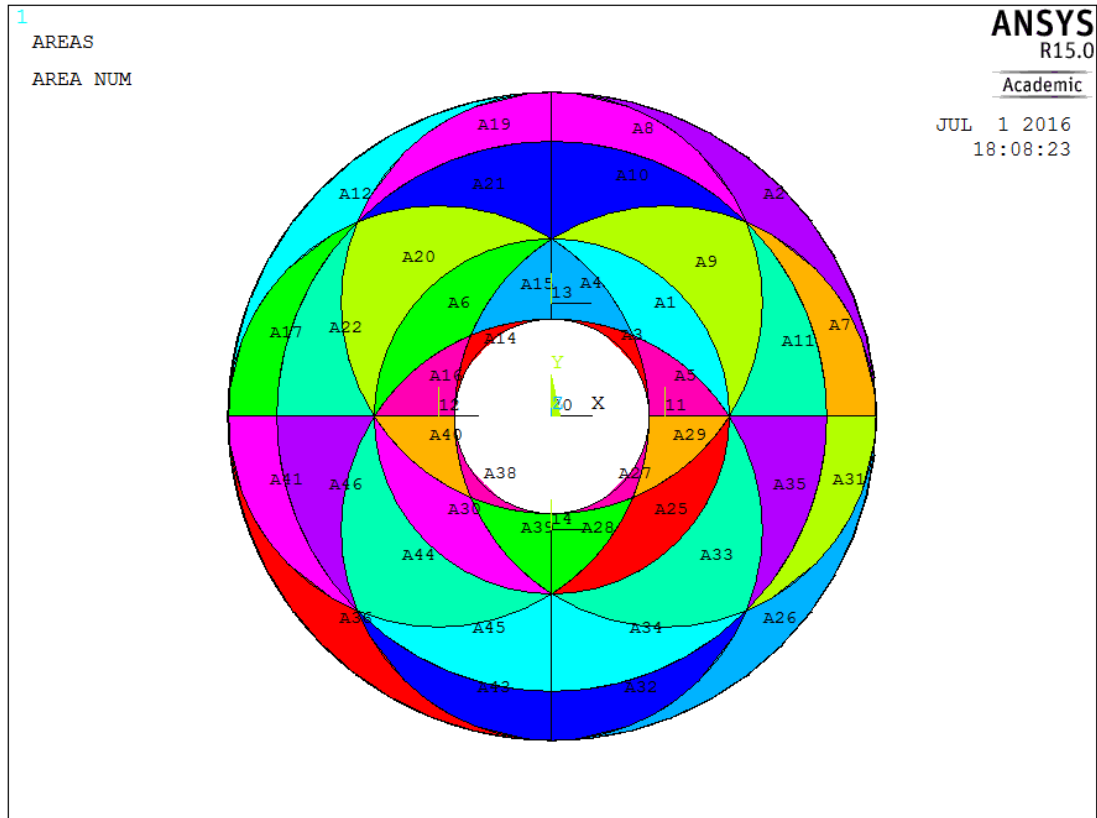
Figure 5.11 View of the areas forming the mosaic pattern composite disc sub structure

A more concise mesh control had to be used for this model due to the sharp edges of the outer and inner areas of the disc. As a result, the element size for the mentioned areas was first set to 0.1 m. A free quad mesh was employed, although a triangle one could also be used especially taking into account the shape of these zones obtaining good outcomes. Then, the elements generated were refined twice using the minimal level of refinement available, or level 1, which produces an element of half the length of the original element [21]. The rest of the areas were meshed utilising a free quad mesh of 0.05 m element size and no further refinement was necessary. The main aim to use a more refined mesh in the inner/outer zones was to control the shape and the size of the disc elements merging with the cylinder ones and to avoid errors in the grid creation. See Figure 5.12.

The models with a more advanced structure, also known as mosaic pattern composite structures, were designed following the guidelines specified above. However, for the first attempt (the small scale model), fibre reinforcement and only one fibre

orientation per area as stated by Sayem in [20] were utilised as observed in Figure 5.12, where the fibre orientations have been highlighted with coloured arrows matching the colour of the origin of the cylindrical coordinate system that they track. The fibre reinforcement option available in ANSYS APDL allows the user to simulate a cluster of fibres placed according to the structure needs in order to enhance its mechanical properties. Certain key zones were reinforced using smear layers of the same material so that the stiffness of the structure could be improved. A secure bond between the reinforcing fibres and the base element is assumed by ANSYS and the motion of the reinforcing fibres is determined solely by the motion of the base element as the relative movement between the mentioned components is not allowed [21].

Despite the potential of this tool no influence in the properties of the structures was noticed. Moreover, the lack of flexibility in the design made extremely difficult to reduce the mass and comply with the imposed specifications at the same time. Thus, this option was discarded. More flexibility was given to the design as requested in search of decent results that would set the path to track. Following the preceding established with the CA generator structure, a factorial design of experiments was carried out utilising the same thicknesses and fibre orientations but in this occasion for each area. It was checked that the most suitable fibre orientation for the rim was still 0 degrees and the addition of any ply of any thickness or fibre orientation makes the deflection go up. Once the most favourable orientations were found (for either the disc areas or the rim), the thicknesses were optimised so that the overall weight of the structure could be minimised. Thickness of areas with small sizes was increased as much as possible so the thickness of the largest areas could be decreased. This trade off process of optimisation went on until the deflection limit was reached.
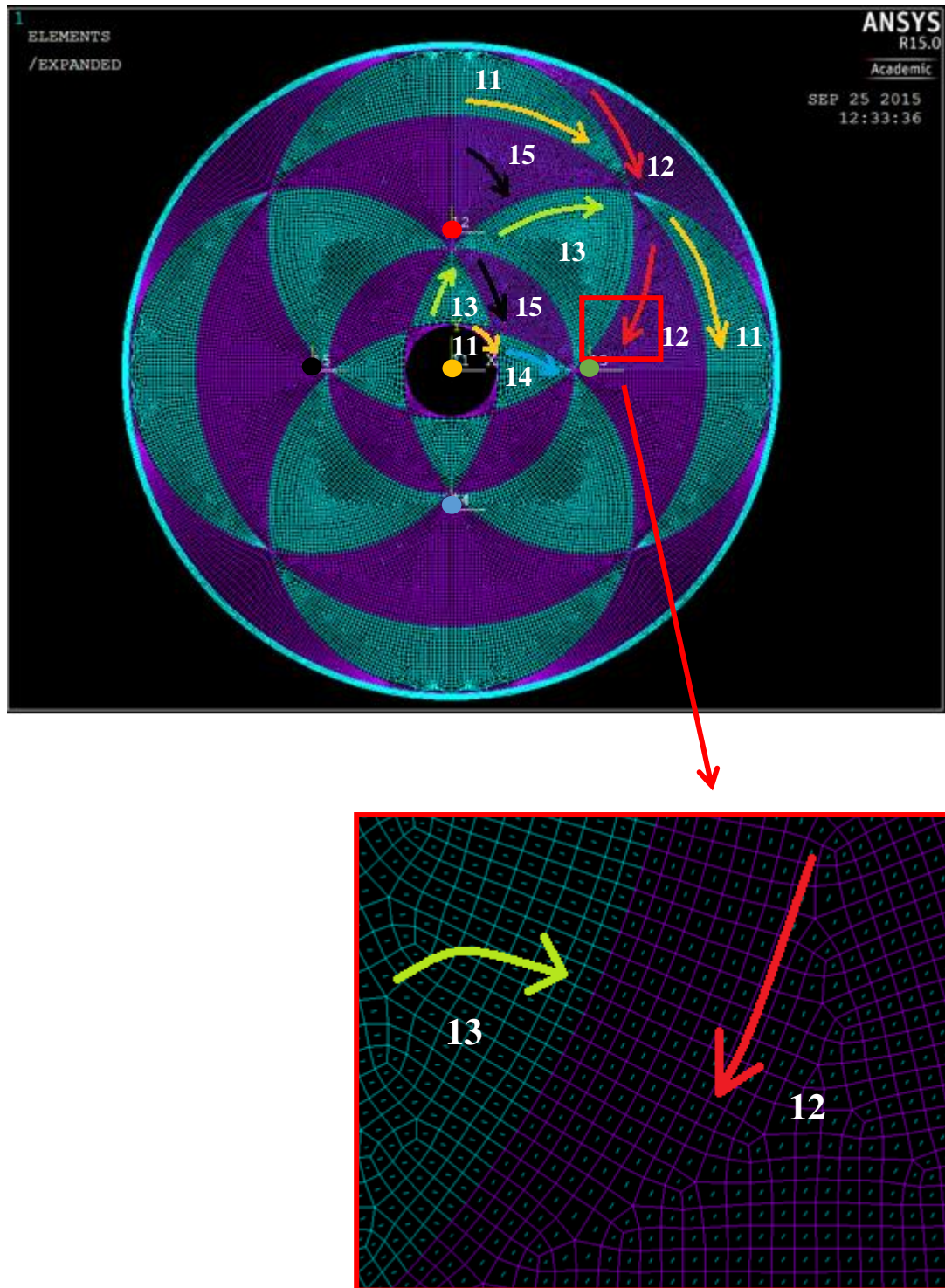
Figure 5.12 Detailed view of the composite rotor disc structure based on Morozov's model highlighting variable fibre orientation (small green bits) and reinforcement in purple [25]

5.4.3 Conventional Approach vs. Mosaic Pattern Approach

A comparison between the stress plots for a CA and mosaic pattern composite structures is depicted in Figure 5.13. Stress concentrations in the disc sub structure have been cancelled in the mosaic pattern structure due to the effect of the fibres interlacing.
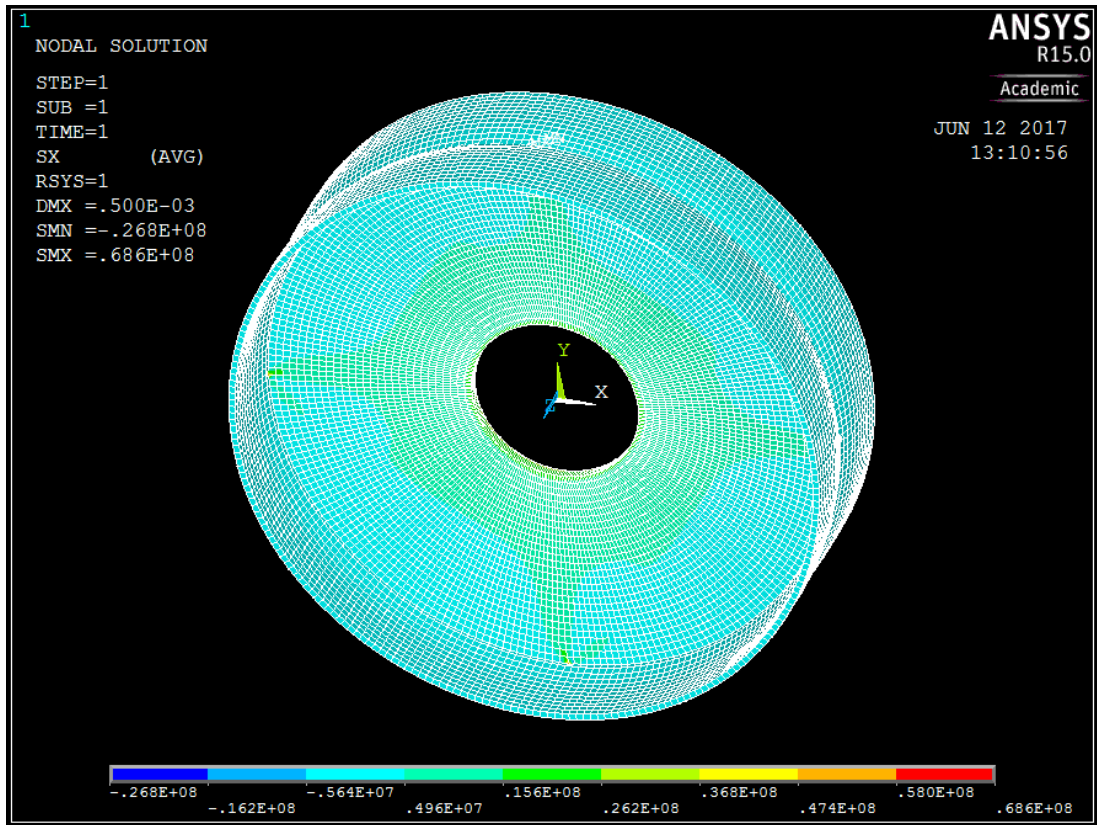
(a)
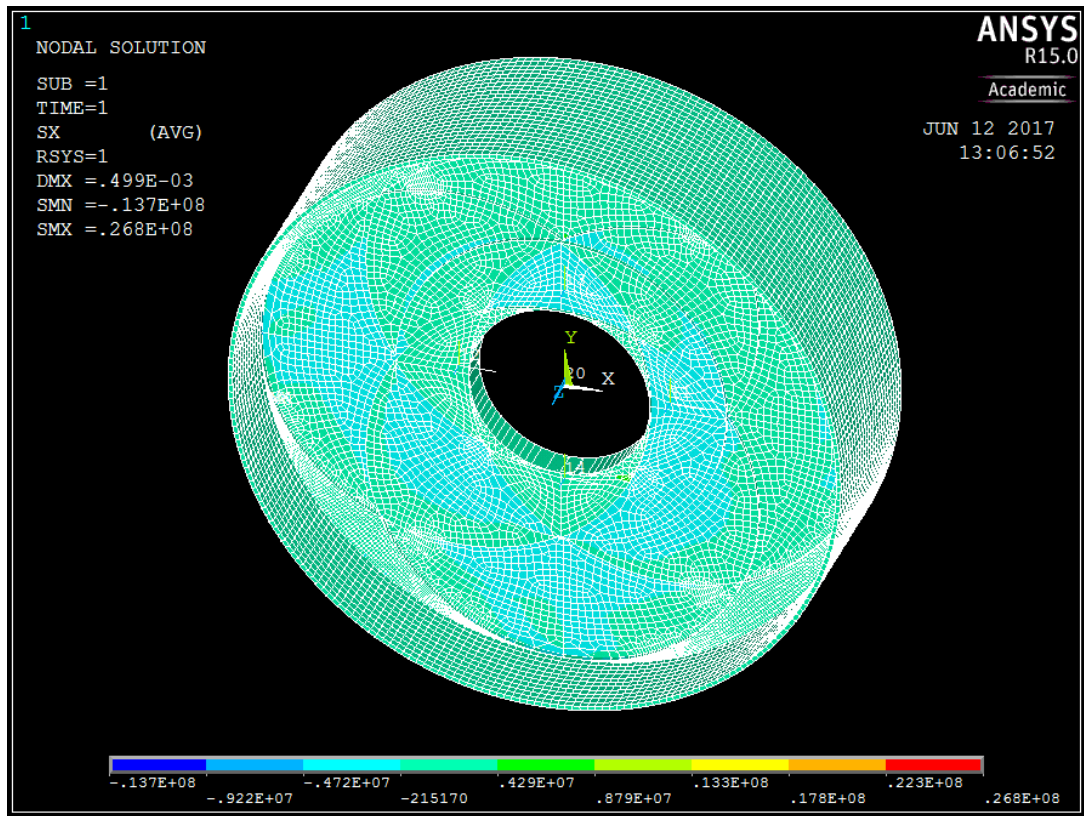
(b)

Figure 5.13 Contour plots highlighting stress in the radial direction (a) CA composite rotor structure (b) Mosaic pattern composite rotor structure

The contour plot illustrated in Figure 5.13(b) shows a result of -0.472×10^7 Pa of tensional stress across the disc, with certain areas working again under tension at even less stress (-215170 Pa) for the more advanced model, while the CA model shows a combination of stress loading of distinct order of magnitude (tension and compression of -0.564×10^7 and 0.156×10^8 Pa respectively) that will have a big negative influence in the life of the structure.

Table 5.3 shows the effect of reducing the thickness of the critical areas of the large scale model mosaic pattern disc sub-structure on the deflection and by definition on the stress. Areas 2 and 3 were not at play as they produced either no noticeable improvement or unacceptable deflections with large stress concentrations.

Table 5.3 Effect Caused by the Reduction of Critical Areas Thickness

Areas	Thickness Reduction (mm)	Mass (kg)	Total Deflection (mm)
1	4	8	0.2
4/5	2	4	0.1
8/7	2	8	0.2
9	2	8	~ 0.1
10/11	2	9	0.4

As understood, the combination of areas 10 and 11, which correspond to midspan areas of the disc sub structure as Figure 5.11 illustrates, are the ones giving the highest deflection, although they are also taking away the highest amount of material with 9 kg per 0.2 mm of thickness reduction. The combination of areas 4 and 5 give the lowest deflection but with the lowest mass reduction, whereas area 1 and the combination of areas 8 and 7 offer fair results with 8 kg per 0.2 mm of deflection. The best outcomes were obtained by minimising the thickness of area 9. As seen, 8 kg of mass drop was achieved per 0.2 mm of thickness reduction which gives ~ 0.1 mm of deflection.

5.5 Results

Different materials and design approaches for electrical machine supporting structures have been presented in this investigation. Suitable disc steel structures have been proposed for both the small and big scale models. As presented in Chapter 4, the total mass (includes rotor and stator structures) of the small scale model made of steel was 313.2 kg with 114.76 kg for the rotor and 198.46 kg for the stator. A further optimisation of this structure was carried out obtaining a total mass of 266.7 kg, with a mass of 91.1 kg for the rotor and 175.6 kg for the stator. This means a drop of about 15 %.

With the lightest steel structure configuration identified for the small scale model, the use of composite materials in the structure design was attempted tracking two distinct methods named conventional approach, 'CA', and mosaic pattern approach. They have been already described in Sections 5.3 and 5.4.

In the case of the CA small structure, the rotor mass was 34.1 kg, while the stator mass went up to 41.4 kg giving a total of 75.5 kg. If a comparison with the optimised steel structure is made, it can be appreciated that a significant reduction of nearly 72 % was achieved.

For the mosaic pattern fibre orientation generator structures, it was estimated that the mass for the small scale rotor structure is 16.96 kg. The stator structural mass was 33.25 kg. This makes a sum of 50.21 kg, which gives us a difference of about 25.3 kg with the conventional configuration model. This means an overall reduction in mass of about 33.5 %. The results obtained for the small scale model structures have been plotted in Figure 5.14 for comparison.
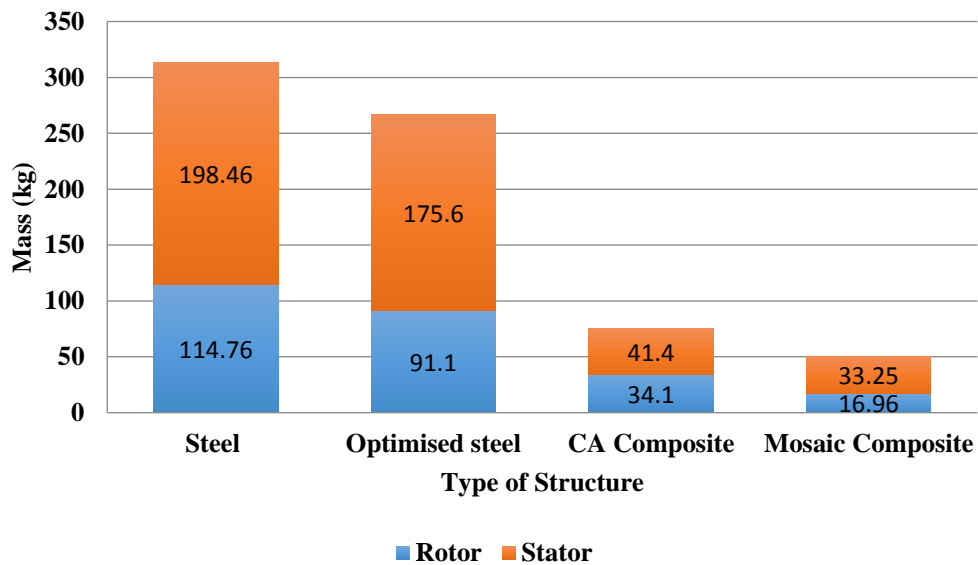
Figure 5.14 Small Scale Model (Mass vs. Type of Structure)

Large scale models corresponding to a 3 MW electrical machine supporting structure were developed following the same procedure. A steel structure was modelled, as described in Chapter 4, achieving a result of 9809 kg for the rotor structure and 9451

kg for the stator. Adding up these values, it was obtained an overall mass 19260 kg. After further optimisation, a decrease of 38 % was acquired. The total mass for the optimised model corresponded to 12000 kg with the rotor accounting for 5694 kg. The mass of the stator structure was 6306 kg and as it can be seen, its optimisation contributed less to the weight reduction than the rotor one.

Regarding the composite structures, in the case of the CA large scale model, the rotor structure had a mass of 2488.5 kg, whereas the stator one was of 4346 kg. The total mass of the generator structure was 6834.5 kg, which means a drop of 43 % if compared to its optimised counterpart made of steel.

For the mosaic pattern approach large scale model, the rotor had an estimated mass of about 2418 kg. The mass of the stator structure was about 4550 kg giving us an overall value of 6968 kg. The difference between this model and the one with the conventional layout was 133.5 kg and it can be neglected. A tiny saving in mass of 70.5 kg could be made for the rotor, while for the stator a negative result of 204 kg was understood. Figure 5.15 shows the outcomes achieved for the large scale structures.
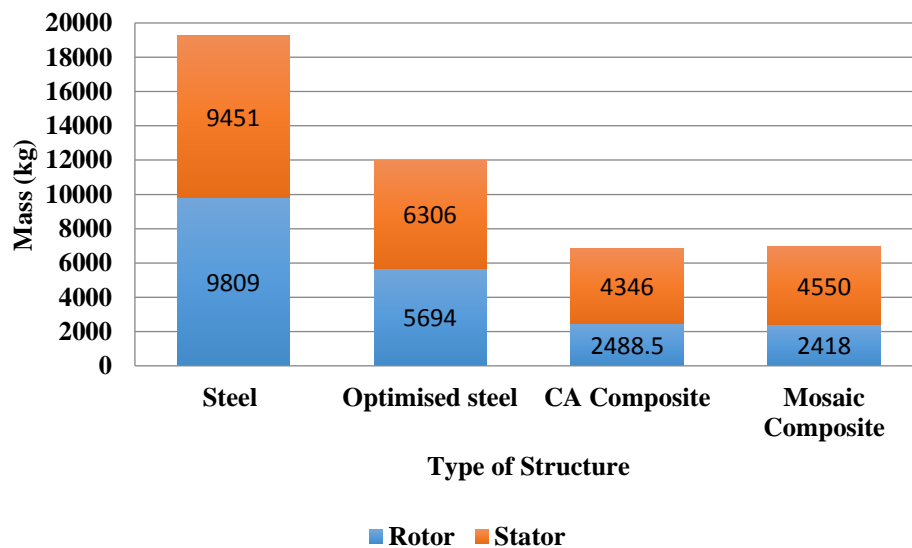
Figure 5.15 Large Scale Model (Mass vs. Type of Structure)

Figure 5.16 shows the result achieved for the final design of the mosaic pattern approach stator structure. The concentration of deflection highlighted in green on the

cylinder corresponds to the location of the tangential forces, which were placed like that as the available ANSYS license had a limited number of nodes that could be loaded. With a load uniformly distributed along the rim, it is thought that less deflection would be obtained allowing for further optimisation of the structural mass.
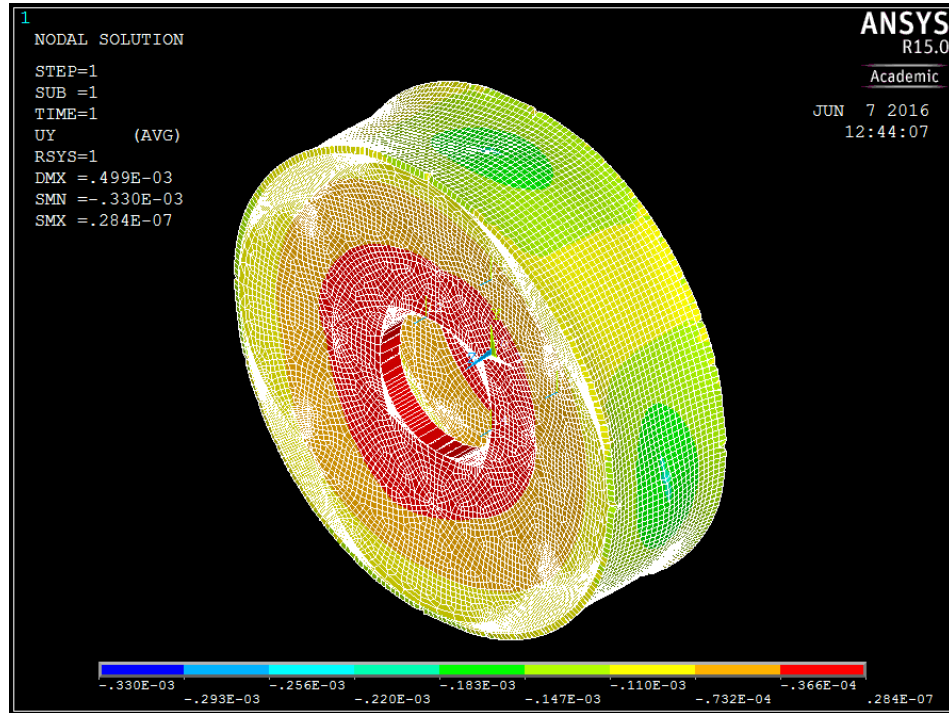
Figure 5.16 Contour plot displaying maximum deflection in the hoop direction of the mosaic pattern approach composite stator structure

Having said that, further improvements might be achieved by considering designs with larger number of areas as proposed by Sayem in [20] that would provide with the necessary flexibility to the design.

5.6 Discussion

Structures made of steel have been assumed and analysed with the main of reducing their mass. Under radial, torque and gravitational loading conditions and constraints as described in Section 5.3, the minimum mass for a conventional steel structure was of 313.2 kg. However, if the steel structure is optimised a substantial difference can

be obtained. The total mass for an optimised steel generator structure would be 266.7 kg, which means that an overall mass drop of 15 % can be achieved.

On the other hand, two different ways of designing electrical generator supporting structures made with discs for direct-drive wind turbines using low density materials, such as composites, have been also presented. First, a small scale model was created following the conventional approach and tested under the typical loads acting on the drivetrain of a direct driven machine of 0.42 m radius, 0.21 m axial length, 2.08 mm airgap, 140.1 rpm rotor speed and 6,817 Nm torque corresponding to a 100 kW wind turbine. Then, a mosaic pattern configuration was modelled and tested under the same parameters. After a comparison, a difference in mass between the two models of 25.3 kg was achieved. This is equivalent to a reduction of up to 33.5 %. Furthermore, whether a comparison with the optimised steel model is made an overall mass reduction of 72 % in the case of the conventional model and 82 % in the case of the more advanced mosaic pattern design have been reached.

It could be observed that higher mass savings can be acquired for the rotor structure than for the stator structure. For instance, in the mosaic pattern approach model case, a decrease of almost 50 % was achieved for the rotor, while a 20 % was reached for the stator. This difference can be explained by looking at the sort of loading acting on the structures in question. The rotor structure is subject to a radial expansion load uniformly distributed along the outer surface of the rim, besides the tangential and gravitational loads. On the contrary, the stator is subject to a radial load acting on the inner surface of the rim and pointing inwards besides the tangential and gravity loads. This means that the rotor structure is mainly working under tension when the stator is working under compression. Performance of composites decreases when they work under compression. Typically, mechanical properties of composites working under compression are about 30 % lower than when subject to tensile stresses. Due to this important factor, the thicknesses of the largest areas that form the disc sub-structures of the stator had to be increased.

In addition, the configuration of the structures is completely different with the rim of the rotor being supported by a disc concentrically located and the cylinder of the stator being maintained by two discs placed at its edges. The stator layout can be

considered much weaker as the area of the rim not being supported is larger than that of the rotor.

Generally speaking, it can be said that the mosaic pattern model without reinforcements and using multiple fibre orientations gave better results if compared with the conventional model because of the addition of more flexibility to the design. The use of fibre reinforcement and a fixed fibre orientation for each area was seen as a constraint during the early stage of the design as mass optimisation could not be carried out if the structural requirements wanted to be fulfilled. For this reason it was discarded.

By dividing the disc sub structure area into smaller zones that can have different layups, the designer introduces more variables to play with to this parametric model. The use of several plies with unlike fibre orientations that follow five distinct coordinate systems allows the designer to manage the stress by spreading it or simply concentrating it in purpose into smaller areas. With this, minimisation of thickness of large areas can be achieved. Special care has to be taken regarding the nature of the stress. When designing a structure like this, the avoidance of cyclic loading of large amplitudes is a must. Taking into account the brittle behaviour of this sort of materials, the variable thickness of the structure will play a crucial role in its working life.

The design of the composite structure for the large scale model with a radius of 2 m and an axial length of 1.2 m was made following the same procedure as for the small scale one. Very significant mass reductions were acquired for both models, the conventional one and the mosaic pattern one if compared with a structure made of steel. As explained in Chapter 4, the steel structure was optimised by using the Design Explorer tool of ANSYS Workbench giving a result for the mass of the whole structure of 12000 kg. The rotor accounts for 5694 kg while the stator weights 6306 kg. In the worst case scenario, a mass drop of 6968 kg could be achieved by utilising composite structures, which means a decrease of nearly 42 %. Bearing this mind, it can be said that the use of this type of lightweight materials is a viable option whether a significant structural mass reduction is pursued.

Nevertheless, it is essential to point out that the mosaic pattern design was not able to make any further improvement to the mass reduction. Yet, the structural performance of both the rotor and the stator were enhanced as the cyclic loading acting on the discs and on the rim individually was eliminated.

It is considered that further mass reductions could be achieved if the designer goes a step beyond and introduces even more flexibility to the mosaic pattern model. Models (a) and (b) displayed in Figure 5.17 have been analysed in this research. Due to time constraints, designs (c) and (d) could not be explored. However, the author thinks that they would introduce the required resilience to approach more ambitious optimisations. As suggested in Section 5.4, the use of more variables would add more complexity to the design. For this, the development of a script that automates the process is recommended. A powerful computer would be necessary to handle and process the amount of data that these simulations would generate.

Looking at the structural design of the machine from the manufacturing perspective, it can be easily asserted that the more complexity added to the design, the more expensive will be to manufacture the structure. Therefore, the cost of manufacturing, which would include the cost of material, wages of skilled labours, the use of special tooling and handling equipment amongst others, should be estimated before pursuing such investigation. Nevertheless, if the amount of material to be removed is large enough the overall cost could be balanced.

The structural performance has been enhanced, as it has been demonstrated, by utilising the mosaic pattern model. Working life of the structure is another important input to be included when carrying out the risk analysis of the project.

Last but not least, certain simplifications and assumptions were made during the accomplishment of this study. For example, thermal aspects were no considered. The fibres utilised to form composite materials own very low coefficients of thermal expansion. Nonetheless, the sensitivity of the composite structure thermal expansion coefficient to variations from fibre orientations can be significant as thermal response of the composite materials can be tailored directionally as desired by placing the laminates in the appropriate manner [26]. Due to the complexity and the variety of

approaches that could be followed, it was thought that a more concise analysis was required. For this reason, a deep investigation of this field and its effects on the design of any composite structure proposed is recommended.

On the other hand, it was considered that steel back iron does not add any strength or stiffness to the structure. By taking into account this feature, more accurate structural optimisations might be achieved.

Finally, this research has no concerns about the connection of any composite structure presented here to the shaft, bearings, turret, bed plate and rotor and stator back iron that can be very challenging. Taking the aircraft industry as an example, titanium fasteners are usually employed to join metallic parts with composites, in order to avoid galvanic corrosion. This would add an extra weight that would be necessary to include. In addition, the cost of these hardware devices would need to be taken into consideration.
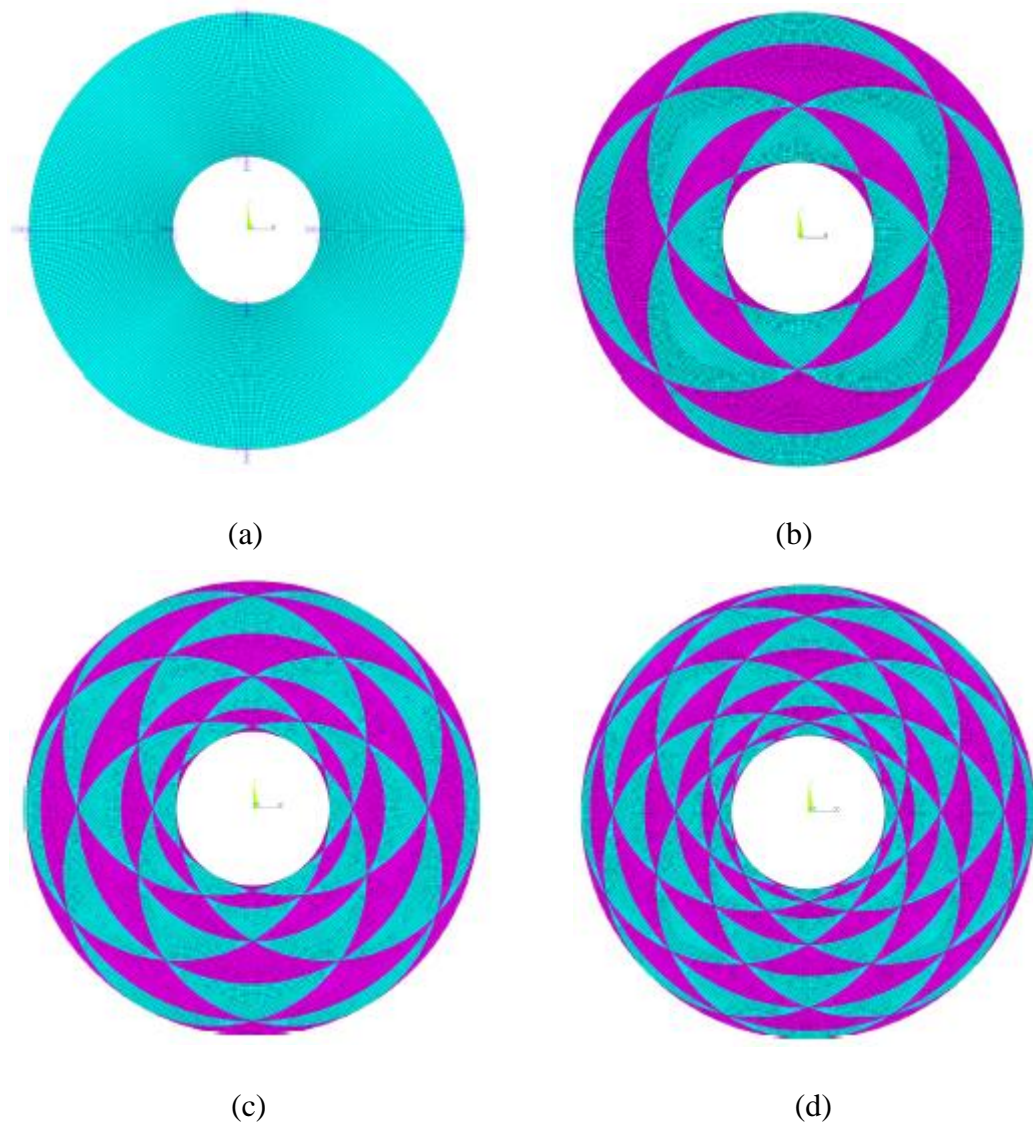
Figure 5.17 Potential disc sub-structure designs (a) Conventional model (b) mosaic pattern approach disc (c) 6-unit disc (d) 8-unit disc [20]

5.7 Conclusions

In this chapter, the possibility of using low density materials in order to minimise the mass of the overall structure has been explored. Two different approaches have been utilised: a conventional method and a more advanced approach, which divided the full area of the disc sub-structure into smaller zones. Both techniques were employed to optimise the mass of the rotor and the stator of two models one at a small scale and another at a large scale. A comparison between the small scale model created

following the conventional approach and an optimised steel structure under the same loads and constraints showed that the composite structure was 72 % lighter than the steel one.

Afterwards, an evaluation of the mass of the CA structure and the structure modelled tracking the mosaic pattern approach revealed a difference of 33.5 % in favour of the mosaic pattern design, as well as a better structural performance. The mass of this model was also contrasted with the one of a model made of steel working under the same circumstances, giving a mass drop of about 82 %.

A similar procedure was chased for the large scale model. The masses of the models designed following the conventional and the mosaic pattern approaches were contrasted with their optimised counterpart made of steel revealing a drop in mass of about 60 %. Later on, the masses and performances of the two composite structures were compared. No significant difference in mass was observed, although the more advanced mosaic pattern model showed a better structural performance. Further improvements might be acquired if more flexibility is added to the design.

Looking at the results obtained, it can be concluded that the use of materials with higher Young's Modulus to density ratios, such as composites, is without doubt, an option to be taken into consideration when attempting the design of lightweight electrical generator structures or any other type of weight sensitive rotating machinery working in a similar environment.

The high cost of these materials and the complexity that they introduce into the design could make the engineers reject its use. During the feasibility study that needs to be accomplished before giving the go-ahead to the project, the advantages brought to the design by the composite materials cannot be ignored. As explained in Section 5.2.4, larger components can be produced. Less number of parts will be then joint and less number of fasteners will be needed saving money, weight and time. The decrease in the amplitude of fatigue loads and cancellation of stress concentrations achieved with a concise design would contribute to extend the lifespan not only of the generator but also of the entire wind turbine. Moreover, if well designed, thermal and corrosion issues might be taken out of the equation. The opinion of highly skilled

engineers with capacity to assess correctly the economic impact of all of these factors would be needed at this early phase.

5.8 References

[1]   A. American Composites Manufacturers, "Where are composites used?", www.acmanet.org/composite/where-are-composites-used, 2016. Last Accessed [05/05/2016].

[2]   G. Shrestha, H. Polinder, D. Bang, and J. A. Ferreira, "Structural Flexibility : A Solution for Weight Reduction of Large Direct-Drive," in *IEEE Transactions on Energy Conversion*, 2010, vol. 25, no. 3, pp. 732–740.

[3]   H. Lind, S. O. Stiesdal, "*Wind Turbine*," Patent, WO 2013/083386 A2.

[4]   ANSYS, "*ANSYS Webinar on advanced composite structures analysis,*" 2015.

[5]   University of Plymouth, "Laminate Thickness and Vf," *Laminate thickness and Vf presentation, University of Plymouth*. www.tech.plym.ac.uk/. Last Accessed [01/09/2016].

[6]   Gurit, *Gurit - Wind Energy Handbook (Guide to composites)*, GTC-3rd–0509 ed. www.gurit.com.

[7]   Ronald F. Gibson, *Principles of composite material mechanics*. McGraw-Hill Inc, 1994.

[8]   Aviation Structural Mechanic (H&S) 3&2, "How airplanes are built and how to maintain them," *http://navyaviation.tpub.com/14018/css/Composite-Material-56.htm*. Last Accessed [01/09/2016].

[9]   US Dept. of Defense Handbook, "Composite Materials Handbook. Polymer Matrix Composites", vol. 3, June (2002).

[10]   University of WashingtonX, "*Composite materials overview for engineers AA432x,*" 2015.

[11]   S. C. Nolet,TPI Composites, "Composite Wind Blade Engineering and Manufacturing," *http://web.mit.edu/windenergy/windweek/Presentations/Nolet_Blades.pdf*, 2011.

[12]   C. World, "ATL and AFP Defining the Megatrends in Composite Aerostructures," *http://www.compositesworld.com/articles/atl-and-afp-defining-the-megatrends-in-composite-aerostructures*. 2016. Last Accessed [01/09/2016].

[13]   G. P. Thomas, "Resin Transfer Moulding," *http://www.azom.com/article.aspx?ArticleID=8620*. Last Accessed [01/09/2016].

[14]   Advanced Process Technology Inc., "Vaccum Assisted Resin Transfer Moulding," *http://www.advancedprocess.com/vartm-vacuum-assisted-resin-transfer-m*, 2015. Last Accessed [01/09/2016].

[15]   V. V. V. and E. V. Morozov, "Optimal Composite Structures," in *Advanced*

Mechanics of Composite Materials, 2nd Edition, Elsevier Ltd, 2007, pp. 437–480.

[16] Z. Su, L. Y. Ã, and Y. Lu, "Guided Lamb waves for identification of damage in composite structures : A review," *J. Sound Vib.*, vol. 295, pp. 753–780, 2006.

[17] I. Dresden, "Composite Delamination," *http://www.ima-dresden.de/*, 2008. Last Accessed [01/09/2016].

[18] J. G. (NASA. Goree, "Preliminary Investigation of Crack Arrest in Composite Laminates Containing Buffer Strips," 1978.

[19] A. Abdul-aziz, G. Baaklini, and J. Trudell, "Structural Analysis of Composite Flywheels : An Integrated NDE and FEM Approach," Cleveland, Ohio, 2001.

[20] M. Sayem, E. V. Morozov and K. Shankar, "The effect of filament winding mosaic pattern on the stress state of filament wound composite flywheel disk," *Compos. Struct.*, vol. 107, pp. 260–275, Jan. 2014.

[21] ANSYS Apdl, *Help topics*. ANSYS, 2015.

[22] M. Sayem, E. V. Morozov, and K. Shakar, "The effect of filament-winding mosaic patterns on the strength of thin-walled composite shells," *Compos. Struct.*, vol. 76, pp. 123–129, 2006.

[23] Altaeros Energies, "www.altaerosenergies.com/," 2014. Last Accessed [01/09/2016].

[24] The Pennsylvania State University, "https://methodology.psu.edu/ra/most/factorial," *Introduction to Factorial Experimental Design*, 2016. Last Accessed [01/09/2016].

[25] P. Jaen-Sola, A. S. Mcdonald, and E. Oterkus, "A Lightweight Approach for Airborne Wind Turbine Drivetrains," in *European Wind Energy Association International Conference*, Paris (France), Nov. 2015, pp. 1–9.

[26] R. R. Johnson, M. H. Kural, and G. B. Mackey, "Thermal Expansion Properties of Composite Materials", Lockhead Missiles and Space Company, Inc., NASA Contractor Report 165632, Sunnyvale, California, 1981.

Chapter 6

Dynamics of a direct drive generator

6.1 Introduction

In previous chapters, the structural integrity of the electrical generator has been analysed by carrying out static studies using FE tools. In this chapter, the machine will be studied from a dynamic point of view. As a rotating piece of machinery, the generator vibrates when its natural frequencies are excited introducing potentially large amplitude oscillations into the forces acting on it that could cause structural fatigue, noise and, in the worst case scenario, the sudden collapse of the structure. The main aim of this chapter is to develop suitable approaches and to investigate a

set of possible designs that would ensure the dynamic integrity of the machine without significantly increasing its weight.

When designing a wind turbine system special consideration must be taken when looking at these machines from a dynamic viewpoint as they inherently vibrate during operation. This vibration produced by the excitation of the structure natural frequencies can increase the magnitude of fatigue forces leading to an early breakdown. Following the guidelines and specifications stated in [1] and [2], Bywaters *et al.* presented results for various sets of modal analyses accomplished for wind turbines with different rated powers and drivetrain configurations [3]. Figure 6.1 displays the Campbell diagram for a 3 MW machine operating between 8.5 and 17 rpm.
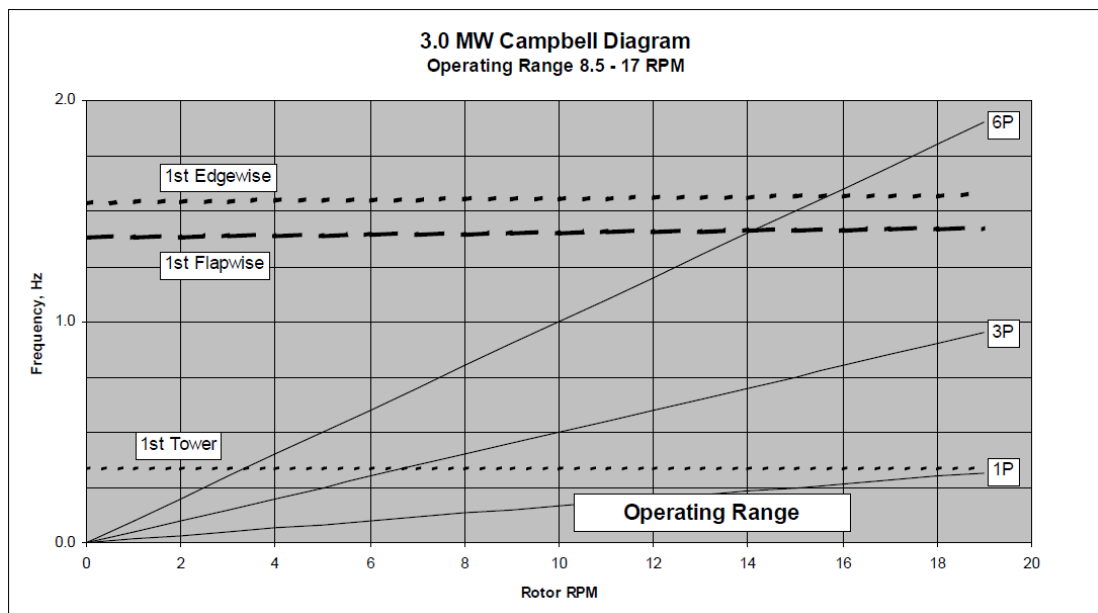
Figure 6.1 Campbell diagram for a 3 MW machine [3]

A Campbell diagram, named after Wilfred Campbell who first introduced the concept, also called interference diagram, represents the frequency in Hertzs versus the rotational speed of the rotating piece of machinery in rpm, in this case, the wind turbine rotor. The development of the natural frequencies corresponding to the mode shapes are presented in function of the rotational speed of the rotor as horizontal lines. To excite the structure, any of the excitation frequencies, which in this graph

corresponds to the 1P, 3P and 6P inclined lines; have to intercept any of the natural frequencies. The most dangerous natural frequencies to be excited are typically the lowest ones as they have more possibilities of coinciding with a larger number of excitation frequencies [4].

As seen, Figure 6.1 shows the 1st mode for the tower at around 0.3 Hz, whereas the 1st modes flapwise and edgewise of the wind turbine rotor take place at around 1.375 and 1.55 Hz respectively. Excitation frequencies are calculated according to the wind turbine rotor rotational speed, 'P'. This technique has been utilised, as it will be described in the next section, to find out whether the optimised generator disc structure is at risk dynamically speaking and if so, what the frequencies to be avoided are.

The analysis and optimisation of the mechanical and structural design of a radial flux direct drive generator rated between 0.75-3 MW for land based and fixed bottom offshore wind turbine applications were carried out in [5] and [6]. Authors in [6] claimed no vibration issues with the generator according to the results achieved from a collection of experimental studies on a 1.5 MW machine allowing an eccentricity of up to 50 % under extreme loads.

A permanent magnet synchronous generator was dynamically evaluated and the effects on the turbine operational speed range caused by the harmonics of the cogging torque and torque ripple quantified in [7], [8] and [9]. In [10] and [11], the bearing working life and the structural suitability of a permanent magnet generator with an outer rotor were surveyed. Hub and nacelle design were suggested too. Large scale direct drive generators feasibility (10 MW) is under investigation as seen in [12].

In [13], Sethuraman characterised the dynamic behaviour of the direct drive power train of a floating wind turbine following the well-known two step de-coupled approach proposed by Xing *et al.* [14], [15]. This method, originally created for analysing conventional geared wind turbines, utilises the data obtained from an aero-elastic simulation code, on global motion response and loads as inputs for a detailed drive train model created in a Multi-Body Simulation piece of software which

enables kinematic and dynamic analyses of mechanical systems. However, as the main purpose of this research was to study a direct drive machine, the author also needed to address how significant the dynamic effects and feedback forces from the drivetrain were.

A new concept for the design of a 5 MW direct drive generator is presented by Shrestha *et al.* in [16]. The main goal was to reduce the weight of a large diameter machine by introducing axial flexibility in the generator support structure. The data retrieved from modal analyses are given highlighting the fact that the use of transverse plate stiffeners for a hollow rotor structure not only provides axial stiffness and limits the radial deflection but also helps keep the first bending mode frequency in a safe region without significantly increasing machine´s weight. See Figure 6.2 for a detailed view of the proposed structure.
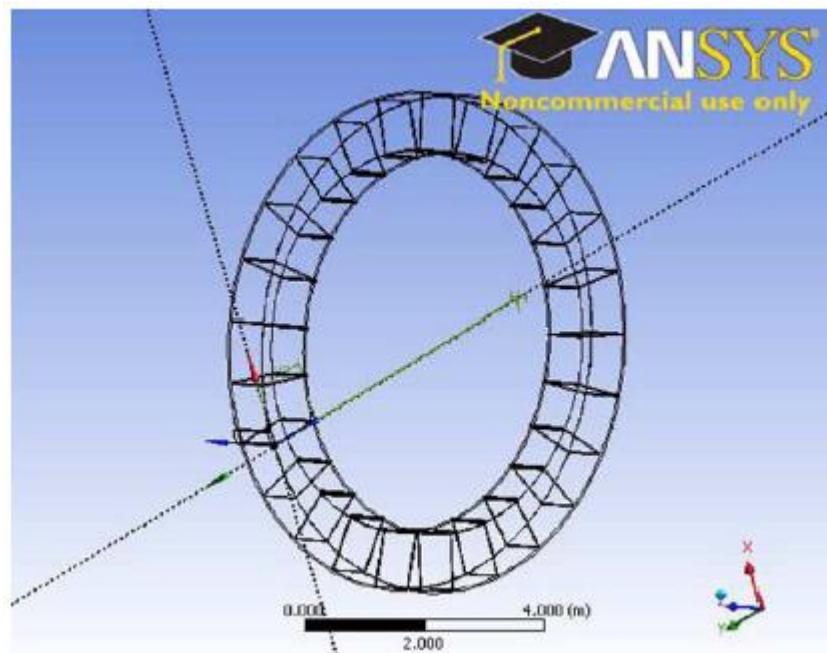
Figure 6.2 Wire frame view of the rotor structure with transverse plate stiffeners [16]

Zavvos shows in [17] the outcomes acquired from the modal analyses he made over three different 5 MW direct drive electrical machines: radial, axial and transverse flux. The first was also studied having distinct structural configurations, such as disc and armed. He found that axial and transverse flux machines and radial flux

machines made with discs have a moderate risk of experiencing vibrations, with the axial flux machine being the most vulnerable to fatigue. On the opposite side were the conventional radial flux machines made with hollow arms, which was the least susceptible to fatigue type of generator.

In [18], Kirschneck produced a two way model, which links mechanical and magnetic systems, that identifies the dynamics of a specific electrical machine. Going through a collection of all the relevant modelling techniques and formulae, he derived a set of equations that can be used to optimize the structural mass of the generator and to determine the effect of the excitation forces.

Chapter 6 is composed of 6 sub sections: Section 6.1 reviews the state of the art in the technology. Although several studies on the dynamics of the wind turbine drivetrain have been published, only a few concentrate on the direct drive generator structure. In Section 6.2, the distinct options explored to improve the dynamic behaviour of the machine are explained in detail. All the outcomes obtained from the said research are presented in Section 6.3. These results are analysed and discussed in Section 6.4, leading to conclusions and recommendations for further design enhancements in Section 6.5.

6.2 Methodology

6.2.1 Evaluating structural natural frequencies

A finite element modelling package, such as SolidWorks, was employed in this chapter so as to estimate the lowest mode shapes of the generator structures. The theory behind the modal analyses carried out with this piece of software leans on the structural linear vibrations principle.

Starting with basics, if we want to explain why a body vibrates, it is essential to recall the energy conservation principle. Assuming a mass 'm' suspended on a spring of stiffness 'k', as shown in Figure 6.3, consider that the mass is pulled up from its static equilibrium position by y_{max} and then released.
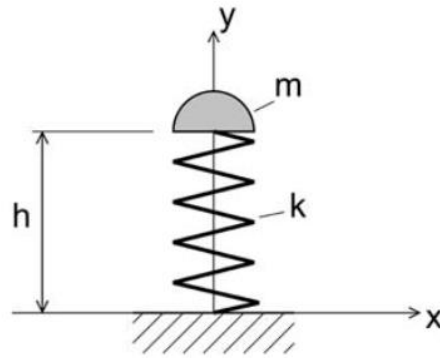
Figure 6.3 Spring-mass arrangement [19]

When the spring deforms some energy gets stored in it. This energy is known as the potential energy or 'V_{max}' and represents the maximum energy transmitted to the spring by deforming it by y_{max}. After realising the mass, the spring will start oscillating up and down until recovering its original position. The energy gained with the motion of the mass is called kinetic energy and can be described by the following equality,

$$E_k = \frac{1}{2} m \dot{y}^2 \tag{6.1}$$

with $\dot{y}$ being the mass linear velocity, which corresponds to the mass displacement time derivative. The potential energy stored in the spring at a midway position y is

$$V = \frac{1}{2} k y^2 \tag{6.2}$$

Assuming an ideal spring, the sum of the kinetic energy gained with the mass motion and the potential energy acquired by the spring at any moment in time must be equal to V_{max}. Therefore,

$$V_{max} = \frac{1}{2} m \dot{y}^2 + \frac{1}{2} k y^2 \tag{6.3}$$

It can be observed that an energy transformation occurs in a spring-mass system, from potential to kinetic and vice versa while V_{max} always remains constant. It happens that when $y = \pm y_{max}$, V is equal to V_{max} and $\dot{y} = 0$. However, when $y = 0$, which represents a static displacement, $\dot{y} = \dot{y}_{max}$. As already mentioned, this periodic move from extreme positions is named oscillation and can be characterized by the next two parameters: the period of oscillation, which is the time elapsed between two consecutive maximum deformations, and the amplitude of oscillation, which is the maximum displacement of the mass from its static equilibrium position or 'y_{max}'.

Knowing that the mass moves in a periodic fashion with an amplitude of y_{max}, the process can be described by the following the function,

$$y = y_{max} sin\left(2\pi \frac{t}{T} + \alpha\right) \tag{6.4}$$

where t is the time, T is the oscillation period and α is a constant which is defined by the requirement that at $t = 0$, $y = y_{max}$. As seen, y_{max} is known leaving T as the only unknown (besides α) in the equation. After derivations, y and $\dot{y}$ can be substituted in expression (6.3), obtaining

$$\left[\frac{m(2\pi)^2}{T^2} - k\right] y_{max}^2 cos^2\left(2\pi \frac{t}{T} + \alpha\right) = 0. \tag{6.5}$$

For equation (6.5) to be true at any moment in time, the term in brackets must be equal to zero,

$$\left[\frac{m(2\pi)^2}{T^2} - k\right] = 0 \tag{6.6}$$

hence the period of oscillation is defined as a function of mass and stiffness according to equation (6.7):

$$T = 2\pi\sqrt{\frac{m}{k}} \tag{6.7}$$

Note that the oscillation period does not depend on the initial disturbance. The number of oscillations per unit time is called oscillation frequency (typically expressed in oscillations per second or Hertz) and it corresponds to the inverse of T [19]. Then,

$$f = \frac{1}{2\pi} \sqrt{\frac{k}{m}} \, .$$

(6.8)

The evaluation of resonant frequencies, also known as natural frequencies, of simple or composite structures is based on the concept explained above. This evaluation would require the use of more complex equations or stress analysis packages depending on the complexity of the structural configuration, which is the case of rotor and stator structures. The example provided owns only one degree of freedom, whereas more complex layouts have various. This implies having several modes of deflection and therefore, several excitation modes and natural frequencies.

As seen from equation (6.8), it is possible to avoid resonance by design influencing the structural stiffness or mass or both. Moreover, by having full control of the system you may be able to avoid dynamic loading at these frequencies.

In Chapter 4 was found that generator disc structures are much lighter than armed structures, as the hollow arms cannot cope with the tangential loading as well as the disc sub-structures do unless the thickness of the arms is considerably increase with the subsequent rise in mass. With the optimum configuration identified, the first 5 natural frequencies of the rotor and stator structures have been assessed, by performing modal analyses, and plotted in a Campbell diagram. For that, the SolidWorks Simulation© add-on package was used. The frequency analysis study option was selected among the distinct types of studies available. Then, structural steel was assigned to all the components forming the structures as their material. Its characteristics are the same as the ones employed in chapter 4: Young's modulus, $E = 2.1 \times 10^{11}$ Pa, Poisson's ratio, $v = 0.3$ and density, $\rho = 7850 \frac{kg}{m^3}$. The next step was to constrain the structures at the shaft and to create an appropriate mesh. In SolidWorks, it is possible to adjust the mesh element size manually by making use of a slider which goes from a finer mesh to a coarser one. The piece of software also

suggests an element size by default that is supposed to give accurate results in a reasonable period of time. In addition, two types of adaptive meshes are available too: h-type and p-type. The h-adaptive mesh diminishes the size of the elements in an iterative manner, locally or globally depending on the settings specified by the user, until convergence is accomplished, while the p-adaptive mesh increases the element order (linear, quadratic, cubic, etc,.), again locally or globally depending on the specifications, in an iterative way until convergence is achieved. See Figure 6.4 for further clarifications on element order. Similar results should be obtained by using any of these two techniques which are very useful instruments especially at the time of finding stress singularities. For instance, when looking at sharp corners, which do not exist in the real world, 3D finite element tools, tend to overestimate the stress no matter how fine the mesh is. This phenomenon is known as a stress singularity. The stress results go higher and higher as the user refines the mesh without levelling off or converging. So as to make sure that good outcomes have been acquired the trend tracker option included in the adaptive mesh tree can show the user if a levelling off have been reached and when.
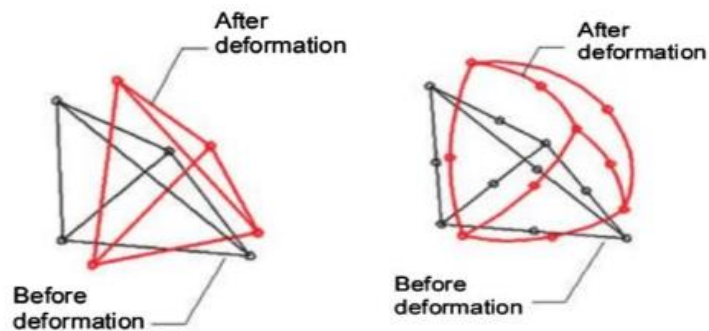
Figure 6.4 (a) First order (linear tetrahedral solid element with no nodes at the midpoints); (b) Second order for a higher quality mesh (parabolic tetrahedral solid element with nodes at the midpoints) [20]

For these studies the mesh density suggested by the FE package was utilised. A linear tetrahedral high quality mesh with 7,682 elements and 15,640 nodes was created. The element size was 148.5 mm.

The estimation of the first five mode shapes of the rotor and the stator structures was performed with no loads applied at any time.

6.2.2 Dynamically designing a direct drive generator supporting structure

Few studies have been published on the design of large diameter direct drive generator structures. Most of them concentrate all the attention on the effects of the external loads acting on the whole drivetrain but not many look at how these forces affect the components forming the electrical machine structure individually. As mentioned, the natural frequencies of the structure to be designed must be either avoided or passed as quickly as possible. The potential excitation frequencies that could activate the structure natural frequencies are as follows [17],

- The frequency of the wind turbine rotational speed (1P).
- The fundamental electrical frequencies (*p*P, with *p* being the number of pole pairs per stage).
- The frequency of the rotor blades passing in front of the tower (3P and 6P).

In this regard, designers of this type of devices often follow an empirical rule that natural frequencies between 70 % and 130 % of the exciting frequency must be avoided [16].

The lowest natural frequencies of both the rotor and the stator structures can be estimated utilising FE techniques. Different excitation frequencies are able to trigger the cited natural frequencies. This research has been carried out considering the three types of frequencies defined above. With this, distinct options were explored so as to increase the natural frequencies of the structures without adding significant weight.

Figure 6.4 displays the power spectrum of rotor speed of a variable speed conventional geared wind turbine, with the rotational velocity, expressed in rad/s, in the *x* axis and the amplitude of the loads in the *y* axis. The first step when dynamically studying a wind turbine or a wind turbine component is to analyse its power spectrum of rotor speed so that the most dangerous modes can be recognised and avoided later on in the design. As seen in the said picture, the first drive train mode is the most dominant. In our case, as the drive train of a direct drive wind turbine is very different (no gearbox), the amplitude of this mode and its frequency will be distinct. In fact, for a direct drive machine it is expected to have a lower amplitude for the first drive train mode and lower frequencies as the rotor speed is significantly lower. Nonetheless, the geared wind turbine example can be utilised as

a reference due to this sort of highly resonant modes are also present during direct drive machines operation and are the ones to be avoided in order to maintain the integrity of the machine.
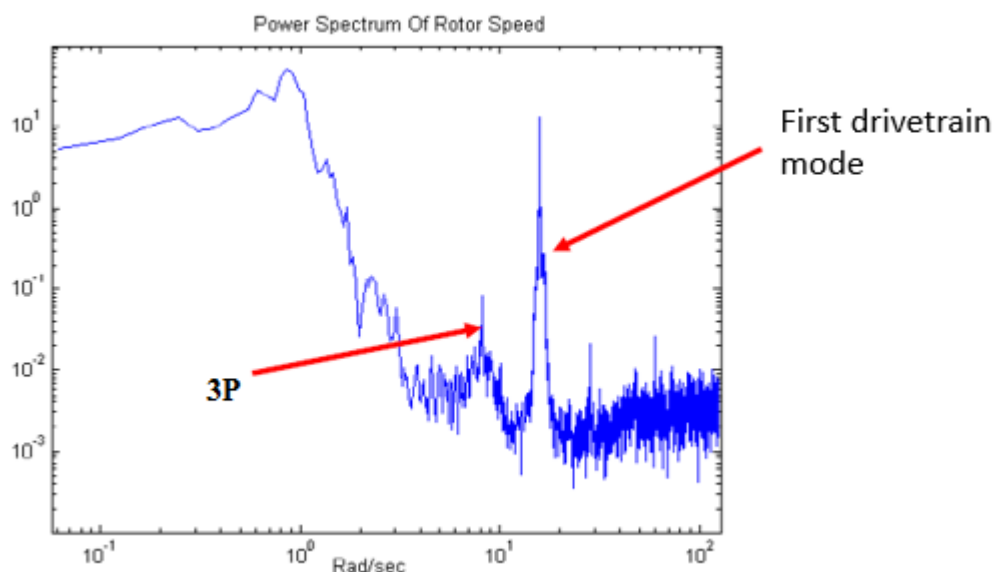
Figure 6.5 Rotor speed power spectrum of a VS conventional geared wind turbine [21]

The rotation of the wind fields generate deterministic and stochastic peaks in frequencies such as 1P, 2P, 3P and so on for the blades of a 3 bladed rotor, while for the drive train and tower the stochastic peaks take place at 3P, 6P and all its multiples and the deterministic peaks happen at 1P, 2P, 4P and all its multiples [21]. As stated by Kirschneck in [18], the dynamic of the structure is dominant while the dynamic of the magnetic field has a rather limited influence. Hence, it is necessary to concentrate the attention on the structural side and to analyse the power spectrum of a direct drive rotor speed to find the most harmful modes for the structure of the electrical machine, to then plot them in a Campbell diagram with the structure natural frequencies and encounter the best way to evade them. As already said, in absence of such information, the author employed the data provided by Zavvos in [17].

Considering a number of pole pairs equal to 60, the excitation frequencies for the drivetrain were encountered for a wide range of rotational speeds going from 0 to 20

rpm. The outcomes were plotted in the frequency interference diagram shown in Figure 6.6 for comparison.
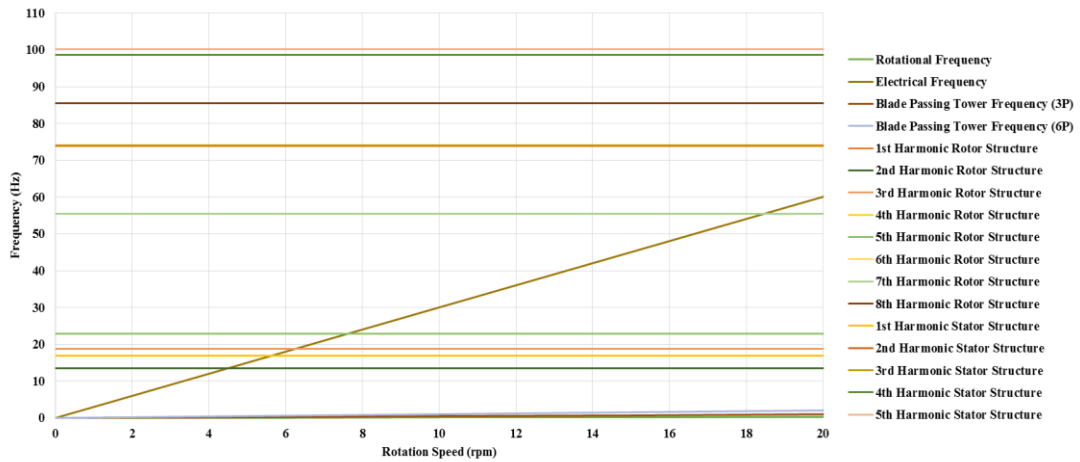
Figure 6.6 Campbell diagram of the system

Looking at the Campbell diagram, it can be seen that the weakest component is the rotor with a frequency for the first mode of 13.403 Hz, whereas the frequency of the first mode for the stator is 16.976 Hz. From Figure 6.6, it can be understood that for a 3 MW direct drive machine optimised structure made with discs the suitable range of operation is between 7.6 and 18.5 rpm. The need to avoid the lowest resonant frequencies forces the designer to sacrifice the collection of energy at the lowest and at the highest wind speeds for the good of the structure. Nevertheless, it would be also possible to step through frequencies using a control system.

Different ways of increasing the natural frequencies of the disc structures have been analysed in this chapter. In addition, another type of structure layout, such as a rotor cone structure, has been proposed and studied. The results acquired for these tests are illustrated in detail in Section 6.3.

6.2.3 Techniques for elevating structure's natural frequencies

There exist 4 distinct ways of elevating the natural frequency of a design [22]:

- Alter the geometry.
- Strategically locate mass elements.
- Change materials (resonant frequencies are directly proportional to the elastic modulus of the materials).
- Modify the features of the shock isolators.

The first three ways have been looked at in this investigation. Since the structural design of the electrical machine has been approached from a general perspective, the fourth manner of pushing up the frequencies has not been studied.

Looking at the structure mode shapes obtained from modal analyses, the sort of technique that might apply to push the natural frequencies up can be identified.

6.2.3.1 Dimensional alteration of structures made with discs

As stated, a 3 MW machine of 4m diameter and 1.2 m axial length made up of steel, as shown in Figure 6.7, has been used. Dimensions t_c and t_d have been varied and modal analyses carried out so that the effect caused by those alterations in the natural frequencies could be studied and quantified.
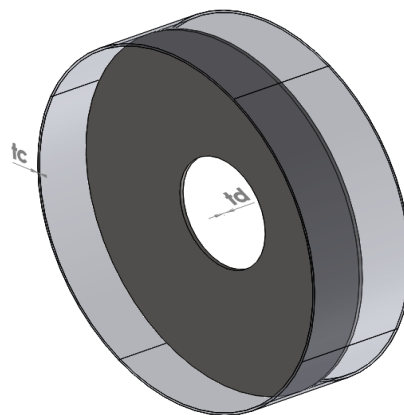
Figure 6.7 Rotor structure as changed in the analysis

The thicknesses, measured in millimetres, of both sub structures were given the following values,

- Cylinder thickness, 't_c': 20, 40, 60, 80, 100, 120 and 140 mm
- Disc thickness, 't_d': 40, 60, 80, 100, 120, 140 and 160 mm

These dimensions were picked looking at the values presented in Chapter 4, in which the contour plots are utilised to optimise the generator structure with a view to minimise its mass. They are all within a realistic range which varies around the optimum obtained results. A total number of 49 modal studies were made. The outcomes achieved were plotted and given in Section 6.3.

The following corresponds to a simplified example of a rotor structure that will help to understand the idea presented in this sub section. If a rotor structure is simplified by assuming that the disc sub structure is equal to a cantilever beam and the outer cylinder is an attachment located at the free end of the beam, as seen in Figure 6.7, a modal analysis can be made so that the effect that each sub structure has in the dynamic behaviour of the overall structure can be appreciated.
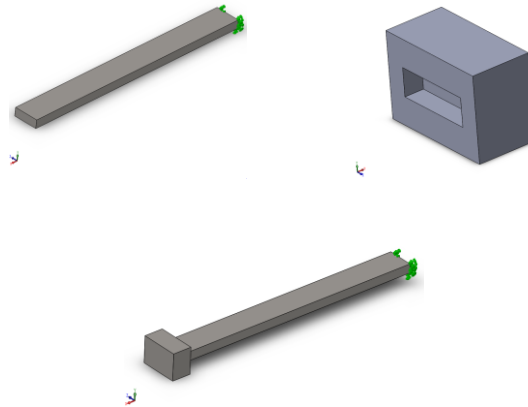
Figure 6.8 Simplified Rotor Structure

As observed in Figure 6.9, the first resonant mode takes place in the Y direction as the area moment of inertia ($I = bh^3/12$), with b being the width and h being the height, is the lowest in that direction. This can be simply explained by saying that the Y direction is the weakest due to it is the thinnest. The characteristics of the model are shown in Table 6.1.

Table 6.1 Simplified rotor model features

b (width in X direction)	0.1 m
h (height in Y direction)	0.035 m
L (length in Z direction)	1 m
m (beam mass per unit length)	28 kg/m
M (attachment mass)	85.8 kg
E (Young's modulus)	2×10^{11} Pa
g (gravity in Y direction)	9.81 m/s^2

The weakest parts of the design show themselves as low frequency modes and as it can be observed in the mentioned picture, the beam is so weak in the Y direction that 3 resonant modes occur in that direction for the beam alone, whereas when the attachment is included 2 modes are obtained.
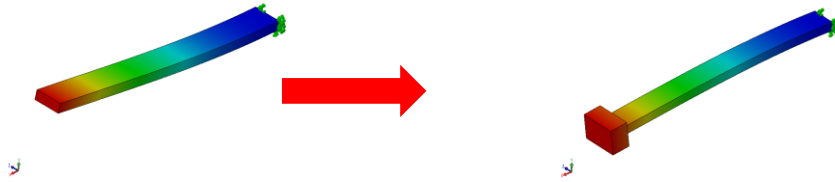
Mode 1 → f = 27 Hz, Shape: Primary Y Direction; f = 18 Hz, Shape: Primary Y Direction

Mode 2 → f = 78 Hz, Shape: Primary X Direction; f = 51 Hz, Shape: Primary X Direction
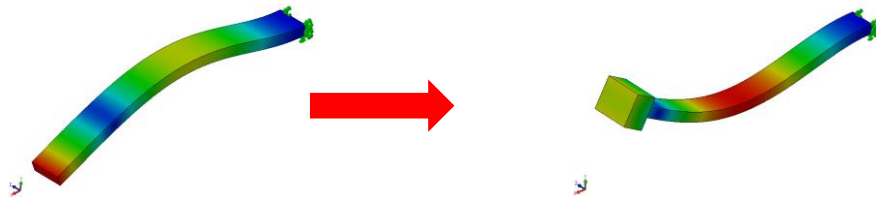
Mode 3 → f = 172 Hz, Shape: Secondary Y Direction; f = 132 Hz, Shape: Secondary Y Direction

Mode 4 → f = 447 Hz; Shape: Primary Z Direction; f = 248 Hz, Shape: Primary Z Direction

(Torsional)

Mode 5 → f = 469 Hz; Shape: Tertiary Y Direction; f = 362 Hz, Shape: Secondary X Direction

Figure 6.9 Simplified Rotor Mode Shapes

In order to validate these outcomes, the resonant modes in the weakest direction of the cantilever beam have been calculated using empirical equations [23]. Figure 6.10 shows the first mode whose shape corresponds to the one acquired with the finite element tool.
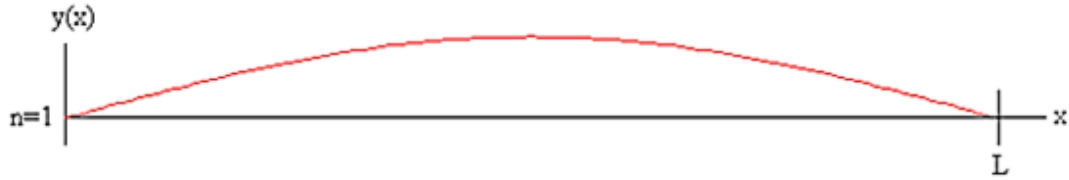
Figure 6.10 First mode shape in Y direction

By employing equation 6.9,

$$f = \frac{3.52}{2\pi L^2} \sqrt{\frac{EI}{m}} \qquad (6.9)$$

where L is the beam length in meters, E is the Young modulus in Pa, I is the area moment of inertia in m^4 and m is the mass per unit length in kg/m, it was found that the first natural frequency was 27.7 Hz. The result obtained using FE techniques was 27.65 Hz.

For the second mode, equation 6.10 was utilised. The mode shape is displayed in Figure 6.11 and again it can be seen that it fairly matches the form acquired by the FE outcome for the cantilever beam.
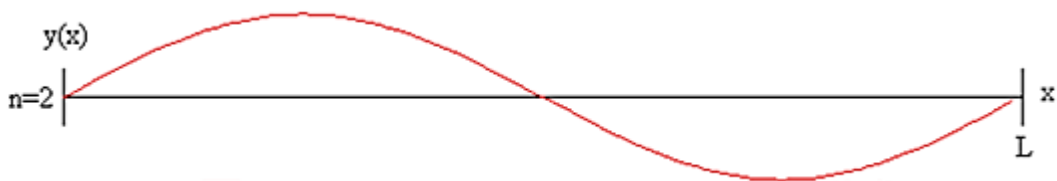
Figure 6.11 Second mode shape in Y direction

As it can be observed, the parameters in equation 6.10 are the same as those in equation 6.11. The only difference between these two equalities is the constant in the first fraction which varies with modes.

$$f = \frac{22}{2\pi L^2} \sqrt{\frac{EI}{m}} \tag{6.10}$$

In this case, the result was 173.4 Hz while the data retrieved form the software was 172.32 Hz.

Finally, mode 3 was calculated utilising equation 6.11.

$$f = \frac{61.7}{2\pi L^2} \sqrt{\frac{EI}{m}} \tag{6.11}$$

Its result was 485.6 Hz whereas SolidWorks gave an outcome of 469.75 Hz. Its shape is shown Figure 6.12.
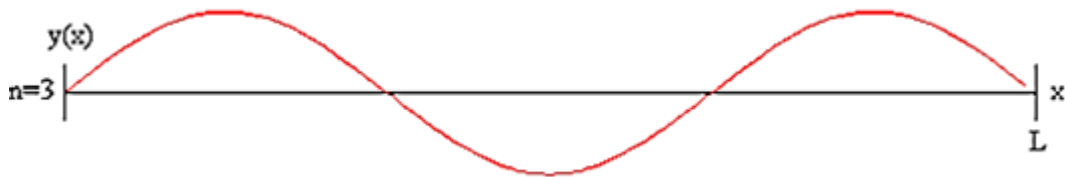
Figure 6.12 Third mode shape in Y direction

For a cantilevered beam with a mass attached to its free end, Young and Budynas [23] derived an empirical equation that is capable of estimating its first natural frequency. Assuming a beam negligible mass, equation 6.12, where g corresponds to the gravity in m/s^2 and M is the mass of the attachment in kg, gave a result of 24.38 Hz. So as to carry out this study in SolidWorks, a material density of 1 kg/m^3 was assumed. The result obtained from the software was 23.8 Hz.

$$f = \frac{1.732}{2\pi} \sqrt{\frac{EIg}{ML^3}} \tag{6.12}$$

If a comparison between the FE data and the outcomes achieved with the equations is made, it can be observed that the largest error obtained was lower than ±5 %. See Table 6.2.

Table 6.2 Analytical vs. FE comparison

Mode	Frequency (Hz)		Error (%)
	Equation	**FE**	
1st without attachment	27.7	27.65	0.2
2nd without attachment	173.4	172.32	0.6
3rd without attachment	485.6	469.75	3.3
1st with attachment	24.38	23.8	2.4

Therefore, it can be said that the results acquired using the software are accurate enough. Once the data was validated, the attention was again focussed on the FE study results. By reviewing the resonant modes acquired with and without the attachment, it is easy to understand that the addition of mass at the free edge of the beam makes the structure even weaker in all directions. A considerable reduction in frequency happens for all the modes with the 5th one experiencing the highest drop from 469 to 362 Hz and changing the mode shape from the Y to the X direction and it would have been worse if a heavier attachment had been used. This is the type of behaviour that can be expected from rotor and stator structures. The results given in Section 6.3 will corroborate this statement.

6.2.3.2 Use of stiffeners

Another way of manipulating the natural frequencies of the structures is through the introduction of other structural components, named stiffeners, which provide the structure with the necessary directional stiffness. When finding the structure's natural frequencies, special attention must be taken to the mode shapes. The different forms adopted by the structure give the designer a clear picture of type of stiffener required and their location. With this in mind, it is important to remember that the main aim of this investigation is to reduce the mass of the machine while meeting structural

requirements. Therefore, the utilisation of stiffeners will be suitable only when a substantial increase in frequency is observed without adding too much mass.

In this research, an isosceles triangular type of stiffener with a thickness of 60 mm joining the cylinder and the disc sub structures has been proposed. Located in the axial direction, its equal length sides are joined to the inner face of the rim and the axial surface of the disc and its dimensions vary with the disc thickness. As shown in Figure 6.13, a finite number of stiffeners equally spaced have been employed. First on one side of the disc only and then on both sides.
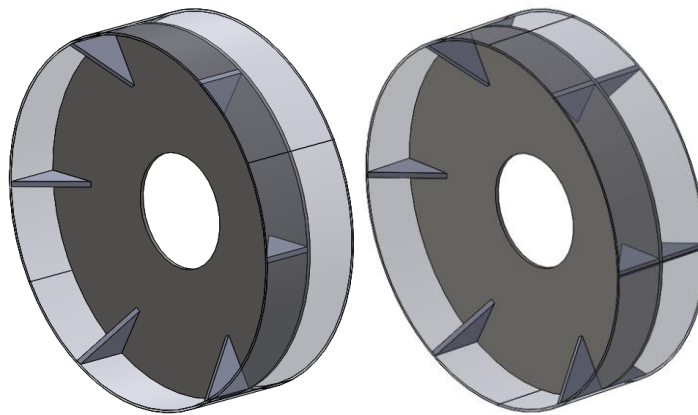
Figure 6.13 Rotor structures with axial stiffeners

A different number of stiffeners, as well as the use of a distinct material with lower density (alloy steel) in their design were also tried with the main aim of minimising the overall mass. Again, all the outcomes obtained from this part of the investigation are given in Section 6.3 of this chapter.

6.2.3.3 Rotor conical structure

In the last sub section, the techniques utilised for incrementing the natural frequencies of an optimised disc structure have been presented. However, other types of simplified structural configurations exist as stated by Stander in [24].

Rotor conical structures provide an axial stiffness that a disc structure misses, while the cone sub structure acts as a disc sub structure bringing radial stiffness to the

model. In this chapter, a rotor conical structure has been optimised according to the deflection criterion as applied to the disc structure and under the same loading conditions but also considering its natural frequencies.

Last but not least, the most dangerous modes of deflection for the rotor conical structure were found. By applying the same loads and constraints as for the disc structure in Chapter 4, the optimised cone structure was tested and the retrieved data analysed.

6.3 Results

As explained in Section 6.2, the natural frequencies of the generator structure must be avoided in order to avoid resonance. Different techniques can be used to increase the said natural frequencies. In this section, the data retrieved from the analyses carried out over 3 distinct types of structural configurations are presented.

As with Chapter 4, one can plot the mass of a disc structure on a 2D plot, with disc thicknesses on the X-axis, cylinder thicknesses on the Y-axis and contours representing rotor or stator structural mass. Another set of contours can be used to show the natural frequency. See Figure 6.14. The frequencies presented in these plots correspond to the first mode shapes. Plots showing the variation of frequency with dimensions for the rest of the modes have been included in Appendix A.
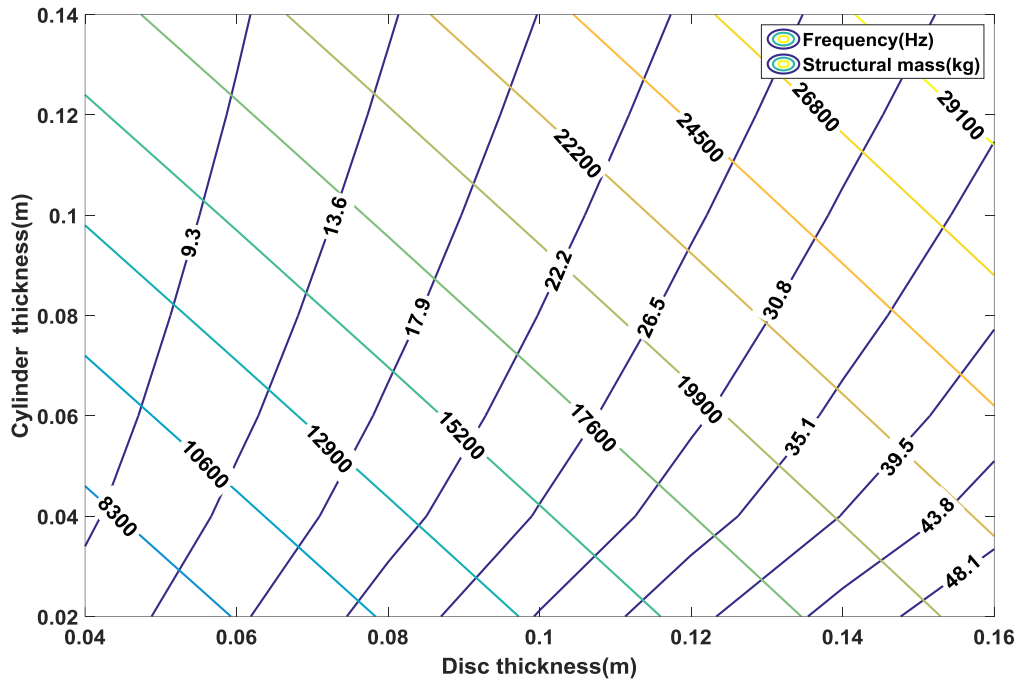
(a)
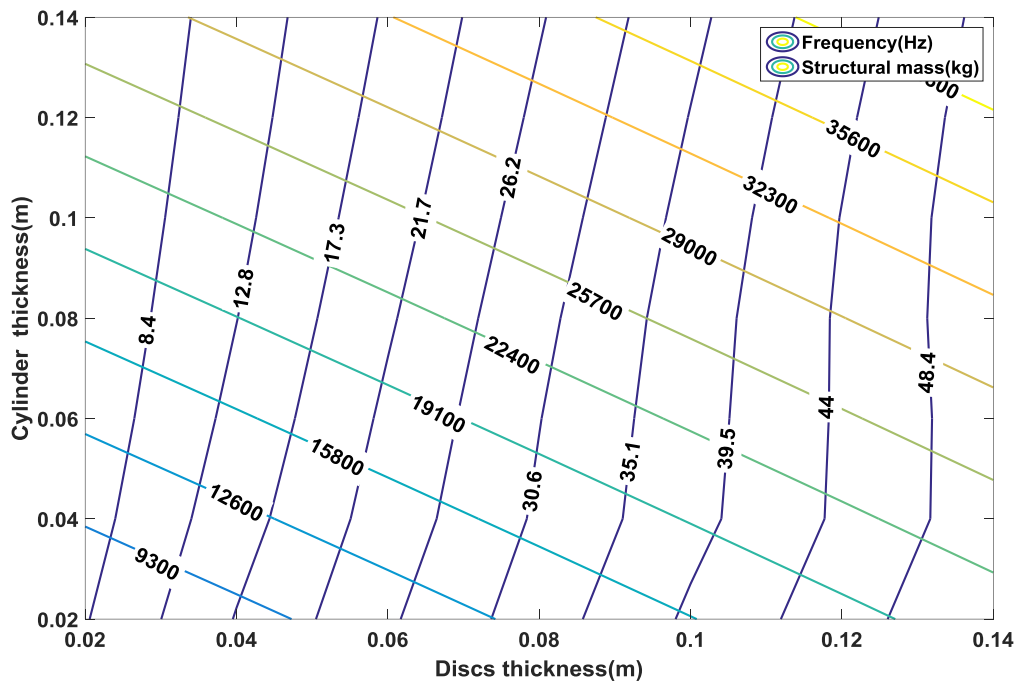
(b)

Figure 6.14 2D Optimisation for 3 MW rotor and stator disc structures with 1st mode natural frequencies criterion

After optimising a disc generator structure by looking at it from a static viewpoint, one can assess its dynamic behaviour and estimate the structure natural frequencies by entering its dimensions in the contour plots given. With the information provided by this reliable and fast method and the resonant frequencies given by the power spectrum of rotor speed a Campbell diagram can be created and the best ways to maintain the machine's integrity identified.

At this point, it is important to mention that the rotor and the stator structures have been studied individually and the potential interactions between them have not been taken into consideration. An inner rotor type was utilised in the studies. The results shown in this section do not apply to machines with outer rotor configurations as the change in geometry will produce different outcomes for the same loading conditions.

Figure 6.15 displays the shapes for the first 5 modes of a typical rotor disc structure. In the first mode, the cylinder sub structure stretches in the horizontal direction making the disc sub structure twist about the vertical axis (in red) as it is illustrated in the figure below. A similar shape is acquired for mode 2 although in this case the cylinder sub structure stretches in the vertical direction making the disc twist about the X axis. The excitation of the third natural frequency would produce a lateral displacement in the Z direction of both the cylinder and disc sub structures. As the disc is fixed at the shaft, the displacement in the Z direction would induce the disc sub structure to acquire a conical shape. In the last two modes presented here, the cylinder sub structure shows large deflection at its edges taking place periodically that produce ripples. The disc sub structure deforms accordingly with the cylinder shape. Although, these modes seem to produce random shapes, it is not difficult to recognise a deformation pattern. The lowest deflection is located on the disc and it follows a square shape that changes in direction with the mode as it can be appreciated.

These modes obtained due to the excitation of the structure natural frequencies create an uneven deformation across the structure that would introduce such instability in the airgap that could cause the collapse of the machine. Two options can be taken into account to avoid this situation:

- To make use of the techniques given in Section 6.2.

- To design a structure capable of withstanding the stress without significantly deforming.

Note that the latter would imply a substantial increase in the structural mass.
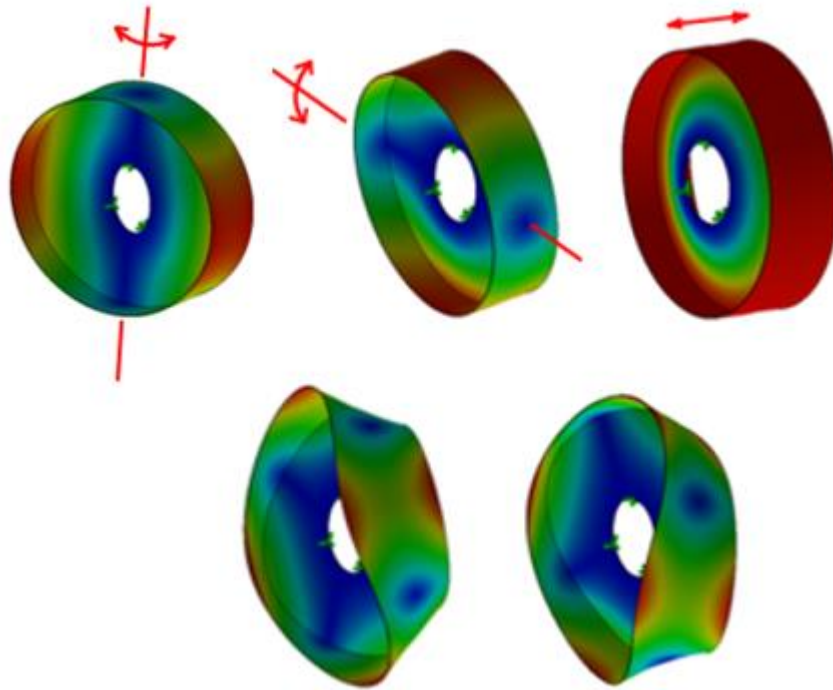
Figure 6.15 First 5 mode shapes of a typical rotor disc structure (1st Mode: top left; 2nd Mode: Middle top; 3rd Mode: top right; 4th Mode: bottom left; 5th Mode: bottom right)

The evaluation of this behaviour helps the design engineers to make decisions on how to alter the natural frequencies of the structures. For instance, in this case where the disc deforms axially due to radial alterations in the cylinder sub structure, the use of stiffeners providing some extra axial stiffness might help. A finite number of stiffeners of isosceles triangular shape with 60 mm of thickness, equally spaced, were implemented in the optimum steel structure, with a mass of 19,260 kg, as described in the previous section, in order to quantify their effect in the structure natural frequencies.

No. of Stiffeners	4	5	6	7	8	9	10
■ One side	13.9	14.1	14.3	14.5	14.8	15.0	15.2
■ Two sides	13.8	14.1	14.3	14.6	14.9	15.1	15.3
■ Cast alloy steel	13.9	14.1	14.3	14.6	14.8	15.1	15.3

■ One side ■ Two sides ■ Cast alloy steel
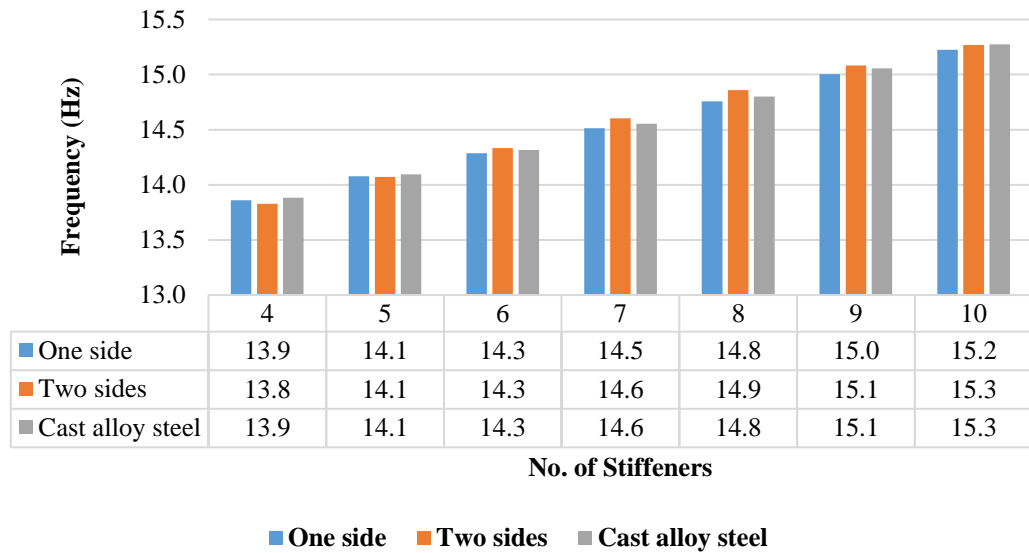
Figure 6.16 Quantification of the effect produced by the implementation of stiffeners in a rotor disc structure

The investigation was started with a modal study of the structure without any stiffener. The result for the first mode shape was 13.403 Hz. Then, 2 stiffeners were introduced on one side of the disc verifying that their effect on the structure natural frequencies was almost negligible, although 154 kg were added to the overall mass. An unacceptable outcome was again obtained for 3 stiffeners; hence the data began to be taken into consideration after them. As shown in Figure 6.16, a different number of stiffeners located on one side first and on both sides second were tried. In addition, a less dense material such as cast alloy steel, with a density of 7,300 kg/m^3 was also assumed for the stiffeners with the main objective of reducing their mass.

It was understood that the structure natural frequency increases linearly with the number of stiffeners placed on one side of the disc. The same behaviour was observed when using stiffeners on both sides with slightly higher frequencies. The utilisation of stiffeners made of cast alloy steel on one side of the disc slightly enhanced the dynamic performance of the structure but the reduction in mass achieved was not very significant as each stiffener weighted 71.65 kg for 77 kg of a stiffener made of conventional structural steel. The data retrieved from the analyses showed that the introduction of stiffeners, either on one side or on both, pushed up

the natural frequencies less than 2 Hz (with 10 stiffeners). However, a mass of 770 kg had to be included for that.

Having the disc structure deeply analysed, another type of structural configuration was looked at. As explained in Section 6.2, rotor conical structures include extra axial stiffness that disc structures miss, while keeping excellent radial stiffness characteristics. A rotor cone structure suitable for the proposed direct drive machine has been optimised this time not only considering the deflection criterion as in Chapter 4, where a complete set of static analyses was carried out, but also the structure natural frequencies that were found utilising finite element methods. The methodology tracked was:

First a cone structure was CAD modelled in SolidWorks as in Chapter 4. Random dimensions were picked for both the thicknesses of the cone and the cylinder sub structures. Their values were 40 and 22 mm respectively. After that, a set of static and dynamic analyses were run for each position and angle of the cone with the main aim of obtaining the mass, the maximum deflection and the first mode shape of the structures. See Table 6.3.

Table 6.3 Cone Structure Optimisation Results

Angle (°)	Mass (kg)	Position 1 δ(m) x10⁻⁴	Position 1 f(Hz)	Position 2 δ(m) x10⁻⁴	Position 2 f(Hz)	Position 3 δ(m) x10⁻⁴	Position 3 f(Hz)	Position 4 δ(m) x10⁻⁴	Position 4 f(Hz)	Position 5 δ(m) x10⁻⁴	Position 5 f(Hz)
30	6873	4.8	19.1	4.4	25.7	4.8	31.3	4.8	33.5	4.4	29.8
35	7080	4.9	20.4	4.6	26.8	4.9	32.8	4.9	36	4.4	33
40	7384	4.7	21.1	4.5	27.4	4.9	33.5	4.9	37.5	4.4	35.3
45	7775	4.8	21.1	4.5	27.5	5	33.4	5	38	4.5	37.6
50	8281	4.9	21	4.7	26.9	5.1	32.4	5	37.1	4.6	38.1
55	8958	5	21	4.9	25.4	5.3	30.3	5.2	34.7	4.7	36.7
60	9881	5.2	19.4	5.1	23.2	5.7	27.3	5.4	31	4.9	33.1
65	11200	5.7	17.3	5.5	20.1	5.9	23.3	5.7	26	5.2	27.6
70	13205	7.1	14.5	6.6	16.3	6.7	18.3	6.6	20	5.9	21

As seen, the lowest deflections are acquired when the cone is placed in position 5. In addition, the highest natural frequencies for the first mode shape are also achieved in this position. By looking at the second column of position 5, it can be observed that the frequency increases with the cone angle until reaching 50º. After that, it starts going down again. Since the breakeven point took place at 50º of position 5, this arrangement was taken as the optimum.

Then, it was checked which sub structure put more weight into the overall structure when adding the same thickness (5 mm). It could be understood that the cone sub structure included 87 kg more than the cylinder. With the targeted sub structure found, its thickness was diminished while the thickness of the cylinder was kept constant achieving a final result of 17 mm thickness for the cone and 22 mm for the cylinder. That gave a total mass of 5,062 kg and a radial deflection of 4.827×10^{-4} m. Tangential and axial deflections were also checked observing that they were still within the limits. The natural frequencies for the first five mode shapes were as follows,

- 1st Mode shape → 26.92 Hz

- 2nd Mode shape → 27.23 Hz

- 3rd Mode shape → 27.64 Hz

- 4th Mode shape → 27.66 Hz

- 5th Mode shape → 36.18 Hz

Once the optimum thicknesses were found, a sanity check was carried out obtaining that 50º cone angle at position 5 was still the best layout.

With the finest configuration encountered, the dimensions of the rotor, 't_{con}' and 't_{cyl}', were altered and modal analyses run in order to quantify the effect of increasing the thicknesses of the sub structures in the overall frequency. The obtained results showed that the natural frequencies of the rotor structure rise with the thickness of the cone in a linear manner. However, as the cylinder thickness goes up, the natural frequencies go down following a linear trend again. See Figure 6.17. The plots for the rest of the modes can be seen in Appendix A.

$$f = 291.99 t_{con} + 18.473$$
$$R^2 = 0.9971$$

(a)

$$f = -46.891t_{cyl} + 30.28$$
$$R^2 = 0.6875$$
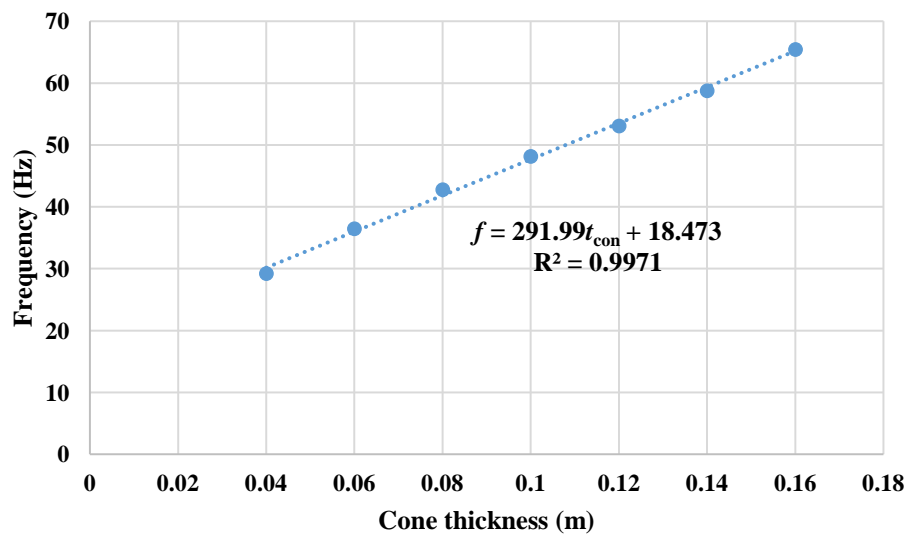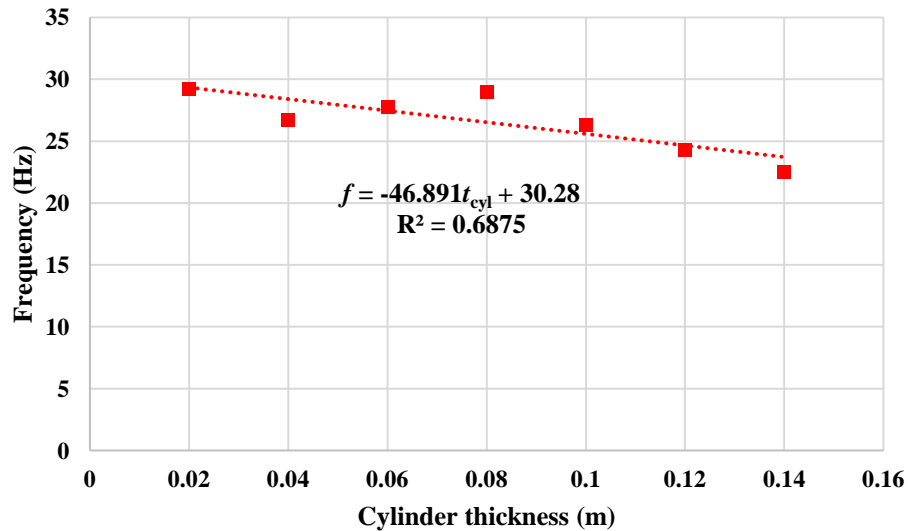
(b)

Figure 6.17 Frequency variation as dimensions are altered; (a) With cylinder thickness maintained at 0.02 m; (b) with cone thickness kept at 0.04 m

Finally, with the conical structure optimised and studied, the most dangerous modes of deflection were identified. Figure 6.18 shows the outcomes achieved for the different existing modes of deflection starting from 0 and ending with 4. The deflection was calculated using the same loads as for the disc structure in Chapter 4 that are eventually higher than the ones used in the optimisation of the structure. Only radial loads were applied to obtain these data, whereas tangential and gravitational were also utilised for the optimisation. Hence, this information must be seen only as a reference when designing conical structures. From the graph, it is easy to see that the highest deflection is obtained for mode 3 and therefore, this mode can be considered as the most damaging for this type of structures. So as to withstand the demanding loading conditions the use of thicker sub structures or the introduction of stiffeners are the most straightforward solutions that can be adopted.
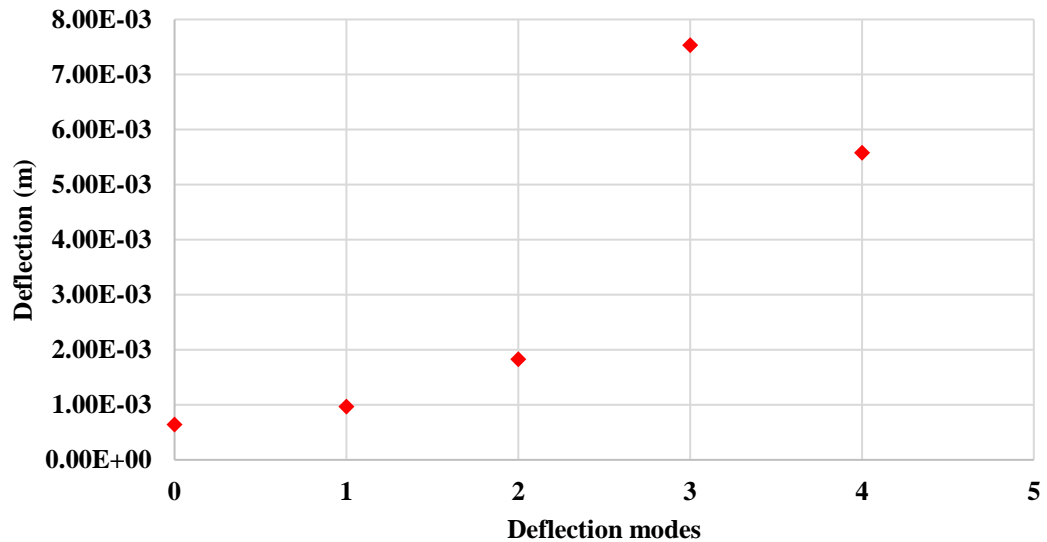
Figure 6.18 Deflection vs. Modes of Deflection (Cone Structure)

6.4 Discussion

Three distinct types of structural arrangements have been analysed in this chapter. A useful tool developed for disc structures to help the engineers during the early stage of their dynamic design has been presented. It consists of contour plots where the natural frequencies and the structural mass vary with thicknesses of the sub structures forming the generator components. Alternatively, the use of stiffeners has been introduced as a potential solution to push up the natural frequencies of the structures without sensibly augmenting their mass. A series of modal analyses were carried out over the optimised structure having stiffeners equally spaced. Firstly, they were placed on one side of the disc sub structure and then on both sides. It was understood that the utilisation of this sort of stiffeners puts too much weight (77 kg per stiffener) on the structure while the first natural frequency only increases by around 0.2 Hz per stiffener. However, it was observed that the use of stiffeners on only one side was much more efficient than on both sides in terms of frequency and mass. For this reason, it was thought that a less dense material, such as cast alloy steel, might be employed to further reduce the mass of such layout. The results obtained from the modal studies revealed that the addition of structural mass was still high. Nonetheless, the author believes that a distinct shape type of stiffener made of a

214

lower density material might be employed. At this point, it is important to highlight that the techniques suggested in this chapter have been only tried on rotor structures. It was considered good practice to make an attempt to find suitable methods for more simple structures before proposing them for stator structures.

On the other hand, rotor conical structures were assumed. Attracted by their good axial stiffness features, a conical structure was optimised with a view of minimising its mass considering deflection limitations and the frequencies of the lowest mode shapes. It was found that a rotor structure with a cone angle of 50º placed at the 5th position with 17 mm thickness for the cone and 22 mm for the cylinder presented the best outcomes. That gave a total rotor mass of 5,062 kg. Whether this data is compared to the one of the optimised disc structure, it can be observed a drop in mass of more than 48 % and 33 % if it is contrasted with the further optimised steel structure, although it is still heavier than any of the composite models. Moreover, the natural frequencies of the first five mode shapes of the rotor conical structure were all between 27 and 37 Hz, which means an increase of 58 % in the worst case scenario if compared with the disc structure. However, this increment in the natural frequencies of the first mode shapes can be interpreted as an issue too. This increase means that for the example given in this chapter, the electrical resonant frequency would cross all the natural frequencies of the rotor at higher rotation speeds. This would force the engineer to sacrifice a lot of energy collection in order to maintain the integrity of the machine unless the structure is designed to withstand the stress or the thickness of the cone is significantly elevated so that the resonant frequency is avoided. The structure would see its mass considerably augmented anyway.

The last step of this investigation on rotor cone structures included the data acquired from a set of conventional static studies made over the optimised conical structure which showed that the highest deformation takes place under mode of deflection 3. It is thought that this is a key factor that must be taken into account when designing this kind of supporting structures for electrical generators.

Chapters 3, 4 and 5 look at the design of the machine structure from a static point of view. The loads were estimated using a parametric model and applied to rotor and stator structures with different characteristics and made of distinct materials. Yet, no

external loads (except torque) or influence were included during the optimisation process. Rotation of the rotor and transient loads (wind induced forces, short circuit,..) should be taken into account in future models. Exploration of the rotor and stator interference and bearing location are other features that have not been considered in these analyses. By checking the Campbell diagram presented in this chapter, it can be seen that the highest rotor modes and lowest stator modes are fairly close (this combination could easily lead to a structural collapse). In order to avoid them, it would be necessary to have the electrical machine working in a range between 7.6 and 18.5 rpm. This means that the wind energy that could be harvested below 7.6 rpm and over 18.5 rpm is lost. A potential solution would be to increase the thickness of the disc sub structure with the consequent rise in mass. Another solution would be to make use of rotor conical structures. However, it was understood that the use of this particular geometry did not push up the frequency far enough, thus an elevation of the cone sub structure thickness would be again needed. The last solution that can be noticed by having a look at the said diagram goes through altering the number of pole pairs so that the slope of the electrical frequency line can be changed. With a higher number of poles, the inclination of the line would go down interfering with the lowest rotor and stator modes at higher rotational speeds which would force us to narrow down the machine operating range. In addition, saturation problems could arise. But, if the number of poles is decreased, the slope of the line would go up giving us more room for machine operation. Nonetheless, it is important to notice that by doing so the highest stator modes could get excited at lower rotational speeds. Also, with lower number of poles thicker rotor and stator yokes would be necessary which would make the machine heavier.

During a short circuit event, the magnetic field could react causing rotor eccentricity, transferring the entire load from the generator structure to the bearing. Moreover, the excitation of the structural modes can generate changes in the inductance of the coils introducing higher harmonics in the currents. Therefore, a more accurate model of the bearing that replicates their characteristic non-linear behaviour would be required.

In Chapter 6, the dynamic behaviour of the structure has been studied and tried to improve. Several techniques have been described and tested here. The results achieved were filtered until finding the appropriate data that could be useful for a design engineer looking at this sort of devices. Again, no external influence was considered in these studies.

6.5 Conclusions

In this chapter, a useful instrument for the dynamic design of disc structures has been presented. The use of the provided contour plots allows the engineer to make accurate estimations of the weight and the natural frequencies of the structure to be produced. Later on, the introduction of stiffeners was proposed with the main aim of elevating the structure natural frequencies without adding too much weight. The best results were obtained by placing the stiffeners on one side of the disc sub structure with the frequency of the overall structure increasing linearly with their number. Nevertheless, as the studies demonstrated, the augment in frequency was not significant enough for the amount of material that is put on and for this reason their use was discarded.

Due to its potentially good radial and axial stiffness characteristics, a rotor conical structure was proposed. It was observed that its performance is superior to that of a disc structure with less mass needed to support the same loads and natural frequencies almost 2 times higher. Having said that, the author believes that conical structures should be taken into consideration when approaching the design of a generator structure due to their outstanding static and dynamic characteristics. More research would be necessary on this field as with the use of the already described methods and materials the mass of these structures might be further optimised. For instance, a composite material conical structure would present fewer issues than a disc structure at the time of joining the sub structures as the cone slope creates a larger surface of attachment that would facilitate the transition of the composite fibres from one sub structure to another. With this, a considerable reduction in the number of fasteners and in the manufacturing time would be achieved. It would be

even possible to think that the structure might be constructed as a whole and not in two pieces (cone and cylinder) eliminating the need for fasteners and the challenging process of attachment. The introduction of external loads and influence would be indispensable in order to carry out an accurate optimisation study.

6.6 References

[1]   IEC 61400-1. Wind Turbine Generator Systems, Part 1: Safety Requirements. 2nd edition. 1999.

[2]   Germanischer Lloyd. Non-Marine Technology, Part 1: Regulations for the Certification of Wind Energy Conversion Systems. Rules and Regulations, IV. 1999.

[3]   G. Bywaters, V. John, J. Lynch, P. Mattila, G. Norton, J. Stowell, M. Salata, O.Labath, A. Chertok, D. Hablanian,Northern Power Systems WindPACT Drive Train Alternative Design Study Report April 12, 2001 to January 31, 2005.

[4]
        http://www.energy.kth.se/compedu/webcompedu/S5_Aeroelasticity/B1_Introd uction_to_Aeroelasticity/C3_Bladed- Disk_Vibrations/S5B1C3_files/Campbell_diagram.htm,[Online] Last Accessed 19/10/2016.

[5]   R.Poore, T. Lettenmaier,Alternative Design Study Report: WindPACT Advanced Wind Turbine Drive-train Designs Study. NREL/SR-500-33196., August 2003.

[6]   G. Bywaters, P. Mattila, D. Costin, J. Stowell, V. John, S. Hoskins, J. Lynch, T. Cole, A. Cate, C. Badger, B. Freeman, Northern Power NW 1500 Direct-Drive Generator. NREL/SR-500-40177, October 2007.

[7]   J. Heikkinen, J. Sopanen, V. Ruuskanen, J. Nerg,Dynamic analysis of a direct-driven permanent magnet generator drive train including flexible turbine blades, ASME International Design Engineering Technical Conferences Computers and Information in Engineering Conference, IDETC/CIE 2011,Washington, DC, USA, Aug. 2011.

[8]   J. Islam , D. Svechkarenko , R. Chin , A. Szucs , J. Mantere , R. Sakki, Cogging torque and vibration analysis of a direct-driven PM wind generator with concentrated and distributed windings, 15th International Conference on Electrical Machines and Systems (ICEMS), Sapporo, 21-24 Oct. 2012.

[9]   J. Sopanen, V. Ruuskanen, J. Nerg, J. Pyrhonen, Dynamic Torque Analysis of a Wind Turbine Drive Train Including a Direct-Driven Permanent-Magnet Generator, IEEE Transactions on Industrial Electronics, (2011).58, (9), pp. 3859-3867.

[10]   E.B.Smith, Nacelle Design for a 10MW reference wind turbine, M.S thesis. Thesis, NTNU, 2012.

[11]   S. S. Klair, Design of Nacelle and Rotor Hub for NOWITECH 10MW Reference Turbine, MS Thesis, NTNU, 2013.

[12]   L. Frøyd, O.G. Dahlhaug, Rotor Design for a 10 MW Offshore Wind Turbine, Proceedings of the Twenty-first (2011) International Offshore and Polar Engineering Conference, Maui, Hawaii, USA, 19-24 June 2011.

[13]   L. Sethuraman, "Hydrodynamics and drive-train dynamics of a direct-drive floating wind turbine", PhD thesis, University of Edinburgh, Edinburgh, 2014.

[14]   Y. Xing, M. Karimirad, T. Moan, Effect of Spar-Type Floating Wind Turbine Nacelle Motion on Drivetrain Dynamics, In Proceedings of EWEA 2012 Annual Event, Copenhagen, Denmark,16-19 April 2012.

[15]   Y. Xing, M. Karimirad, T. Moan, Modelling and analysis of floating spar-type wind turbine drivetrain, Wind Energy, (2012).(DOI: 10.1002/we.1590), pp.1-23.

[16]   Shrestha *et al.*, "Structural Flexibility: A Solution for Weight Reduction of Large Direct-Drive Wind-Turbine Generators", IEEE Transactions on Energy Conversion, Vol. 25, No. 3, Sept. 2010.

[17]   A. Zavvos, "Structural Optimisation of Permanent Magnet Direct Drive Generators for 5MW Wind Turbines", PhD thesis, University of Edinburgh, Edinburgh, 2013.

[18]   M. Kirschneck, "Mastering Electro-Mechanical Dynamics of Large Off-Shore Direct-Drive Wind Turbine Generators", PhD thesis, TU Delft, Delft (The Netherlands), 2016.

[19]   https://sites.ualberta.ca/~yousefim/bfiles/Ebooks/Vinogradov%20-%20Fundamentals%20of%20kinematics%20and%20dynamic%20of%20machines%20and%20mechanisms.pdf, [Online] [Accessed 10 March 2017].

[20]   http://www.prismengblog.com/2016/05/31/faster-solidworks-simulations-with-draft-quality-mesh, [Online] Last Accessed 19/10/2016.

[21]   W. Leithead, Wind Turbine Technology 2, Wind CDT material course, University of Strathclyde, Glasgow, 2012.

[22]   SolidWorks, http://www.solidworks.com/sw/products/simulation/frequency-analysis.htm, [Online] Last Accessed 19/10/2016.

[23]   R. J. Roark and W. C.Young, 'Roark's Formulas for Stress and Strain', McGraw-Hill International Editions, Singapore, 1989, 6th Edition.

[24]   J. N. Stander, G. Venter, and M. J. Kamper, "Review of direct-drive radial flux wind turbine generator mechanical design," 2011.

Chapter 7

Discussions and Conclusions

7.1 Chapter summaries

This thesis addresses the structural analysis and the different ways of efficiently designing low speed, high torque radial flux permanent magnet electrical generators for direct drive wind energy converters with a view to minimise their mass. In this chapter, a summary of each chapter is presented. The outcomes obtained from this investigation will be discussed accompanied by the conclusions drawn.

Chapter 2 introduces the reader to renewables and the diverse types of wind energy converters. Looking more in detail, two alternatives for the drivetrain are available:

one which utilises a gearbox to step up the low speed of the wind turbine rotor so that it can be connected to a conventional high speed electrical generator and one in which the electrical generator is directly connected to the turbine rotor. The latter, also known as a direct drive system, removes the gearbox from the arrangement minimizing the number of mechanical moving parts making the device potentially more reliable and efficient and less noisy.

However, with the layout where the gearbox is eliminated, the electrical machine copes with a very large torque and forces, hence it needs to be bigger, heavier and more robust than conventional high speed generators. Whereas the common way to approach the design of such machines was to focus all the attention on the mass of the active material and give the highest priority to the electrical aspects, in this investigation the author has concentrated on the amount of material required to maintain the structural integrity of the generator taking into account mechanical matters.

In Chapter 3, the distinct existing types of simplified radial flux generator structures are shown as described in [1] and the concepts of structural stiffness and magnetic stiffness introduced [2]. Due to the variety of forces acting on the direct drive generator, the structure can deform in many different ways which can be characterized by a mode number, 'n'. These modes of deflection can affect the magnetic flux density in the generator airgap inducing forces that try to close it. The most significant load is known as the normal component of Maxwell stress and the necessary stiffness to resist it has been calculated employing a parametric model, which links magnetic and structural design, previously proposed by Tavner and Spooner in [3]. This method has been corrected, enhanced and further developed. Equalities capable of computing the required structural stiffness for conventional synchronous machines and permanent magnet machines have been generated. A permanent magnet machine has been assessed using this model and FEMM for validation.

Chapter 4 presents three techniques that have been used to estimate the minimum stiffness and mass that the generator structure needs to withstand static loads without sensibly deforming. The mentioned three methods, which correspond to finite element, analytical and hybrid, have been categorised according to their flexibility and suitability to produce accurate results against the benchmark of finite element analysis. The hybrid approach consists of combination of the data acquired from dimensional homogeneity studies and the results achieved from finite element analysis. This versatile method is capable of producing accurate results for Mode 0 and Mode 1 deflection much quicker than the FE method. The analytical technique is also much faster than the finite element approach although it is only suitable to predict the stiffness of certain types of structures which are under Mode 0 deflection. However, although much slower, the FE method is able to estimate the stiffness of any type of structure under any sort of deflection mode. Moreover by using the retrieved data from FE analyses, 2D structural contour maps, where the cylinder and the disc thicknesses are set as the independent and dependent variables respectively, can be generated and utilized as a mean for finding the minimum structural mass of the generator.

Structural stiffness modelling of disc and armed structures is also presented in Chapter 4. The outcomes obtained from the analyses carried out using the said three techniques are shown and evaluated. A comparison between disc and armed structures is presented revealing that structures with hollow arms are not able to resist high torque loads as well as structures made with discs do unless the thickness of the arms is considerably increased. This leads to an increase in mass. Thereafter, a disc structure suitable for a 3 MW direct drive generator was optimised with the main aim of minimising its weight considering normal, tangential and gravitational loads. For the mass minimisation, as well as the loads, a stiffness and mass trade-off study of the rotor and stator structures was carried out. By setting the minimum stiffness of each structure forming the generator as a threshold, and considering the minimum stiffness needed by the entire machine, its mass can be diminished by targeting the heaviest structure that typically corresponds to the stator. Other ways of reducing the mass of electrical machines disc structures are suggested and put in

practice and a distinct structural configuration, such as rotor conical structures, proposed and analysed. Both disc and conical structures are studied under several deflection modes.

Chapters 2, 3 and 4 provide the reader with the necessary information to understand the theory and the issues behind the static design of a supporting structure for a multi MW electrical machine. Different design tools, which can be employed during the early stages of the design process for the estimation of the required minimum structural stiffness, are developed and described.

Chapter 5 introduces the reader to composite materials. An overview of the theory behind and the work done in the past in related fields using these materials is given. A small scale disc structure corresponding to a 100 kW generator was first modelled following what it is called the conventional approach, in which the plies forming the stacking sequence are placed according to the Cartesian coordinate frame. Then, the disc structure was again modelled but this time following an innovative approach utilised for the design of flywheels, in which the fibres are placed following 5 different cylindrical coordinate systems. The disc sub structure was divided into 11 distinct areas where the plies formed by the said fibres were located. An optimisation of this type of structure was finally made obtaining a difference in mass with its optimised counterpart made of steel of 82% and 33.5% if compared with the composite structure modelled following the conventional approach.

A model of the larger direct drive generator corresponding to a 3 MW machine was also created utilising composite materials employing the conventional and the more advanced approach. In this case, the difference in mass is about 60%. However, the more advanced structure resulted in a slightly heavier than the conventional approach one due to a lack of adaptability in the design. Diverse ways of implementing the needed adaptability to pursue more ambitious optimisations are proposed.

In Chapter 6 the optimised steel structure is studied from a dynamic point of view making use of modal analyses. The main aim was to work out the natural frequencies of the structure and the distinct ways of changing them so that the excitation

frequencies do not match them. The thickness of both the disc and the outer rim sub structures were varied revealing that thicker cylinders reduce the natural frequencies of the overall structure, whereas thicker discs have the opposite effect. Different numbers of stiffeners, first located on one side of the disc sub structure and then placed on both sides, were tried too. It was observed that the structural mass was increased, while the natural frequencies did not increase as expected. A distinct material with lower density was tried in order to see how the reduction in weight of the stiffeners would affect the overall mass. The result achieved showed that the increase in mass was still high for the small increase in the natural frequencies of the structure. With all of these options exploded, it was thought of another kind of structural configuration such as a conical structure where the cone contributes with a higher axial stiffness. The location of the cone sub structure was altered – with respect to the cylinder – until the ideal position was found. The structure was then optimised following the same parameters as with the disc structure, obtaining an optimum cone angle of 50 degrees, and analysed using FE tools. The studies revealed a superior performance of the conical structure if compared to the disc structure with less mass needed to withstand the same loads and natural frequencies almost 2 times higher. The advantages and drawbacks of utilising rotor conical structures are discussed.

7.2 Discussion

In this section, the gained insights from the chapters above are outlined and discussed. The broad approach of this thesis includes the next ideas:

1. The use of simple generator structures that can reproduce the types and character of airgap deflection and mass features of real generators used in industry.

2. Development of design tools and knowledge that can be used in the early phase of the design process to estimate the required minimum structural stiffness at the lowest mass that allows fast calculations and straightforward optimisations.

3. To find a simplified structure made with conventional materials that can meet major structural requirements in a lightweight manner.

4. To explore the possibility of employing low density materials, such as composites, in the supporting structure design in order to minimise its overall mass.

5. Whether stiffness through static modelling is sufficient or if dynamic modelling is also necessary.

7.2.1 Evaluating stiffness

Simplified structural generator models have been analysed using different approaches. A method coupling the magnetic and mechanical design has been developed and described in Chapter 3. It is a versatile 2D magnetic model which by assuming a deflection computes the airgap closing force and the airgap stiffness of two different types of electrical machines under distinct modes of deflection. Then, by making a comparison with the results obtained from the mechanical model fed with the outcomes of a finite element structural model of the machines, the structure in question can be considered suitable or not to successfully carry the imposed loads. The given data corroborated the applicability and accuracy of this technique to estimate the required stiffness that can be utilized during the design stage, after the manufacturing process and as part of a condition monitoring system. In Chapter 4, another three distinct methods capable of calculating the necessary stiffness and structural mass of the entire machine with high accuracy were presented and evaluated. As proved, they can be used to optimize the structure so that it can withstand the major internal stresses present during operation at the lowest mass.

All of the mentioned techniques are very easy to use. In addition, their high versatility make them very useful especially at the early stages of the design process. They would accelerate the calculations and give the designer the possibility of carrying out a quick estimation of the needed stiffness and mass.

Further structural optimizations could also be made by using topology optimization packages. Their use after the studies made with the tools mentioned above is

recommended by the author as additional mass savings can be achieved through the elimination of parts which do not contribute to carry the loads.

On the other side, it is important to highlight that these methods have been developed taking into account the major internal loads that can act on the generator structure. This means that the electrical machine is completely isolated from the rest of the turbine and that no external loads, except torque, have been considered. Generator dynamics have not been included either. Therefore, these techniques only apply to the generator supporting structure design from a static viewpoint.

7.2.2 Lightweight materials for generator supporting structures

The use of low density materials, such as composites, has been considered in the design of the generator structure with the main aim of reducing its overall mass. The anisotropic nature of composite materials makes them harder to model and introduces additional complexity to the structure design. Nevertheless, the graphical interface of the software and its flexibility to change parameters makes the modelling and optimisation process more straightforward. The results obtained showed that an advanced composite material structure can deal with loads as well as a structure made of steel does. By tailoring its structural properties, it was possible to find an arrangement capable of spreading out the stress across the structure and withstand the loads keeping the deflection limits within the specified range. In addition, the better fatigue properties of composite materials help to extend the lifespan of the entire wind turbine and their higher Young's modulus to density ratios reduces the overall generator mass by about 60 %. It is important to note that the plies utilised for modelling the structure were assumed perfectly manufactured. This means that no defects and ideal alignment of fibres were considered. In reality, it is not possible to perfectly align the fibres and although very small, the possibility of having voids or any other kind of imperfection is something to take into account. These factors can affect the structural weight reduction achieved although not heavily.

During the machine modelling and optimisation stage, thermal considerations were not assumed. Wind turbine electrical generators operate for long periods of time at really high temperatures. Thermal expansion properties of composite structures can

also be tailored to meet the needs of the design potentially introducing further enhancements and that is why the author believes that further research must be done in this area. The inherent dynamic features of the electrical machine and the influence of external loads on its composite structure have not been investigated here. However, the characteristics of the structure with tailored high stiffness and low mass suggests that it is possible to achieve satisfactory dynamic features and still have a lighter machine. Extensive investigation on further mass optimisation of the mosaic pattern composite structure is required as with the introduction of higher design adaptability additional mass savings can be achieved. The interaction between the rotor and the stator yokes, made of iron, with the composite structure should also be studied. In the aerospace industry, the attachment of composite structures typically implies the utilisation of titanium fasteners which are lighter than its steel counterparts and that not only introduces the necessary stiffness but also impedes galvanic corrosion. The fact of employing carbon/epoxy for the structure and titanium fasteners will considerably increase the cost of the machine. Its manufacturing process will be more expensive than that of a conventional generator steel structure. Different options can be studied in order to diminish the cost of the machine structure and its manufacturing process such as using rotor conical structures. The cone angle can benefit the integration of the cone sub structure fibres into the outer casing, opening the door to manufacture the structure as only one piece eliminating so the need for fasteners and reducing the weight and the production time. Bearing all of this in mind and once the suggested research has been carried out, the author would propose to build up a model of the structure and test it before undertaking large scale projects. A detailed economic study considering the advantages and drawbacks derived from the use of composites to produce a generator structure is needed before giving the go-ahead or rejecting the task.

7.2.3 Direct drive electrical generator dynamics

Several tools have been developed and evaluated for the static design of simplified direct drive electrical machine structures. However the inherent dynamic nature of

the wind turbine led the author to look at the generator from a dynamic perspective in Chapter 6.

Considering an ideal bearing configuration in which the external loads coming from the hub are directly transmitted to the tower, only the major internal loads acting on the generator structure have been assumed for its design and analysis. Nevertheless, the external loads have an important influence on the internal loads that must be taken into account. This influence strongly depends on how well integrated in the wind turbine system the generator is. The structure has to be capable of dealing with internal stresses with larger amplitudes and variable frequencies produced by the induced effect of the external loads without sensibly deforming. In order to make this possible it is estimated that an extra 10 % of stiffness as composed to static case needs to be added to the structure in every direction.

Resonance is another issue that needs to be addressed so as to maintain the integrity of the machine. For that, a range of possibilities has been explored in Chapter 6. To increase the structure natural frequencies, the use of stiffeners introducing more support into sensitive zones is a solution widely adopted by manufacturers. Other options include the utilisation of low density materials in the structure design or a change in geometry. By looking at the Campbell diagram of the example provided in Chapter 6, the operation range of the machine could be identified. In addition, it was observed that the said operational range narrows down as the structure natural frequencies increase due to the match with the fundamental electrical frequency. Due to this, other possibilities were proposed but this time the attention was focused on the electrical side. In order to expand the machine range of operation so that the energy capture can be maximized the number of pole pairs can be modified. An increase would mean that the electrical frequency would cross the lowest modes of the rotor and the stator at higher rotational speeds reducing the operational range even further. But if the number of pole pairs is diminished the slope of the line would increment. With this, it would be possible to avoid the lowest modes of both the rotor and the stator structures although it would require having thicker rotor and stator yokes, which would elevate the mass of the generator. In any case, the author

believes that it is necessary to go through this trade-off process so that the optimum integrated design is achieved according to the requirements of the project.

7.3 Revisiting the thesis research question

In Chapter 1, the research question is stated as:

"*Can electromagnetic and structural stiffness models be used effectively to minimise the mass of electrical generators for direct drive wind turbines?*"

In order to find an answer, it is necessary to know the minimum needed stiffness so that all the loads acting on the generator can be resisted without deforming to find the minimum required mass.

In this project, a number of models were generated. The way in which they can be used during the design and optimisation stages was also described and explained. In Chapter 3, an electromagnetic-mechanical stiffness model was developed. The retrieved results showed how versatile and accurate the model is so as to calculate the minimum required structural stiffness of two different types of electrical machines. Chapter 4 illustrates the distinct techniques available and establishes a hierarchy according to their suitability and accuracy to estimate the minimum stiffness and mass of electrical machine structures. In Chapter 5, models of generator structures made of low density materials are analysed revealing a high positive impact on the effort to reduce the machine's supporting structure mass. As the mentioned chapters covered the design of the generator from a static perspective, in Chapter 6, the generator structures were studied from a dynamic point of view. The outcomes helped to understand the influence of the dynamics in the electrical machine design. It was estimated that an extra 10 % of stiffness, as composed to the static case, in every direction is necessary to deal with the internal stresses with larger amplitudes and variable frequencies produced by the induced effect of the external loadings although this figure might vary as the influence of the external loads on the generator structure strongly depends on how well the electrical machine is integrated in the wind turbine. It could be said that the answer to the research

question is affirmative as the models presented in this thesis were proved to be effective when they were used to reduce the structural mass of the machine.

7.4 Contribution to knowledge

This thesis has contributed to knowledge in a number of ways:

- A consistent set of equations coupling electromagnetic and mechanical designs of different types of electrical machines, which is used to model the minimum required stiffness, has been derived and validated for different modes using finite element tools. A case study illustrating the suitability of the magneto-mechanical model has been introduced (Chapter 3).

- Distinct structural design tools have been developed, validated and categorized according to their flexibility and suitability to estimate the necessary stiffness of sub structures and complete structures (Chapter 4).

- Diverse structural configurations have been analysed and compared in order to identify the arrangement that is capable of coping with the loads with the minimum mass. The optimum disc model, found by using 2D contour maps of stiffness and mass of rotor and stator structures, was studied under several deflection modes and further optimised using a commercial piece of software. A rotor conical structure was proposed and analysed under different deflection modes (Chapter 4).

- A new concept for the design of electrical machine disc structures using low density materials has been introduced and verified for small and large scale generators. The structural mass reduction achieved with this design is investigated (Chapter 5).

- The options available to alter the natural frequencies of a structure have been presented and analysed through modal studies. A dynamic study of the optimum disc structure has been conducted, establishing structural excitation sources and how to interact with them. A new structural configuration (rotor conical) has been dynamically studied and optimised (Chapter 6).

The work in this thesis has contributed to a number of other publications:

Structural stiffness analysis of radial flux permanent magnet direct drive generators in Chapter 3 in [2]; A comparative study of methods for modelling the structural stiffness of generator components in Chapter 4 in [4] and A New Method for Coupling Structural and Magnetic Models for the Design and Optimization of Radial Flux PM Generators for Direct-Drive Renewable Energy Applications in [5]; A lightweight approach for airborne wind turbine drivetrains in Chapter 5 in [6].

7.5 Further work

This thesis covers a number of topics that are of vital importance in the design of electrical generators structures. Due to time limitations, it did not go deeper into the fields it addresses. In order to improve the techniques introduced in this dissertation further research is necessary. The following points need to be investigated in more detail:

- The model coupling magnetic and mechanical designs it is a static representation that neglects axial end effects and does not consider any external influence. Further investigation should be carried out so that these points can be covered.

- The optimised generator models produced in this thesis do not consider thermal issues or any other external load coming from the wind turbine rotor. External loads compromise any load coming from the wind turbine rotor (including thrust). External loads have a significant influence on internal loads. As said, the degree of influence depends on how well integrated the generator is in the wind turbine structure. The electrical machine is directly connected to the hub through a shaft. Misalignments and other factors that can affect the normal operation of the generator and the integrity of its structure should be also analysed.

- The majority of the simplified structures proposed by Stander in [1] have been studied. However, supporting structures made with spokes or star shapes are still missing. Further optimisations might be possible with the use of such layouts.

- The mosaic pattern structural model produced for the 3 MW direct drive machine using composite materials in Chapter 5 was not able to reduce the weight of the structure more than the conventional approach model because of the lack of flexibility in its design. Additional optimisations could be made by making use of mosaic pattern structures with more sub divisions in the disc sub structure. This would increase considerably its cost of manufacturing; hence a detailed economic study should be made before approaching this task.

- Avoidance of structure's natural frequencies is a key matter that must be addressed with the highest precision possible. Extensive research should be carried out on this field with the main aim of maximising the machine operation range with the minimum mass.

- A deeper investigation on the distinct methods for minimising the mass of conical structures is desirable.

7.6 References

[1]   J. N. Stander, G. Venter, and M. J. Kamper, "Review of direct-drive radial flux wind turbine generator mechanical design," 2011.

[2]   P. Jaen-Sola and A. S. McDonald, "Structural Analysis and Characterization of Radial Flux PM Generators for Direct-Drive Wind Turbines," *3rd Renew. Power Gener. Conf. (RPG 2014)*, Naples (Italy) Sept. 2014.

[3]   P. J. Tavner and E. Spooner, "Light Structures for Large Low-Speed Machines for Direct-Drive Applications." in *Proc. International Conference on Electrical Machines*, Chania, Greece, 2006.

[4]   P. Jaen-Sola and A. S. McDonald, "A Comparative Study of Methods for Modelling the Structural Stiffness of Generator Components", *IET Power Electronics, Machines & Drives (PEMD)*, Glasgow (UK), Apr. 2016.

[5]   A. S. McDonald and P. Jaen-Sola, "A New Method for Coupling Structural and Magnetic Models for the Design and Optimization of Radial Flux PM Generators for Direct-Drive Renewable Energy Applications", *IET Renewable Power Generation Journal*, Dec. 2016.

[6]   P. Jaen-Sola and A.S. McDonald, "A Lightweight Approach for Airborne Wind Turbine Drivetrains", European Wind Energy Association International Conference (EWEA), Paris (France), Nov. 2015.

Appendix

Natural frequencies: Disc rotor structure

$$f = 349.58t_\mathrm{d} - 3.5856$$
$$R^2 = 0.9998$$

(a)

$$f = 366.1t_\mathrm{d} + 0.0431$$
$$R^2 = 0.9999$$
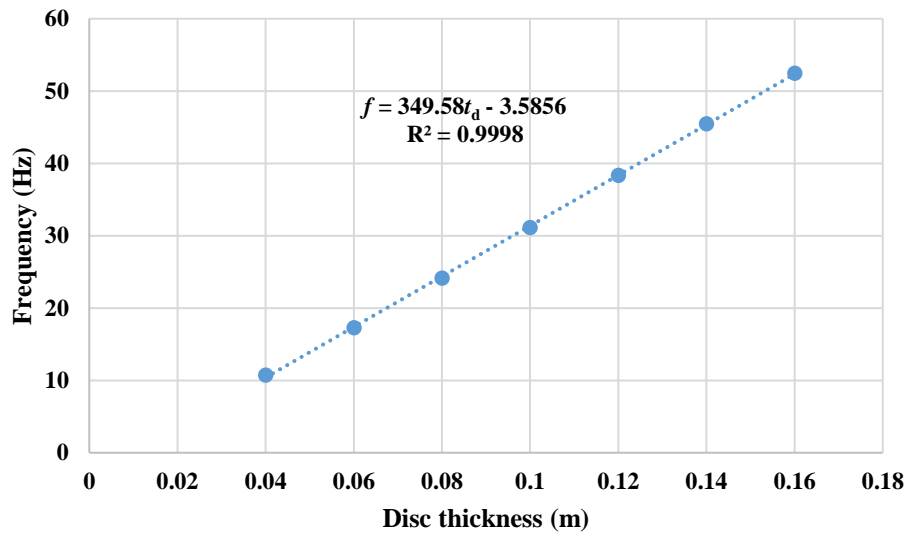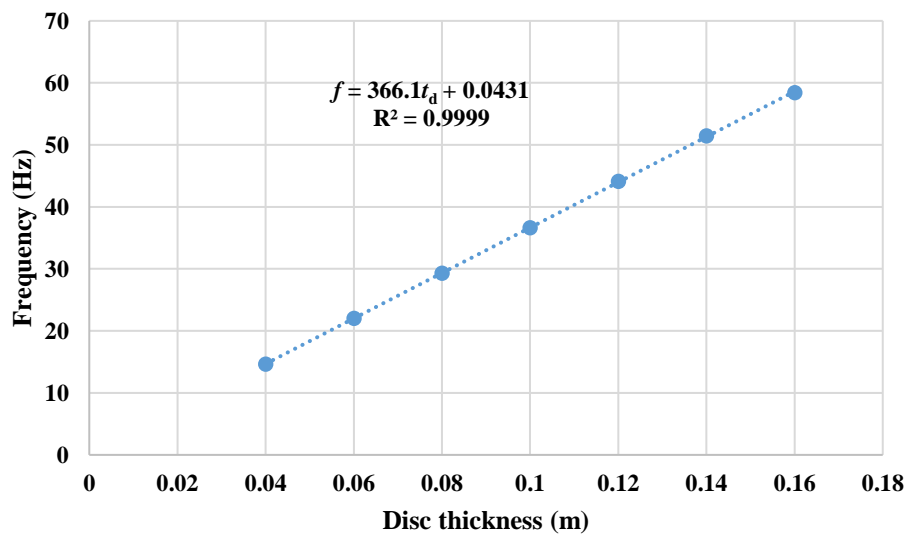
(b)
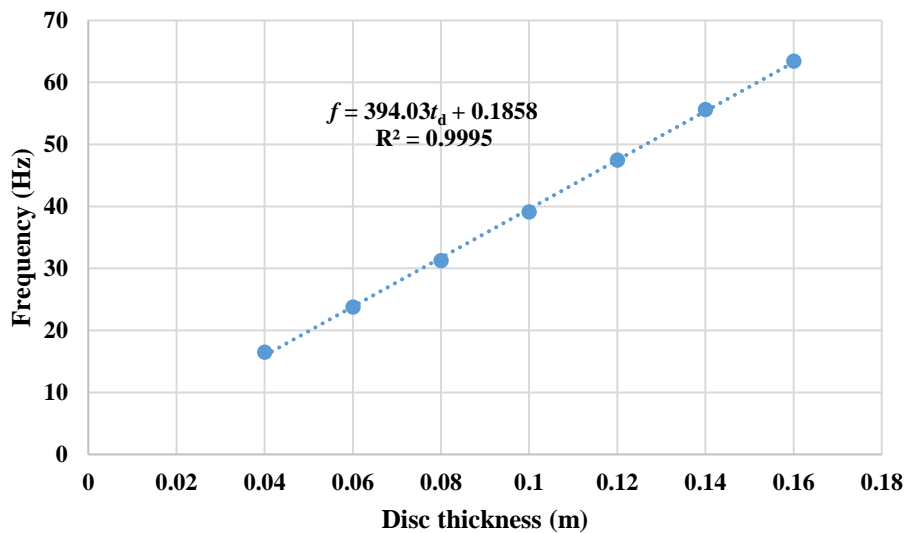
(c)
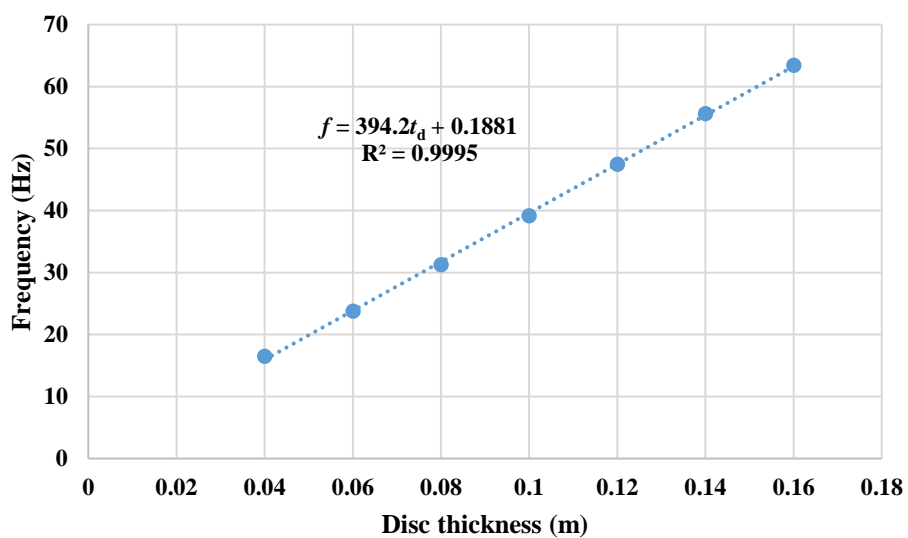
(d)

Figure A.1 Frequency variation as dimensions are altered with rotor cylinder sub structure thickness maintained at 0.02 m; (a) 2nd mode; (b) 3rd mode; (c) 4th mode; (d) 5th mode
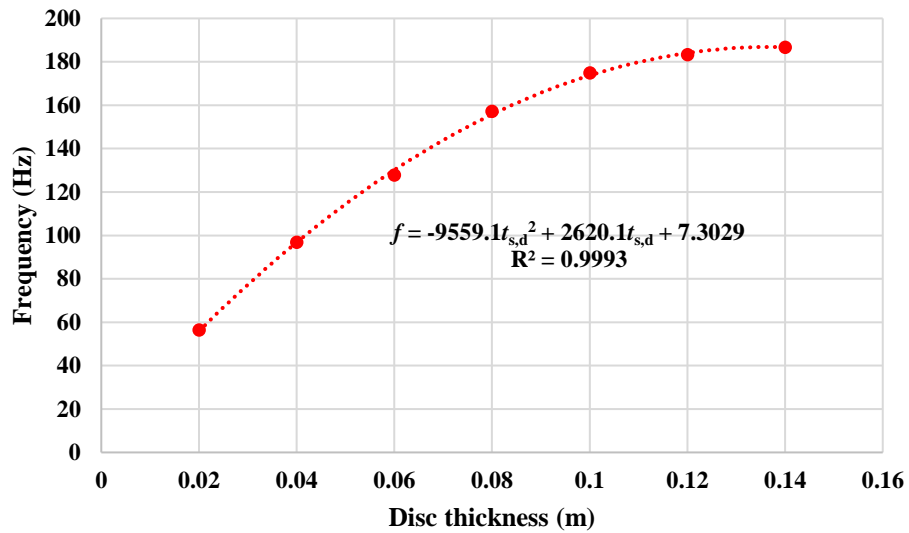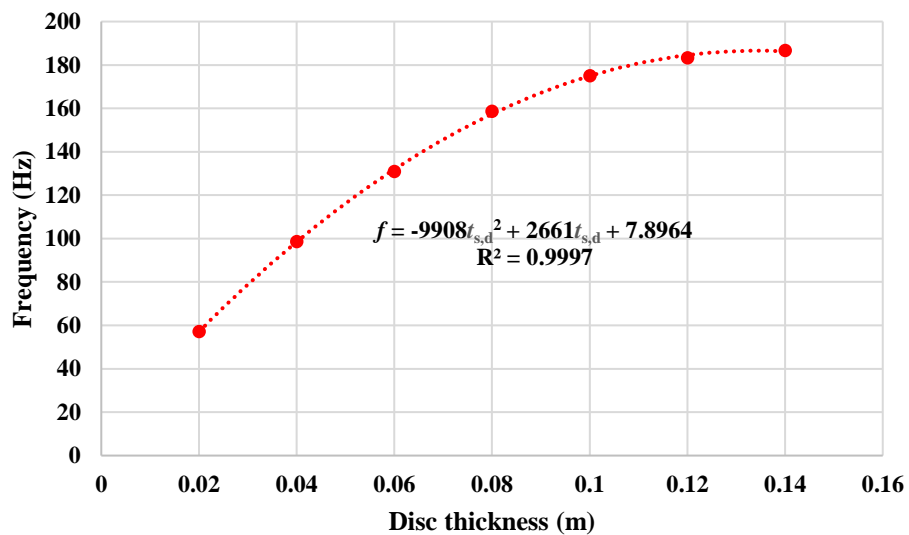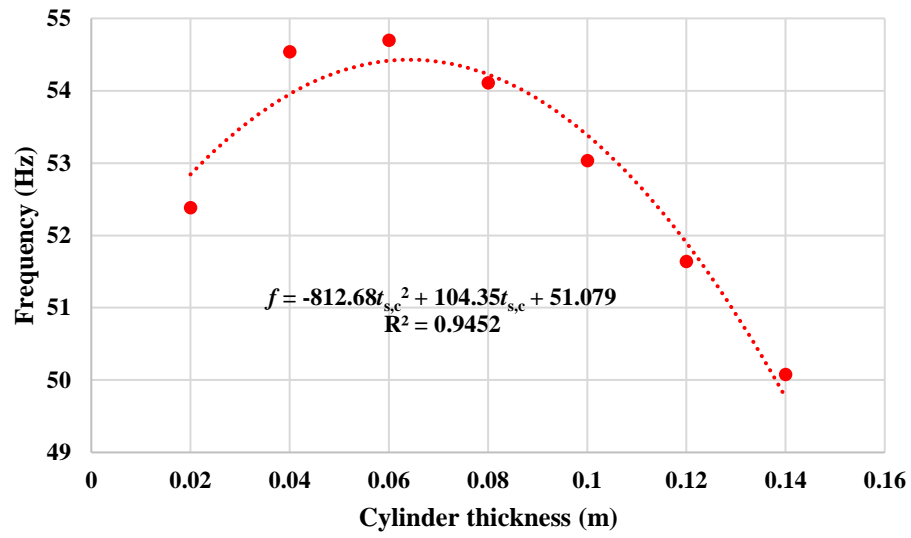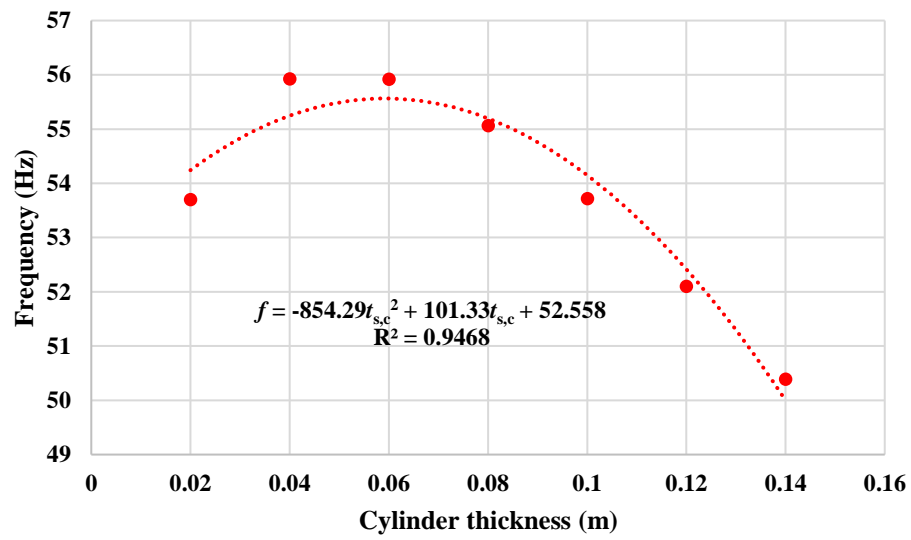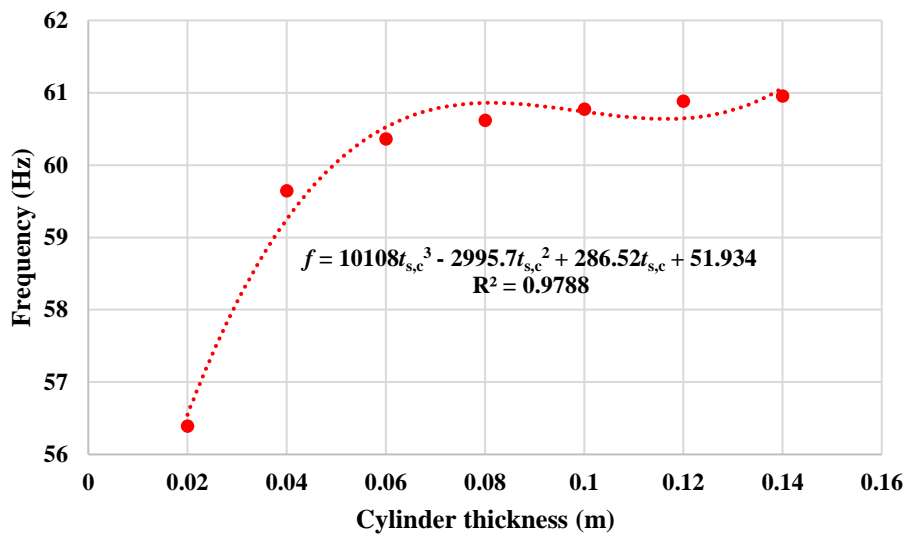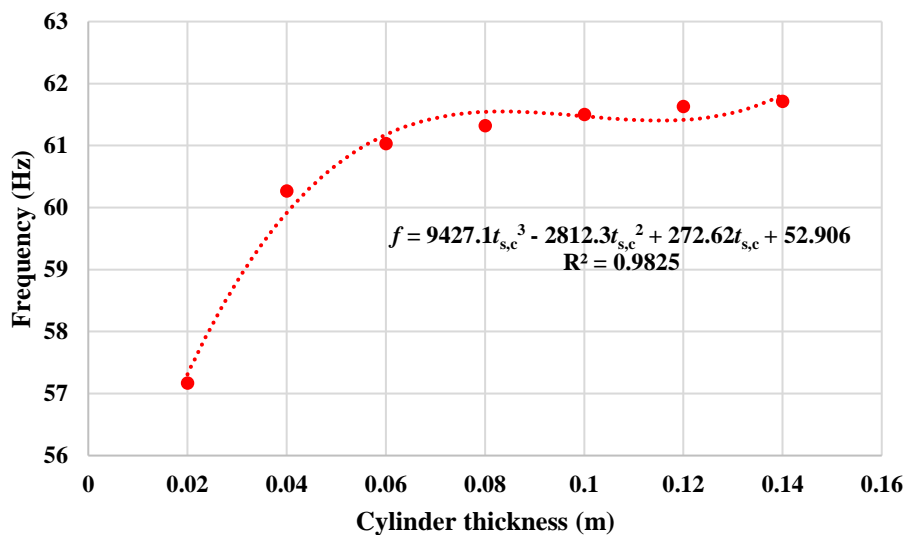
236

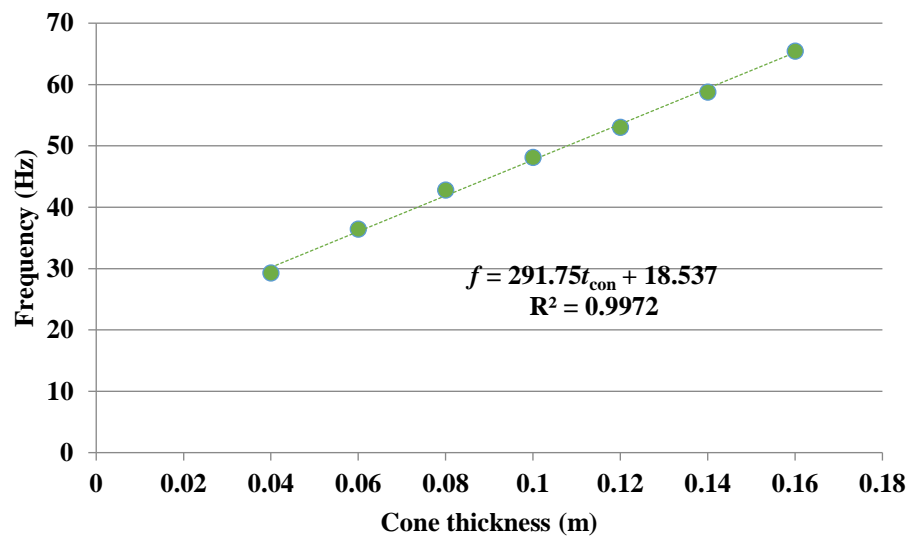$$f = 462.71t_{c}^2 - 141.26t_{c} + 19.747$$
$$R^2 = 0.9969$$

(a)

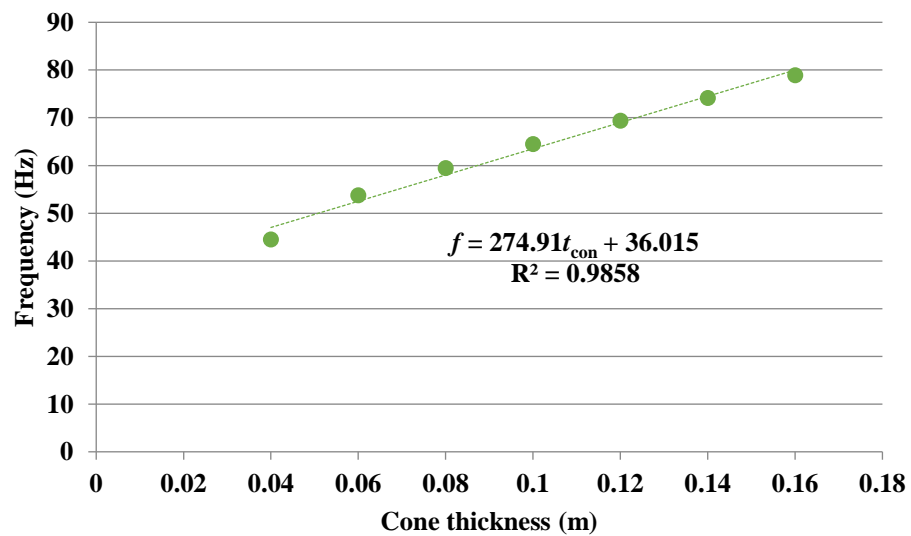$$f = -72.263t_{c} + 23.102$$
$$R^2 = 0.9858$$
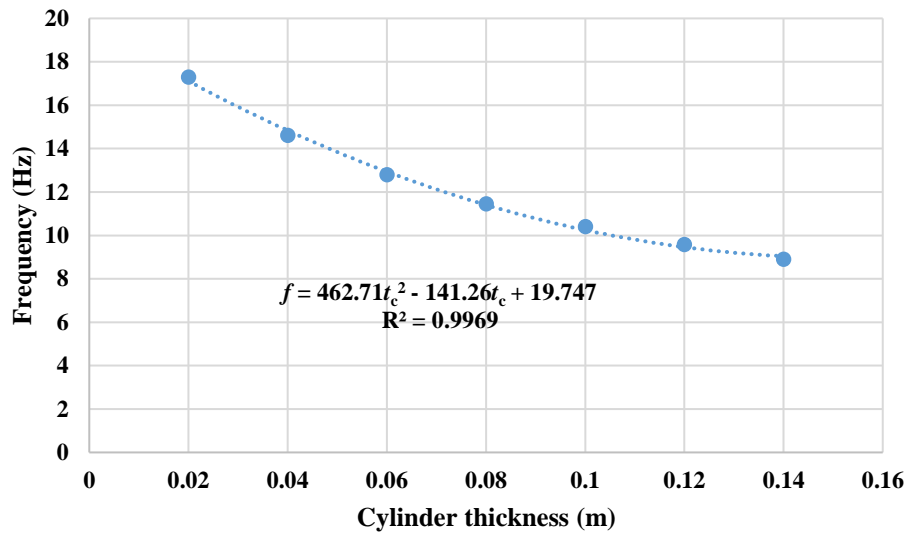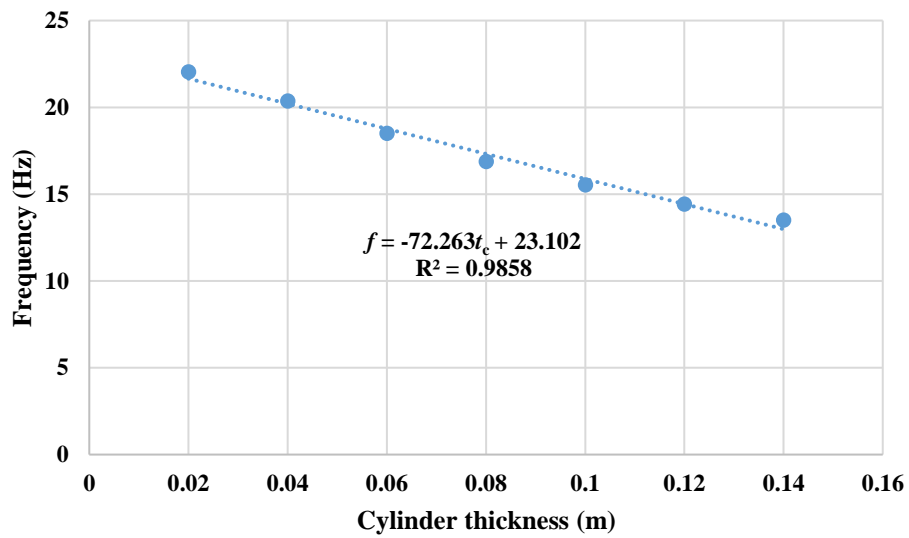
(b)
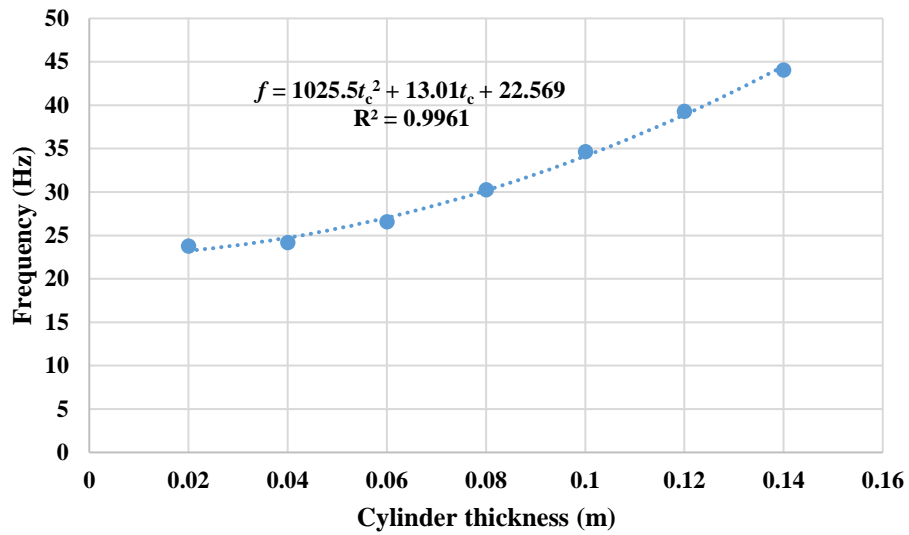
(c)
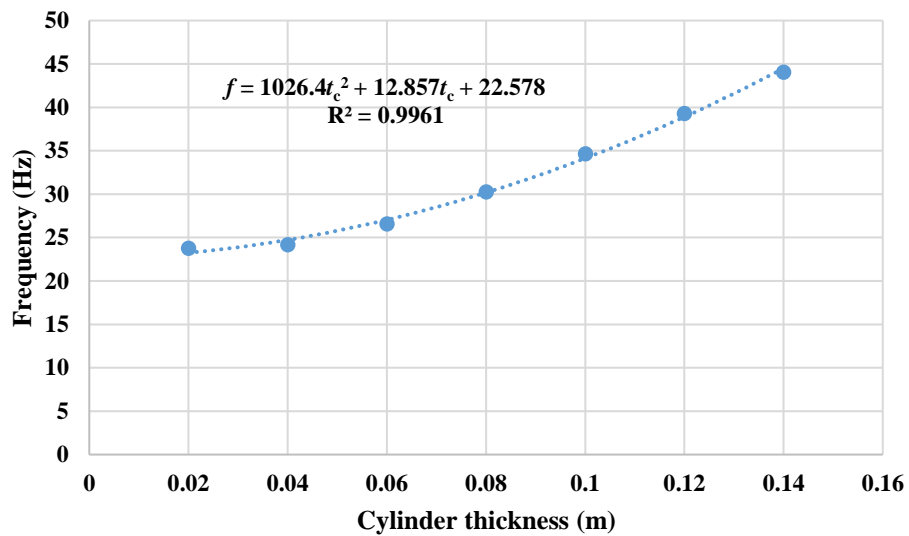
(d)

Figure A.2 Frequency variation as dimensions are altered with rotor disc sub structure thickness maintained at 0.06 m; (a) 2nd mode; (b) 3rd mode; (c) 4th mode; (d) 5th mode

Natural frequencies: Disc stator structure

$$f = -4296t_{s,d}^2 + 1009.6t_{s,d} + 36.9$$
$$R^2 = 0.9716$$

(a)

$$f = -4092.4t_{s,d}^2 + 970.33t_{s,d} + 38.681$$
$$R^2 = 0.9745$$
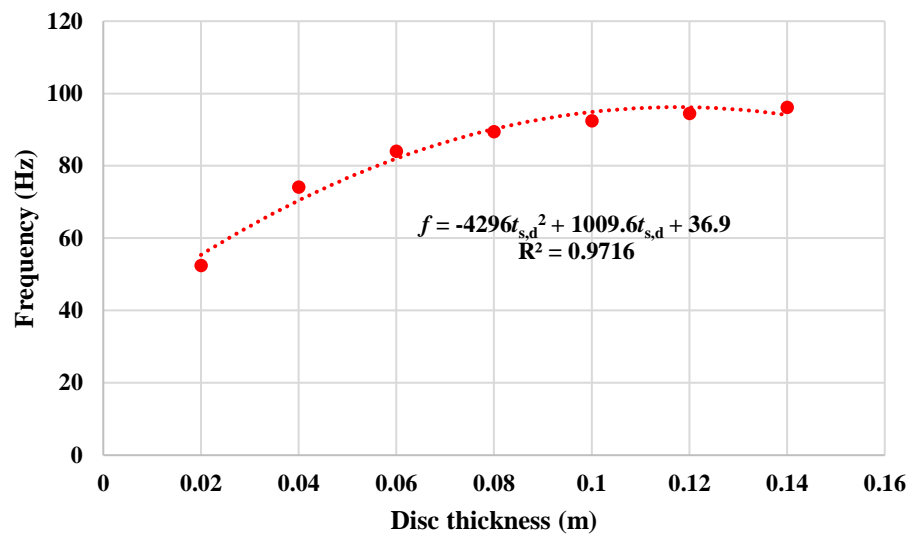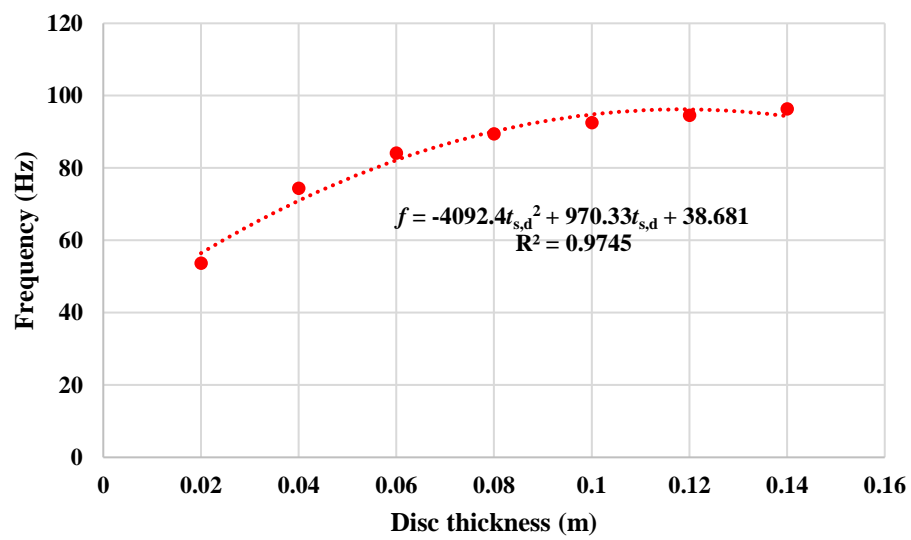
(b)

(c)

(d)

Figure A.3 Frequency variation as dimensions are altered with stator cylinder sub structure thickness maintained at 0.02 m; (a) 2nd mode; (b) 3rd mode; (c) 4th mode; (d) 5th mode
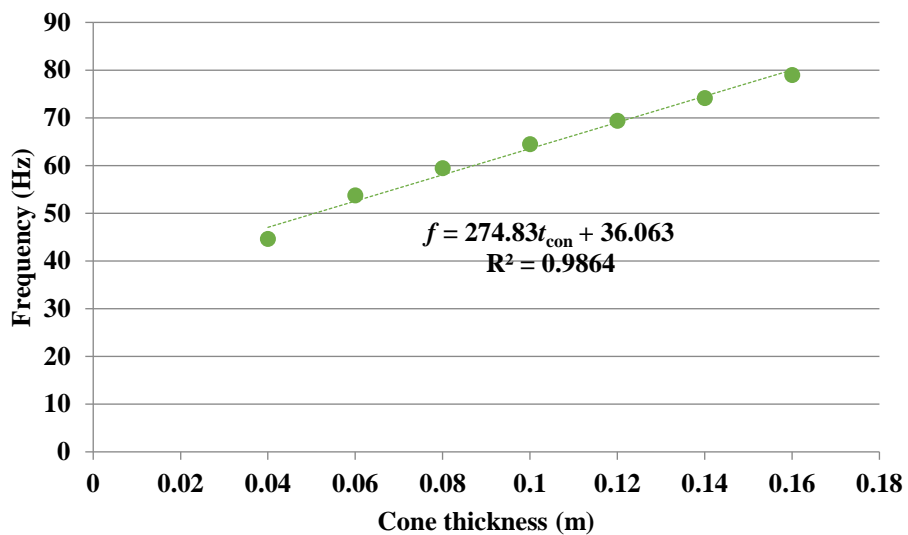
$$f = -812.68{t_{s,c}}^2 + 104.35t_{s,c} + 51.079$$
$$R^2 = 0.9452$$

(a)

$$f = -854.29{t_{s,c}}^2 + 101.33t_{s,c} + 52.558$$
$$R^2 = 0.9468$$

(b)

(c)

(d)

Figure A.4 Frequency variation as dimensions are altered with stator disc sub structure thickness maintained at 0.02 m; (a) 2nd mode; (b) 3rd mode; (c) 4th mode; (d) 5th mode
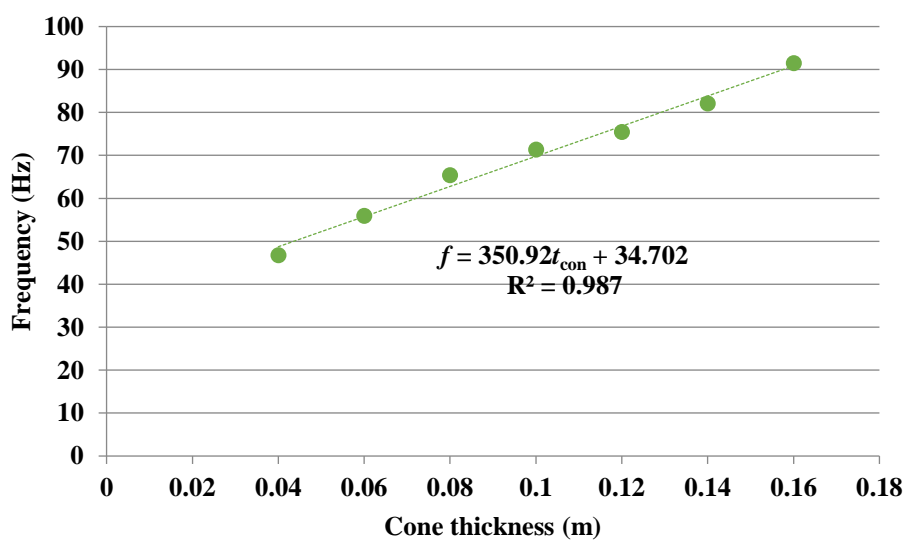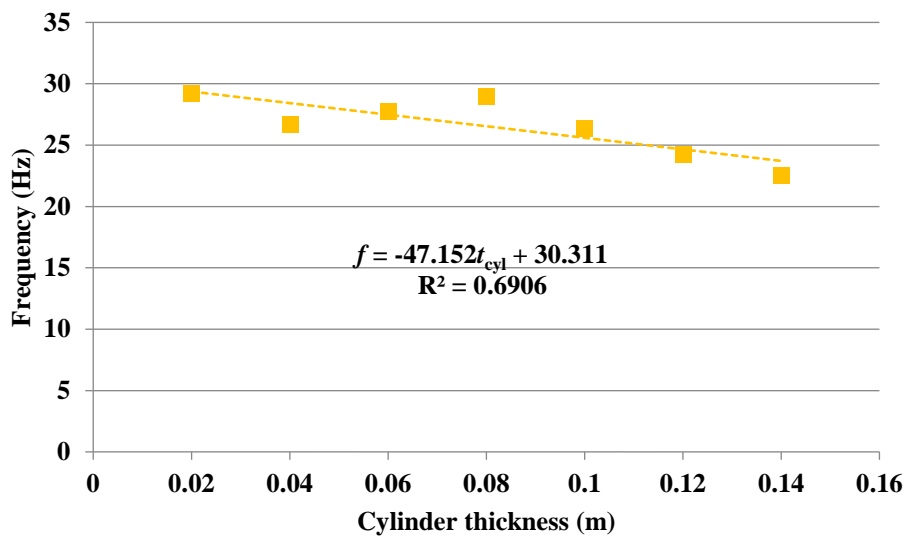
Natural frequencies: Rotor conical structure

$$f = 291.75t_{con} + 18.537$$
$$R^2 = 0.9972$$

(a)

$$f = 274.91t_{con} + 36.015$$
$$R^2 = 0.9858$$

(b)

$f = 274.83t_{con} + 36.063$
$R^2 = 0.9864$
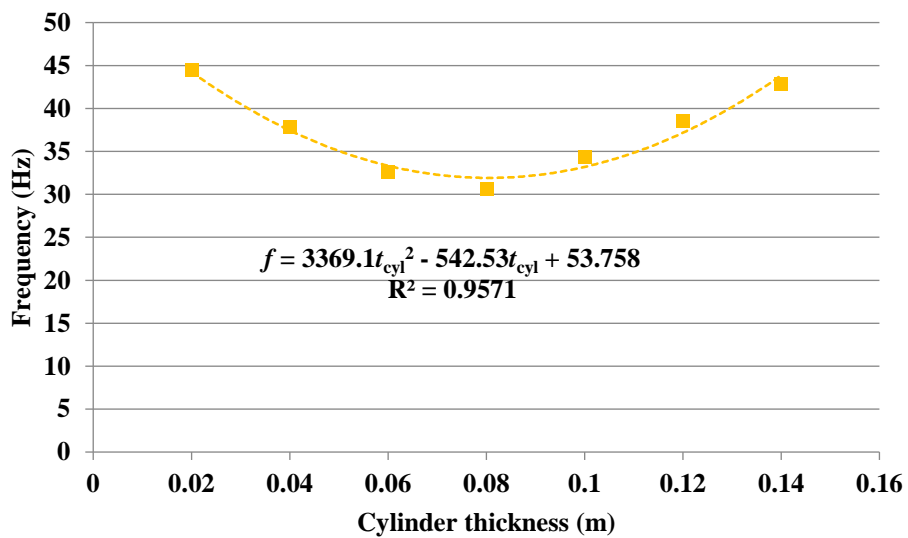
(c)

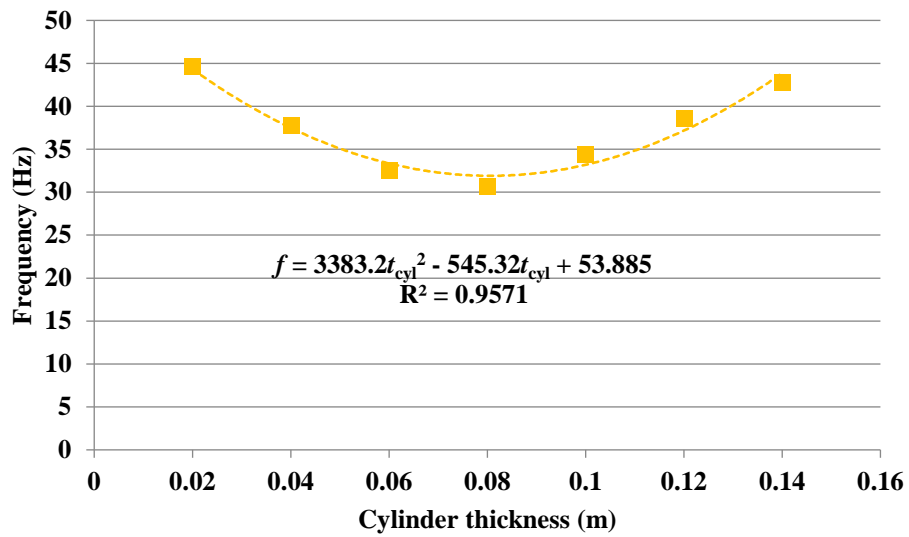$f = 350.92t_{con} + 34.702$
$R^2 = 0.987$

(d)

Figure A.5 Frequency variation as dimensions are altered with cylinder thickness maintained at 0.02 m; (a) 2nd mode; (b) 3rd mode; (c) 4th mode; (d) 5th mode
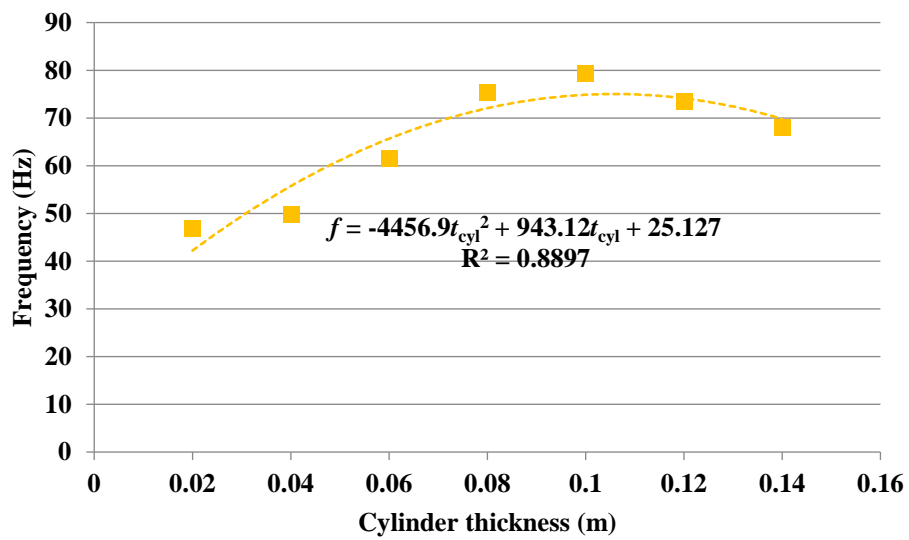
(a)

(b)

(c)

(d)

Figure A.6 Frequency variation as dimensions are altered with cone thickness kept at 0.04 m; (a) 2nd mode; (b) 3rd mode; (c) 4th mode; (d) 5th mode